Coordination of dynamic metallo-supramolecular polymers (MEPEs)

Dissertation zur Erlangung des naturwissenschaftlichen Doktorgrades der Julius-Maximilians-Universität Würzburg

vorgelegt von

Stefanie Martina Munzert

aus Kronach

Würzburg 2017

Eingereicht bei der Fakultät für Chemie und Pharmazie am

_____

Gutachter der schriftlichen Arbeit

1. Gutachter: _____

2. Gutachter: _____

Prüfer des öffentlichen Promotionskolloquiums

1. Prüfer: _____

2. Prüfer: _____

3. Prüfer: _____

Datum des öffentlichen Promotionskolloquiums

_____

Doktorurkunde ausgehändigt am

_____

für meinen Bruder Felix

Table of Contents

Danksagung

Ich bedanke mich bei allen, die zum Gelingen dieser Arbeit beigetragen haben. Mein besonderer Dank gilt:

Herrn Prof. Dr. Dirk G. Kurth für die Überlassung des Themas und zahlreiche Anregungen und Diskussionen sowie für das in mich gesetzte Vertrauen, die mir gewährten Freiräume und seine uneingeschränkte Unterstützung.

Ebenfalls bedanken möchte ich mich bei Herrn Dr. Guntram Schwarz, der mit unendlicher Geduld und Hilfsbereitschaft immer zur Seite stand.

Herrn Prof. Dr. Robert Luxenhofer, der mich an seinem umfangreichen Wissen über die Polymerchemie teilhaben ließ und wichtige Anstöße zur vorliegenden Arbeit lieferte.

Herrn Prof. Dr. Markus Sauer und Herrn Priv.-Doz. Dr. Sören Doose (Lehrstuhl für Biotechnologie und Biophysik der Universität Würzburg) für die Verfügbarkeit der Stopped-flow-Anlage.

Herrn Prof. Dr. Sextl für die ausgezeichneten Arbeitsbedingungen am Lehrstuhl für Chemische Technologie der Materialsynthese.

Der Deutschen Forschungsgemeinschaft für die finanzielle Unterstützung im Rahmen des DFG-Projekts INST 93/774–1 FUGG.

Der „Jubiläums-Stiftung zum 400-jährigen Bestehen der Universität“ für ein Reisestipendium zur Gordon Research Conference „Self-Assembly & Supramolecular Chemistry“ in Lucca (Italien).

Alexander Braun, Andreas Stephan, Christian Bauer und Paul Schmid für ihre Hilfe bei der Durchführung der DLS-, SLS- und Viskositätsmessungen.

Allen Kollegen am Röntgenring für die schöne Zeit, die gute Zusammenarbeit und das freundschaftliche Arbeitsklima.

List of Publications

The work of this thesis is based on the following publications:

A *"Kinetic Studies of the Coordination of Mono- and Ditopic Ligands with First Row Transition Metal Ions"*

Stefanie Martina Munzert, Guntram Schwarz, Dirk G. Kurth, *Inorg. Chem.* **2016**, 55, 2565-2573.

B *"The kinetics of growth of metallo-supramolecular polyelectrolytes in solution"*

Stefanie Martina Munzert, Simon P. Stier, Guntram Schwarz, Haim Weissman, Boris Rybtchinski, Dirk G. Kurth, *Chem. Eur. J.* **2017**, doi: 10.1002/chem.201701417.

C *"Tailoring length and viscosity of dynamic metallo-supramolecular polymers in solution"*

Stefanie Martina Munzert, Guntram Schwarz, Dirk G. Kurth, *RSC Adv.* **2016**, 6, 15441-15450.

List of Abbreviations

a.u.	arbitrary unit
BDC	1,4-benzene-dicarboxylate
CHEF	chelation-enhanced fluorescence
cryo	cryogenic
DLS	dynamic light scattering
DMF	dimethylformamide
DMSO	dimethyl sulfoxide
EM	effective molarity
eq(s)	equation(s)
et al.	et alia, and others
EtOH	ethanol
KMH	Kuhn-Mark-Houwink
MEPE	metallo-supramolecular polyelectrolyte
MOF	metal-organic framework
NMR	nuclear magnetic resonance
PAC	polyelectrolyte-amphiphile complex
PET	photoinduced-electron-transfer
ref	reference
SLS	static light scattering
TEM	transmission electron microscopy
THF	tetrahydrofuran
tpy	terpyridine
UV/Vis	ultraviolet / visible
vol %	percentage by volume
wt %	percentage by mass

Ligands used in this work

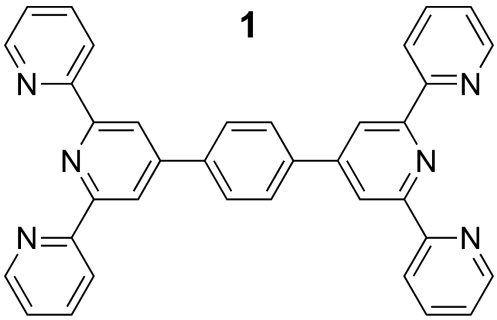

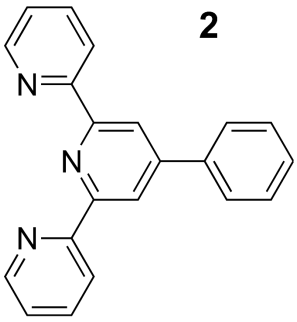

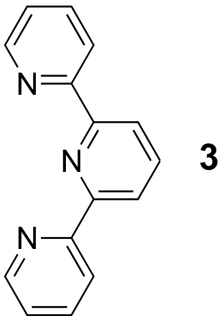

Note:

The conformation of the pyridine units in the uncoordinated terpyridine ligands and in ethanolic solution is trans-trans with respect to the nitrogen atoms. Nevertheless, the ligand units are in most cases depicted in the cis-cis conformation to emphasize the ability to act as a chelating ligand.

1

From Self-Assembly to Metallo-supramolecular polyelectrolytes

Parts of this Chapter are based on the publications listed on page VIII.

1.1 Introduction

Metal ion induced self-assembly combines the properties of organic ligands and the magnetic, electronic, optical, and catalytic potential of metal ions. Dependent on the interactions between metal ions and ligands, self-assembly leads to a variety of structures. Kinetically labile transition metal complexes are employed to construct in metal-organic frameworks (MOFs).[1-5] In this case polymeric species are not dominant in solution, which means that the coordination network only exists as crystalline solid as it is formed by concomitant metal ion coordination and crystallization.[6] Materials built up by kinetically labile interactions can assemble, disassemble and reconstruct and are responsive and adaptive to external parameters, such as external fields, ionic strength, pH, solvent and temperature.

Based on the coordination geometry of the metal ion and the structure of the ligands, the design of a variety of different structures is possible, for example the self-assembly of well-defined discrete cyclic nanostructures mediated by transition metal ions, which is reviewed by Stang et al.[7] Thus, the design of two-dimensional molecular polygons, like rhomboids[8-10] and helicates,[11-19] molecular triangles,[20-25] squares,[9, 26-31] pentagons[14, 32-33] and larger ring systems[34] as well as three-dimensional nanoscopic cages, like self-assembled prisms[35-37] and cylinders,[38-39] is reported.[7] Scheme 1 shows some corresponding examples.

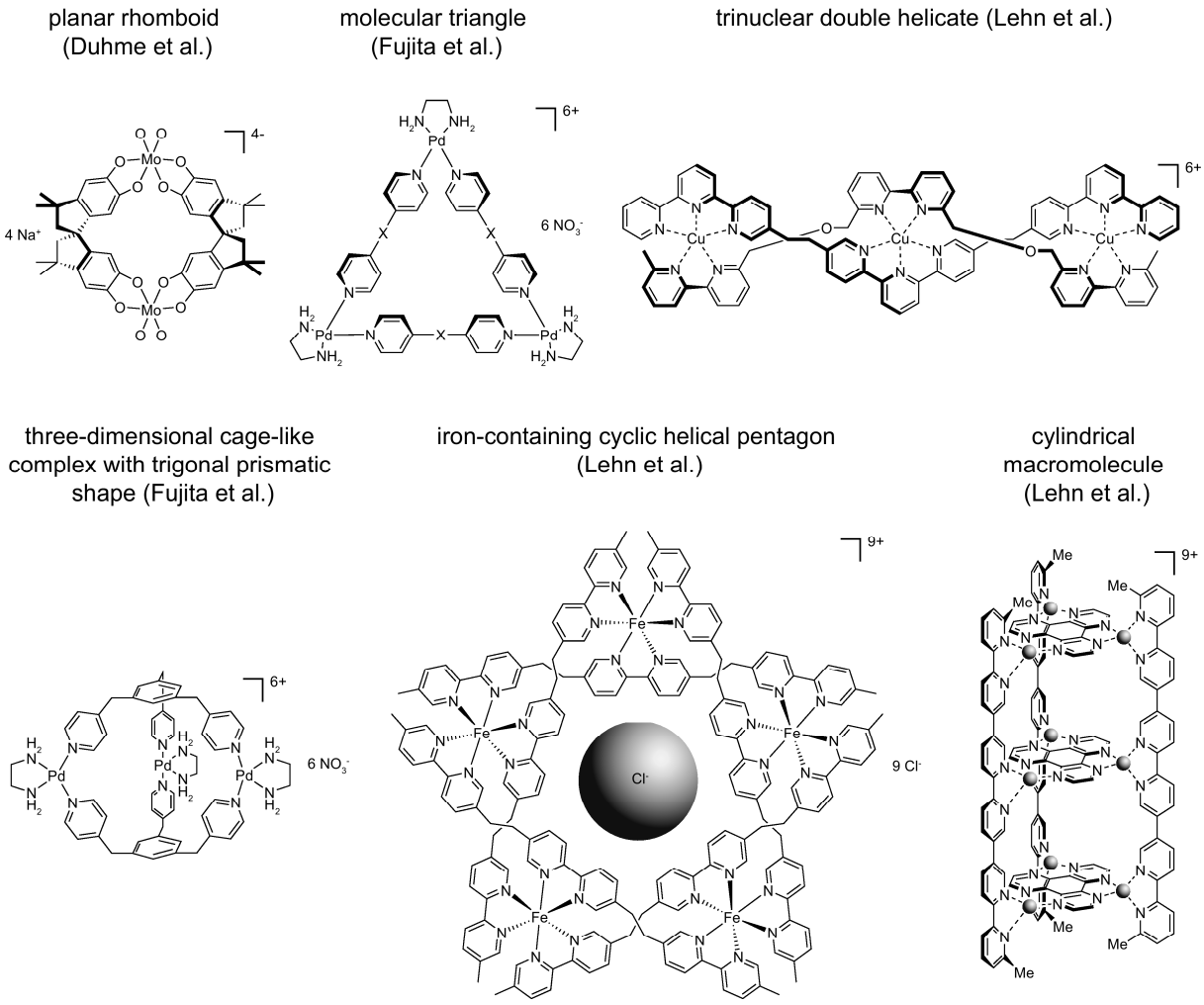

Scheme 1. Selected examples of well-defined discrete cyclic nanostructures mediated by transition metal ions. Adapted with permission from [7], [11], and [39]. Copyrights 2000 American Chemical Society, 1996 National Academy of Sciences, and 1999 John Wiley and Sons.

If the ligand planes are arranged perpendicular at each metal center, a linear and rigid extension of the ligand system leads to a grid-like two-dimensional coordination network with regularly arrayed metal ions. These architectures are mainly based on tetrahedrally and octahedrally coordinated metal complexes of azaaromatic ligands containing bidentate or tridentate subunits as Zhao et al.[40-41] and Lehn et al.[42-46] have

reported.[42] Scheme 2 shows a [3×3] grid self-assembled from a tris-terdentate ligand and octahedrally coordinated transition metal ions.

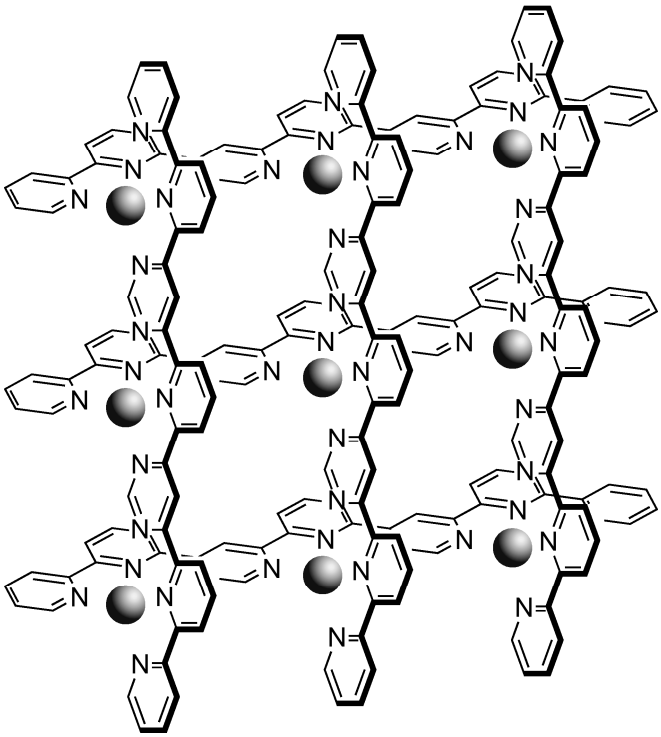

Scheme 2. Schematic representation of a [3×3] grid and octahedrally coordinated metal ions. Adapted with permission from ref [46]. Copyright 2002 John Wiley and Sons.

Metal ion induced self-assembled structures offer many applications as dye-sensitized solar cells,[47] spin-state control[48], electrochromic[49-53] and catalysis.[54-60] The large surface area of MOFs enables the uptake of gases by variation of the functional groups and thus, the pores of the architecture as mainly Yaghi et al. have reported.[4-5, 61-65]

If the binding constants are sufficiently high, metal ion induced self-assembly can lead to polymeric assemblies in solution.[6] For example, stimuli-responsive polymers show property changes in response to an environmental stimulus, which is used to synthesize

gels as Beck et al.[66] have reported. The group produced supramolecular polyelectrolyte gel-like materials exhibiting thermo-, chemo-, and mechanoresponsive, as well as light-emitting properties by the usage of metal-ligand interactions.[66]

In general, metallo-supramolecular systems are based on coordinative bonds and are variable by changing geometry and coordination number of the ligands and by using different transition metal ions. Coordination of organic ligands and metal ions results in a variety of supramolecular structures ranging from mononuclear compounds to nanosized assemblies, soluble coordination polymers, gels all the way to solid state networks.[63, 67-70] In case of ditopic bis-terpyridines, such as **1**, rigid-rod like metallo-supramolecular coordination polyelectrolytes (MEPEs) form in solution with transition metal ions such as Fe^{2+}, Co^{2+}, Ni^{2+} or Zn^{2+} (see Scheme 3).[50, 52-53, 71-84]

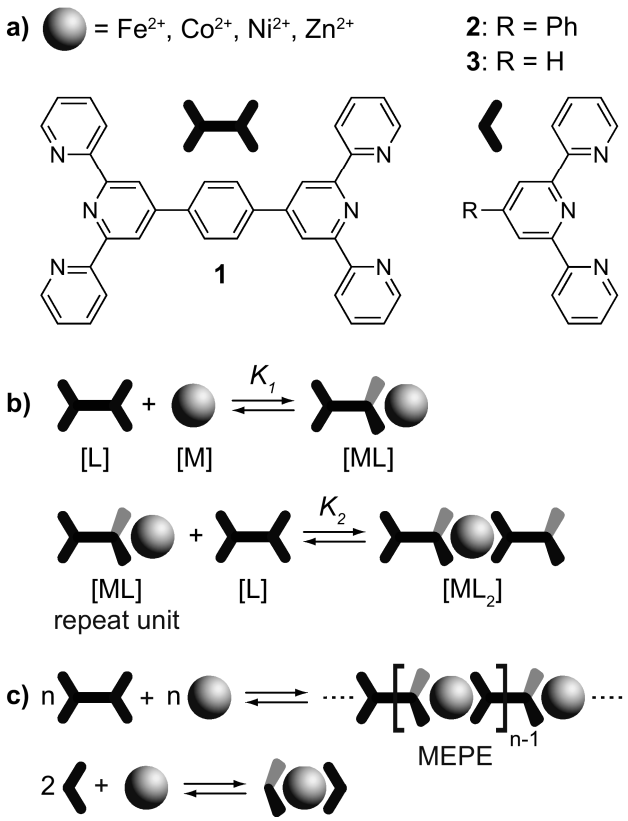

Scheme 3. Metal ion induced self-assembly of 1,4-bis(2,2′:6′,2′′-terpyridine-4′-yl)benzene (**1**) results in metallo-supramolecular coordination polyelectrolytes (MEPEs). 4′-Phenyl-2,2′:6′,2′′-terpyridine (**2**) and 2,2′:6′,2′′-terpyridine (**3**) form mononuclear complexes with Fe^{2+}, Co^{2+}, Ni^{2+}, and Zn^{2+}. The compounds are shown in part (a). The ligands are trans-trans configured in EtOH and cis-cis in acetic acid solution (75 vol %) due to hydrogen bonding between the protons and the free electron pair of the central nitrogen atom.[85-87] As shown in part (b), K_1 and K_2 are the binding constants for the stepwise coordination of **1** to the metal ion, whereas part (c) illustrates the overall reaction of the components. The acetate counter ions are omitted for clarity. Adapted from ref [88] with permission from The Royal Society of Chemistry.

Due to the chelating effect of ligand **1** (see Scheme 3), the binding strength to 3d transition metal ions, e.g. Fe^{2+}, Co^{2+} and Ni^{2+} is sufficient to support macromolecular assemblies even in aqueous solutions.[84] With many metal ions coordination results in a pseudo-octahedral geometry. In case of rigid bis-terpyridines, such as **1**, rigid-rod like metallo-supramolecular coordination polyelectrolytes (MEPEs) form in solution,

whereas the monotopic ligands, such as **2** or **3**, result to mononuclear metal complexes (Scheme 3).[89]

The resulting MEPEs are soluble in water, aqueous acetic acid and polar solvents like EtOH or MeOH. Figure 1 shows the ethanolic solutions of Fe-, Co-, and Ni-MEPE. By addition of $Fe(OAc)_2$ in acetic acid solution (75 vol %) to a solution of ligand **1** in acetic acid solution (75 vol %), the resulting Fe-MEPE shows a deep blue color, whereas the complexation of ligand **1** with Co^{2+}, and Ni^{2+} in acetic acid solution (75 vol %) leads to a red and yellow color, respectively.[89]

Figure 1. Colors of ethanolic Fe-, Co-, and Ni-MEPE solutions (from left to right).

The MEPEs offer interesting features, like electrochromic[49-51] and electrorheological properties and can be incorporated in various architectures, including films,[52-53, 82] liquid crystals[90] or nanostructures.[91] Polyelectrolyte amphiphile complexes based on Fe-MEPE embedded in alkyl phosphate layers exhibit a structure induced and partially reversible spin-crossover between diamagnetic low-spin and paramagnetic high-spin state. The change in the spin state alters not only the magnetic state but the optical properties of the complex as well.[92] Thus, MEPEs are suitable systems for spin-crossover or thermochromic materials.[83, 92] The properties and applications of the MEPEs will be presented in detail in Chapter 1.2.3.2.4.1.

1.2 Structures

1.2.1 Self-assembly and supramolecular chemistry

Self-assembly refers to the spontaneous aggregation of molecular or macromolecular building blocks into well-defined supramolecular structures through noncovalent interactions like hydrogen bonds,[93-100] coordinative bonds,[50, 66, 69-71, 73, 75, 77, 83, 101-112] ionic interactions,[113] hydrophobic interactions,[114-118] and π-π stacking,[119-142] as shown in Scheme 4.[69, 102, 104-105, 108, 112]

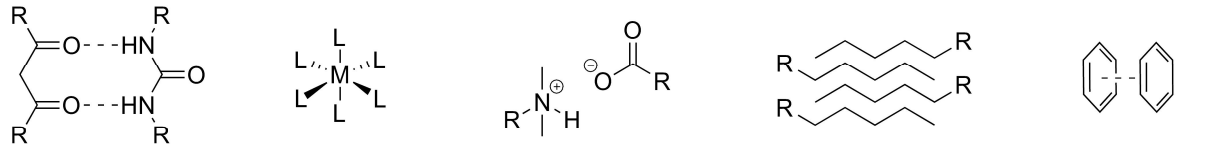

Scheme 4. Basic physical molecular interactions exploitable for supramolecular systems. Adapted with permission from [102]. Copyright 2016 American Chemical Society.

Two- and three-dimensional systems, i.e. rigid rods, side-chains, and cross-linked supramolecular polymeric structures can form, depending on the geometry of the interacting components. Scheme 5 shows some of the different types of supramolecular polymers, which can be designed by the self-assembly of complementary monomers.[69, 102, 104-105, 108, 112, 143-148]

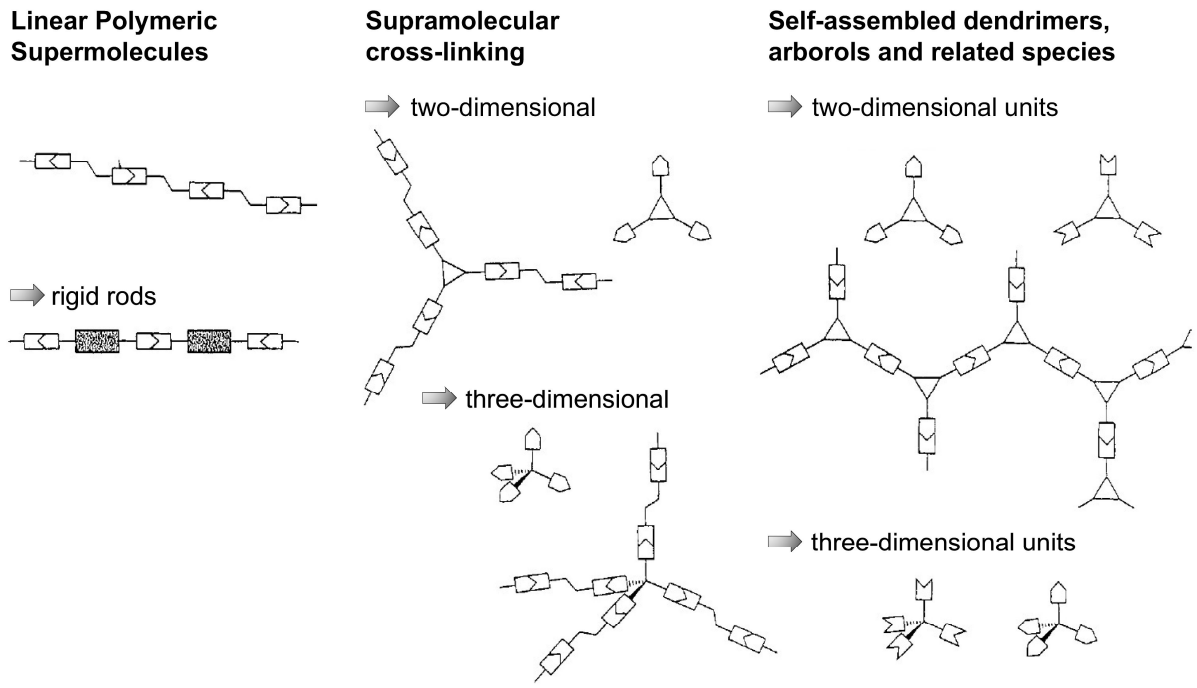

Scheme 5. Different types of supramolecular polymers by self-assembly of complementary monomers through noncovalent interactions. Adapted with permission from ref [69]. Copyright 2002 John Wiley and Sons.

The ligands shown in Scheme 5 can form main-chain, side-chain or branched structures. Linear polymeric supramolecules can be designed by using ditopic ligands. By using flexible spacers between two functional receptors, the resulting linear structures are flexible and may be circular. If rigid ditopic molecules are used, the resulting structure are rigid rods (see the left side in Scheme 5). Supramolecular structures can also be linked by using polytopic ligands, as shown in the middle part of Scheme 5, leading to two- and three-dimensional cross-linked supramolecular structures. Furthermore, the design of two- and three-dimensional repetitively branched supramolecules (dendrimers and arborols) is possible (see the right side of Scheme 5).[69, 102, 104-105, 108, 112, 149]

Thus, the properties of supramolecular polymers are determined by the nature of the molecular components and by the type of bonds, acting between them in solution.

These polymers can change the molecular-size distribution of their species through reversible adaptation to external factors such as concentration, temperature, solvent, and stoichiometry as well as the addition of cross-linking and end-capping agents that means they are stimuli-responsive.[69, 102, 104-105, 108, 112]

Dependent on the building blocks of supramolecular structures, they give rise to electrochemical,[77] electrochromic,[49-53] magnetic,[68, 150] spin-crossover,[76, 92] and self-healing properties[66, 71, 93, 101, 111, 113, 117] for applications in films or layers,[52-53, 76, 82, 92, 103, 151] liquid crystals,[76, 90, 92, 103, 151] nanostructures,[91, 152-165] optically switchable molecular compounds,[76, 92, 150, 166-167] and even for 3D printable hydrogels,[102] electrorheological fluids,[91, 168] metal-organic frameworks (MOFs) with gas storage,[63, 67-68] catalysis properties,[54-60] and organic light-emitting diodes (OLEDs).[128-129]

1.2.2 Metal ion coordination

In general, the coordination of metal ions to organic ligands leads to discrete architectures including complexes, grids, helicates and extended assemblies that occur as crystalline or amorphous solids, nanoparticles, or soluble polymers as well as thin films. MOFs are built up by networks of metal centers or inorganic clusters connected by organic linkers through metal-ligand coordination bonds leading to three-dimensional networks, whereas supramolecular coordination complexes consist of metal ions self-assembled to ligands with multiple binding sites and a specific angularity. Kinetically labile transition metal complexes mainly result in MOFs and are characterized as crystalline solids.[1-5] In these cases the binding constants are small and extended assemblies hardly form in solution which means, the coordination network forms through crystallization of the discrete species present in solution and only exists in the solid state.[6] In recent decades, the ligand diversity for generating

metal-organic materials ranges from cyanide to pyridyl- and carboxylate based donors.[169-170] For example, the pigment "Prussian Blue" showing a mixed-valent Fe^{2+}/Fe^{3+} network bridged by cyanide ligands is known since the early 1700s (see Figure 2).[170-171]

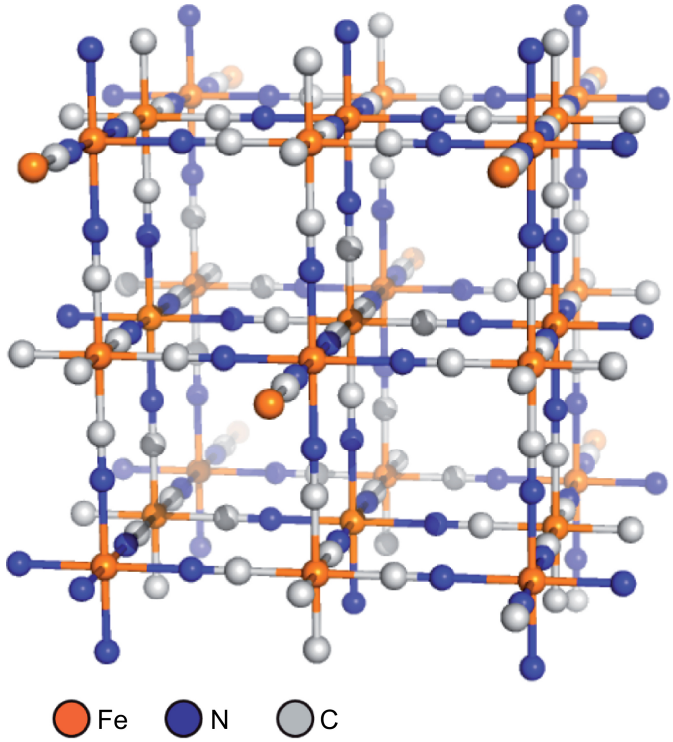

Figure 2. Structure of Prussian Blue, the first synthetic coordination polymer. Alternating octahedral sites of Fe^{2+} and Fe^{3+} ions are bridged by cyanide ligands to generate a cubic 3D array. Reprinted with permission from [170]. Copyright 2013 American Chemical Society.

Nowadays, the two most used ligands for supramolecular coordination complex and MOF formation are O-donors and N-donors that means carboxylate- and pyridyl-based ligands, as shown in Scheme 6 and Scheme 7, respectively.[170]

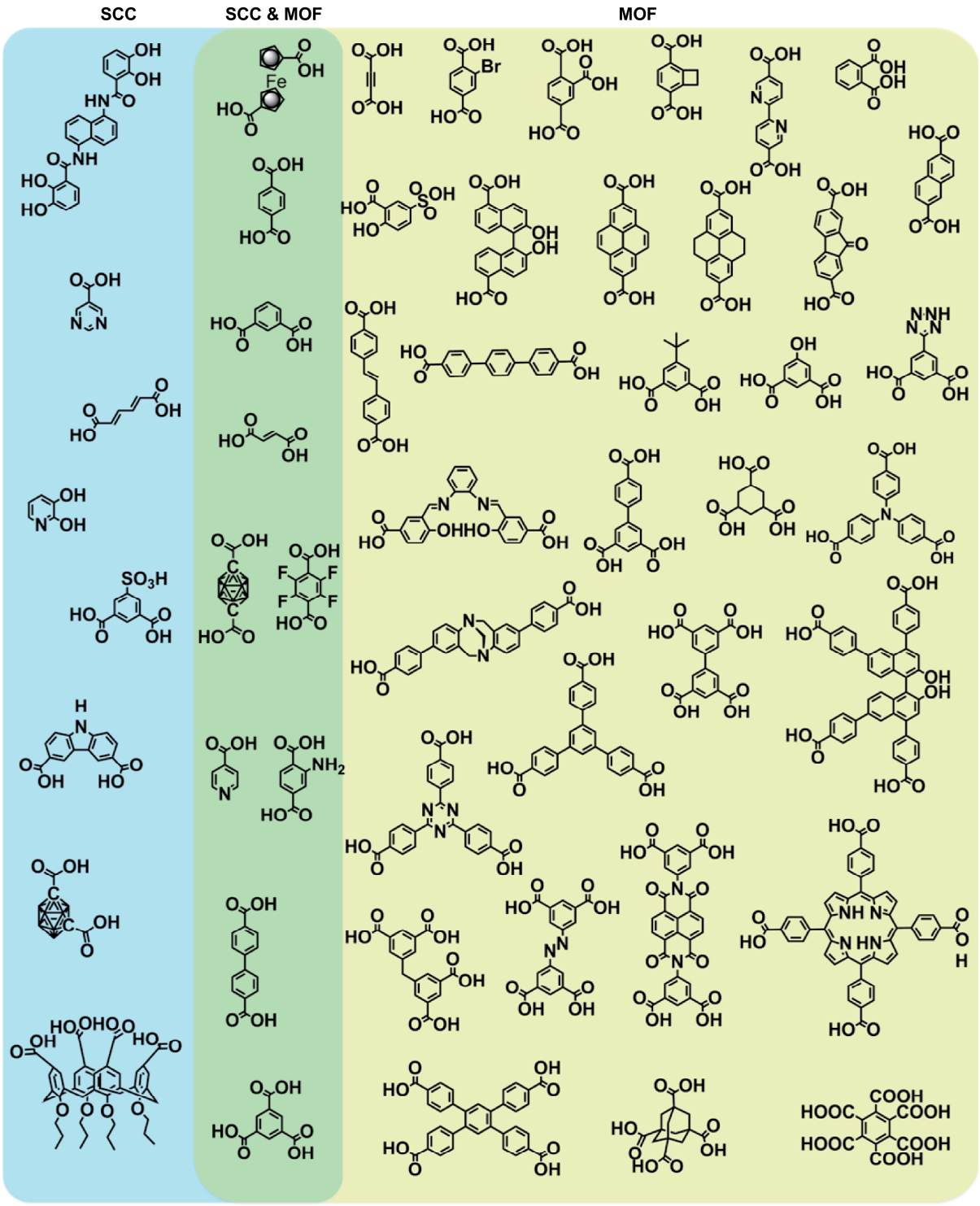

Scheme 6. O-donor based building blocks for supramolecular coordination complexes (SCCs) and MOFs. Adapted with permission from [170]. Copyright 2013 American Chemical Society.

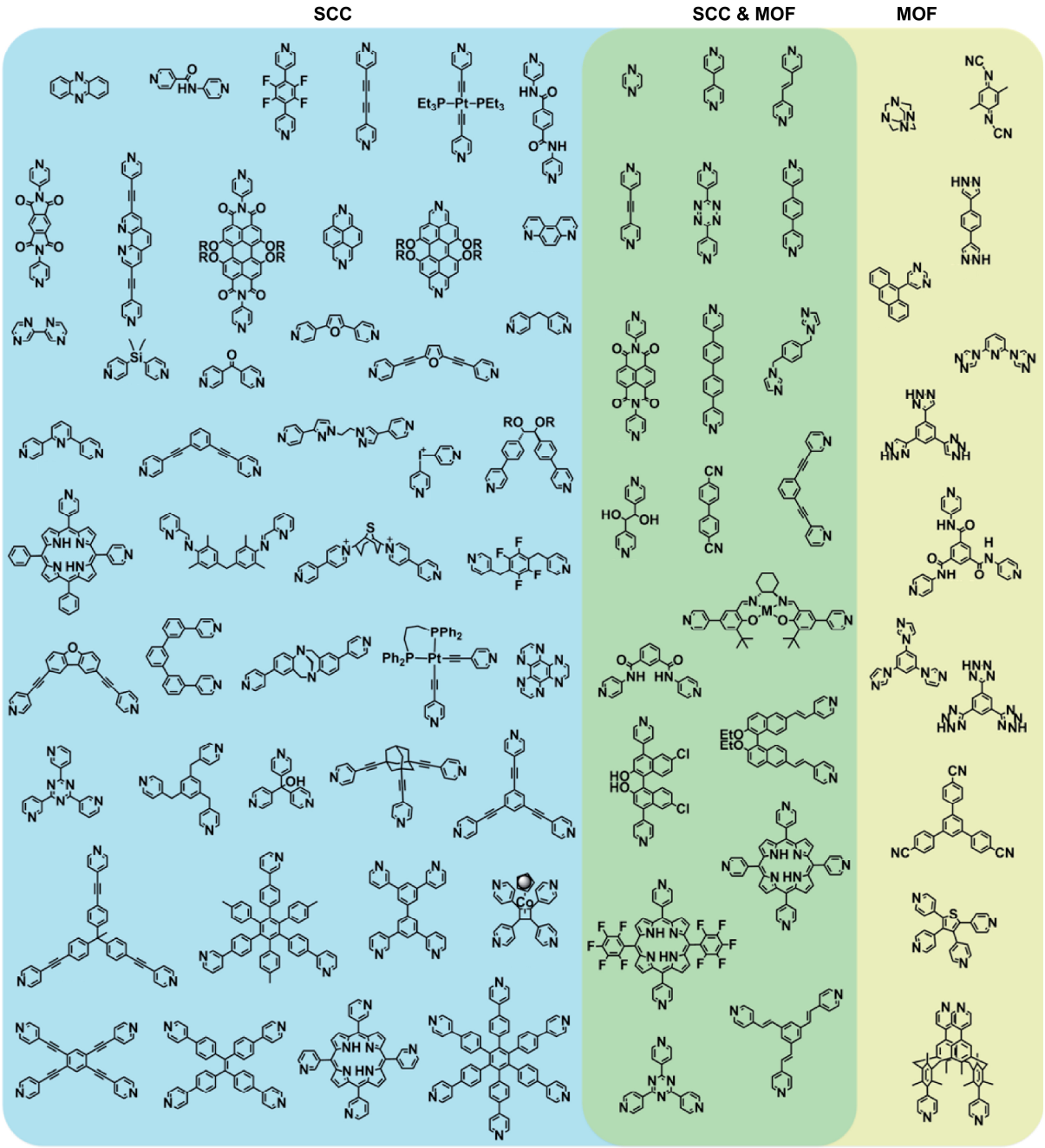

Scheme 7. N-donor based ligands as building blocks for supramolecular coordination complexes (SCCs) and MOFs. Adapted with permission from [170]. Copyright 2013 American Chemical Society.

As can be seen in Scheme 6 and Scheme 7, supramolecular coordination complexes are dominated by N-donor based ligands, while carboxylate ligands are more

commonly used to form MOFs.[170] For example, the N-donor ligand 4,4′-bipyridine forms a two-dimensional square network material with $Cd(NO_3)_2$, as shown in Figure 3, which is able to clathrate aromatic guests with high shape specificity.[55, 170]

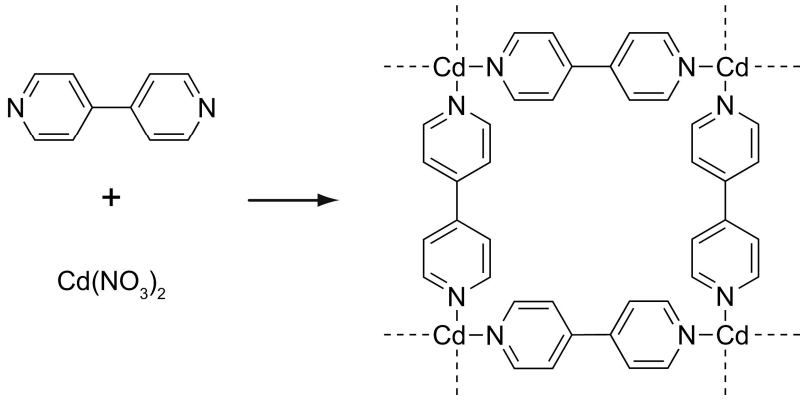

Figure 3. Formation of a two-dimensional square network material with 4,4′-bipyridine as the ligand and Cd^{2+} as a metal ion. The counter ions are omitted for clarity. Adapted with permission from [55]. Copyright 1994 American Chemical Society.

An example of a 3D assembly using the N-donor based ligand 4,4′-bipyridine is given by the Ru-based cube of Thomas et al.[172] When ([9]ane-S_3)Ru(DMSO)Cl_2 is combined with 4,4**′**-bipyridine in a 8:12 ratio, the chlorides and DMSO ligands are displaced. The supramolecular cube assembles slowly in 2 weeks in solution, presumably due to slower ligand exchange kinetics. Each Ru site acts as the vertex of the cube, with 4,4**′**-bipyridine representing the edges (see Scheme 8).[172]

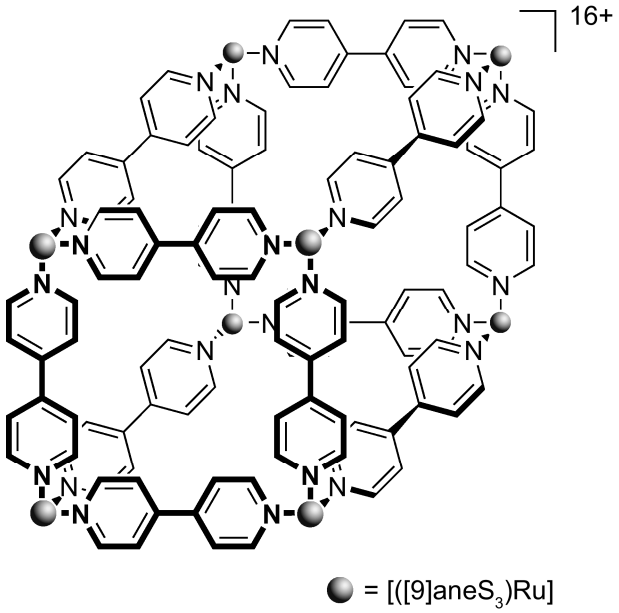

Scheme 8. Combining ([9]ane-S3)Ru(DMSO)Cl_2 with 4,4′-bipyridine in an 8:12 ratio leads to a 3D assembly, where the chlorides and DMSO ligands are displaced. Adapted from ref [172] with permission from The Royal Society of Chemistry.

Batten et al.[67-68] reported another interesting example by the design of a supramolecular nanoball for solvent and hydrogen gas storage. In the first step of synthesis the N-donor ligand tris[3-(4′-pyridyl)pyrazol-1-yl]hydroborate is used to form an intermediate building block by addition of Cu^+ (see Figure 4). Subsequent addition of a range of divalent metal salts leads to the self-assembly of analogous nanoball species by coordination to the secondary binding sites of the ligand.[67-68]

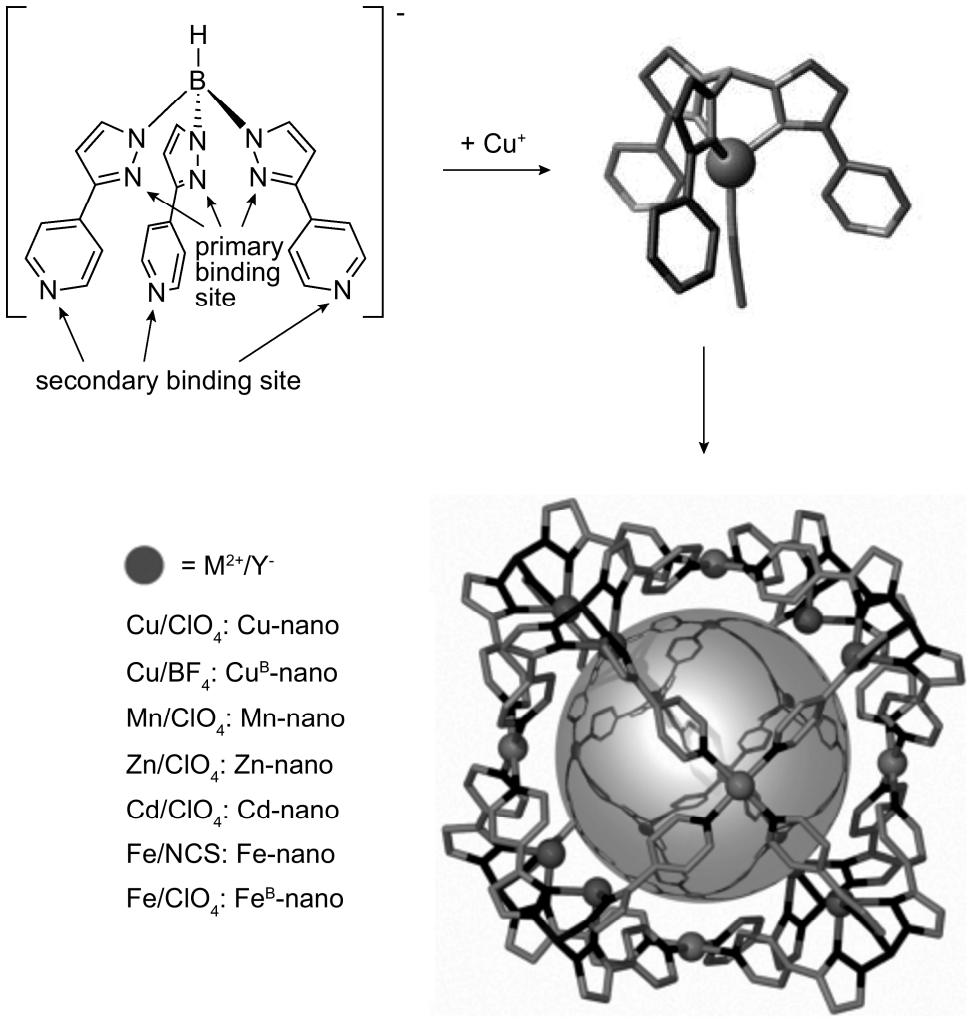

Figure 4. The bifunctional ligand, tris[3-(4'-pyridyl)pyrazol-1-yl]hydro-borate (upper left side) is used to form an intermediate building block (upper right side). Subsequent addition of a range of divalent metal salts leads to the self-assembly of the analogous nanoball species by coordination to the secondary binding sites of the ligand. Adapted with permission from ref [67] and [68]. Copyright 2009 John Wiley and Sons.

As can be seen in Figure 4, Batten et al.[67-68] present an example of metal-varied discrete cage-like materials that are synthesized by the intermediate production of a metal complex. Here, Cu-nano is a suitable candidate for hydrogen storage. That means the MOF is able to uptake 1.2 wt % hydrogen (at 77 K and 1 bar), equating to approximately 34 hydrogen molecules per nanoball.[67-68]

Besides N-donor ligands, also O-donor that means carboxylate based ligands are used to form MOFs as already indicated in Scheme 6. The carboxylate-based linear 1,4-benzene-dicarboxylate (BDC) can be regarded as a counterpart to 4,4′-bipyridine, because it also contains two Lewis-basic moieties. A well-known example of a BDC MOF is given by $(BDC)_3 \cdot (DMF)_8(C_6H_5Cl)$, also known as "MOF-5".[64, 170]

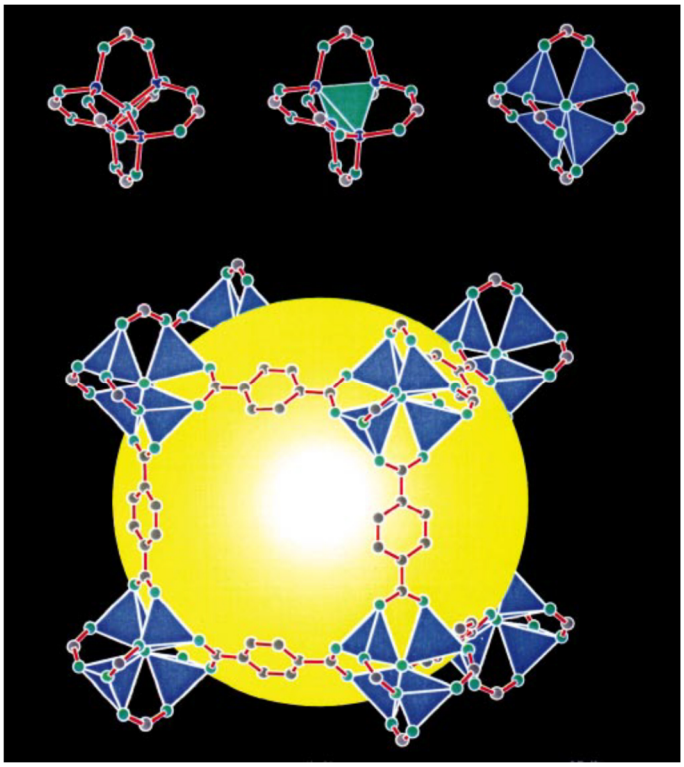

Figure 5. Construction of the MOF-5 framework. Top left, the $Zn_4(O)O_{12}C_6$ cluster is shown as a ball and stick model (Zn in blue, O in green, and C in grey). Top middle, the same cluster is shown with the $Zn_4(O)$ tetrahedron indicated in green. Top right, the cluster is shown with the ZnO_4 tetrahedra indicated in blue. The bottom shows one of the cavities in the resulting MOF-5 framework indicated by a yellow sphere. Adapted by permission from Macmillan Publishers Ltd: Nature [64], copyright 1999.

An expanded form of the tritopic analogue of BDC in which phenyl spacers are added is used to link zinc acetate to form "MOF-177", which possesses a surface area of 4500 m^2/g as shown in Figure 6.[61, 170]

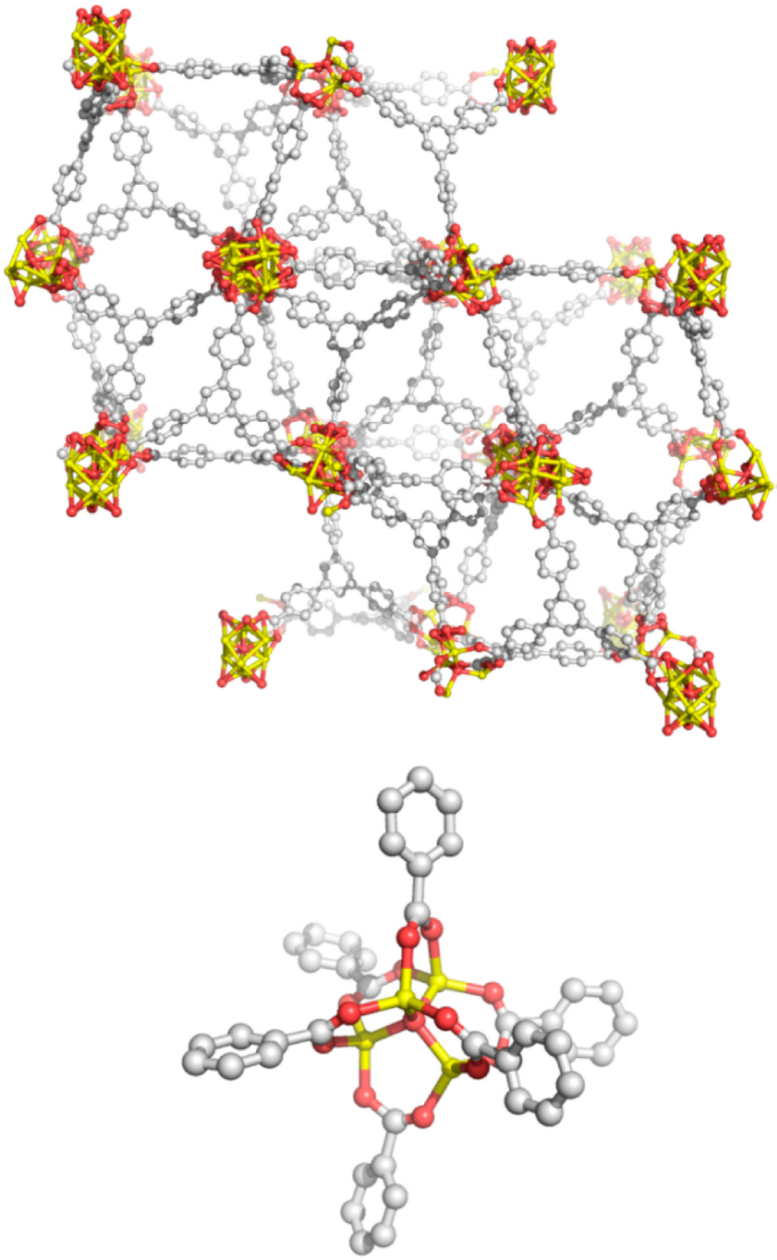

Figure 6. Construction of the MOF-177 framework by assembly of zinc acetate with the tritopic carboxylate ligand 1,3,5-benzenetribenzoate. On the bottom, the zinc acetate scaffolds are shown, which lead to disordered metal nodes (top). Zn is shown in yellow, C in gray, and O in red. The hydrogen atoms are omitted for clarity. Reprinted with permission from [170]. Copyright 2013 American Chemical Society.

The following subchapters give an overview concerning the kinetics and the mechanism of replacement reactions of coordination complexes of transition metal

ions with 2,2′:6′,2′′-terpyridine, as well as the published kinetic data. Furthermore, two important effects concerning the fluorescence properties of metal ion coordination complexes are presented.

1.2.2.1 Kinetics and mechanism of replacement reactions of coordination complexes of transition metal ions with 2,2′:6′,2′′-terpyridine

The reaction of metal ions and ligands in solution generally involves successive replacement of coordinated solvent molecules by the appropriate donor atoms of the incoming coordinating ligands. According to Eigen and Wilkins[173] the central metal ion (M^{2+}) and the ligand (L) first form an outer-sphere complex followed by the rate-determining step, the replacement of a solvent molecule (S) by the ligand in the inner sphere complex:[174-176]

$$[\mathrm{M(S)}_m]^{2+} + \mathrm{L} \overset{K_0}{\rightleftharpoons} [\mathrm{M(S)}_m]^{2+}, \mathrm{L} \xrightarrow{k_{ex}} [\mathrm{M(S)}_{m-1}\mathrm{L}]^{2+}, \mathrm{S} \quad (1)$$

with K_0 being the equilibrium constant for the formation of the outer-sphere complex, and k_{ex} being the rate constant for exchange of a solvent molecule between the inner sphere and the bulk solvent. Reactions following this rate law are controlled by the rate of water ligand dissociation, are largely insensitive to the nature of the incoming ligands and are governed by ligand field effects.[177] The reaction scheme predicts the rate law to be first order in M^{2+} and in L. With M^{2+} in excess, k is the second-order rate constant for the overall forward reaction:

$$k = K_0 k_{ex} \quad (2)$$

If a negative volume of activation is measured, the mechanism is associative (*A*). In this case, the intermediate shows an increased coordination number. In contrast, in

dissociative substitution mechanism (*D*), the intermediate shows a reduced coordination number. Due to the mainly bond-breaking character of dissociative substitution mechanisms the volume of activation is positive. When the reaction is concerted and there is partial, and equal, association and dissociation of the entering and leaving groups, it is an interchange mechanism. Moreover, one can distinguish the interchange mechanism (*I*) with an associative (I_a) or a dissociative activation mode (I_d), in which the transition states are characterized mainly by bond-formation or bond-breaking, respectively.[176-179] The water exchange reaction of first row transition metal ions, i.e. Mn^{2+}, Fe^{2+}, Co^{2+}, Ni^{2+} as well as the coordination of these metal ions to bi- and terpyridine ligands were studied by Caldin,[174] Ellgen,[175] Hayward,[180] Hubbard,[181] Merbach,[182] Moore,[183] van Eldik,[184] and Wilkins.[78, 185] In water exchange studies, Co^{2+} and Ni^{2+} show positive volumes of activation indicating a dissociative interchange (I_d) mechanism. However, Fe^{2+} shows an almost zero value and the value for Mn^{2+} is negative. These results are rationalized in terms of a mechanistic changeover along the series with Mn^{2+} showing associative and Ni^{2+} dissociative behavior, respectively.[181-182] Measurements of volumes of activation indicate that coordination reactions of the metal ions Fe^{2+}, Co^{2+}, and Ni^{2+} with bi- and terpyridines take place as an I_d mechanism. Thus, the changeover in the solvent-exchange mechanism for the first row transition metal elements also applies to complex formation reactions involving these metal ions and neutral ligands.[184] Finally, there is evidence that the chemical nature of the entering ligand also affects the rate, e.g. in chelation-controlled substitutions.[186]

1.2.2.2 Binding constants of the formation of transition metal ions and 2,2′:6′,2′′-terpyridine

Wilkins et al.[78] have shown that the addition of a terpyridine ligand to the metal ion is controlled by the first attachment, followed by rapid completion of the chelate.[78, 81] Each step is associated with a binding constant, K_1 and K_2, respectively (see Scheme 3b).[78] The binding constants are defined by

$$K_1 = \frac{[\mathrm{ML}]}{[\mathrm{M}] \cdot [\mathrm{L}]} \tag{3}$$

$$K_2 = \frac{[\mathrm{ML_2}]}{[\mathrm{ML}] \cdot [\mathrm{L}]} \tag{4}$$

with $[\mathrm{M}]$, $[\mathrm{L}]$, $[\mathrm{ML}]$ and $[\mathrm{ML_2}]$ being the concentrations of the uncoordinated metal ions (M^{2+}), the uncoordinated ligands (**1**, **2**, or **3**), and the both coordinated species ($[ML]^{2+}$ and $[ML_2]^{2+}$), respectively (see also Scheme 3b). The binding constants, K_1 and K_2, for the coordination of ligand **3** to Fe^{2+}, Co^{2+}, and Ni^{2+}, and Zn^{2+} are published by Wilkins et al.[78] and Ziessel et al.[187] (see Table 1).

Table 1. Literature values of binding constants, K_1 and K_2, for the coordination of different terpyridine ligands to the metal ions Fe^{2+}, Co^{2+}, Ni^{2+}, and Zn^{2+} at 25 °C. The values from ref [78] are measured in water with ligand **3** and bromide as counter ion, while the values from ref [187] are measured in acetonitrile with 4,4-difluoro-8-(6''-methyl-2',2'':6'',2'''-terpyridin-6'-yl)-1,3,5,7-tetramethyl-2,4-diethyl-4-bora-3a,4a-diaza-s-indacene as ligand and perchlorate as counter ion. Adapted with permission from ref [188]. Copyright 2017 John Wiley and Sons.

	Fe^{2+} (ref [78])	**Co^{2+} (ref [78])**	**Ni^{2+} (ref [78])**	**Zn^{2+} (ref [187])**
$lg[K_1]$	7.1	8.4	10.7	8.4 ± 0.5
$lg[K_2]$	13.8	9.9	11.1	6.4 ± 1.0
$lg[K_1 \cdot K_2]$	20.9	18.3	21.8	14.8 ± 0.5
$lg[K_2]/lg[K_1]$	1.9	1.2	1.0	0.7 ± 0.1

The high binding constants are caused by the chelate effect of ligand **3**. The coordination of **3** to a metal ion releases three solvent molecules per coordination step, which leads to an increasing entropy. Furthermore, the pyridine rings act as electron donors, whereas Fe^{2+}, Co^{2+}, and Ni^{2+} release d-electrons into the empty π*-orbitals of the ligand. The resulting π backdonation enhances the tendency for the formation of bis-tpy-complexes compared to mono-tpy-complexes, as can be seen in Table 1, where K_2 is larger than K_1 for the coordination of terpyridines to the metal ions Fe^{2+}, Co^{2+}, and Ni^{2+}. This can be noticed especially for the coordination of **3** to Fe^{2+} with $lg[K_2] - lg[K_1] = 6.7$ (see Table 1). The particular stability of $[Fe(\mathbf{3})]^{2+}$ is based on a high crystal field stabilization energy due to the d^6 low-spin electron configuration.[189] According to the spectrochemical series, the electron configuration is presumably high-spin in the mono-tpy-complex, since the crystal-field splitting is lower by a (3N3O) coordination compared to a (6N) coordination.[190] The change from high- to low-spin causes an energy gain, which is the reason for the high K_2 for the coordination of **3** to Fe^{2+}.

Hence, in the case of Fe^{2+}, Co^{2+}, and Ni^{2+} the bis-tpy-complex that is the species of a metal ion complexed to two terpyridine ligands (see Scheme 3) is the preferred species even if an excess of metal ions is present in solution.[70, 78, 89, 187]

Assuming that the binding constants, K_1 and K_2, are applicable to the formation of MEPEs, the average number of MEPE repeat units per chain that is the polymer length can be estimated.

1.2.2.3 Fluorescence increasing and quenching effects in transition metal ion complexes

While measuring the fluorescence properties of fluorescing ligands, an enhanced or a decreased fluorescence intensity, respectively, can be observed upon coordination to transition metal ions. These phenomena can be explained by two important effects: the chelation-enhanced fluorescence (CHEF) and the photoinduced electron transfer (PET) effect. Both effects are shown in Figure 7.

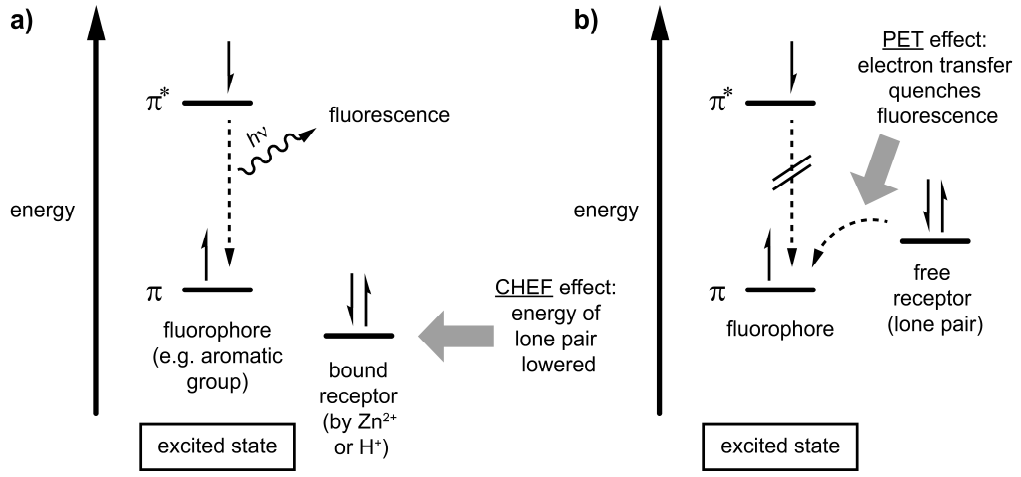

Figure 7. Origin of the chelation-enhanced fluorescence (CHEF) and the photoinduced-electron-transfer (PET) effect in the excited states of fluorophores: (a) fluorescence enhanced by the CHEF effect; (b) fluorescence quenched by the PET effect. Reprinted with permission from [89]. Copyright 2016 American Chemical Society.

In the event of a CHEF effect, lone electron pairs of the ligands are bound by protonation or by coordination. In both cases, the energy of the lone pairs is dropped below that of the ground state π level of the fluorescing ligand, as shown in Figure 7a. Therefore, the probability of transferring excited-state electrons from the excited π* level to the ground state π level is increased. As a consequence, the excited ligand molecule can return to the ground state π level unimpeded thus enhancing emission.[191]

In case of a PET effect, the lone pairs of the excited ligands are not bound by protonation or by complexation. Thus, the lone pairs transfer electrons into the ground state π level of the fluorescing ligand leading to a decreased probability of a return of ligand's excited-state π* electrons to the ground state π level. As a consequence, the emission of photons is reduced, which leads to a decreased fluorescence intensity (see Figure 7b).[191]

Both effects play an important role in coordination of terpyridine ligands to the transition metal ions, Fe^{2+}, Co^{2+}, Ni^{2+}, and Zn^{2+}. Depending on the metal ion, the fluorescence intensity of ligand **1** is enhanced or quenched, respectively, which is an important requirement for performing stopped-flow measurements and thus for obtaining a deeper insight to the kinetics of formation of the MEPEs.[89]

1.2.3 Supramolecular polymers

In contrast to traditional covalent polymers, supramolecular polymers are held together by noncovalent bonds, like coordinative bonds, π-π interactions, or hydrogen bonding. The design of such systems that is the spontaneous generation of a well-defined macromolecular architecture by self-assembly of molecular components under a given set of conditions without usage of any catalysts, has attracted considerable attention.[105, 112, 143-148] In the following subchapters some examples of supramolecular polymers are presented.

1.2.3.1 Supramolecular polymers based on hydrogen bonds and π-π interactions

H-bond-mediated self-assembly systems are a way in developing supramolecular structures with weak reversible interactions. For example, Lehn et al.[93] reported supramolecular polymers, built up by the association of two homoditopic heterocomplementary monomers through sextuple hydrogen-bonding arrays, as shown in Scheme 9.

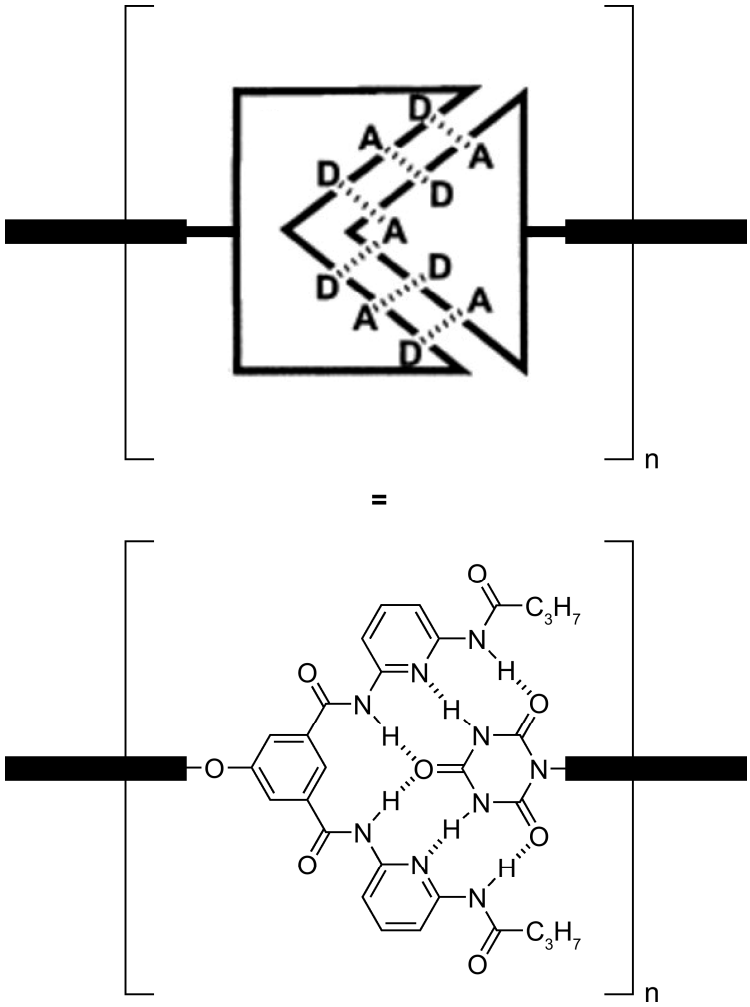

Scheme 9. Complementary hydrogen-bonded molecular recognition units. Adapted with permission from ref [93]. Copyright 2002 John Wiley and Sons.

The group used heterocyclic derivatives of diaminopyridine and uracil consisting of triple hydrogen-bonding donor (D) and acceptor (A) sites by usage of complementary components ADA and DAD, as shown in Scheme 9.[93-94] The self-assembly of these derivatives leads to a supramolecular liquid crystalline polymer of triple helical superstructure. If these complementary building blocks are connected by a spacer, the resulting ditopic components lead to rigid-rod supramolecular polymer systems in a nonpolar solvent, as shown schematically in Scheme 10.[93, 99]

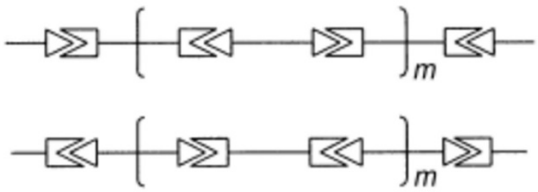

Scheme 10. Schematic representation of the complementary building blocks. Reprinted in part with permission from ref [93]. Copyright 2002 John Wiley and Sons.

Additionally, different hydrogen bond based supramolecular polymers are reported by Meijer,[95, 98] Cohen Stuart,[192-195] Bouteiller,[196] and Yagai.[197] For example, Meijer et al.[198] reported the self-assembly of supramolecular polymers based on the S-chiral oligo(*p*-phenylenevinylene) as shown in Figure 8.

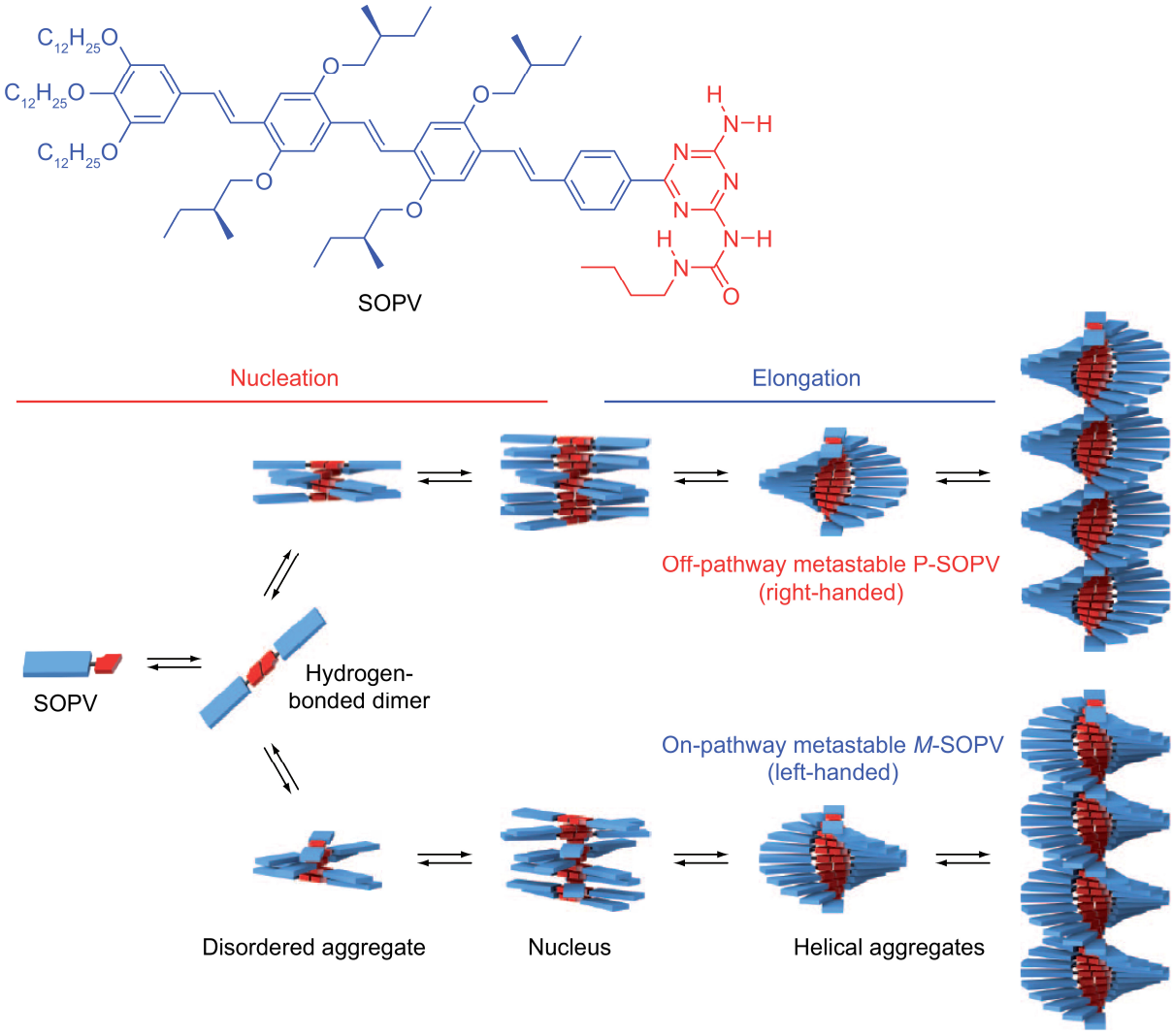

Figure 8. The two aggregation pathways of SOPV, including the growth of two competing assemblies. The righthanded P-helices form quickly but are less stable than the left-handed M-helices, which form more slowly. Reprinted by permission from Macmillan Publishers Ltd: Nature [198], copyright 2012.

The self-assembly of "SOPV" in apolar solutions is first initiated by formation of a quadruple hydrogen-bonded dimer which further self assembles into helical stacks via π-π interactions. The growth is described by a nucleation-elongation growth mechanism. The steady-state concentration of the aggregates is determined by two

different binding constants that is K_n for the nucleation phase and K_e for the elongation phase.[198]

Another well-known example of supramolecular polymers based on π-π interactions has been reported by Würthner et al.[123] The group synthesized perylene bisimides which form different types of aggregates that means H- and J-type aggregates, as shown in Figure 9.

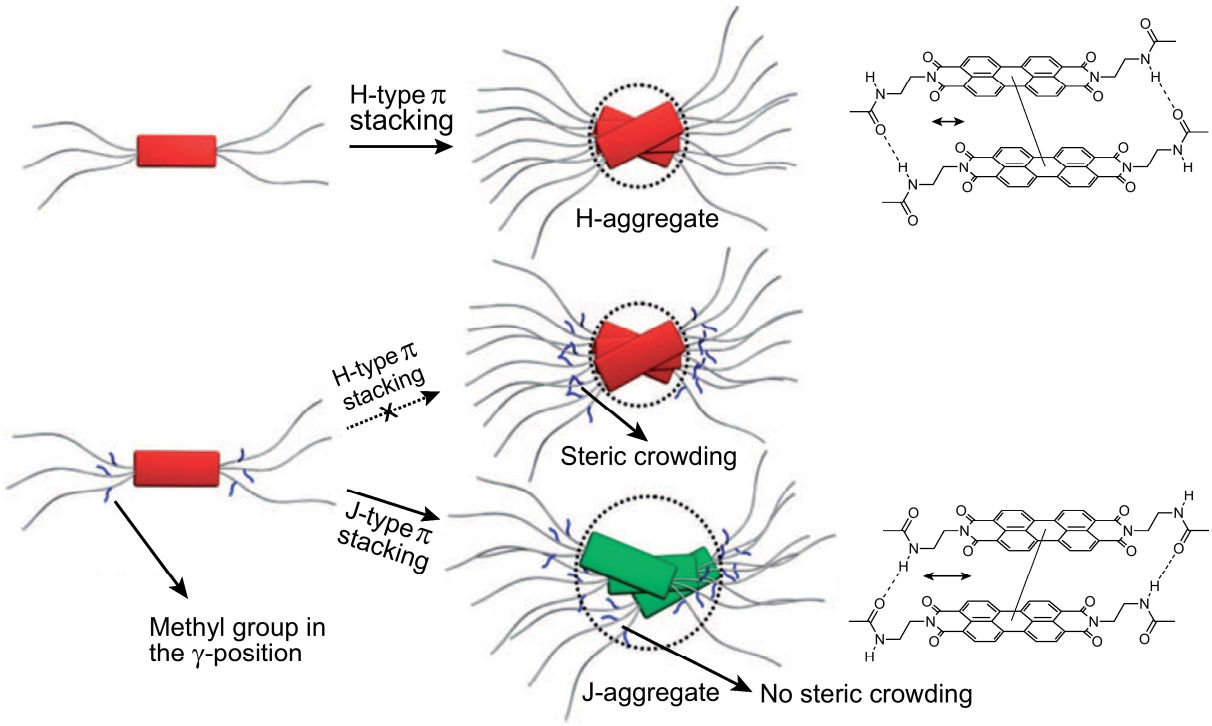

Figure 9. Left side: Perylene bisimide chromophores with linear (top) and branched (bottom) alkyl substituents. Middle: An increasing steric demand of the alkyl side-chains hinders the formation of H-aggregates and leads to J-aggregates. Right side: Packing model for H- (top) and J-type (bottom) π stacking. In both cases additional rotational offsets are needed to enable both close π-π contact and hydrogen bonding. Adapted with permission from ref [123]. Copyright 2008 John Wiley and Sons.

The type of aggregates depends on the steric demand of the side-chains. An increasing steric demand of the alkyl side-chains hinders the formation of H-aggregates and leads

to J-aggregates. The macroscopic orientation of the perylene bisimide aggregate orientation can be switched completely reversibly simply by switching a magnetic stirrer on and off.[123]

1.2.3.2 Metallo-supramolecular polymers

Metal containing polymers can be subdivided in three different types, as shown in Figure 10. In (a) metal ions or complexes are attached to the polymer at the side-chain, whereas in (b) the metal centers are part of the main-chain. In (c) metal ions are embedded into a polymer matrix via physical interactions.[199]

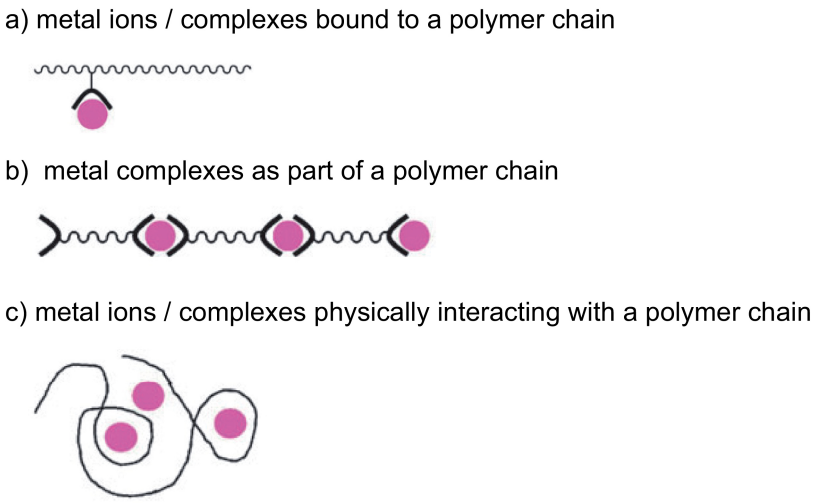

Figure 10. Overview of the general types of metal containing polymers. Reprinted in part from ref [200] with permission from The Royal Society of Chemistry.

Metallo-supramolecular polymers, which are a specific class of supramolecular polymers, are classified as structures where metal ions are part of the polymer chain

(see Figure 10b).[199] In this chapter the focus will be on metallo-supramolecular polymers built up by metal ions and organic ligand molecules.

1.2.3.2.1 Porphyrin and carbene based metallo-supramolecular polymers

Metalloporphyrins are known as building blocks for the design of metallo-supramolecular polymers. Here, the central metal ion coordinates to a planar framework and to additional ligands in an axial direction. As reported by Abd-El-Aziz et al.,[201] porphyrin containing coordination polymers can be formed to basically three different geometries as shown in Figure 11. In the most cases, nitrogen based ligands are used for the linkage of the porphyrin rings.[199, 201]

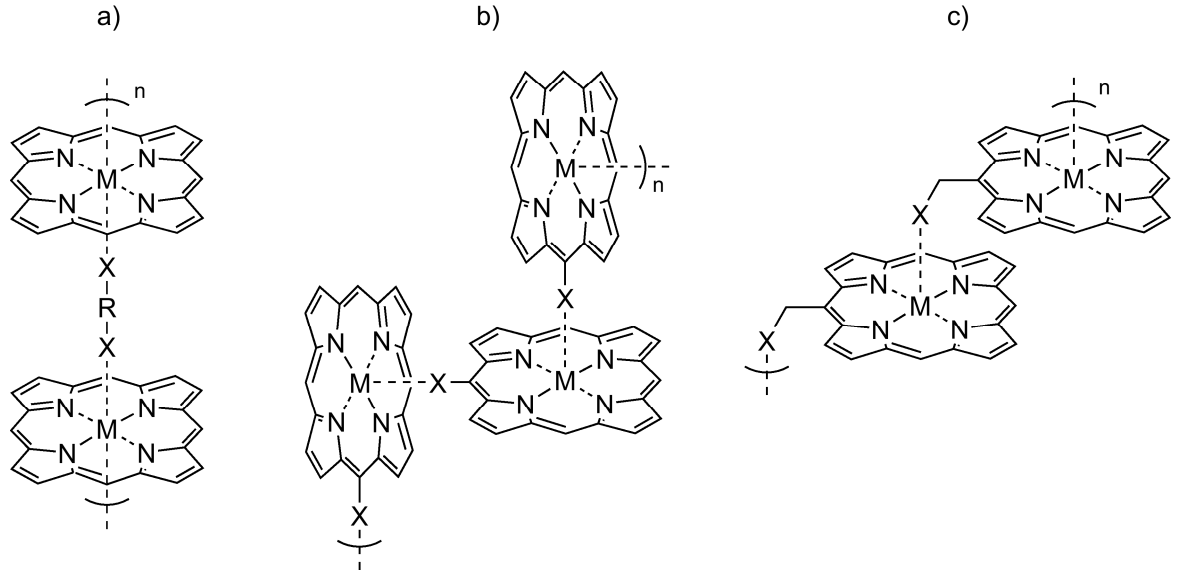

Figure 11. Three possible geometries of porphyrin containing coordination polymers. Adapted from ref [199] with permission from The Royal Society of Chemistry.

For example, Würthner et al.[202] reported the self-assembly of a Zn^{2+} containing porphyrin-(perylene bisimide)-porphyrin triad with different ditopic ligands as shown

in Scheme 11. Instead rectangular assemblies, the group obtained the formation of zig-zag-shaped polymers, presumably due to the bulkiness of the ligands.[199, 202]

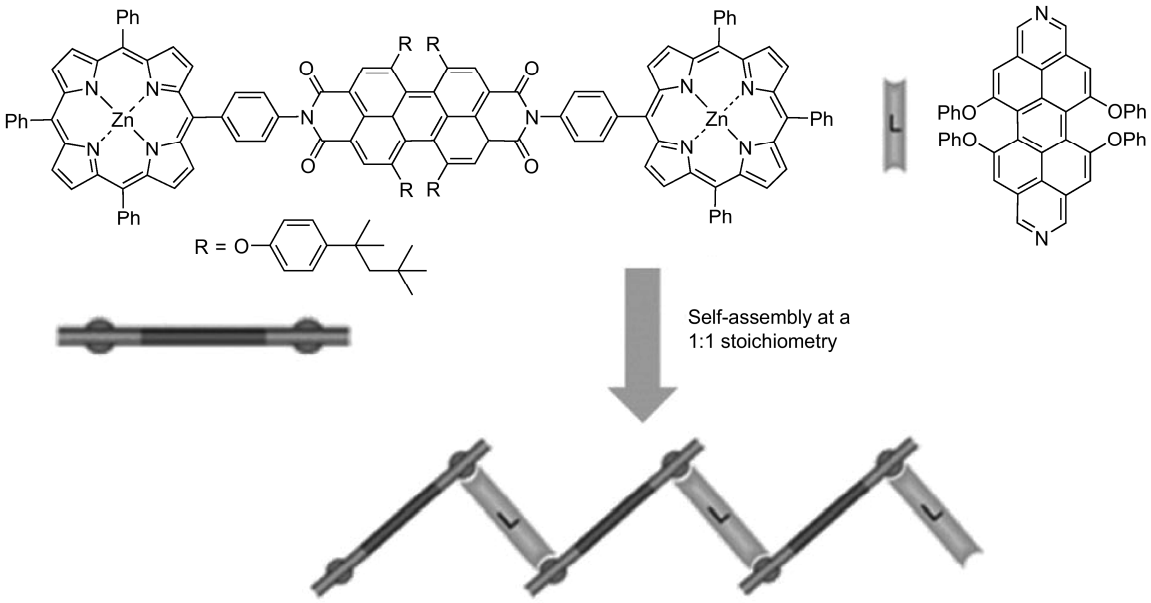

Scheme 11. Structure of a zig-zag-shaped metallo-supramolecular coordination polymer built up by zinc porphyrin-(perylene bisimide)-zinc porphyrin triads. Adapted from ref [199] with permission from The Royal Society of Chemistry.

Rigid bis-*N*-heterocyclic carbene derivatives can also be used for the construction of metallo-supramolecular polymers as shown in Figure 12. Stable metallopolymers incorporating these ligands and Pd^{2+} or Pt^{2+} ions are reported in the literature.[199, 203-208]

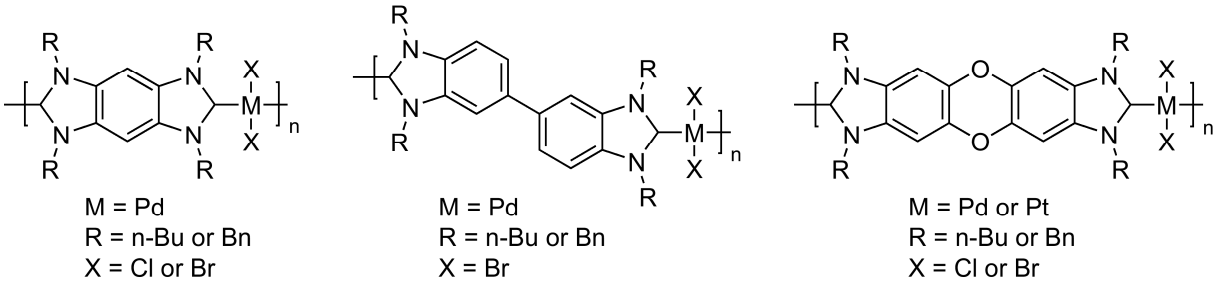

Figure 12. Schematic representation of metallopolymers containing telechelic *N*-heterocyclic carbene ligands. Adapted from ref [199] with permission from The Royal Society of Chemistry.

1.2.3.2.2 Metallocene based metallo-supramolecular polymers

Metallo-supramolecular polymers via metal-arene π-complexation are reported to form four different types of geometries (type A to D) as shown in Figure 13. Metallocene based metallo-supramolecular polymers of type A are reported mainly by Siebert et al.[209-213] For example, the polycondensation of substituted tris-(allyl)dinickel-(μ-2,3-dihydro-1,3-diborolyl) complexes yields the Ni^{2+}-containing "polydecker" complexes (see Figure 13, bottom, left).[209-213]

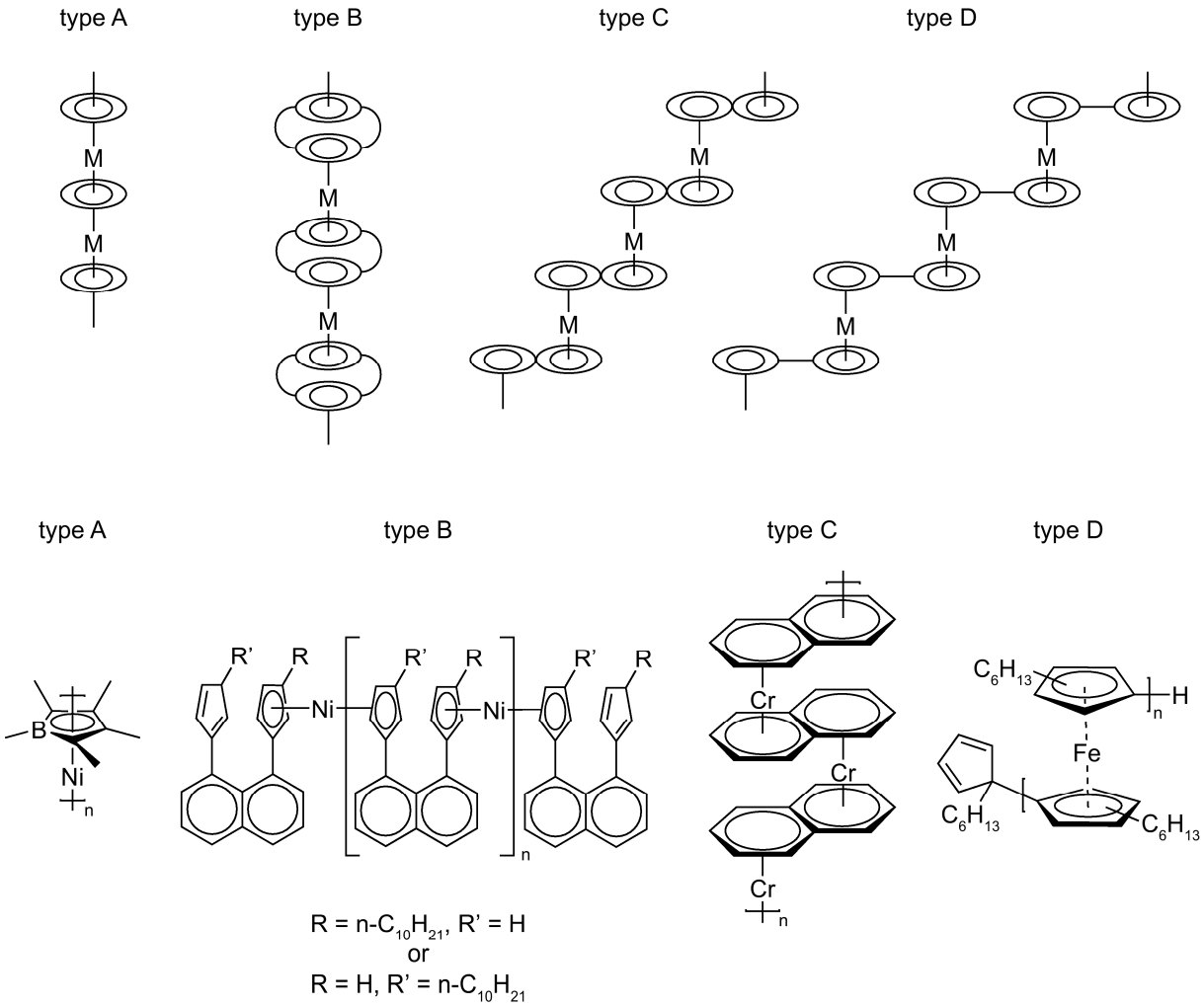

Figure 13. The four generally different types of metallocene based metallo-supramolecular polymers (top) and the corresponding examples (bottom). Adapted with permissions from [214] and [199] from The Royal Society of Chemistry and the American Chemical Society.

A variety of type-B polymeric metallocenes are investigated by Rosenblum et al.[214-218] Here, the metallocene units are ordered face-to-face with naphthalene or biphenyl as a spacer group (see Figure 13).[214-218] Metallocene based metallo-supramolecular polymers of type C are known from Lagowski et al.,[219] for example poly[μ-η^6,η^6-naphthalene)chromium].[219] Finally, The fulvalene dianion shown in Figure 13 (bottom, right) represents a building block that can already be used for the synthesis of polyferrocenylenes (type D).[199, 220]

1.2.3.2.3 Pyridine based metallo-supramolecular polymers

In the following, the focus is on pyridine based metallo-supramolecular polymers. For example, metallo-supramolecular polymers that are water-soluble at every metal ion to ligand ratio were presented by Cohen Stuart et al.[70] as they used flexible bifunctional ligands which differ in spacer length, coordinated to Zn^{2+} ions (see Scheme 12).[70]

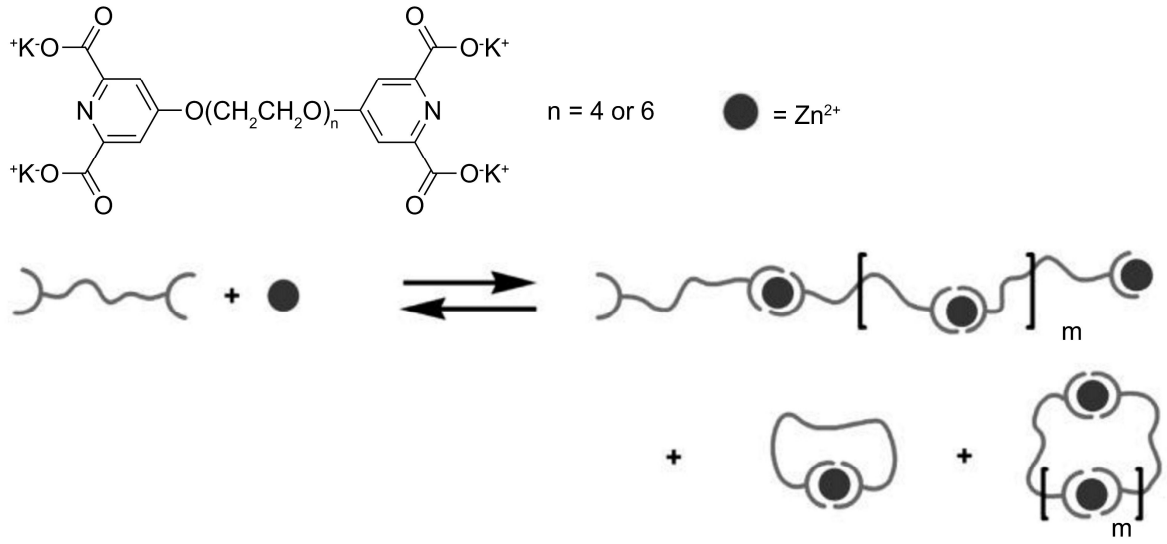

Scheme 12. Schematic representation of the water-soluble bifunctional ligands, and the formation of polymers and rings. Adapted with permission from [70]. Copyright 2003 American Chemical Society.

Since the used ligand is flexible, the formation of linear polymers and rings is obtained. The group followed the formation of the polymers as a function of the metal ion to ligand ratio, the total ligand concentration, and the temperature by viscosity measurements. Viscosity and ^{1}H NMR measurements confirm the reversibility of the coordination bonds and the formation of rings at low concentrations. If the metal ion to ligand ratio is 1:1, viscosity reaches a maximum. Furthermore, a model developed by Jacobson and Stockmayer[221] was used to calculate the molecular weight

distributions of chains and rings. The model is in qualitative agreement with the experimental results.[70]

The coordination properties of the tridentate ligand 2,2′:6′,2′′-terpyridine with metal salts was reported in 1992 by Constable et al.[73] The ditopic 2,2′:6′,2″-terpyridine ligands are ideal structural units, which form supramolecular polymers with a metal center by self-assembly (see Scheme 13). The ditopic "back-to-back" terpyridine ligands are used to assemble linear coordination polymers, including six-coordinated metal centers.[73]

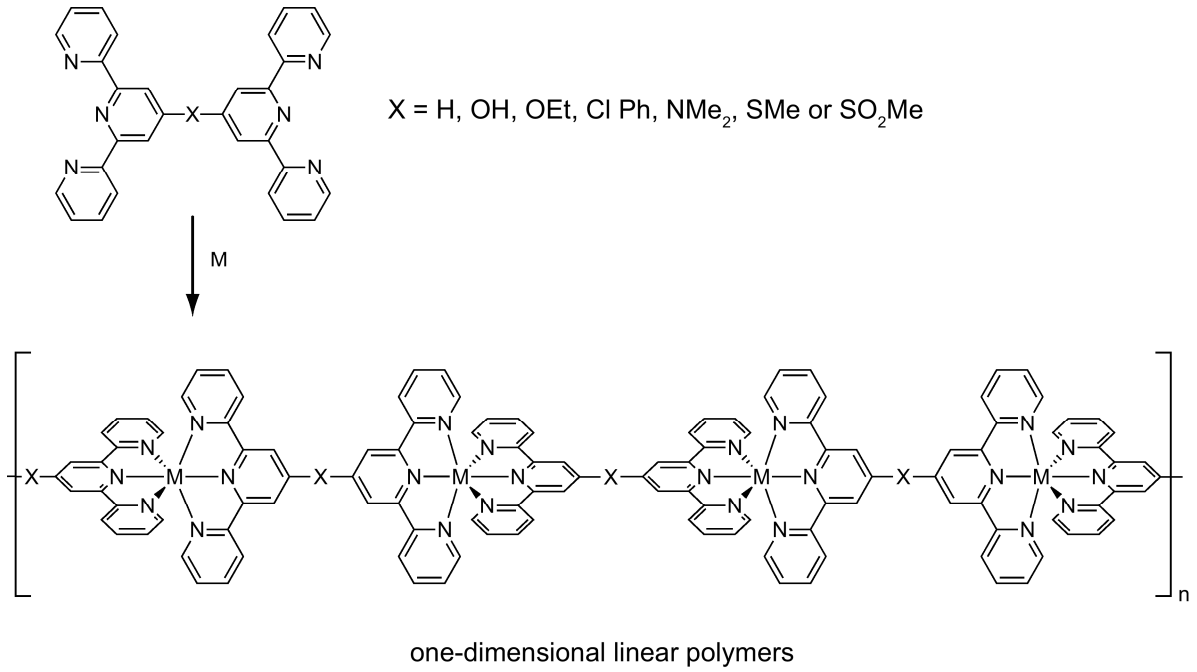

Scheme 13. The use of "back-to-back" 2,2′:6′,2″-terpyridine ligands to assemble coordination polymers or oligomers bearing specific terminator groups (X = spacer unit). Adapted from ref [73] with permission from The Royal Society of Chemistry.

Not surprisingly, an increasing denticity of (poly)pyridyl ligands leads to an increased complex stability due to the chelation effect as reported by Würthner et al.[222] For the single interaction of Zn^{2+} with a pyridine ligand a binding constant of 10^3 M^{-1} can be

found, whereas the binding constant increases to > 10^8 M^{-1} for the Zn^{2+}-terpyridine system.[199, 222]

Ditopic ligands carrying terpyridine units and their self-assembly with metal ions can also be used for the design of fluorescent supramolecular polymers as the same group[75] has reported in 2005. They used perylene bisimide fluorophores as a spacer group between two terpyridine moieties, as shown in Scheme 14.[75]

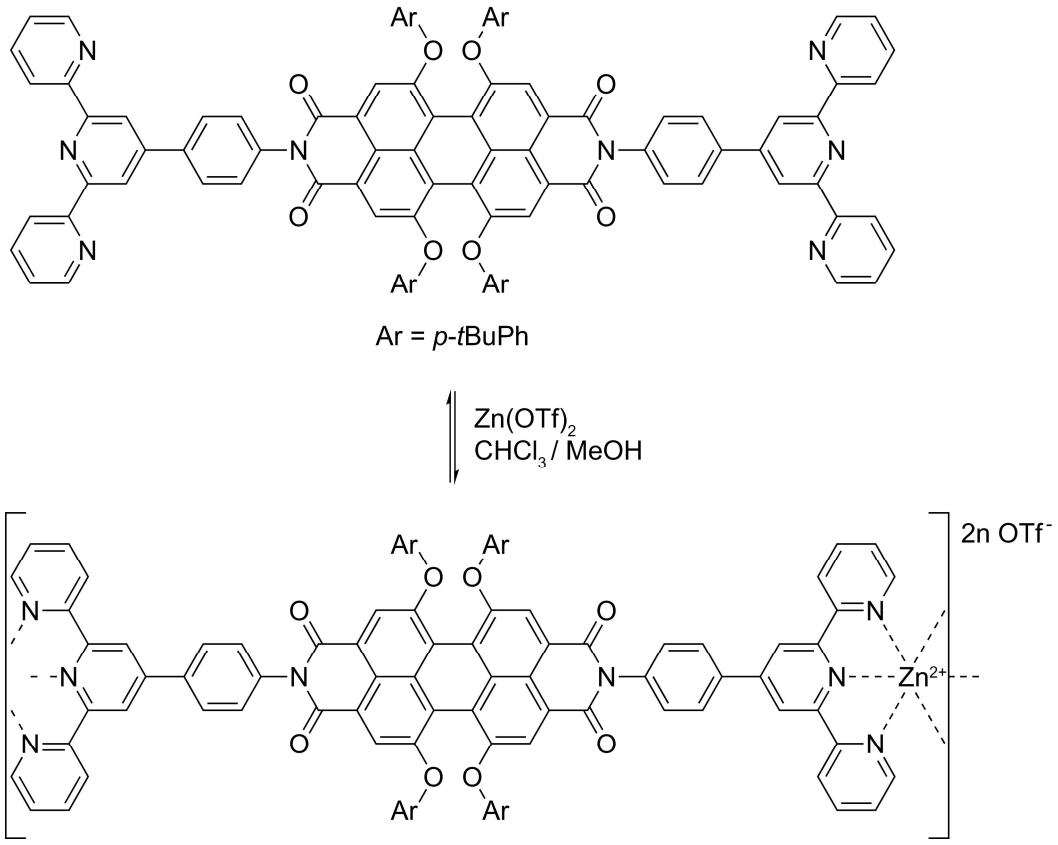

Scheme 14. Coordination of a terpyridine-functionalized perylene dye with $Zn(OTf)_2$ leads to the corresponding Zn-coordinated polymer. Adapted with permission from [75]. Copyright 2005 American Chemical Society.

The complexation of this ditopic terpyridine ligand with a series of first row transition metal ions that is Fe^{2+}, Co^{2+}, Ni^{2+}, Cu^{2+}, and Zn^{2+}, leads to fluorescing metallo-supramolecular dimers and polymers at room temperature. Diffusion ordered NMR

spectroscopy and fluorescence anisotropy measurements reveal that the terpyridine-Zn^{2+} complex is characterized by a thermodynamically stable (that means a high binding constant) yet kinetically labile (that is a fast ligand exchange) coordination bonding. For both dimer and polymer, reversible coordination was observed depending on the metal ion to ligand ratio. If the ratio exceeds 1:1, the chain-length of the supramolecular polymers is drastically decreased. Furthermore, the compounds obtain high fluorescence quantum yields.

Metal-coordination polymers also obtain potential for the development of self-healing materials, as the groups of Rowan[66, 71] and Schubert[101, 111] have shown. In 2011 Rowan et al.[66, 71] reported a healable metallo-supramolecular polymer based on a ligand containing poly(ethylene-*co*-butylene) core with 2,6-bis(1'-methylbenzimidazolyl)-pyridine ("Mebip"), complexed to Zn^{2+} that can be mended through exposure to light (see Scheme 15).[71]

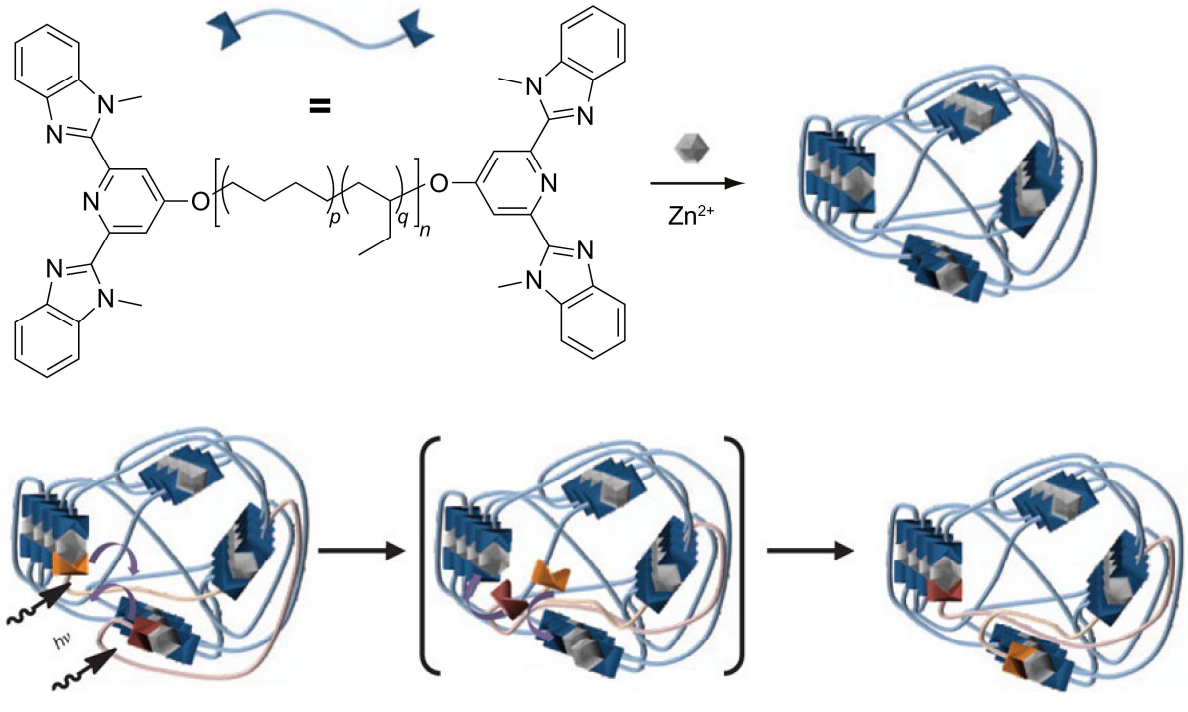

Scheme 15. Top: "Mebip"-ligand and its polymerization by addition of $Zn(NTf_2)_2$. Bottom: Proposed optical healing of the metallo-supramolecular network. Adapted by permission from Macmillan Publishers Ltd: Nature [71], copyright 2011.

On exposure to ultraviolet light, the metal-ligand motifs are electronically excited and the absorbed energy is converted into heat. This causes temporary disengagement of the metal-ligand motifs and a concomitant reversible decrease in the polymers' molar mass and viscosity,[74] thereby allowing quick and efficient defect healing. Light can be applied locally to a damaged site, so objects can in principle be healed under load. The formation of lamellar morphologies in which a hard phase comprising the metal-ligand complexes physically crosslinks soft domains of the poly(ethylene-cobutylene) cores is the main determinant for the thermomechanical characteristics of the materials studied. The data suggest that the dynamics of the light-induced depolymerization and, thereby, the healing behavior are governed by the presence of an excess of free ligands and the nature of the metal-ligand bond. The group assumes that the concept

of photothermally induced healing of supramolecular materials should be applicable to any supramolecular polymer with a binding motif that is sufficiently dynamic. They anticipate that this approach to healable materials, based on supramolecular polymers and a light-heat conversion step, can be applied to a wide range of supramolecular materials that use different chemistries.[71]

Another self-healing metallo-supramolecular polymer system was reported by Schubert et al.[101, 111] in 2013. Polymer coatings based on crosslinked metallo-supramolecular polymers were synthesized containing the metal-ligand coordination in the side-chain of flexible alkyl methacrylate polymers, as shown in Scheme 16.[101]

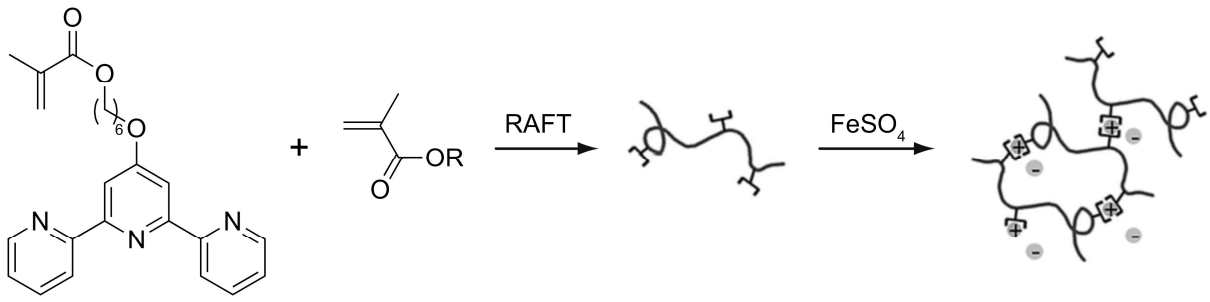

R = CH_3, C_4H_9 or $C_{12}H_{25}$

Scheme 16. Schematic representation of the synthesis of the Fe^{2+} crosslinked polymer network by reversible addition-fragmentation chain transfer (RAFT) polymerization technique and a following complexation with the metal ion. Adapted with permission from ref [101]. Copyright 2013 John Wiley and Sons.

First, the terpyridine containing polymers are received from copolymerization of a terpyridine with alkyl methacrylate monomers, in order to adjust the amount of the crosslinking units as well as to tune the thermal and mechanical properties of the resulting polymer networks. The reversible addition-fragmentation chain transfer (RAFT) polymerization technique is used to obtain well defined polymers with

adjustable composition.[80] Subsequently, the terpyridine containing copolymers are crosslinked by the addition of iron(II)sulfate, as shown in Scheme 16. The copolymer network containing lauryl methacrylate is able to heal scratches which the group ascribes to the high flexibility of the polymer backbone. In all cases, the crosslinked copolymer networks did not melt during the healing process. As no residual solvent is present, the formation of an organogel can also be excluded. Therefore, the above described healing is based on an intrinsic self-healing capability of the materials.[101]

In conclusion, the field of metallo-supramolecular polymers offers many attractive possibilities in varying metal ions and ligands. But so far, the details of the kinetics of the growth of the presented metallo-supramolecular polymers are mostly unknown. Thus, it is important to understand the underlying polymerization mechanisms in detail. The following subchapter gives an overview of polymerization mechanisms in general and the different possible polymerization mechanisms in supramolecular polymerization.

1.2.3.2.4 Metallo-supramolecular polyelectrolytes (MEPEs) studied in this thesis

1.2.3.2.4.1 Applications

In 2007 and 2008 Kurth et al.[50-51] reported the photophysical, electrochemical and electrochromic properties of MEPEs. Different types of MEPEs were assembled from different bisterpyridine ligands and investigated in terms of their electrochromic properties. By self-assembly of rigid, π-conjugated ditopic terpyridine ligands to Fe^{2+}, Ru^{2+}, and Co^{2+}, metallo-supramolecular polyelectrolytes form in solution, as shown in Scheme 17.[50-51]

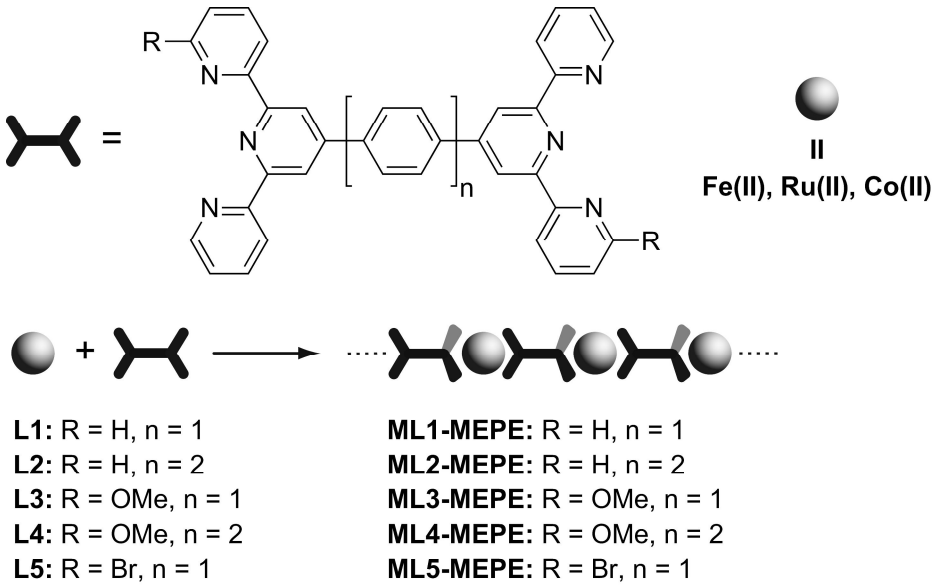

L1: R = H, n = 1
L2: R = H, n = 2
L3: R = OMe, n = 1
L4: R = OMe, n = 2
L5: R = Br, n = 1

ML1-MEPE: R = H, n = 1
ML2-MEPE: R = H, n = 2
ML3-MEPE: R = OMe, n = 1
ML4-MEPE: R = OMe, n = 2
ML5-MEPE: R = Br, n = 1

Scheme 17. Structures of different ditopic terpyridine ligands and the corresponding MEPEs, where electrochromic properties can be demonstrated. **M** indicates the metal ions Fe^{2+}, Ru^{2+}, and Co^{2+}, **L** represents the ligands, and MEPE stands for metallo-supramolecular coordination polyelectrolytes. Adapted with permission from and [51]. Copyright 2008 American Chemical Society.

By dissolving the MEPEs in a mixture of MeOH and H_2O, the different polymers display different colors spanning the entire visible regions, as shown in Figure 14.[50-51]

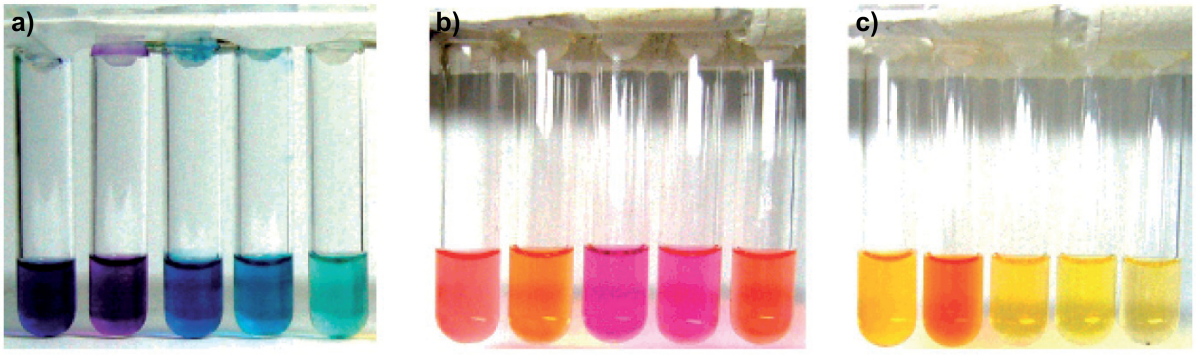

Figure 14. Colors of (a) **FeL1-MEPE** - **FeL5-MEPE** (0.25 mM, MeOH), (b) **RuL1-MEPE** - **RuL5-MEPE** (0.05 mM, MeOH/H_2O (v/v = 4/1)) (B), and (c) **CoL1-MEPE** - **CoL5-MEPE** (0.5 mM, MeOH). Adapted with permission from and [51]. Copyright 2008 American Chemical Society.

Kurth et al.[50-51] have shown that the electrochromic properties of the MEPEs are affected by the nature of the substituents at the peripheral pyridine rings that is "R" in Scheme 17. The response times can be tuned by the design of the ligands that means by variation of the spacer unit between the terpyridine units and by variation of the substituents at the peripheral pyridine rings, which makes the MEPEs attractive as electrochromic materials.[50-51]

Also the properties of electrorheological fluids (ERFs) based on Fe-MEPE-silicate composites were reported from Kurth et al.[91, 168] The ERFs are designed by usage of self-assembled Fe-MEPE and the corresponding mononuclear complexes, as shown in Figure 15.

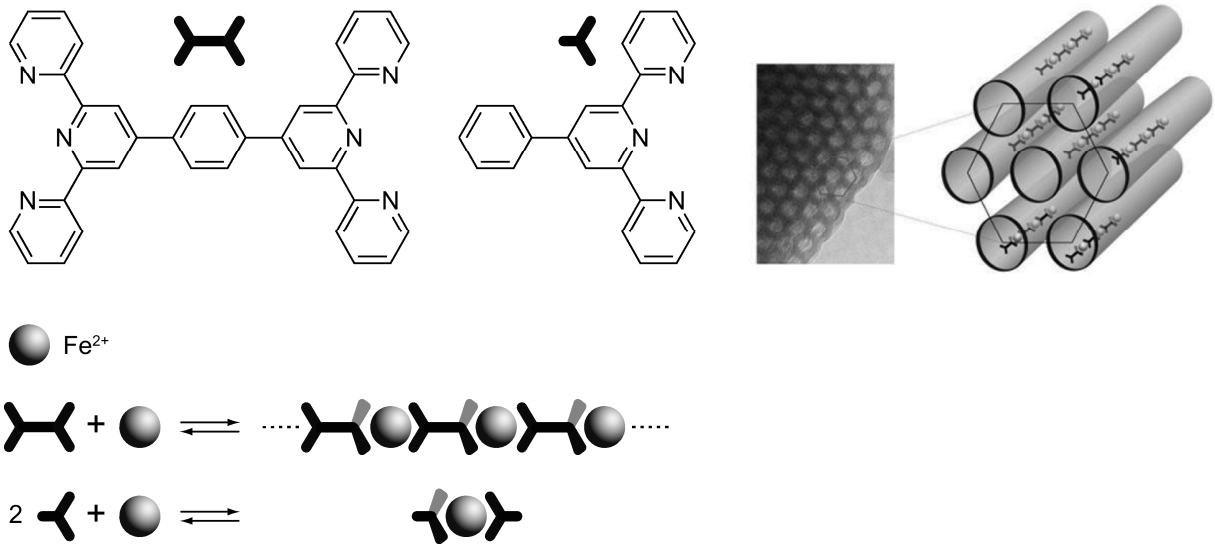

Figure 15. Top left: Fe-MEPE and the corresponding mononuclear complex are based on Fe^{2+} and ligands **1** or **2**, respectively. Bottom: Scheme of the self-assembly process. The counterions are omitted for clarity. Top right: TEM image of a SBA-15 particle edge revealing the hexagonal orientated mesopores and schematic illustration of MEPEs incorporated in the pores. Adapted with permission from [168]. Copyright 2013 American Chemical Society.

For this purpose, Fe-MEPE was incorporated in mesoporous SBA-15 silica resulting to a 10 wt % Fe-MEPE/SBA-15 composite. Dispersion of the composite in silicone oil leads to a fluid obtaining a strong electrorheological effect, even at low concentration of the active component (0.16 wt %).[168, 223-226]

MEPEs can also be used for the synthesis of metallo-supramolecular polyelectrolyte-amphiphile complexes. The self-assembly of an aqueous solution of MEPE with a chloroform solution containing long-chain dialkyl-phosphoric acid esters leads to polyelectrolyte-amphiphile complexes (PACs) via electrostatic interactions, as shown in Scheme 18. This leads to an architecture, where the polymers are embedded in between the amphiphile layers.[76, 90, 92, 103, 151]

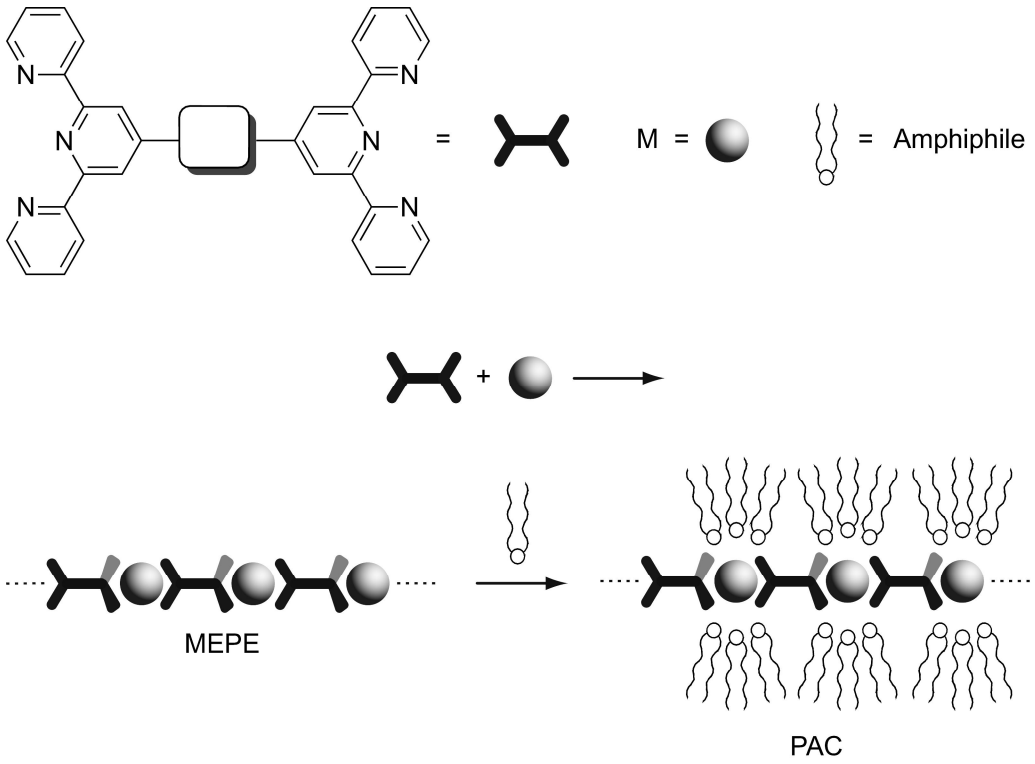

Scheme 18. Self-assembly of metal ions and ditopic bis-terpyridine ligands in aqueous solutions results in a positively charged metallo-supramolecular coordination polyelectrolyte (MEPE). Due to the octahedral coordination geometry a one-dimensional, positively charged macromolecule is formed. The square connecting the two terpyridine groups indicates a suitable spacer or functional component. Sequential self-assembly of MEPE and amphiphile gives a polyelectrolyte-amphiphile complex (PAC). The solubility properties of PAC suggest that the amphiphiles are primarily located around the hydrophilic metal-ion centers, as depicted in the scheme. The amphiphiles presumably form a charged hydrogen-bonded network that binds to MEPE through electrostatic interactions. Adapted with permission from ref [103]. Copyright 2002 John Wiley and Sons.

The electrostatic interactions result from the positive charged MEPEs with the negative charged head groups of the amphiphiles, where six amphiphiles bind per MEPE repeat unit. The polar metal-ion coordination centers are efficiently shielded by the amphiphiles, which leads to a hydrophobic nature of the PAC and solubility in common apolar organic solvents.[76, 90, 92, 103, 151]

PACs obtain liquid-crystalline properties: upon heating above room temperature, the systems show a spin-crossover (SCO) process. PACs based on Fe-MEPE embedded between alkyl phosphate layers exhibit a structure induced and partially reversible spin-crossover between diamagnetic low-spin and paramagnetic high-spin state (see Scheme 19). The change in the spin state modifies not only the magnetic state but the optical properties of the complex as well.[76, 92]

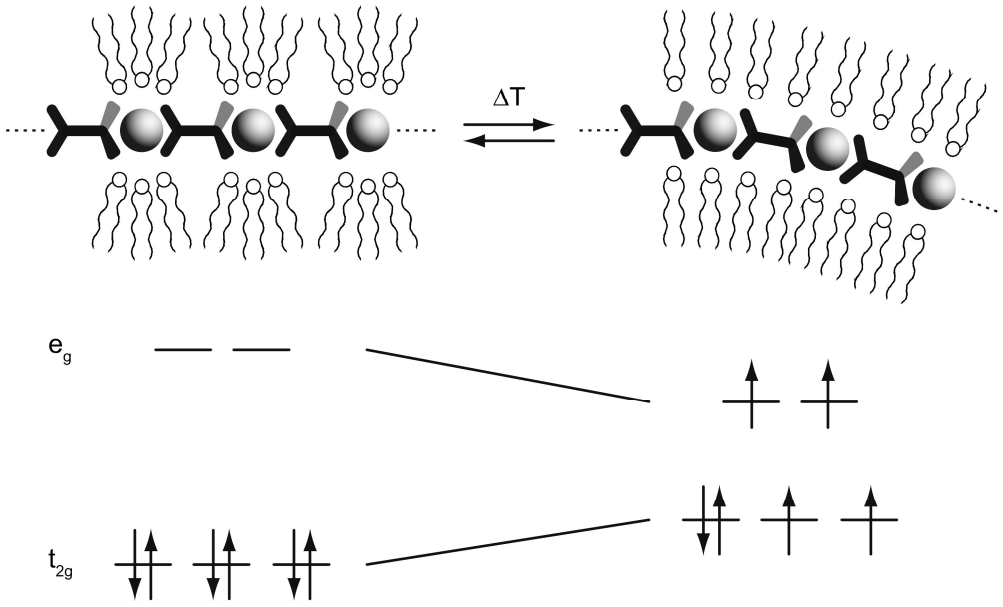

Scheme 19. Upon heating of the multilayer, the alkyl chains of the mesophase melt, resulting in a distortion of the metal ion coordination geometry. The unfavorable coordination of the terpyridines around Fe^{2+} results in a lowering of the energy gap between the d-orbital subset, giving rise to a reversible transition from a diamagnetic low-spin state to a paramagnetic high-spin state. Adapted with permission from ref [76]. Copyright 2008 Elsevier.

1.2.3.2.4.2 Modeling the chain-length of MEPEs

The chain-length of MEPEs is affected by the metal ion to ligand ratio, y:

$$y = \frac{[\mathrm{M}]_0}{[\mathrm{L}]_0} \tag{5}$$

with $[M]_0$ being the initial concentration of metal ions, and $[L]_0$ the initial concentration of the ligands (see also Scheme 3). Close to y = 1, small changes in this ratio affects the conductivity, chain-length and viscosity deviations of the final MEPE solutions as reported by Dormidontova et al.[72] and Kurth et al.[84, 227] The impact of a change in y can be illustrated by calculating the number average degree of polymerization, $\bar{X}_n$, if the metal ion to ligand ratio, $y < 1$:[88, 228]

$$\bar{X}_n = \frac{1 + y}{1 - y} \tag{6}$$

or if the metal ion to ligand ratio, $y > 1$:

$$\bar{X}_n = \frac{1 + y^{-1}}{1 - y^{-1}} \tag{7}$$

with the assumption that the extent of reaction is 100%.[228] For example, y = 0.99 ± 0.005 results in $\bar{X}_n$ = 266 ± 134, which is an inacceptable error in adjusting a desired chain-length.[88] Using the law of mass action, the average number of repeat units per chain, $\langle\bar{n}\rangle$, can be calculated. For this purpose, the coordination of ligand **1** to the metal ion, M^{2+}, is described by a set of chemical equilibria. In the following, several equilibrium constants are defined, with [M] being the concentration of the transition metal ions, M^{2+}, and [tpy] being the concentration of the terpyridine receptors. The binding constants for the formation of $[M(tpy)]^{2+}$ and $[M(tpy)_2]^{2+}$ as well as for the formation of protonated terpyridine groups, $[H(tpy)]^{+}$, $[H_2(tpy)]^{2+}$, or $[H_3(tpy)]^{3+}$ in acidic solution are defined in the following. The charges are omitted for clarity. Here,

K_1 and K_2 are the equilibrium constants for the formation of the metal-ligand complexes:

$$K_1 = \frac{[\mathrm{M(tpy)}]}{[\mathrm{M}] \cdot [\mathrm{tpy}]} \tag{8}$$

$$K_2 = \frac{[\mathrm{M(tpy)_2}]}{[\mathrm{M(tpy)}] \cdot [\mathrm{tpy}]} \tag{9}$$

The acid dissociation constants, $K_{H^+,x}$, of $[H_x(tpy)]^{x+}$ are defined as

$$\left(K_{H^+,1}\right)^{-1} = \frac{[\mathrm{H(tpy)}]}{[\mathrm{tpy}] \cdot [\mathrm{H^+}]} \tag{10}$$

$$\left(K_{H^+,2}\right)^{-1} = \frac{[\mathrm{H_2(tpy)}]}{[\mathrm{H(tpy)}] \cdot [\mathrm{H^+}]} \tag{11}$$

$$\left(K_{H^+,3}\right)^{-1} = \frac{[\mathrm{H_3(tpy)}]}{[\mathrm{H_2(tpy)}] \cdot [\mathrm{H^+}]} \tag{12}$$

With the initial concentration of the terpyridine receptors, $[tpy]_0$, it follows:

$$\begin{aligned}[\mathrm{tpy}] + [\mathrm{M(tpy)}] + [\mathrm{M(tpy)_2}] + [\mathrm{H(tpy)}] + [\mathrm{H_2(tpy)}] + [\mathrm{H_3(tpy)}] \\ = [\mathrm{tpy}]_0 = 2 \cdot [\mathrm{L}]_0\end{aligned} \tag{13}$$

And with the initial concentration of metal ions, $[M]_0$, one arrives at:

$$[\mathrm{M}]_0 = [\mathrm{M}] + [\mathrm{M(tpy)}] + [\mathrm{M(tpy)_2}] \tag{14}$$

With $[M(tpy)_2]^{2+}$ representing the concentration of $[M(tpy)_2]^{2+}$ units in the MEPE chain and [tpy], $[M(tpy)]^{2+}$, $[H(tpy)]^{+}$, $[H_2(tpy)]^{2+}$, and $[H_3(tpy)]^{3+}$ being end groups, the average number of MEPE repeat units, $[ML]^{2+}$, per chain, $\langle\overline{n}\rangle$, can be described as

$$\langle\bar{n}\rangle = 2 \cdot \frac{[\mathrm{M(tpy)_2}]}{[\mathrm{tpy}] + [\mathrm{M(tpy)}] + [\mathrm{H(tpy)}] + [\mathrm{H_2(tpy)}] + [\mathrm{H_3(tpy)}]} \tag{15}$$

Equations (8) to (15) are solved by Mathematica providing a numerical approximated solution, with $pK_{H^+,1}$= 1.7, $pK_{H^+,2}$ = 3.5, $pK_{H^+,3}$ = 4.7,[229] and $[M]_0$ = 6.7 × 10^{-3} M. The calculated average number of repeat units per chain, $\langle\bar{n}\rangle$, that is the polymer length, is shown in Figure 16.

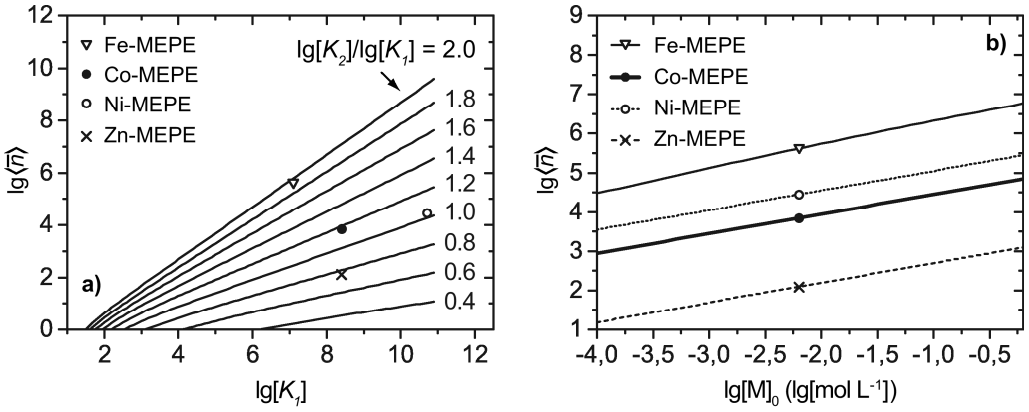

Figure 16. Average number of repeat units per chain, $\langle\bar{n}\rangle$, as function of (a) K_1 and K_2, and (b) as a function of the initial concentration of M^{2+}. In (a) the parameters are set to $[L]_0$ = $[M]_0$ = 6.7 mM, pH = 7, and y = 1 with varying K_1 and K_2, whereas in (b) the parameters are set to pH = 7, y = 1, and K_1 and K_2 according to Table 1, while $[M]_0$ is varying. The average chain-length of MEPEs increases with increasing binding constant K_1 and with increasing ratio lg[K_2]/lg[K_1], as well as with increasing initial concentration $[M]_0$. In (a) the symbols correspond to the literature values of lg[K_2]/lg[K_1] (see also Table 1), whereas in (b) the symbols correspond to $lg[M]_0$ = -2.2 ($[M]_0$ = 6.7 mM). Adapted with permission from ref [188]. Copyright 2017 John Wiley and Sons.

Here, the repeat unit is defined as a ligand and a metal ion as shown in Scheme 3. Figure 16a shows the average number of repeat units as a function of binding constants K_1 and K_2. The chain-length increases with increasing K_1 and with increasing ratio lg[K_2]/lg[K_1]. Figure 16b shows the average number of MEPE repeat units per chain with increasing concentration, $[M]_0$. As expected, chain-length increases with increasing initial concentration of the metal ion, $[M]_0$. As can be seen in Figure 16a, lg$\langle\bar{n}\rangle$ amounts to 5.6, 3.9, 4.5 and 2.1 for Fe-, Co-, Ni- and Zn-MEPE, respectively, which corresponds

to number average molar masses of 2.8 × 10^8 g mol^{-1}, 5.7 × 10^6 g mol^{-1}, 2.3 × 10^7 g mol^{-1}, and 9.1 × 10^4 g mol^{-1}. Therefore, according to the theoretical predictions from Figure 16, the molar mass follows the order Zn-MEPE < Co-MEPE < Ni-MEPE < Fe-MEPE, if pH = 7 and y = 1. Protonation of the ligand competes with metal ion coordination. Using the law of mass action, the concentrations of M^{2+}, $[ML]^{2+}$, and $[ML_2]^{2+}$ can be calculated as a function of pH. The results are shown in Figure 17.

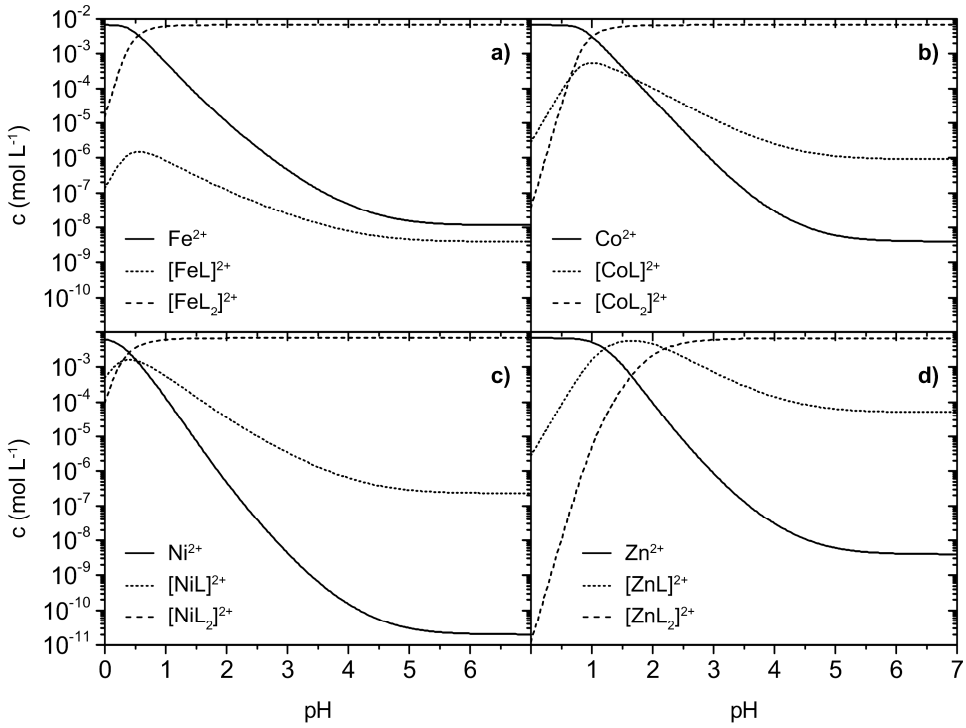

Figure 17. Concentrations of M^{2+}, $[ML]^{2+}$, and $[ML_2]^{2+}$ for (a) Fe^{2+}, (b) Co^{2+}, (c) Ni^{2+}, and (d) Zn^{2+}, respectively, as function of pH with given binding constants K_1 and K_2 according to Table 1. The initial ligand concentration $[L]_0$ is set to 6.7 mM with y = 1. The critical pH blocking the formation of chains rises from < 1.5 in the case of Fe^{2+}, Co^{2+}, and Ni^{2+} to 2.2 in the case of Zn^{2+}. Adapted with permission from ref [188]. Copyright 2017 John Wiley and Sons.

Interestingly, long chains form in solution above pH = 1, if the affinity of the ligand and the metal ions is high enough, e.g. Fe^{2+}, Co^{2+}, and Ni^{2+}. In order to analyze the chain-

length of the MEPEs, acetic acid solution (75 vol %) is the solvent of choice. If Zn^{2+} is used as a metal ion in acetic acid solution (75 vol %) with pH = 1.8, $[ZnL]^{2+}$ complexes predominate that means, no long chains form. Figure 18 shows the calculated average number of MEPE repeat units per chain, $\langle\overline{n}\rangle$, as function of the pH as well as of the metal ion to ligand ratio, y.

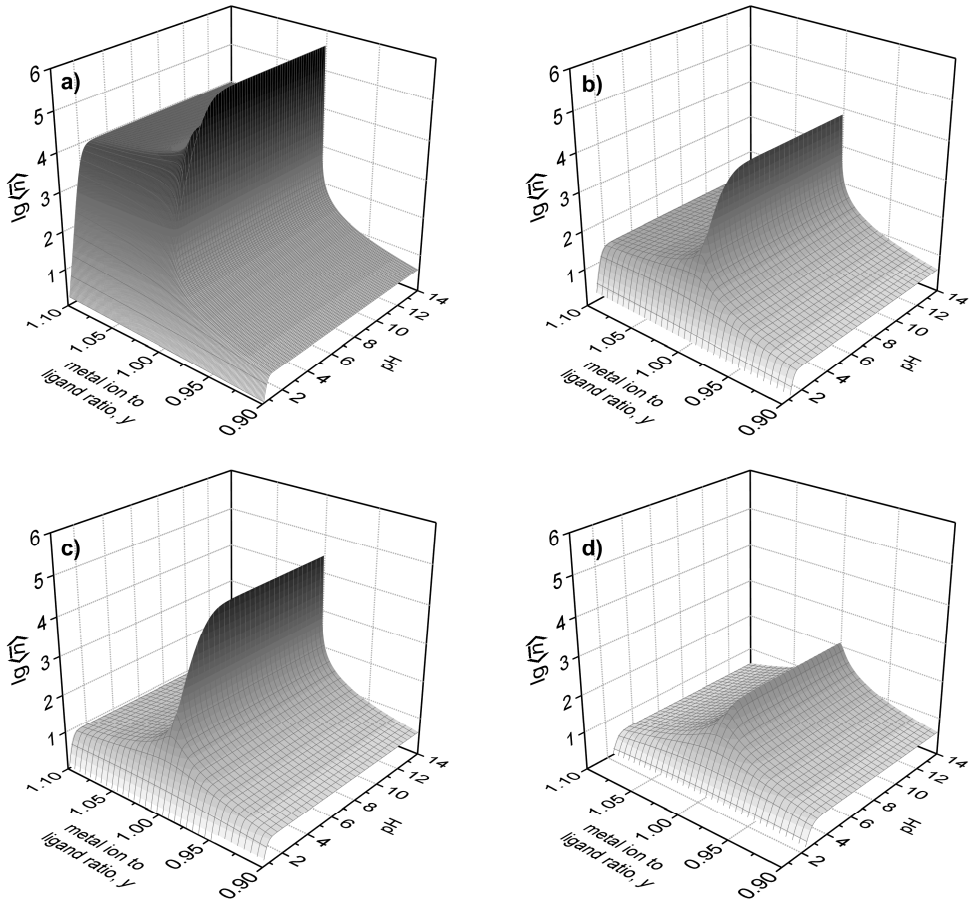

Figure 18. Average number of MEPE repeat units, [ML], per chain, $\langle\overline{n}\rangle$, as function of pH and metal ion to ligand ratio, y, with (a) Fe^{2+}, (b) Co^{2+}, (c) Ni^{2+}, and (d) Zn^{2+} as a metal ion. The initial ligand concentration $[M]_0$ is set to 6.7 mM. The chain-length reaches its maximum at y = 1.00. Adapted with permission from ref [188]. Copyright 2017 John Wiley and Sons.

The chain-length reaches its maximum at y = 1.00. In case of Fe^{2+}, $\lg[K_2]$ is around twice as high as $\lg[K_1]$ (see Table 1 in Chapter 1.2.2.2) and the maximum of $\lg\langle\overline{n}\rangle$ is > 10^5. The

chain-length is asymmetric with respect to y as shown in Figure 18a. In case of Co^{2+} and Ni^{2+} where the difference between K_1 and K_2 is smaller, the average number of repeat units is smaller compared to Fe-MEPE and the asymmetry with respect to y is negligible (Figure 18b and Figure 18c). However, coordination of **1** to Zn^{2+} leads to relatively short chains nearly unaffected by y, because $K_2 < K_1$ (Figure 18d). At pH = 1.8 as in acetic acid solution (75 vol %) and y = 1.00, $\lg\langle\bar{n}\rangle$ amounts to 2.5, 1.4, and 2.0 for Fe-, Co-, and Ni-MEPE, respectively, which corresponds to number average molar masses of 2.1 × 10^5 g mol^{-1}, 1.7 × 10^4 g mol^{-1}, and 7.7 × 10^4 g mol^{-1}. As already mentioned, complexation of Zn^{2+} to ligand **1** mainly leads to $[Zn\mathbf{1}]^{2+}$ complexes at these conditions.

These results are in agreement with Monte Carlo simulations presented by Dormidontova et al.[72] They have shown that the maximum degree of polymerization in metallo-supramolecular polymers occurs at the metal ion to ligand ratio of y = 1.00.[72] In case of the non-linear chain-length dependence in the proximity of y = 1.00, small changes in y cause large variations in chain-length, e.g. by experimental errors and impurities (see Figure 18).[72, 84, 227]

1.2.4 Ways to control supramolecular polymerization

The chain-length of polymers can be tuned by using chain stoppers. For supramolecular polymers this so-called “stopper experiment” was first reported by Meijer et al.[97, 100] The group designed supramolecular polymers based on quadruple hydrogen bonding and decreased the degree of polymerization and therefore the polymer's chain-length by usage of end-caps that can be formed by a photochemical process as shown in Scheme 20.

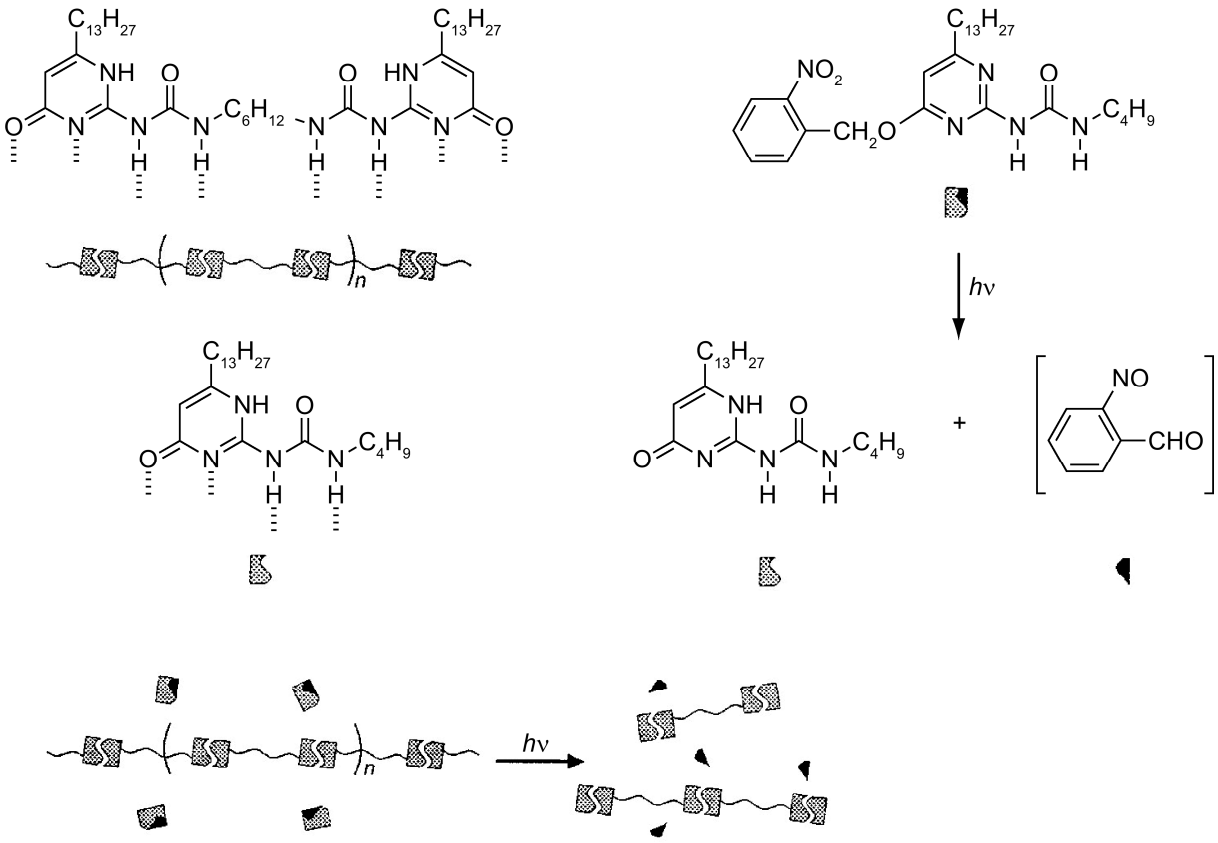

Scheme 20. Bifunctional compound (upper left), which forms supramolecular polymer chains, and monofunctional compound (upper right), which acts as an end-cap. Adapted from ref [97] with permission from The Royal Society of Chemistry.

Thus, they are able to trigger the viscosity of the solution by light.[97, 100] Chain stopper molecular systems were later applied to different other hydrogen bond based supramolecular polymers by Meijer,[95, 98] Lehn,[93] Cohen Stuart,[192-195] Bouteiller,[196] and Yagai.[197]

Besides hydrogen based supramolecular polymerizations, the polymerization of porphyrin based polymers can also be controlled by the usage of chain stoppers. For example, Hunter et al.[107] constructed porphyrin polymers by coordination of aminoporphyrins as shown in Scheme 21.[107]

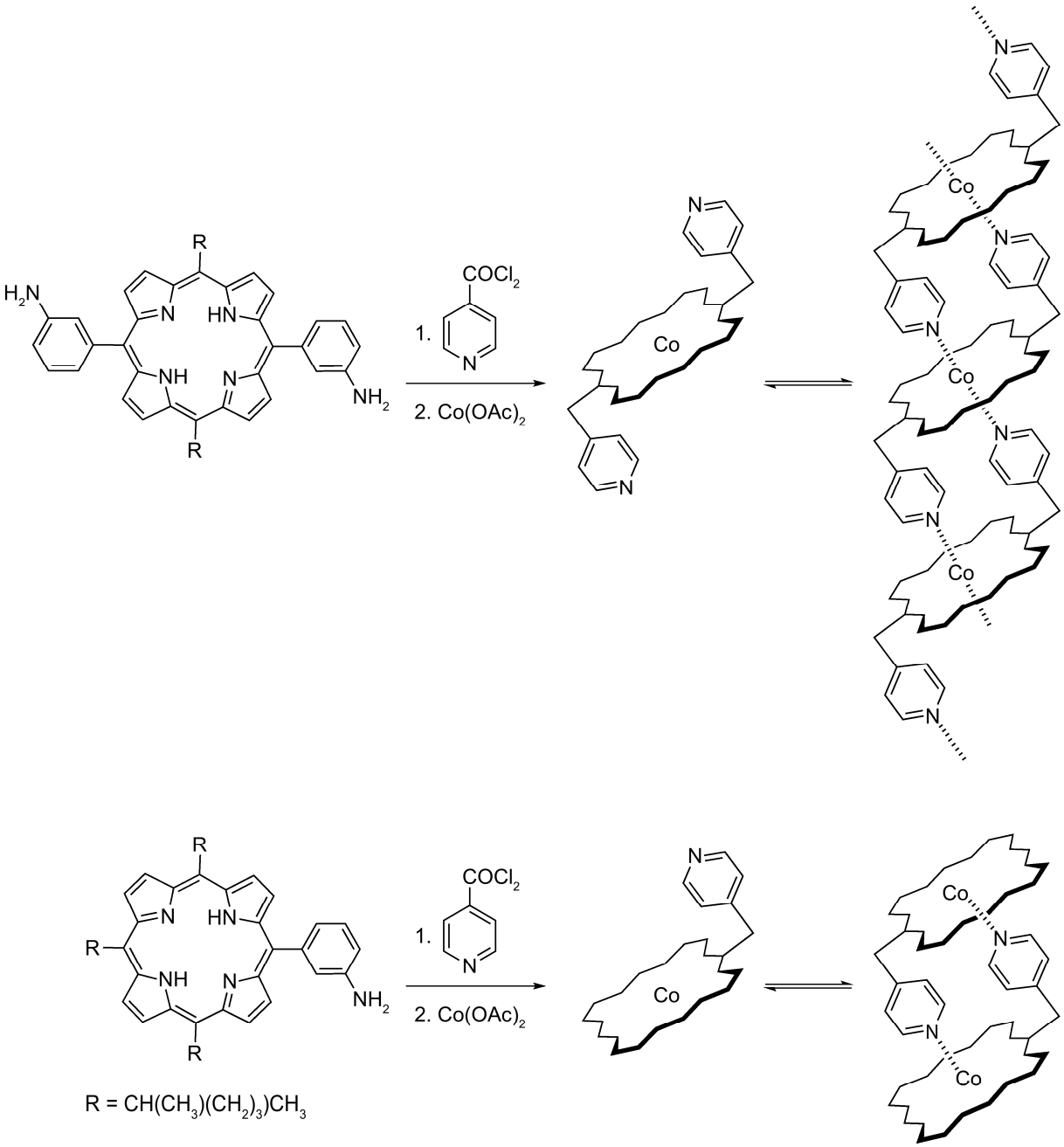

Scheme 21. Self-assembly of a cobalt porphyrin polymer (top) and a cobalt porphyrin dimer (bottom) via coordination of two covalently attached pyridine ligands. Both aminoporphyrins were prepared from the corresponding nitroporphyrins using 4-pyridinecarbonyl chloride and $Co(OAc)_2$. Adapted with permission from ref [107]. Copyright 2000 John Wiley and Sons.

Size exclusion chromatography (SEC) indicates the formation of stable, high molecular weight polymers. Here, the monofunctional cobalt porphyrin acts as a chain stopper,

which can be used to control the mean molecular weight of the cobalt porphyrin polymer.[107]

1.3 Mechanism

1.3.1 Polymerization mechanisms

Polymerization mechanisms can be distinguished in two classes: chain growth and step growth polymerizations (see Figure 19).

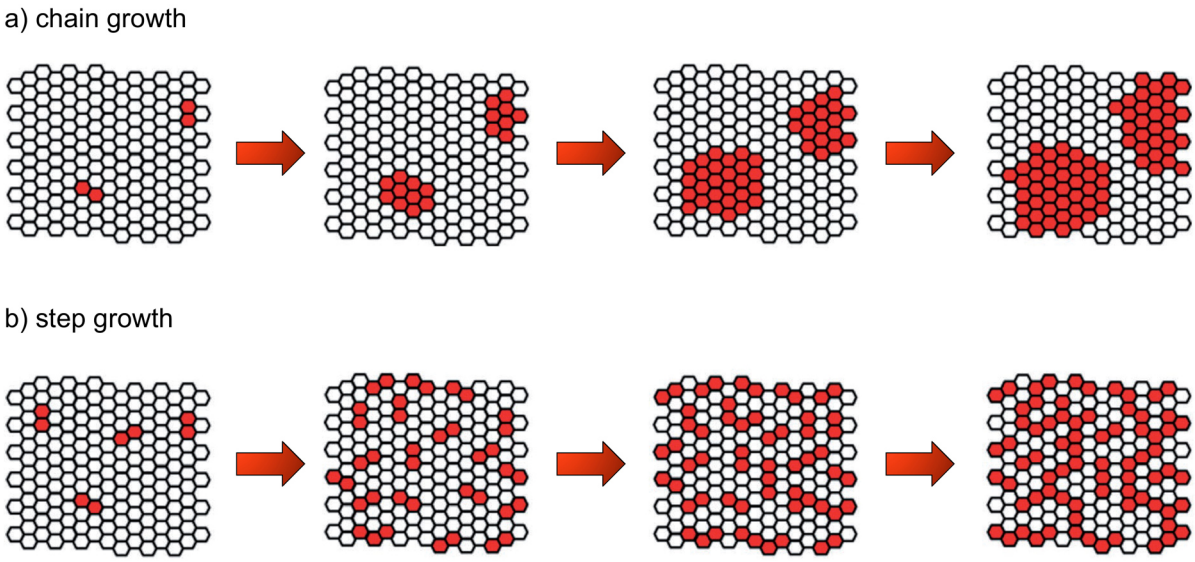

Figure 19. Step growth and chain growth mechanism in 2D array of monomers. White colored lattice sites represent the unreacted monomers while the red colors exhibit the polymerized sites. Adapted from ref [230] with permission from The Royal Society of Chemistry.

In chain growth polymerization an initiator is used to produce an initiator species, R^*, with a reactive center, which may be a free radical, cation, or anion. Polymerization takes place by addition of monomer molecules to the active site of a growing polymer chain and the addition of each monomer unit regenerates the active site as shown in

Figure 19a.[231] In contrast to step growth polymerization, the different-sized species such as dimer, trimer, tetramer, and n-mer do not react with each other. An example for a chain growth mechanism is the polymerization of vinyl monomers as shown in Scheme 22. The growth of the polymer chain ceases when the reactive center is deactivated by one or more of a number of possible termination reactions.[228, 232]

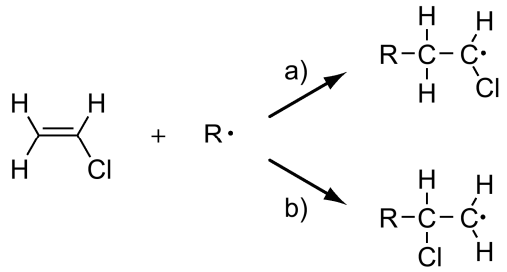

Scheme 22. Polymerization of vinyl monomers.[232]

Chain polymerizations without the ability of chain termination reactions are called "living polymerization".[228] For example, Szwarc et al. [233-234] reported the anionic living polymerization of styrene in THF. First, styrene is activated by an initiator. As shown in Scheme 23, the resulting anion leads to a situation where termination reactions cannot occur anymore. The terminal anions will stay at the ends of the polymer and polymerization proceeds until all monomers are integrated.[228, 233-234]

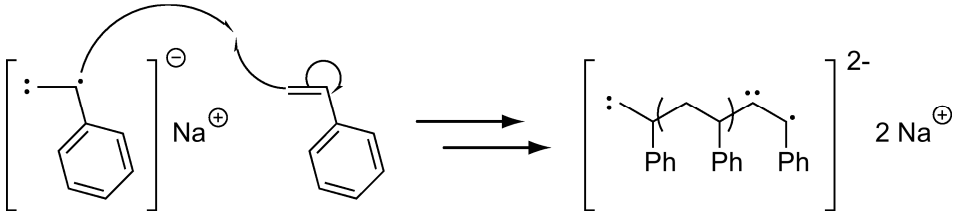

Scheme 23. Anionic living polymerization by activation of styrene in THF. The resulting anion hinders any termination reaction.[233-234]

Living polymerizations are a common method for synthesizing block copolymers since the polymer can be synthesized in different stages with different monomers.[228, 233-234]

The situation is different in step growth polymerizations which proceed from monomer to dimer, trimer, tetramer, pentamer, and so on until large-sized polymers have been formed as shown in Figure 19b. The reaction occurs between any of the different-sized oligomers present in the reaction system.[228] Step polymerizations are furthermore classified as "condensation polymerizations", if a small molecule, like water, is eliminated in the polymerization process. Common examples for a step growth polymerization are polyamides, which are built up by diamines and diacids by elimination of water[228, 235] or polycarbonates, which are formed by the reaction of aromatic dihydroxy reactants with phosgene by elimination of hydrogen chloride as shown in Scheme 24.[228, 236]

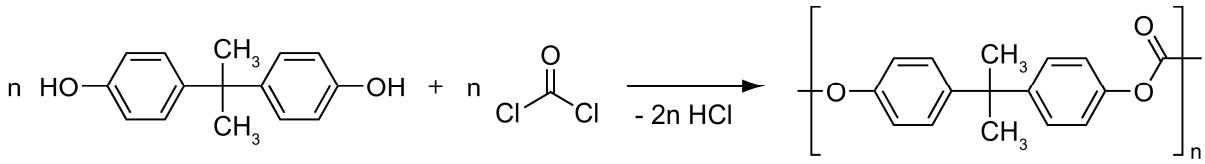

Scheme 24. The polycondensation of bisphenol A and phosgene leads to polycarbonate by elimination of hydrogen chloride.[236]

In contrast, "addition polymers" are classified by Carothers[237] as step growth polymers formed from monomers without loss of a small molecule. A well-known example for addition polymers are polyurethanes, which are formed by the reaction of diols with diisocyanate.[228, 238]

Generally, polymer growth of a linear step growth polymerization can be described as

$$\bar{X}_n = [\mathrm{A}]_0 kt + 1 = \frac{1}{1-p} \tag{16}$$

with $\bar{X}_n$ being the number-average degree of polymerization, $[\mathrm{A}]_0$ the concentration of monomers at the beginning of the polymerization, k the rate constant, t the time, and p the monomer conversion.[239] Carothers[240] established a connection of the weight-average degree of polymerization, $\bar{X}_w$, to the monomer conversion, p:

$$\bar{X}_w = \frac{1+p}{1-p} \tag{17}$$

with $\bar{X}_w$ being defined as

$$\bar{X}_w = \frac{\bar{M}_w}{M_m} \tag{18}$$

with $\bar{M}_w$ being the weight-average molar mass of the polymer, and M_m being the molar mass of the monomer, A. With eqs (16) and (17) the weight-average degree of polymerization, $\bar{X}_w$, can be described as a function of time:

$$\bar{X}_w = 2[\mathrm{A}]_0 kt + 1 \tag{19}$$

With $\bar{X}_w$ at hand, the monomer conversion, p, can be calculated by rearranging eq (17):

$$p = \frac{\bar{X}_w - 1}{\bar{X}_w + 1} \tag{20}$$

By usage of eqs (19) and (20) the monomer conversion, p, at a time, t, can be calculated if the rate constant k is known.[239]

1.3.2 Growth mechanisms in supramolecular polymerization

In the field of supramolecular polymerization, three major models are distinguished in literature: In the so-called "isodesmic supramolecular polymerization" (ISP), also known as the "equal K model", "free association model" or "multistage open association

model", each additional step is equivalent and independent of the polymer length as shown in Scheme 25a.

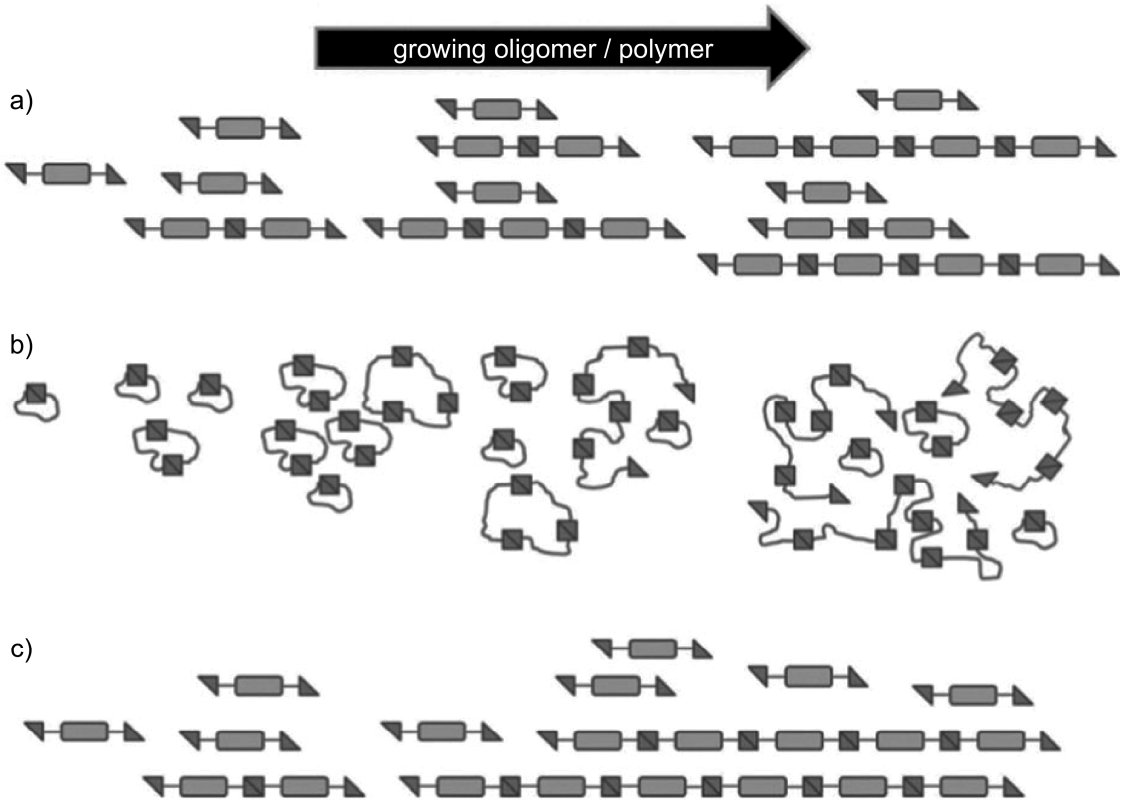

Scheme 25. Schematic representation of the three mechanisms for supramolecular polymerization mechanisms: (a) isodesmic supramolecular polymerization (ISP), (b) ring-chain mediated supramolecular polymerization and (c) cooperative supramolecular polymerization (CSP). Adapted from ref [199] with permission from The Royal Society of Chemistry.

That means, that all reactive sites of the monomers, oligomers and polymer chains have the same reactivity and every step during polymerization exhibits the same equilibrium constant. In isodesmic growth polymerizations, no critical temperature or concentration of the monomers is required for the polymerization to occur.[199, 228]

The second polymerization mechanism occurs if oligomers can also react to closed rings of polymers, as shown in Scheme 25b. If the monomer concentration is below a

critical concentration, the ends of small oligomers are more likely to undergo an intramolecular reaction and form a polymer ring. Above a specific critical concentration, the probability of intermolecular reactions is increased, which leads to the growth of long polymer chains.[143, 188, 241-246] In ring-chain mediated supramolecular polymerization two equilibrium constants can be defined: one for the intra- and one for the intermolecular reaction. The so-called "effective molarity" is then defined as[143, 199]

$$\mathrm{EM} = \frac{K_{\mathrm{intra}}}{K_{\mathrm{inter}}} \tag{21}$$

If EM > 1 cyclization if favored, whereas linear chains are formed if EM < 1.[199, 228] Ring-chain mediated supramolecular polymerizations are reported in the literature.[227, 247-252] For example, Newkome et al.[250] reported the formation of linear ([methylphenylenebis(terpyridine)]$_n$Ru$^{2+}{}_{n-1}$) complexes and macrocycles by a single-pot reaction as shown in Scheme 26.

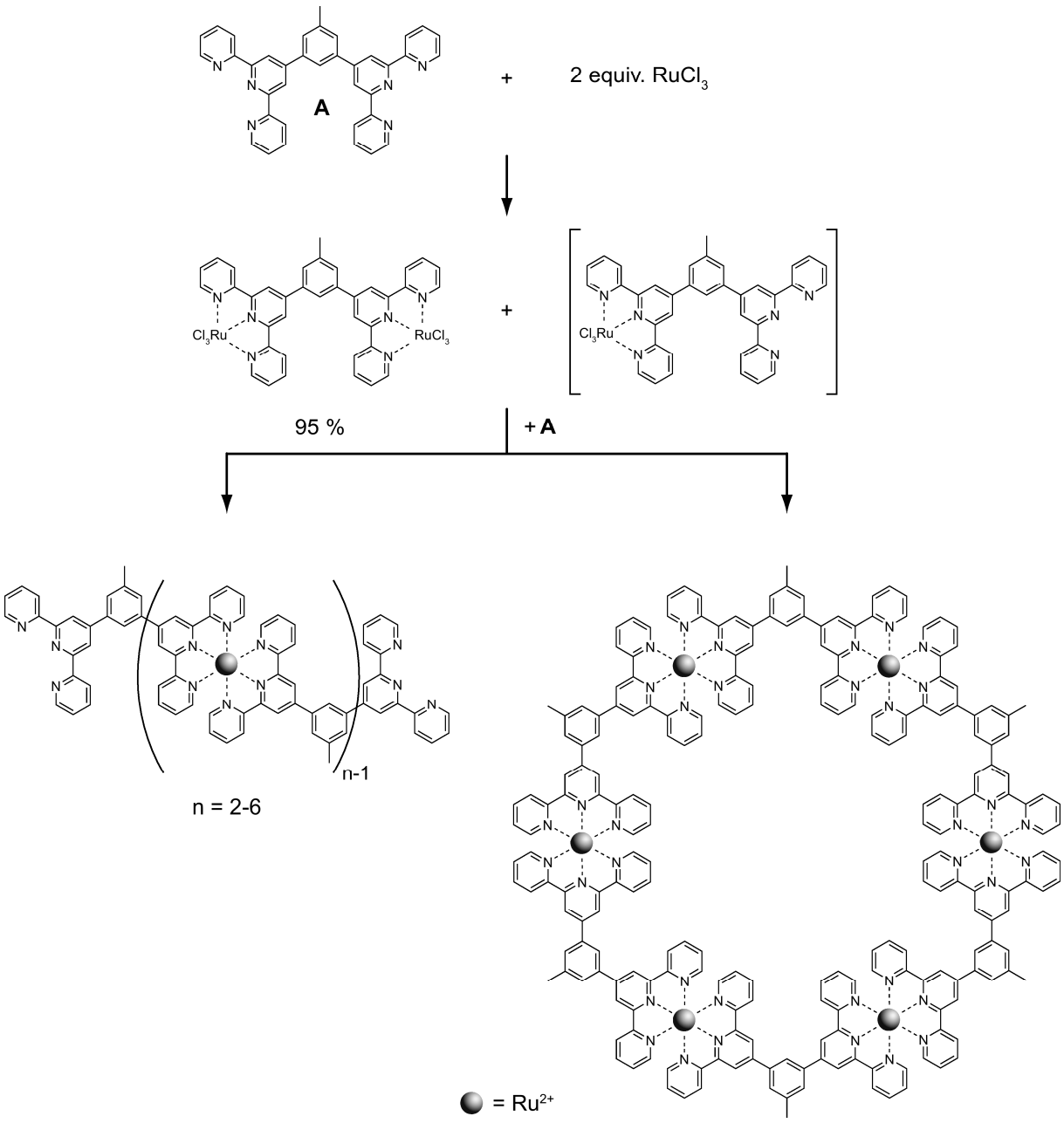

Scheme 26. Synthesis of the bis(Ru^{3+}) and mono(Ru^{3+}) monomers and the formation of the linear ([methylphenylenebis(terpyridine)]$_n$$Ru^{2+}{}_{n-1}$) complexes (left) and macrocycle (right) by a single-pot reaction. Adapted with permission from ref [250]. Copyright 2006 John Wiley and Sons.

The third polymerization mechanism is called the "cooperative model", or "nucleation-elongation polymerization" (NEP) as shown in Scheme 25c. This mechanism involves

two consecutive periods of growth: an initial nucleation process (K_N), followed by an elongation growth process (K_E). In nucleation-elongation mechanism, the bonds between monomers are weak, hindering the spontaneous formation of polymers, but after a nucleus is formed, further monomer addition becomes favorable, at which point polymer growth begins as known in polymerization of helices. In contrast to isodesmic chain growth polymerizations (ISP), long polymer chains will form only above a certain temperature and monomer concentration.[143, 198-199, 228, 239, 253-259]

As already mentioned, the aim of this thesis is to obtain a better understanding in the growth kinetics of MEPEs. In Chapter 3, the kinetics of growth are presented in detail based on the assumption of an isodesmic growth mechanism. Since association constants provide information on the binding strength and therefore the length of supramolecular polymers the following subchapter will give an overview of literature known association constants in supramolecular polymers.

Association constants of supramolecular polymers. The association constant, K_a, for the polymerization of supramolecular polymers is defined as

$$K_a = \frac{k_1}{k_2} \tag{22}$$

with k_1 and k_2 being the rate constants of the forward and reverse polymerization reaction, respectively. Relatively low association constants, K_a, are obtained for cylindrical β-sheet peptide assemblies (K_a = 1.2 × 10^1 M^{-1} to 2.6 × 10^3 M^{-1}), which stack through backbone-backbone hydrogen-bonding to form nanotubular structures as shown in Figure 20.[242, 260]

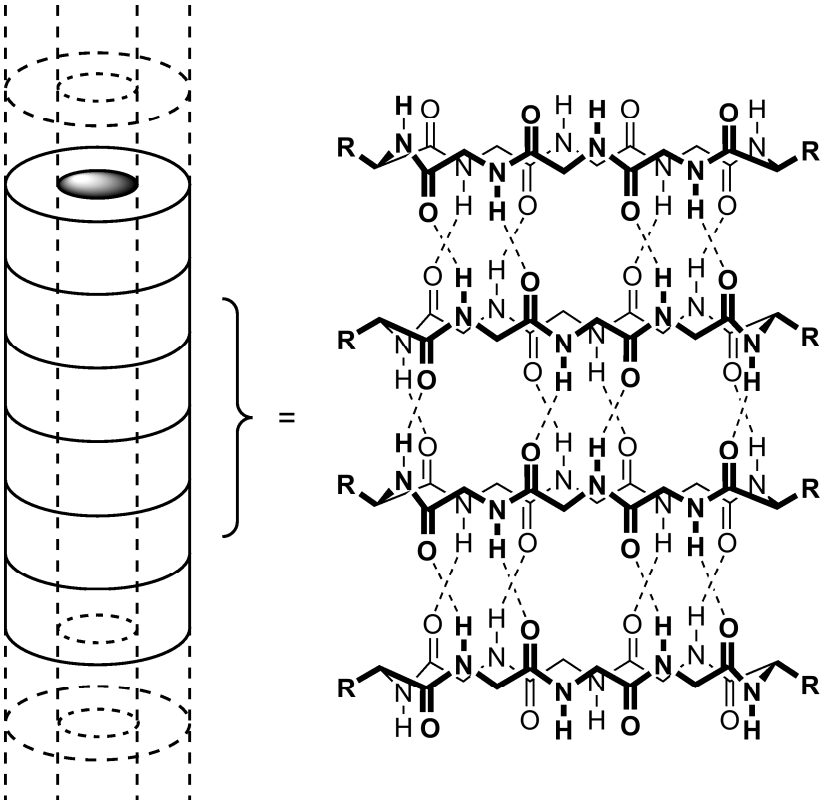

Figure 20. Self-assembling cyclic nanotubes, where the subunits are designed to adopt flat, disklike conformations and stack through antiparallel backbone-backbone hydrogen-bonding. Adapted with permission from [260]. Copyright 1998 American Chemical Society.

Phenylene ethynylene macrocycles undergoing solvent induced π-stacked organization exhibit slightly higher association constants in the range of K_a = 5.0 × 10^1 M^{-1} to 1.5 × 10^4 M^{-1}, whereas Meijer et al.[98] introduced supramolecular polymers based on the self-complementary quadruple hydrogen bonding ureidopyrimidinone and ureidotriazine, which obtain "moderate" (K_a = 2 × 10^4 M^{-1}) to "high" (K_a = 6 × 10^7 M^{-1}) association constants between the units.[98, 100, 241-242, 257, 261-262] One polymer based on zinc porphyrin, covalently linked to an appropriate pyridine side arm, forms macrocyclic dimers with high association constants in the range K_a = 10^6 M^{-1} to 10^8 M^{-1}.[107, 242] Finally, Gong et al.[263] describe the design of a self-complementary

six-H-bonded duplex with an association constant up to 7 × 10^9 M^{-1} as shown in Scheme 27.[242, 263]

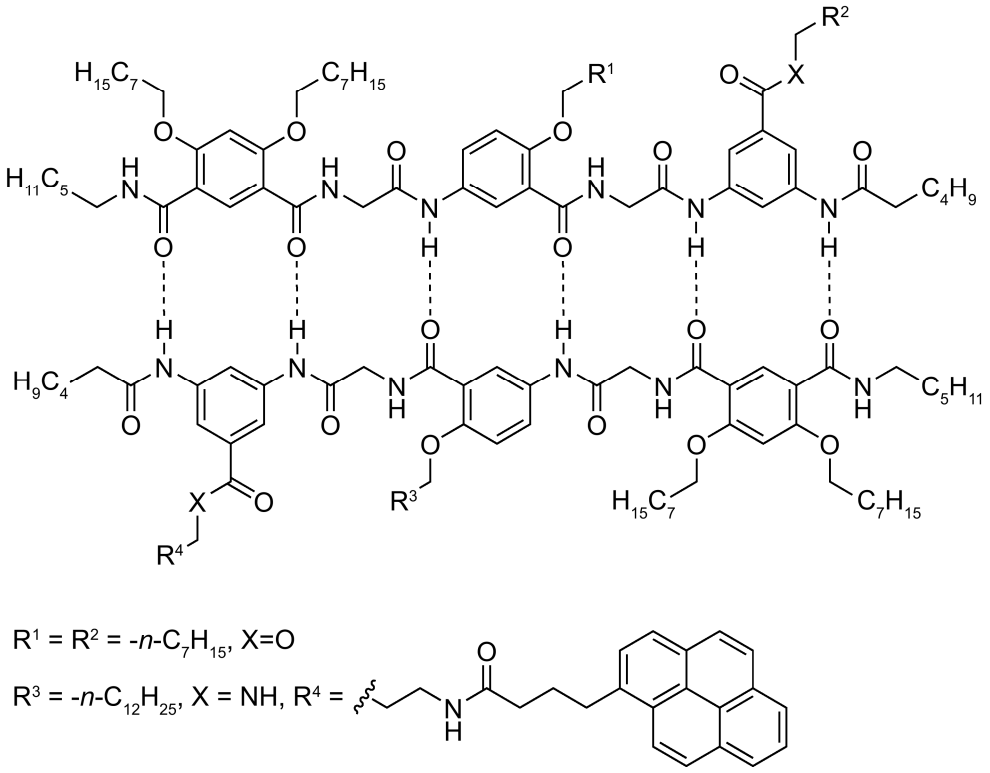

Scheme 27. Six-H-bonded, self-complementary duplex that contains the AADADD-DDADAA array. Adapted from ref [263] with permission from The Royal Society of Chemistry.

The hydrogen-bonded complexes are based on rigid heterocycles with multiple H-bonding donor (D) and acceptor (A) sites. In general, increasing the number of H-bonds leads to an increasing stability of the corresponding H-bonded duplex.[263]

The association constant, K_a, influences the number average degree of polymerization, $\bar{X}_n$, according to

$$\bar{X}_n \sim (K_a c)^{0.5} \tag{23}$$

with c being the overall concentration of ditopic monomers.[194] The number and weight average degrees of polymerization are shown theoretically in Figure 21.

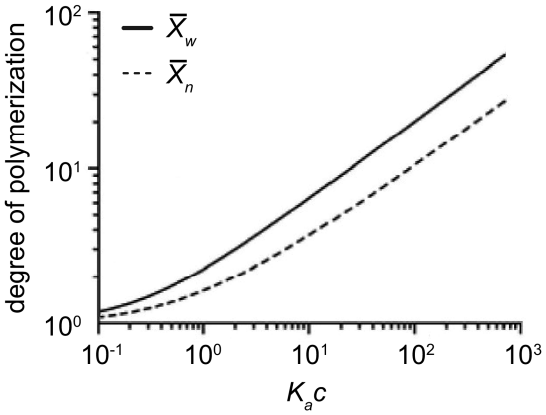

Figure 21. Concentration-dependent properties of isodesmic supramolecular polymers in ideal solutions. Number and weight average degrees of polymerization as a function of $K_a c$. Adapted in part with permission from [143]. Copyright 2009 American Chemical Society.

As can be seen, the fraction of monomer incorporated in polymeric species is increasing with the concentration, c. Furthermore, a high equilibrium constant K_a is needed (K_a > 10^6 M^{-1}) to obtain supramolecular polymers with high degrees of polymerizations in dilute solutions (c < 1M).[143]

1.4 Conclusion and aim of this thesis

Despite the widespread use of metal ion coordination, the mechanisms of formation in coordination networks and soluble polymers are poorly understood. Tailoring the structure and properties of metallo-supramolecular architectures requires a better understanding of the kinetic and thermodynamic properties of metal ion ligand interactions. For instance, one could make predictions of the size of metallo-supramolecular assemblies as well as their dynamic response to external stimuli if the binding constants and ligand substitution rates were available. Therefore, investigation of the kinetics of metal-ligand coordination as well as the kinetics of polymer growth of the MEPEs seems a promising way to understand the properties of metal ion ligand interactions.[89, 188] Tailoring specific chain-lengths of the MEPEs also presents a method to adjust the properties of these polymers.[88] Studies on these concepts are presented in the following Chapters of this thesis.

Aim of this thesis. The mechanisms and the kinetics of complex formation and polymer growth of MEPEs are poorly understood and tailoring the size and dynamic response of the MEPEs are not possible so far. Thus, a motivation of this thesis is to understand the kinetics of coordination of the ditopic ligand **1** to Fe^{2+}, Co^{2+}, and Ni^{2+} and to obtain a better understanding of the metal ion ligand interactions and their complexation. Based on the already known binding constants and rate constants, reported by Wilkins et al.[78] the intension is the verification of these results and the transferability to the kinetics of the coordination of the ditopic ligand **1** to Fe^{2+}, Co^{2+}, and Ni^{2+}. Aim of this thesis is to present a full kinetic rate law for the complexation of MEPEs. Furthermore, the absorption and emission properties of the MEPEs as well as of the corresponding complexes are of great interest as well as the impacts on

enhanced or reduced emission intensity. Another motivation is to understand the impact of concentration, pH, metal ion to ligand ratio, and binding constants on the polymer growth kinetics and the final chain-length of the polymers in solution. Thus, it is necessary to develop a theoretical model to predict the polymer length and the verification of this model by means of the experimental determination of the MEPE's growth and their final average chain-length. The thesis presents conditions for obtaining high degrees of polymerization and a procedure to adjust the chain-length and viscosity of the systems will be developed by usage of a monotopic chain stopper. In addition, aim of the thesis is to develop a full kinetic rate law for the polymer growth inclusive of the determination of forward and reverse polymerization rate constants and the corresponding association constants. Furthermore, the motivation is to determine constants for converting the weight average molar mass to the viscosity.

2

Kinetic Studies of the Coordination of Mono- and Ditopic Ligands with First Row Transition Metal Ions

This Chapter is based on: *"Kinetic Studies of the Coordination of Mono- and Ditopic Ligands with First Row Transition Metal Ions",* S. M. Munzert, G. Schwarz, D. G. Kurth, *Inorg. Chem.* **2016**, 55, 2565-2573.

Abstract: The reactions of the ditopic ligand **1** as well as the monotopic ligands **2** and **3** with Fe^{2+}, Co^{2+}, and Ni^{2+} in solution are studied. While the reaction of **1** with Fe^{2+}, Co^{2+}, and Ni^{2+} results in metallo-supramolecular coordination polyelectrolytes (MEPEs), ligands **2** and **3** give mononuclear complexes. All compounds are analyzed by UV/Vis and fluorescence spectroscopy. Fluorescence spectroscopy indicates that protonation as well as coordination to Zn^{2+} leads to an enhanced fluorescence of the terpyridine ligands. In contrast, Fe^{2+}, Co^{2+}, or Ni^{2+} quench the fluorescence of the ligands. The kinetics of the reactions are studied by stopped-flow fluorescence spectroscopy. Analysis of the measured data is presented and the full kinetic rate laws for the coordination of the terpyridine ligands **1**, **2**, and **3** to Fe^{2+}, Co^{2+}, and Ni^{2+} are presented. The coordination occurs within a few seconds, and the rate constant increases in the order $Ni^{2+} < Co^{2+} < Fe^{2+}$. With the rate constants at hand, the polymer growth of Ni-MEPE is computed.[89]

2.1 Introduction

In order to understand the growth and complexation of MEPEs based on Fe^{2+}, Co^{2+}, Ni^{2+}, and ligand **1**, a comprehensive analysis of the coordination kinetics using stopped-flow measurements in solution is presented. The monotopic ligands 4′-phenyl-2,2′:6′,2′′-terpyridine (**2**) and 2,2′:6′,2′′-terpyridine (**3**) (Scheme 3) are used for control experiments. Based on the kinetic data presented by Wilkins et al.[78] it is expected that coordination in MEPEs occurs on a time scale, which is readily available by conventional stopped-flow methods.[89]

2.2 Results and discussion

2.2.1 UV/Vis and emission properties

Here, the focus is on the overall rate that is the formation of bis-terpyridine complexes. The rate is determined from the fluorescence quenching of the ligands **1**, **2**, and **3** upon metal ion binding with Fe^{2+}, Co^{2+}, and Ni^{2+}. It is assumed that the emission signal is proportional to the concentration of uncoordinated terpyridine receptors. Furthermore, it is expected that the selected metal ions have a strong preference for binding two terpyridine receptors because $K_2 >> K_1$. As a result, the emission decay that is the consumption of terpyridine receptors is directly related to the overall rate of two terpyridine groups coordinating to the metal ion. The emission as a function of time is monitored with the stopped-flow technique. The rate, v, of coordination is obtained from the slope of the emission decay. First, the absorption and fluorescence properties of the ligands and the corresponding complexes, are presented followed by a discussion of stopped-flow analysis. Here, the interest is on the coordination of the

ligands to Fe^{2+}, Co^{2+}, and Ni^{2+} given that the coordination of Zn^{2+} to ligand **1** does not lead to polymers as mentioned above.

Figure 22 shows the UV/Vis absorption spectra of ligand **1** in (a) acetic acid solution (75 vol %) and in (b) EtOH, as well as of Fe-, Co-, Ni-, and $[Zn(\mathbf{1})]^{2+}$ in (a) acetic acid solution (75 vol %), (b) EtOH, and (c) H_2O.

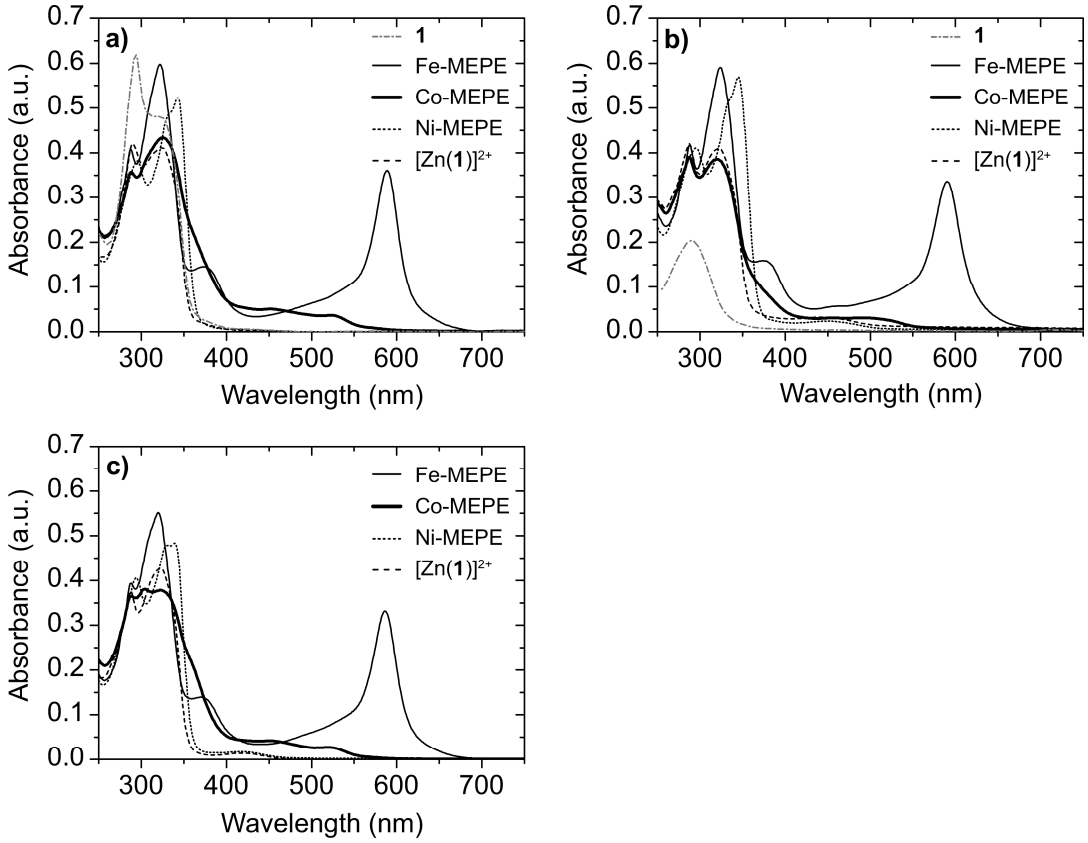

Figure 22. Absorption spectra of ligand **1** in (a) acetic acid solution (75 vol %) and in (b) EtOH, as well as of $[Zn(\mathbf{1})]^{2+}$, Fe-, Co-, and Ni-MEPE in (a) acetic acid solution (75 vol %), (b) EtOH, and (c) H_2O recorded at 20 °C. The concentration of the metal ions and of ligand **1** is 10^{-3} M in all samples. Because ligand **1** shows scattering background in EtOH under these conditions, a baseline correction was applied. Adapted with permission from [89]. Copyright 2016 American Chemical Society.

With simple counter ions like acetate, MEPEs are soluble in water, aqueous acetic acid, and polar solvents like EtOH or MeOH. On the other hand, ligand **1** is soluble in aqueous acetic acid, but less soluble in polar solvents such as water, EtOH, or MeOH. At a concentration of at least 10^{-3} M, which is needed for measuring meaningful absorption spectra, ligand **1** forms a precipitate in EtOH or MeOH giving rise to scattering. For this reason, the absorption spectrum of ligand **1** is recorded in acetic acid solution (75 vol %) (Figure 22a). The UV/Vis absorption spectra of MEPEs recorded in acetic acid solution (75 vol %), EtOH, or H_2O do not show any significant difference in the spectral envelope.

Protonated ligand **1** displays two distinct absorption bands associated with π-π* transitions at 292 and 321 nm. Due to the low solubility in EtOH, ligand **1** shows a broad and featureless absorption band at around 290 nm in EtOH (see Figure 22b); at a concentration sufficient for measuring absorption spectra the solution turns turbid due to agglomeration of ligand **1**.[85-87]

Similar to the protonated ligand **1**, the spectra of MEPEs show two π-π* transitions with band maxima occurring at around 287 and 321 nm, respectively. Coordinating to the metal ion forces the terpyridine receptor to the cis-cis configuration.[87, 264] The blue color of Fe-MEPE originates from the additional absorption band at approximately 580 nm, a metal-to-ligand charge-transfer (MLCT) band, typical for Fe-terpyridine complexes.[265] Co-MEPE has a red color originating from the d-d transitions in the range from 400 to 550 nm.[103] The orange color of Ni-MEPE is associated with a d-d transition at 341 nm, the π-π* transitions are slightly shifted to 294 and 332 nm. $[Zn(\mathbf{1})]^{2+}$ is colorless due to its d^{10} electron configuration.[111]

Next, the fluorescence data of the complexes are presented. While aqueous acetic acid would be the solvent of choice, the fluorescence spectra are measured in EtOH. First, acetic acid can cause corrosion of the stopped-flow apparatus. Second, fluorescence

spectra are recorded at concentrations of 10^{-4} M and below. At these concentrations, ligand **1** and all other species are soluble in EtOH. Finally, the protons of acetic acid would compete with the metal ions in coordination, adding a further variable to the equation. Figure 23a shows the fluorescence spectra of ligand **1** and $[Zn(\mathbf{1})]^{2+}$ recorded in EtOH.

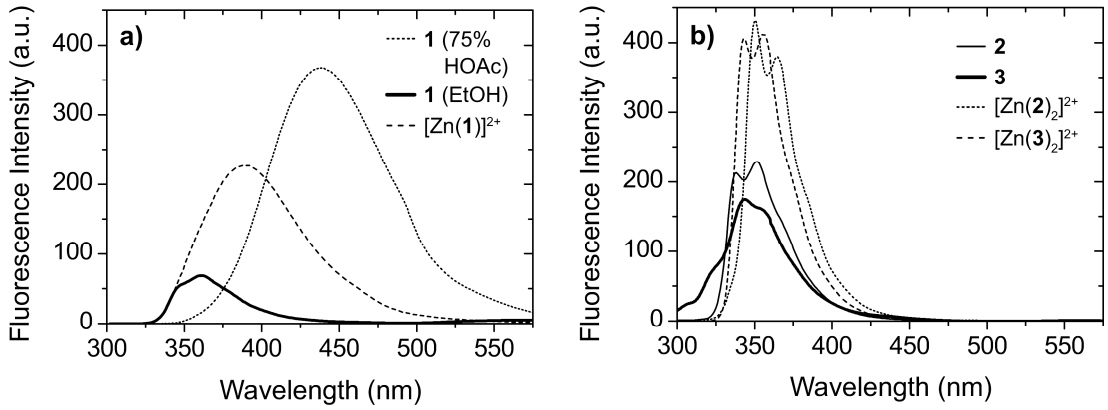

Figure 23. Fluorescence spectra of (a) ligand **1** (dissolved in acetic acid solution (75 vol %) and EtOH) and $[Zn(\mathbf{1})]^{2+}$ (excitation wavelength λ_e = 292 nm, dissolved in EtOH), (b) **2** and $[Zn(\mathbf{2})_2]^{2+}$ (λ_e = 289 nm, EtOH), **3** and $[Zn(\mathbf{3})_2]^{2+}$ (λ_e = 281 nm, EtOH). Spectra are recorded at 20 °C with 10^{-5} M concentration of **1**, **2**, and **3**, respectively. Adapted with permission from [89]. Copyright 2016 American Chemical Society.

The concentration of **1** is 10^{-5} M in both samples. At this concentration, a clear solution is obtained, yet enough signal to record fluorescence spectra. The low intensity of the Rayleigh scattering signal suggests that ligand **1** is dissolved and that aggregates, which form at higher concentrations, are absent. Formation of aggregates at higher concentrations is readily observed by an increasing Rayleigh scattering signal.[266]

Dissolved in EtOH ligand **1** shows a broad emission band with a maximum at 360 nm (Figure 23a). It is noted that in acetic acid solution (75 vol %) **1** reveals an enhanced emission band at 438 nm. Similarly, $[Zn(\mathbf{1})]^{2+}$ shows an increased emission, with a

maximum at 389 nm. Protonation of the terpyridine receptors as well as coordination of Zn^{2+} enhances the fluorescence intensity due to the chelation-enhanced fluorescence (CHEF) effect (see Figure 7a in Chapter 1.2.2.3).[191]

Ligands **2** and **3** show fluorescence bands at 338, 344, and 352 nm, respectively (see Figure 23b). The complexes $[Zn(\mathbf{2})_2]^{2+}$ and $[Zn(\mathbf{3})_2]^{2+}$ also show an increased emission intensity compared to the uncoordinated ligands, due to the CHEF effect.

The fluorescence intensities of the monotopic ligands **2** and **3** in EtOH (intensity maxima 229 and 174 a.u.) in Figure 23b are higher compared with the intensity of the ditopic ligand **1** in EtOH (Figure 23a, intensity maximum 69 a.u.). It appears that a photoinduced-electron-transfer (PET)[191] effect may be responsible for the decreased fluorescence of the free and unprotonated ditopic ligand **1** in EtOH (see Figure 7b in Chapter 1.2.2.3). It is assumed that the PET effect in EtOH is more effective for the ditopic ligand **1**, consisting of two terpyridine receptors, as for the monotopic ligands **2** and **3**. In contrast, the complexes containing Fe^{2+}, Co^{2+}, and Ni^{2+} do not show fluorescence (see Figure 24).

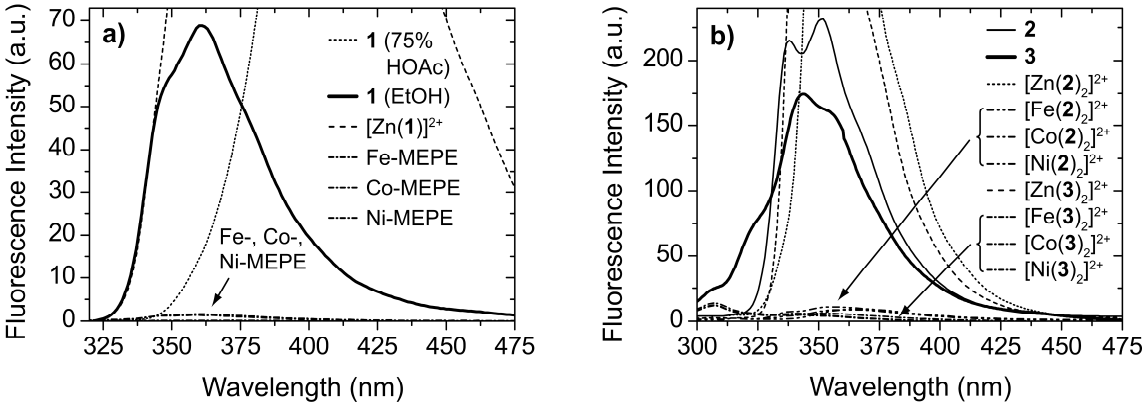

Figure 24. Fluorescence spectra of (a) ligand **1** (dissolved in acetic acid solution (75 vol %) and EtOH), $[Zn(\mathbf{1})]^{2+}$, Fe-, Co, and Ni-MEPE (dissolved in EtOH, λ_e = 292 nm), and (b) **2**, $[Fe(\mathbf{2})_2]^{2+}$, $[Co(\mathbf{2})_2]^{2+}$, $[Ni(\mathbf{2})_2]^{2+}$, $[Zn(\mathbf{2})_2]^{2+}$ (EtOH, λ_e = 289 nm), **3**, $[Fe(\mathbf{3})_2]^{2+}$, $[Co(\mathbf{3})_2]^{2+}$, $[Ni(\mathbf{3})_2]^{2+}$, and $[Zn(\mathbf{3})_2]^{2+}$ (EtOH, λ_e = 281 nm). Spectra were recorded at 20 °C with 10^{-5} M concentration of **1**, **2**, and **3**, respectively. Adapted with permission from [89]. Copyright 2016 American Chemical Society.

The fluorescence quenching is associated with the coordination of the metal ion to the terpyridine receptor. As reported in the literature, the presence of transition metal ions with empty or half-filled d-orbitals like Cr^{3+}, Mn^{2+}, Fe^{2+}, Fe^{3+}, Co^{2+}, Ni^{2+}, and Cu^{2+} quenches the fluorescence presumably through a ligand-to-metal charge-transfer mechanism giving rise to a nonradiative deactivation of the excited singlet state of the ligand.[267-270] In the nonfluorescent complexes, the excited singlet state of the ligands **1**, **2**, and **3** are likely to act as energy donors. The transition metal ions Fe^{2+}, Co^{2+} and Ni^{2+} possess empty or half-filled orbitals (d^6, d^7, and d^8 configuration, respectively), which can be involved in an energy-transfer mechanism where they act as energy-transfer acceptors in a ligand-to-metal charge-transfer. This leads to a nonradiative deactivation of the photoexcited fluorophores **1**, **2**, and **3**.[267-270] Due to the d^{10} configuration, Zn^{2+} does not participate in such an energy-transfer process.[268] Degassing the solutions has no significant effect on the fluorescence properties of all samples.

Figure 25 shows (a) the fluorescence spectra and (b) the fluorescence intensity of ligand **1** as a function of Ni^{2+} concentration. The stoichiometry, δ, of metal ion to ligand concentration is varied from δ = 0 (no Ni^{2+} metal ions present) to δ = 1.0. As the stoichiometry approaches one, the fluorescence is fully quenched as discussed above. Figure 25b shows the fluorescence intensity at λ_{max} = 360 nm as a function of δ.

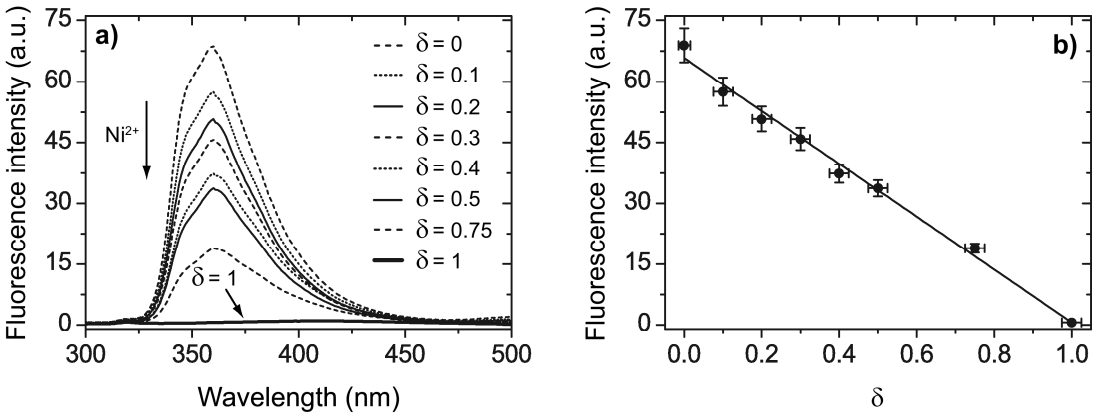

Figure 25. Fluorescence spectra (a) of ditopic ligand **1** on addition of $Ni(OAc)_2 \cdot (H_2O)_4$ (excitation wavelength λ_e = 292 nm) and (b) fluorescence intensity at λ_{max} = 360 nm as a function of stoichiometry, δ = $[Ni^{2+}]/[\mathbf{1}]$. Spectra are recorded in EtOH at 20 °C with 10^{-5} M concentration of **1**. Adapted with permission from [89]. Copyright 2016 American Chemical Society.

A linear decrease of the fluorescence intensity as a function of increasing Ni^{2+} concentration is observed and thus as a function of decreasing concentration of uncoordinated ligand **1**. The dependence of fluorescence intensity I_F on the concentration, c, is given by a form of the Lambert-Beer law:

$$I_F = I_0 \cdot \Phi \cdot (1 - e^{-\varepsilon c d}) \tag{24}$$

with I_0 being the intensity of incident radiation, Φ being the fluorescence quantum yield, ε being the absorptivity, and d being the path length. For low concentrations ($\varepsilon c d$ << 1), the fluorescence intensity is proportional to the concentration:[266]

$$I_F = I_0 \cdot \Phi \cdot \varepsilon cd \quad (25)$$

This is consistent with the observed linearity in Figure 25b, where the intensity is proportional to the concentration of Ni^{2+} and uncoordinated terpyridine receptor, respectively.

To quench the emission of the ditopic ligand completely by coordination with Ni^{2+}, the metal ion to ligand ratio has to be δ = 1. In this case, both terpyridine receptors of the ligand are occupied, except one receptor at the very end of the Ni-MEPE chains. If δ = 0.5, two ligands will associate to $[Ni(\mathbf{1})_2]^{2+}$ complexes, because $K_2 >> K_1$. As shown in Figure 25, fluorescence intensity for Ni-MEPE at δ = 0.5 is quenched to half of the ligand's initial intensity (δ = 0). The metal ion quenches only the coordinating terpyridine receptor, not the entire ditopic ligand. The same results are obtained for Fe^{2+} and Co^{2+} (see Figure 26). This result proves that in the investigated concentration range, fluorescence quenching is linearly related to the coordination of bisterpyridine metal ion complexes.[89]

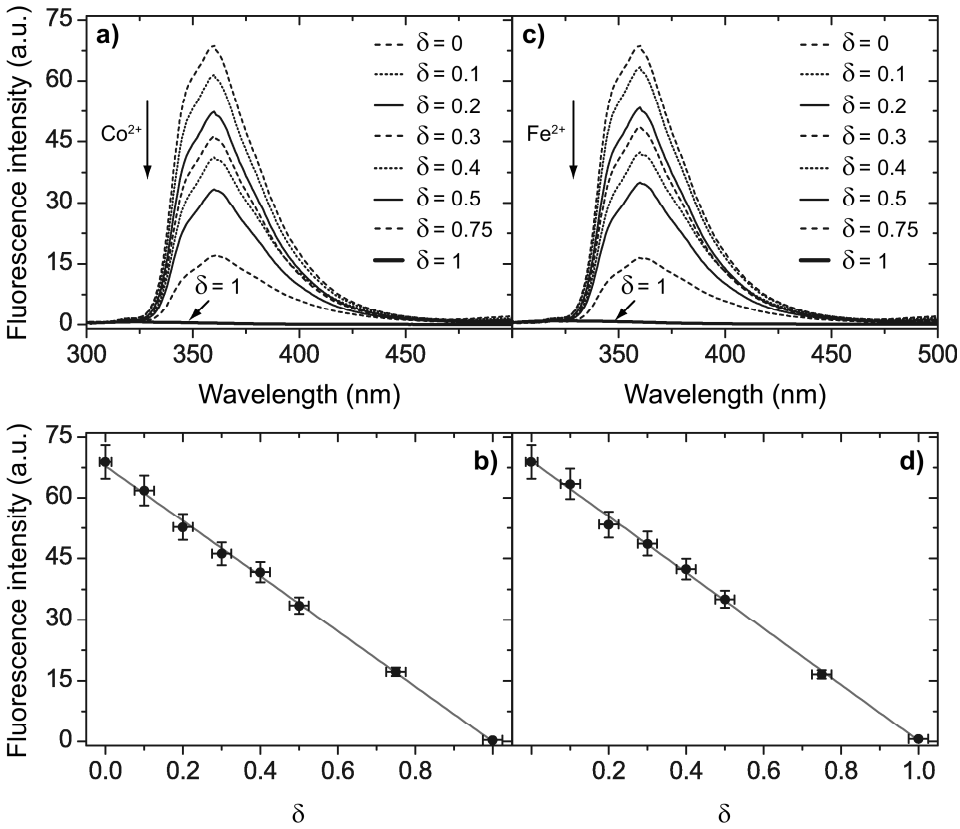

Figure 26. Fluorescence spectra of ditopic ligand **1** on addition of (a) $Co(OAc)_2 \cdot (H_2O)_4$ and (c) $Fe(OAc)_2 \cdot (H_2O)_4$ (excitation wavelength λ_e = 292 nm) and fluorescence intensity at λ_{max} = 360 nm as a function of stoichiometry, (b) δ = $[Co^{2+}]/[\mathbf{1}]$ and (d) δ = $[Fe^{2+}]/[\mathbf{1}]$. Spectra were recorded in EtOH at 20 °C with 10^{-5} M concentration of **1**. Adapted with permission from [89]. Copyright 2016 American Chemical Society.

2.2.2 Fluorescence quenching

Fluorescence spectroscopy is used to monitor the emission intensity decay of the fluorescing ligands **1**, **2**, and **3** as a function of coordination to the metal ions Fe^{2+}, Co^{2+}, and Ni^{2+}. Controlled mixing of the reagents is achieved with a stopped-flow method. In this technique, the ligand solutions **1**, **2**, or **3** and the solutions containing the metal ions Fe^{2+}, Co^{2+}, or Ni^{2+} are forced with sample syringes into the observation cell, where the reaction mixture is studied by fluorescence spectroscopy. For the

reasons mentioned above the reactions are carried out in EtOH at concentrations of 10^{-4} M and below. For the concentration range of interest, a calibration curve is recorded that relates ligand concentration to emission signal as described in Chapter 5.4. In the concentration range a linear relationship between concentration of ligand and emission signal is observed.

The data is analyzed in the following way. The relation between the rate of a reaction and the concentration of a chemical species is given by

$$v = k[\mathrm{M}^{2+}]_0^a[\mathrm{L}]_0^b \tag{26}$$

with v being the rate of the reaction, k being the rate constant, $[L]_0$ being the initial concentration of the respective ligand **1**, **2**, or **3**, and $[M^{2+}]_0$ the initial concentration of the respective transition metal ion. The exponents, a and b, are defined as the order of the reaction.[179] Wilkins et al.[78] proved that the coordination reactions are first order in metal ions and first order in monotopic terpyridine ligands. However, the order of reaction in ditopic terpyridine ligand **1** is investigated. For this purpose, the order is determined by keeping the concentration $[L]_0$ constant, while $[M^{2+}]_0$ is varied and vice versa. With a and b at hand, one is able to calculate the rate constant k and therefore the full rate law for the coordination reaction.

The method of initial rates[179] is used to estimate the order of the reaction related to each reactant. The initial rate varies with the concentration of the respective reactant. Higher initial concentrations of the metal ion result in a faster quenching of the terpyridine's emission. Thus, the rate of coordination increases with increasing initial concentration of the metal ion (see Figure 27).

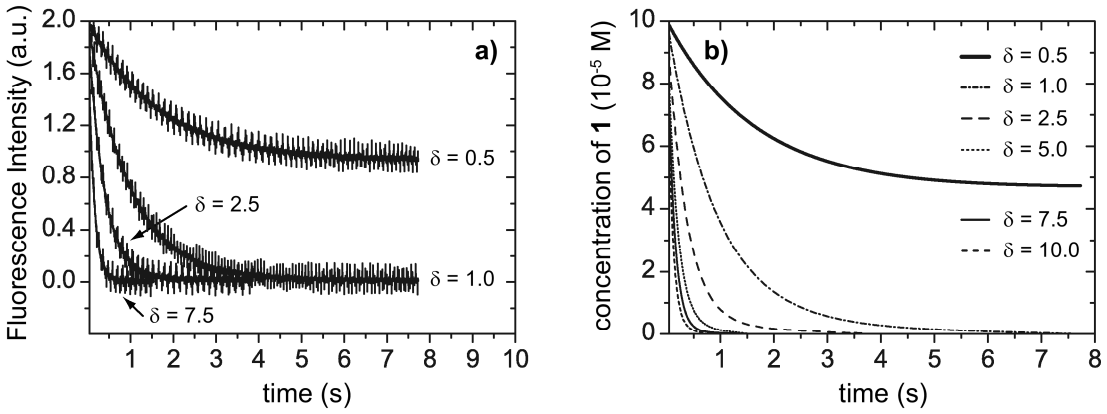

Figure 27. (a) Fluorescence intensity and (b) concentration of uncoordinated ditopic ligand **1** as a function of time for different stoichiometries, $\delta = [Ni^{2+}]_0/[\mathbf{1}]_0$ in EtOH at 20 °C (excitation wavelength λ_e = 292 nm). The initial concentration of $[\mathbf{1}]_0$ is 10^{-4} M, while that of Ni^{2+} is increased from 5×10^{-5} to 10^{-3} M. The concentration of uncoordinated **1** is determined from the emission intensity via a calibration curve. Note that the values of the fluorescence intensities in (a) differ from the fluorescence intensities obtained by steady-state fluorescence spectroscopy in Figure 26, because the spectra were recorded with different spectrometers. Adapted with permission from [89]. Copyright 2016 American Chemical Society.

As the reaction proceeds, the concentration of uncoordinated terpyridine receptors decreases, which is monitored as decaying emission signal. Plotting the emission intensity against time results in decreasing exponential curves, as shown exemplary in Figure 27 for the reaction of **1** and Ni^{2+}. Under these experimental conditions, the coordination of **1** to Ni^{2+} takes place within a few seconds. Figure 27 shows that $\delta = [Ni^{2+}]_0/[\mathbf{1}]_0 = 1.0$ is sufficient to reduce the concentration of uncoordinated ditopic ligand **1** to zero. Due to the ditopic structure of **1** and the strong preference for forming the bisterpyridine complex, $\delta = 1.0$ is sufficient to occupy all terpyridine receptors except at the end of the chain. If $\delta < 1.0$, the emission of uncoordinated terpyridine receptors is detected (Figure 27). These results are in agreement with the steady-state measurements discussed above.

The reaction rate is determined from the slopes of the concentration/time traces at t = 0 (see Chapter 5.4.2). The data is extrapolated to t = 0 because the dead time of the stopped-flow measurement prevents recording data at t = 0. The slope is determined from the curve fit of the experimental data. The resulting rates, v, for the reaction of **1** and Ni^{2+} are summarized in Table 2.

Table 2. Rates v at t = 0 for the reaction of **1** with Ni^{2+} at different concentrations in EtOH at 20 °C. Adapted with permission from [89]. Copyright 2016 American Chemical Society.

$[\mathbf{1}]_0$ (mol L^{-1})	$[Ni^{2+}]_0$ (mol L^{-1})	v (mol L^{-1} s^{-1})
1.0×10^{-4}	1.0×10^{-4}	1.0×10^{-4}
1.0×10^{-4}	2.5×10^{-4}	2.7×10^{-4}
1.0×10^{-4}	5.0×10^{-4}	5.5×10^{-4}
1.0×10^{-4}	7.5×10^{-4}	7.8×10^{-4}
1.0×10^{-4}	1.0×10^{-3}	1.1×10^{-3}

Higher initial concentrations of the metal ion Ni^{2+} lead to higher rates, as Figure 27 already indicated. The reaction order a is calculated by plotting $\ln[v]$ and $\ln[Ni^{2+}]_0$ (see Figure 28) according to

$$v = k[Ni^{2+}]_0^a[\mathbf{1}]_0^b \tag{27}$$

$$\Leftrightarrow \ln[v] = a\ln[Ni^{2+}]_0 + \ln[k] + b\ln[\mathbf{1}]_0 \tag{28}$$

The data follows a straight line with a slope of approximately one indicating that the reaction is first order in Ni^{2+}.

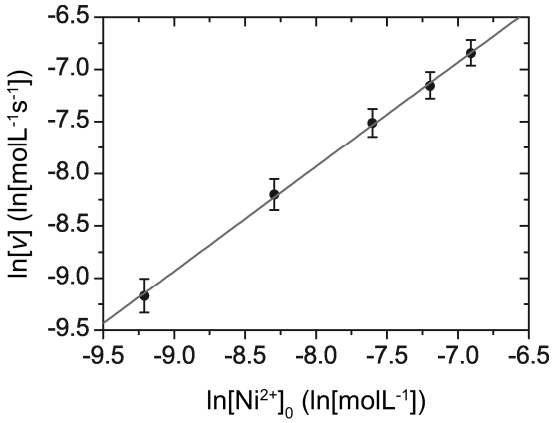

Figure 28. Plot of $\ln[v]$ versus $\ln[\mathrm{Ni}^{2+}]_0$ for coordination of **1** and $Ni(OAc)_2{\cdot}(H_2O)_4$ in EtOH at 20 °C. The slope corresponding to the reaction order, a, is calculated to 1.00. Adapted with permission from [89]. Copyright 2016 American Chemical Society.

Likewise, the order in ditopic ligand **1** is determined by using a constant initial concentration of the metal ion $[Ni^{2+}]_0$ and varied initial concentrations of ditopic ligand $[\mathbf{1}]_0$. Applying the same procedure as for the metal ion the order in **1** is found to be one. The overall order of the coordination reaction of **1** and Ni^{2+} is therefore second order. With a and b equal to one, the rate law reduces to

$$v = k[\mathrm{Ni}^{2+}]_0[\mathbf{1}]_0 \tag{29}$$

The reaction order can be confirmed for the coordination of Fe^{2+} and Co^{2+} to the ditopic terpyridine ligand **1**. The rate constant k is now determined by plotting v that is the slope at t = 0, against different initial concentrations of $[Ni^{2+}]_0$ and $[\mathbf{1}]_0$. Figure 29 shows the obtained data, where k = (8.0 ± 0.4) × 10^3 M^{-1} s^{-1} is obtained.

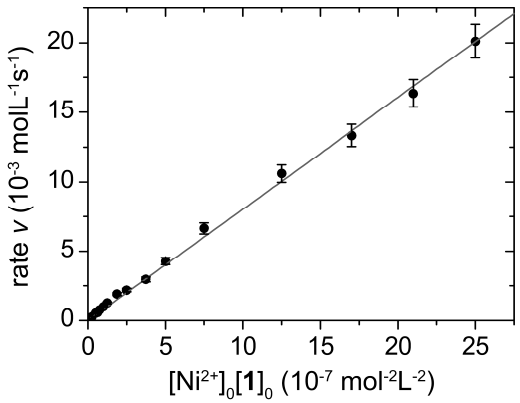

Figure 29. Plot of v versus $[Ni^{2+}]_0[\mathbf{1}]_0$ for coordination of **1** and $Ni(OAc)_2{\cdot}(H_2O)_4$ in EtOH at 20 °C. The slope is the rate constant, k, which is calculated to be (8.0 ± 0.4) × 10^3 $M^{-1}s^{-1}$. Reprinted with permission from [89]. Copyright 2016 American Chemical Society.

Therefore, the full rate law for the coordination of Ni^{2+} to **1** results in

$$v = (8.0 \pm 0.4) \times 10^3 M^{-1}s^{-1}[\mathrm{Ni}^{2+}]_0[\mathbf{1}]_0 \quad (30)$$

The same procedure is repeated for the reactions of **2** and **3** with Fe^{2+}, Co^{2+}, and Ni^{2+}, resulting in $[Co(\mathbf{2})_2]^{2+}$, $[Ni(\mathbf{2})_2]^{2+}$, $[Fe(\mathbf{2})_2]^{2+}$, $[Co(\mathbf{3})_2]^{2+}$, $[Ni(\mathbf{3})_2]^{2+}$, and $[Fe(\mathbf{3})_2]^{2+}$ (see Figure 30).

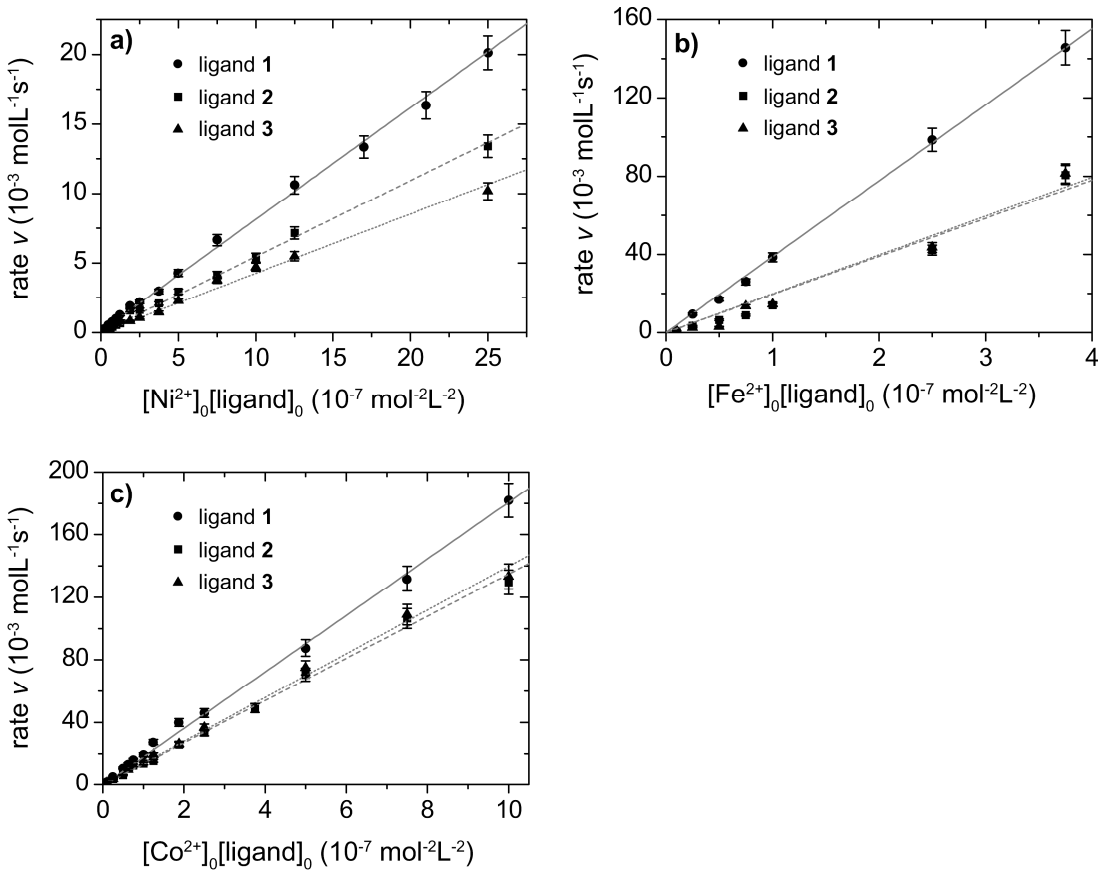

Figure 30. Plot of v versus $[M^{2+}]_0[L]_0$ for coordination of (a) $Ni(OAc)_2{\cdot}(H_2O)_4$, (b) $Fe(OAc)_2{\cdot}(H_2O)_4$, and (c) $Co(OAc)_2{\cdot}(H_2O)_4$ to the ligands **1**, **2**, and **3** in EtOH at 20 °C. The slopes are the rate constants, k. Adapted with permission from [89]. Copyright 2016 American Chemical Society.

Analogously to the reaction of **1** and Ni^{2+} the reaction orders a and b are one, and therefore all evaluated reactions of the metal ions Fe^{2+}, Co^{2+}, and Ni^{2+} with **1**, **2**, and **3** are first order in the reactants and second order in total, which is in agreement with the works of Wilkins[78] and Ellgen et al.[175] Comparing the results, as summarized in Table 3, it can be seen that there is not a simple relation between the metal ion, the ligand, and the resulting rates for coordination.

Table 3. Rate constants k ($M^{-1}s^{-1}$) for the reaction of ligands **1**, **2**, and **3** with Co^{2+}, Ni^{2+}, and Fe^{2+} determined by stopped-flow experiments in EtOH at 20 °C and for comparison literature values for the coordination of the metal ions to ligand **3**. The literature values are measured in water at 25 °C and bromide as counter ion by usage of UV/Vis spectroscopy. Adapted with permission from [89]. Copyright 2016 American Chemical Society.

	1	**2**	**3**	**3 (ref [78])**
Ni^{2+}	(8.0 ± 0.4) × 10^3	(5.5 ± 0.3) × 10^3	(4.3 ± 0.2) × 10^3	1.4 × 10^3
Co^{2+}	(1.8 ± 0.1) × 10^5	(1.3 ± 0.1) × 10^5	(1.4 ± 0.1) × 10^5	2.4 × 10^4
Fe^{2+}	(3.9 ± 0.8) × 10^5	(1.9 ± 0.1) × 10^5	(2.0 ± 0.2) × 10^5	5.6 × 10^4

The obtained rate constants are of the same order of magnitude as presented in a publication by Wilkins et al. for the coordination of **3** to the same metal ions in water at 25 °C, bromide as counterion, and usage of the time-dependent absorption spectra at wavelength of 320 to 335 nm (see Table 3).[78] The reaction rates decrease in the order Fe^{2+} > Co^{2+} > Ni^{2+}. The rate constants are sensitive to the ionic radius r_i and the electronic configuration of the metal(II) ion. The following values apply to the used acetate tetrahydrate complexes $Fe(OAc)_2{\cdot}4H_2O$ (r_i = 78 pm, d^6 configuration), $Co(OAc)_2{\cdot}4H_2O$ (r_i = 74 pm, d^7 configuration) and $Ni(OAc)_2{\cdot}4H_2O$ (r_i = 69 pm, d^8 configuration).[271] The coordination involves the replacement of a ligand coordinated to the metal ion, e.g. H_2O or OAc^-, by the entering ligand **1**, **2**, or **3** in solution. As discussed in Chapter 1.2.2.1, coordination reactions of the metal ions Fe^{2+}, Co^{2+}, and Ni^{2+} and terpyridine take place via an I_d mechanism. The ionic radius decreases from Mn^{2+} to Ni^{2+} and leaves less and less space for the entering ligand. The t_{2g} orbitals are nonbonding whereas e_g* orbitals are antibonding. For σ-bonded octahedral complexes the t_{2g} orbitals are spread out between the ligands and therefore their gradual filling will electrostatically disfavor the approach of a terpyridine molecule toward the octahedron. Thus, the possibility of bond-making is decreased for increased number of electrons filled in t_{2g} orbitals. The e_g* orbitals are directed toward the ligands and

their increased occupancy will increase the tendency of bond breaking, which leads to a weaker coordination. Both effects, combined with steric effects due to a decrease in the ionic radius lead to an increasing dissociative character of the exchange mechanism and thus, a decreasing rate constant from Fe^{2+} to Ni^{2+} for the coordination to the terpyridine ligands **1**, **2**, and **3**.[182, 184, 271] Not surprisingly, ligands **2** and **3** exhibit similar rates. However, coordination reactions of the ditopic ligand **1** proceed approximately twice as fast than the monotopic ligands. While the observed reactivity may be an intrinsic function of ligand **1**, e.g. a result of its structure, it may hint to the fact that the reactivity of the terpyridine receptors toward metal ions is simply additive.[89]

2.2.3 Formation of MEPE chains

Next, the intension is to verify if the kinetic data determined for the formation of mononuclear complexes and if it is also valid for MEPE growth. In a first approximation, an isodesmic step growth polymerization for the formation of MEPE chains is assumed, which means that the reactivity of binding is independent of chain-length. Thus, not only monomers can add to chains, but chains of different length can react with each other.[228, 231, 235-236, 238] It is assumed that there is no energy difference between adding a monomer to an oligomer or to another monomer. The monomer is defined as $[M(\mathbf{1})]^{2+}$ (see also Scheme 3). Thus, the reactivity of polymerizable groups should be independent of chain-length. MEPEs based on ligand **1** are linear and incapable of forming angled structures. In Scheme 28 the formation of MEPEs is shown, with k being the rate constant of the polymerization process.

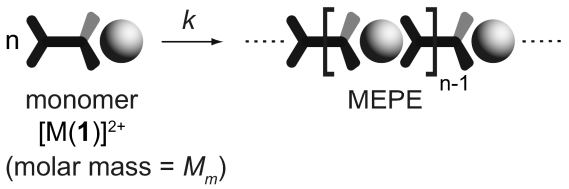

Scheme 28. Self-assembly of MEPEs, with k being the rate constant of the polymerization process. Reprinted with permission from [89]. Copyright 2016 American Chemical Society.

It is assumed that k equals the values found for reaction of **1** with the corresponding metal ion (see also Table 3). A first-order kinetic with respect to the monomer, $[M(\mathbf{1})]^{2+}$ is assumed (see Scheme 28). In Figure 31 the monomer conversion, p, of Ni-MEPE is computed by using eqs (19) and (20) (see Chapter 1.3.1) with $[M(\mathbf{1})]_0^{2+}$ = 6.7 mmol L^{-1} and k = 8.0 × 10^3 M^{-1} s^{-1} (see Table 3).

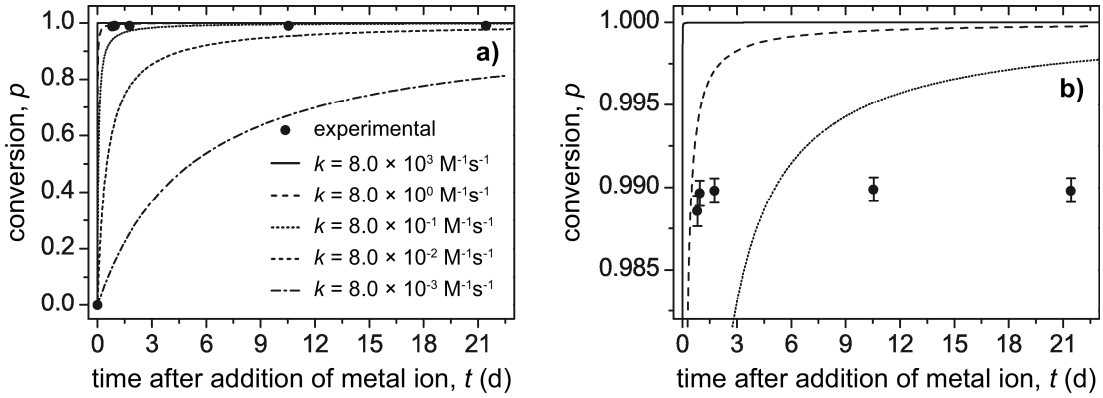

Figure 31. Time dependence of the monomer conversion, p, for polymer chain growth of Ni-MEPE, calculated using eqs (19) and (20). (a) Computed conversion as a function of time ($[M(\mathbf{1})]_0^{2+}$ = 6.7 mmol L^{-1}) with (b) region as p approaches 1. For comparison, polymer growth is computed with the found rate constant k = 8.0 × 10^3 M^{-1} s^{-1} from Table 3 (solid line) and also with rate constants ranging from k = 8.0 × 10^0 M^{-1} s^{-1} to k = 8.0 × 10^{-3} M^{-1} s^{-1}. Finally, this figure shows the MEPE growth in 0.1 M KOAc acetic acid solution (75 vol %) at a temperature of 20 °C ($[M(\mathbf{1})]_0^{2+}$ = 6.7 mmol L^{-1}), measured experimentally by static light scattering (for details concerning the theory of static light scattering, see Chapter 5.4.3.1). Adapted with permission from [89]. Copyright 2016 American Chemical Society.

For verification of the computed data, static light scattering (SLS) is used to investigate the growth of Ni-MEPEs (for details concerning the theory of static light scattering, see Chapter 5.4.3.1). A solution of ligand **1** in 0.1 M KOAc acetic acid solution (75 vol %) and a solution of Ni^{2+} in 0.1 M KOAc acetic acid solution (75 vol %) are mixed and the weight-average molar mass, $\bar{M}_w$ of the resulting Ni-MEPE is obtained by using the SLS technique. With $\bar{M}_w$ at hand, the monomer conversion, p, is calculated according to eqs (19) and (20). The results are shown in Figure 31. It is noted that in a first approximation MEPE growth follows the predicted curve based on the rate of complex formation determined above. However, a closer look at the data (Figure 31b) shows that the MEPE does not quite reach the computed conversion, p. The deviation toward full conversion is not surprising, because an isodesmic step growth polymerization is assumed in a first

approximation. In addition, it is not clear, if the system reaches equilibrium, in particular the reaction rate may slow down as the chains grow due to dissociation and exchange processes of the highly anisometric assemblies. This may further reduce the final conversion, p. Also, it is well-known that polymerization critically depends on the experimental conditions. The rate constant, k, shown in Table 3 is determined in ethanolic solutions, whereas the polymer growth, shown in Figure 31, is measured in 0.1 M KOAc acetic acid solution (75 vol %). Further studies elucidate the details of the growth mechanism of MEPEs, which are presented in Chapter 3.

2.3 Conclusions

In this Chapter data on the overall rates of the coordination reaction of terpyridine ligands and Fe^{2+}, Co^{2+}, and Ni^{2+} are presented. Advantage is taken of the fact that metal ion coordination causes fluorescence quenching of the free ligand. Thus, fluorescence quenching is a direct measure of the reaction rate. The rates are such that the reactions can be followed by stopped-flow measurements. The coordination reactions occur within a few seconds, but there are remarkable differences between the metal ions, due to the electron configuration and the ionic radii. The reaction rates decrease in the order Fe^{2+} > Co^{2+} > Ni^{2+}. On the other side, monotopic ligands **2** or **3** show similar reaction rates, however, ligand **1** reveals a higher rate constant. Since ditopic terpyridine ligands and metal ions form polymers, the next Chapter will focus on the coordination kinetics and the details of polymer growth of MEPEs.

3

The kinetics of growth of metallo-supramolecular polyelectrolytes in solution

This Chapter is based on: *"The kinetics of growth of metallo-supramolecular polyelectrolytes in solution"*, S. M. Munzert, S. P. Stier, G. Schwarz, H. Weissman, B. Rybtchinski, D. G. Kurth, *Chem. Eur. J.* **2017**, doi: 10.1002/chem.201701417.

Abstract: Several transition metal ions, like Fe^{2+}, Co^{2+}, Ni^{2+}, and Zn^{2+} complex to the ditopic ligand 1,4-bis(2,2′:6′,2′′-terpyridin-4′-yl)benzene (**1**). Due to the high association constant, metal ion induced self-assembly of Fe^{2+}, Co^{2+}, and Ni^{2+} leads to extended, rigid-rod like metallo-supramolecular coordination polyelectrolytes (MEPEs) even in aqueous solution. Here, the kinetics of growth of MEPEs are presented. The species in solutions are analyzed by light scattering, viscometry and cryogenic transmission electron microscopy (cryo-TEM). At near-stoichiometric amounts of the reactants, high molar masses are obtained, which follow the order Ni-MEPE ~ Co-MEPE < Fe-MEPE. The experiments indicate that the kinetics of MEPE growth follows a reversible step growth mechanism. The forward polymerization rate constants follow the order Co-MEPE < Fe-MEPE < Ni-MEPE and the growth of MEPEs can be accelerated by adding KOAc.

3.1 Introduction

The results are subdivided in different sections. The first section describes the accurate preparation of MEPEs by conductometry and viscometry. In the second section, results from light-scattering on MEPE growth are presented. Third, a comprehensive analysis of the kinetics of MEPE growth is presented. Finally, the structure and chain-length of MEPEs is illustrated by cryo-TEM.

3.2 Results and discussion

3.2.1 Metal ion to ligand ratio

As already discussed in Chapter 1.2.3.2.4.2, the maximum degree of polymerization in metallo-supramolecular polymers occurs at y = 1. In order to achieve a most accurate metal ion to ligand ratio, y = 1.00, a protocol is developed based on conductometry.[84, 227] Here, the metal ion solution is titrated to a given volume of the ligand solution. Figure 32 summarizes the experimentally determined conductivity data during titration of metal acetate solution (14 mM) to 30 mL of ligand solution (14 mM) as a function of the volume ratio, $V_{M^{2+}}/V_{\mathbf{1}}$.

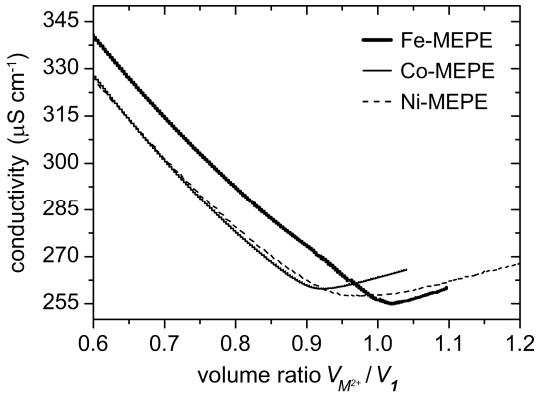

Figure 32. Experimentally determined conductivity data during titration of Fe^{2+}, Co^{2+}, and Ni^{2+} (14 mM) to ligand **1** in acetic acid solution (75 vol %), ($V_{\mathbf{1}}$ = 30 mL; 14 mM) at 20 °C. The minimum of conductivity occurs at a volume ratio of $V_{Fe^{2+}}/V_{\mathbf{1}}$ = 1.020, $V_{Co^{2+}}/V_{\mathbf{1}}$ = 0.923, and $V_{Ni^{2+}}/V_{\mathbf{1}}$ = 0.980, respectively. Due to experimental errors, the data vary from batch to batch. To discern the minimum more clearly, the significant part of the conductivity is shown from $V_{M^{2+}}/V_{\mathbf{1}}$ = 0.6 to 1.2. Reprinted with permission from ref [188]. Copyright 2017 John Wiley and Sons.

Here, $V_{M^{2+}}$ corresponds to the added volume of metal ion solution and $V_{\mathbf{1}}$ to the volume of the ligand solution, respectively. In the absence of experimental errors $V_{M^{2+}}/V_{\mathbf{1}}$ would be unity. As can be seen in Figure 32, this is not the case, the minimum in conductivity, which occurs at y = 1.00, varies from batch to batch due to impurities and experimental errors. Therefore, a stock solution for each metal salt and ligand is prepared, from which the MEPE solutions are prepared under the exact same conditions. The data shown in Figure 32 is recorded from the batches that are used for the measurements presented in this Chapter.

In agreement with previously published data,[72, 84, 227] the conductivity decreases with the addition of the metal acetate solution to the ligand solution. The conductivity of acetic acid solution (75 vol %) is with 200 ± 15 µS cm^{-1} considerably lower than that of the acetic acid solution containing the ligand with 580 ± 15 µS cm^{-1}. The conductivity minimum occurs at a volume of $V_{Fe^{2+}}$ = 30.6 mL, $V_{Co^{2+}}$ = 27.7 mL, and $V_{Ni^{2+}}$ = 29.4 mL, respectively, which corresponds to a volume ratio of $V_{Fe^{2+}}/V_{\mathbf{1}}$ = 1.020, $V_{Co^{2+}}/V_{\mathbf{1}}$ = 0.923,

and $V_{Ni^{2+}}/V_{\mathbf{1}}$ = 0.980. Eventually, the conductivity rises due to the excess of metal ions in solution (Figure 32).

Next, data on the viscosity of the resulting solutions are presented. According to the above mentioned theory, the viscosity should peak at the maximum MEPE chain-length, which is expected at y = 1.00.[72, 84, 227] The viscosity should peak at y-values that coincide with corresponding y-values determined by conductivity.

Accordingly, $V_{\mathbf{1}}$ = 3.00 mL of the ligand solution is mixed with different volumes of the metal acetate solution ($V_{M^{2+}}$ = 2.72 mL to 3.15 mL), corresponding to a volume ratio of $V_{M^{2+}}/V_{\mathbf{1}}$ = 0.907 to 1.050. The dynamic viscosities of the solutions are measured until they plateau as shown in Figure 33.

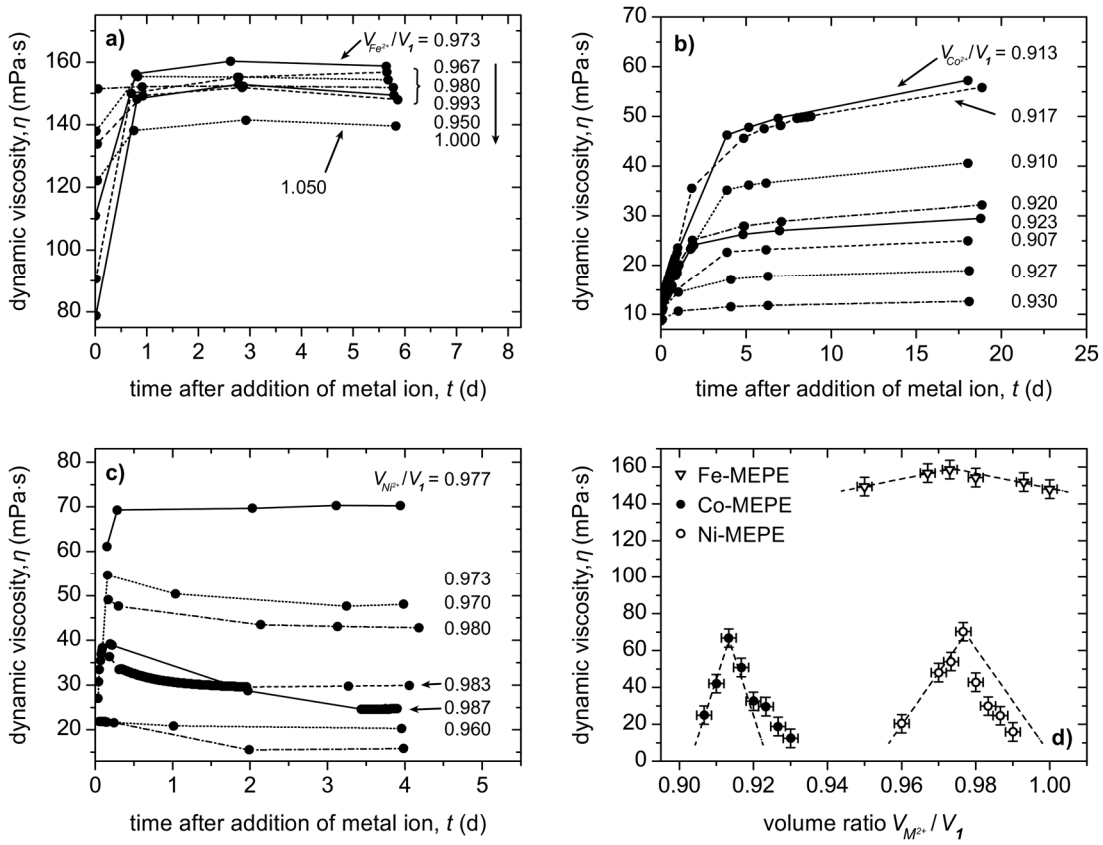

Figure 33. Dynamic viscosity, η, of (a) Fe-MEPE, (b) Co-MEPE, and (c) Ni-MEPE vs. time, t, and (d) volume ratio, $V_{M^{2+}}/V_{\mathbf{1}}$, respectively, using a MEPE concentration of 4.8 g L^{-1} (= 6.7 mM). The time dependent dynamic viscosities (a) are monitored after addition of different volumes of the metal ion solution, $V_{M^{2+}}$, to a solution of the ligand, $V_{\mathbf{1}}$ = 3.00 mL. Figure (d) shows the final dynamic viscosities vs. the volume ratio, $V_{M^{2+}}/V_{\mathbf{1}}$, after an equilibration time of 18 days. All measurements were performed in acetic acid solution (75 vol %) at 20 °C. The dotted lines in (d) are a guide for the eye. Reprinted with permission from ref [188]. Copyright 2017 John Wiley and Sons.

The viscosity, η, is expected to peak at the corresponding volume ratios determined above ($V_{Fe^{2+}}/V_{\mathbf{1}}$ = 1.020, $V_{Co^{2+}}/V_{\mathbf{1}}$ = 0.923, and $V_{Ni^{2+}}/V_{\mathbf{1}}$ = 0.980).

In the case of Fe-MEPE and Co-MEPE an initially increase of the viscosity is observed upon adding metal acetate solution to the ligand solution until the viscosity plateaus (Figure 33a and Figure 33b). In contrast, the viscosity of the Ni-MEPE solutions show a

different behavior. Initially the viscosity increases rapidly but then exhibits a decline and finally reaches a plateau. Notably, the viscosity of the Ni-MEPE solution with a volume ratio of $V_{Ni^{2+}}/V_{\mathbf{1}}$ = 0.977 rapidly increases until it levels off to a final viscosity of η = 70.2 mPa s (Figure 33c). Since polymer chain-length correlates with viscosity, it is concluded, that Fe- and Co-MEPE in acetic acid solution (75 vol %) grow until they reach an equilibration viscosity after 18 and 6 days, respectively. In the case of Ni-MEPE a surprisingly fast initial rise in viscosity is observed followed by a decline until a plateau is reached. Obviously, there is another yet unknown process operative, for instance initial formation of aggregates or gels that equilibrate on a longer time scale. However, there is no spectroscopic evidence yet that would confirm the formation of intermediate species other than MEPEs.

The final dynamic viscosities, η, of the MEPEs are shown in Figure 33d. As can be seen, the maxima occur at $V_{Fe^{2+}}/V_{\mathbf{1}}$ = 0.973, $V_{Co^{2+}}/V_{\mathbf{1}}$ = 0.913, and $V_{Ni^{2+}}/V_{\mathbf{1}}$ = 0.977. The deviation between the conductivity minima ($V_{Fe^{2+}}/V_{\mathbf{1}}$ = 1.020, $V_{Co^{2+}}/V_{\mathbf{1}}$ = 0.923, and $V_{Ni^{2+}}/V_{\mathbf{1}}$ = 0.980) and the viscosity maxima, ($V_{Fe^{2+}}/V_{\mathbf{1}}$ = 0.973, $V_{Co^{2+}}/V_{\mathbf{1}}$ = 0.913, and $V_{Ni^{2+}}/V_{\mathbf{1}}$ = 0.977) is 4.6 %, 1.1 %, and 0.3%, respectively, the values obtained in the titration measurements are slightly larger. The titrations are finished in approximately 2 h, where the MEPE chains are not yet completely equilibrated, as indicated by the time scale of the viscosity measurements. While the procedures occur on different time scales and under different experimental boundary conditions the overall error of approx. 2 % is within the experimental error, including impurities and weighing errors. As can be seen in Figure 33d, the dynamic viscosity of Ni-MEPE decreases stronger in the area of metal acetate excess, in accordance with results from Chapter 1.2.3.2.4.2. As expected, Fe-MEPE solutions exhibit higher viscosities than Co-, and Ni-MEPE solutions, due to a higher binding constant, K_2, between metal ion and terpyridine unit.[78] Furthermore, the viscosity of Fe-MEPE solutions are less affected to variations

of the volume ratio, $V_{Fe^{2+}}/V_{\mathbf{1}}$, compared to Co-, and Ni-MEPE solutions, as indicated by the slope of the dotted lines (see Figure 33d).

It is assumed that under these experimental conditions, MEPE synthesis leads to high chain-lengths, and therefore, an expressive growth should be obtained suitable for studying the kinetics of MEPE self-assembly. In the next section, the growth of MEPEs is presented by monitoring the chain-length at different times using static light scattering. Based on this data, a comprehensive analysis of the kinetics of MEPE growth is presented.

3.2.2 Kinetics of MEPE growth

In order to study the kinetics of MEPE growth, the weight average molar masses, $\bar{M}_w$, of the MEPEs are measured at different times, t, by using static light scattering (for details concerning the theory and the data analysis of static light scattering, see Chapter 5.4.3.1). With $\bar{M}_w$ at hand, the conversion, p, is calculated according to eqs (17) and (18) (see Chapter 1.3.1).

After mixing the solutions of ligand **1** and metal acetate the growth of MEPE is monitored. The obtained values for $\bar{M}_w$ vs. t, are shown in Figure 34, exemplary for Co-MEPE.

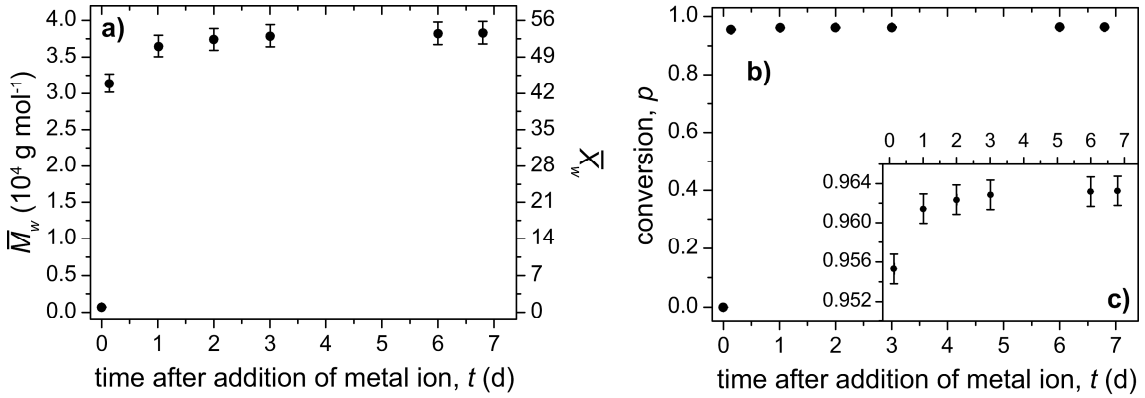

Figure 34. Time dependent (a) weight average molar mass, $\bar{M}_w$, and (b) conversion, p, vs. t of Co-MEPE in acetic acid solution (75 vol %) at a temperature of 20 °C. Inset (c) shows the time dependent conversion in the range of p = 0.948 to 0.966 ($V_{Co^{2+}}/V_{\mathbf{1}}$ = 0.913, Co-MEPE concentration of 4.8 g L^{-1}). The experimental error is within the solid dots (± 7 min) (see text). The reaction volume is kept constant during the experiment. Adapted with permission from ref [188]. Copyright 2017 John Wiley and Sons.

At $t = 0$, the solution of ligand **1** is added to the $Co(OAc)_2$ solution all at once, both dissolved in acetic acid solution (75 vol %). As can be seen in Figure 34a, the weight average molar mass, $\bar{M}_w$, increases with time, t. At the beginning of the reaction, growth proceeds relatively fast and levels off after ~ 6 days at $\bar{M}_w$ = 3.8 × 10^4 g mol^{-1}, which corresponds to a weight average degree of polymerization, $\bar{X}_w$ = 53. Thus, $\bar{M}_w$ is in the same order of magnitude as predicted by the calculations from Figure 18 (1.7 × 10^4 g mol^{-1} at pH = 1.8 and z = 1.00). Figure 34b shows the corresponding conversion of reaction, p, calculated according to eq (20). A volume ratio of $V_{Co^{2+}}/V_{\mathbf{1}}$ = 0.913 is used, as discussed above, at a Co-MEPE concentration of 4.8 g L^{-1} (= 6.7 mM). Since self-assembly of ligand **1** and Co^{2+} proceeds within seconds,[89] it is not possible to obtain data within the first seconds of the reaction. For clarity, a data point at $t = 0$ is added corresponding to the molar mass of the monomer that is $[Co(\mathbf{1})]^{2+}$.

Due to the near-stoichiometric ratio of the reactants (volume ratio of $V_{Co^{2+}}/V_{\mathbf{1}}$ = 0.913) and the absence of cyclization and other side reactions, high conversions (p > 0.95) are

obtained for MEPE growth (see Figure 34). In contrast to common (condensation) polymerizations, metal ion induced self-assembly does not require high temperature, catalyst, or solvent removal. At a first glance, SLS confirms the results from viscosity measurements that MEPE growth occurs on a time scale of days.

Next, the focus is on the analysis of the data in Figure 34 to elucidate the mechanism and kinetics of MEPE growth. Within the experimental conditions the reaction volume is kept constant during polymer growth. Furthermore, it is assumed that side reactions such as branching or ring-closure can be excluded. In the used concentration range, no clouding of the solution or precipitation of MEPE is observed, therefore all metal ions, ligands and MEPE chains in solution are available to react with each other. Also, it is assumed that under the current experimental conditions the polymerization proceeds in a stepwise manner with the weight average molar mass, $\overline{M}_w$, of the MEPE continuously increasing in time. Therefore, the rate of a step polymerization is the sum of the rates of reactions between MEPEs of various sizes. The kinetic analysis is simplified if one further assumes an isodesmic growth mechanism. These simplifying assumptions, often referred to as the "concept of equal reactivity", allow to start the analysis with the equations derived for simple reactions.[228]

The mechanism of step growth polymerizations can be treated by two different theoretical considerations depending on the type of monomer(s) employed.[228] The first involves two different bifunctional monomers in which each monomer possesses only one type of functional group, like it is in MEPE growth, if the metal ion, M^{2+}, and the ligand **1** are regarded as two different bifunctional monomers (see Scheme 29a).

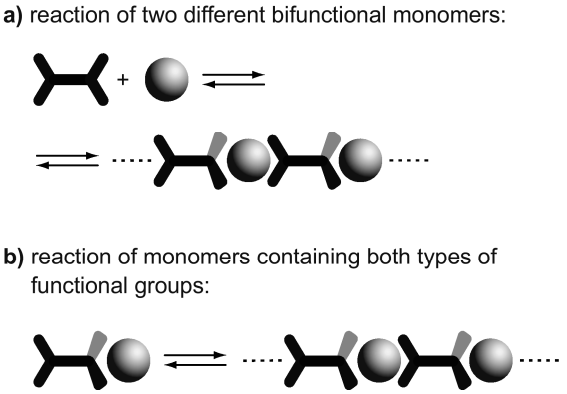

Scheme 29. Theoretical approaches for investigation of MEPE growth involving (a) two different bifunctional monomers in which each monomer possesses only one type of functional group and (b) a single monomer containing both types of functional groups. Reprinted with permission from ref [188]. Copyright 2017 John Wiley and Sons.

The second approach involves a single monomer containing both types of functional groups, like it is in MEPE growth, if the repeat unit, $[M(\mathbf{1})]^{2+}$, is regarded as the monomer (see Scheme 29b). This assumption is reasonable because first it is known that M^{2+} and ligand **1** react to $[M(\mathbf{1})]^{2+}$ within a few seconds in solution and second that due to high binding constant of the chelating terpyridine receptor the concentration of free metal ion and ligand is negligible (see also Figure 17).[89] In the following a closer look at both descriptions is reported.

In order to describe the growth of MEPEs, the applicability of different possible kinetic rate laws is tested on the data in the next section. Depending on the definition of the monomer, the step growth polymerization could either be described as a second-order kinetic mechanism (see Scheme 29a) or as a first-order kinetic mechanism (see Scheme 29b). First, the kinetics of irreversible first-order polymerization kinetics is presented.

3.2.2.1 Irreversible first-order kinetics

Generally, the irreversible first-order kinetics of a species A, is described by

$$\mathrm{A} \xrightarrow{k} \mathrm{B} \tag{31}$$

with A representing a polymerizable group that is the repeat unit, and k being the rate constant of the polymerization reaction. The rate law that is the rate of reaction, v, is defined as the increase of x with time, t:

$$v = \frac{dx}{dt} = k([\mathrm{A}] - x) \tag{32}$$

with x being the extent of reaction, ξ, per unit volume ($x = \xi/V$), t being the time, and $[\mathrm{A}]$ being the initial concentration of the species A.[239, 272] Multiplying with dt and dividing by $([\mathrm{A}] - x)$ to separate the variables followed by integration from $x = 0$ at $t = 0$ to $x = x$ at $t = t$, respectively, yields:[272]

$$\int_0^x \frac{1}{([\mathrm{A}] - x)} dx = \int_0^t k dt \tag{33}$$

Rewriting x as the product of conversion, p, and concentration, $[\mathrm{A}]$:

$$x = p \cdot [\mathrm{A}] \tag{34}$$

simplifies eq (33) to

$$ln\left(\frac{1}{1-p}\right) = kt \tag{35}$$

or by rearranging:

$$p = 1 - e^{-kt} \tag{36}$$

which is the conversion of a first-order reaction of a single component.[272] Here, $[\mathrm{A}]$ corresponds to the initial concentration of the repeat unit, $[\mathrm{M}(\mathbf{1})]^{2+}$. Fitting the

experimentally determined conversion, p, vs. t to eq (36) gives the polymerization rate constant, k. Nonlinear least square curve fitting of the data from Figure 34b by eq (36) is performed applying the Levenberg-Marquardt algorithm (see Chapter 5.4.6).[273-274] The results are shown in Figure 35, χ^2_{red}, is defined as the sum of the squares of the deviations of the calculated and experimental data. The fit of eq (36) to the data in Figure 35 leads to χ^2_{red} = 1.2 × 10^{-3}.

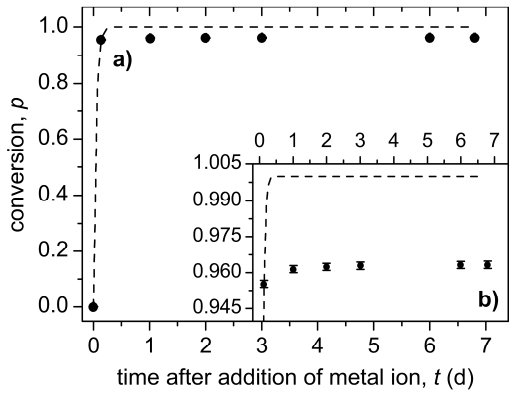

Figure 35. Plot of (a) conversion, p, vs. t according to an irreversible first-order kinetic model with (b) being the inset, exemplary for the growth of Co-MEPE in acetic acid solution (75 vol %) at a temperature of 20 °C. The dashed line shows the nonlinear least square curve fitting of the data by eq (36), applying the Levenberg-Marquardt algorithm with χ^2_{red} = 1.2 × 10^{-3}. Reprinted with permission from ref [188]. Copyright 2017 John Wiley and Sons.

As mentioned above, step growth polymerization can also proceed as a second-order kinetic mechanism, if the metal ion, M^{2+}, and **1** are regarded as bifunctional monomers (see Scheme 29a). Next, the irreversible second-order kinetic rate law is tested on the data.

3.2.2.2 Irreversible second-order kinetics

Generally, the irreversible second-order kinetics of two species A and B, is described as

$$\mathrm{A} + \mathrm{B} \xrightarrow{k} \mathrm{AB} \tag{37}$$

with A and B representing the two polymerizable groups of the repeat unit, and k being as above the rate constant of the polymerization. In this case, the rate law is defined as:[239, 272]

$$v = \frac{dx}{dt} = k([\mathrm{A}] - x)([\mathrm{B}] - x) \tag{38}$$

with x again being the extent of reaction, ξ, per unit volume ($x = \xi/V$), t being the time, and [A] and [B] being the initial concentrations of the metal ion, M^{2+} and **1**, respectively.[239, 272] If the initial concentrations [A] and [B] are equal, the rate expression can be written as

$$v = \frac{dx}{dt} = k([\mathrm{A}] - x)^2 \tag{39}$$

With the same argument as above this equation yields:

$$\int_0^x \frac{1}{([\mathrm{A}] - x)^2} dx = \int_0^t k dt \tag{40}$$

Rewriting x as the product of conversion, p, and initial concentration, [A]:

$$x = p \cdot [\mathrm{A}] \tag{41}$$

eq (40) simplifies to

$$p = \frac{[\mathrm{A}]kt}{[\mathrm{A}]kt + 1} \tag{42}$$

As discussed in the previous section, a near-stoichiometric amount of the reactants is ensured. Therefore, equating the initial concentrations [A] and [B] is justified.

According to eq (42), curve fitting of the experimentally determined conversions, p, vs. t provides the polymerization rate constant, k. Figure 36 shows the nonlinear least square curve fit of the data shown in Figure 34b by eq (42) using the Levenberg-Marquardt algorithm.

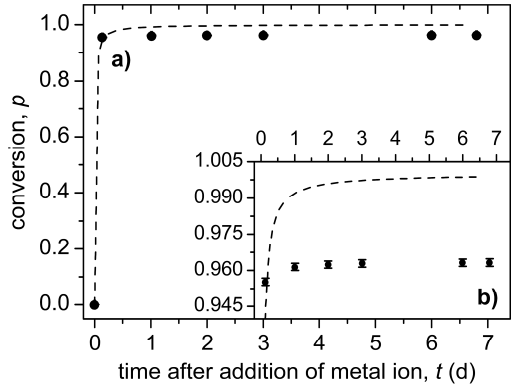

Figure 36. Plot of (a) conversion, p, vs. t according to an irreversible second-order kinetic model with (b) being the inset, exemplary for the growth of Co-MEPE in acetic acid solution (75 vol %) at a temperature of 20 °C. The dashed line shows the nonlinear least square curve fitting of the data by eq (42), applying the Levenberg-Marquardt algorithm with χ^2_{red} = 9.8 × 10^{-4}. Reprinted with permission from ref [188]. Copyright 2017 John Wiley and Sons.

The fit of eq (42) to the data points leads to χ^2_{red} = 9.8 × 10^{-4}, which is a smaller value compared to the previous irreversible first-order kinetic model.

Next, the model will be extended to a reversible first- and second-order kinetic rate law.

3.2.2.3 Reversible first-order kinetics

Generally, the reversible first-order kinetics of a species A, is described by

$$A \underset{k_2}{\overset{k_1}{\rightleftharpoons}} B \tag{43}$$

with A representing the polymerizable repeat unit, and k_1 and k_2 being the rate constants of the forward and reverse polymerization reaction, respectively. The rate law is written as:

$$v = \frac{dx}{dt} = k_1([\mathrm{A}] - x) - k_2([\mathrm{B}] + x) \tag{44}$$

with the variables defined as above.[239, 272] If the initial concentration of the product $[\mathrm{B}] = 0$, the rate expression can be written as

$$v = \frac{dx}{dt} = k_1([\mathrm{A}] - x) - k_2 x \tag{45}$$

and as above, one can write:

$$\int_0^x \frac{1}{([\mathrm{A}] - x) - \left(\frac{x}{K_a}\right)} dx = \int_0^t k_1 dt \tag{46}$$

with $K_a = k_1/k_2$ being the equilibrium constant of the polymerization reaction. Rewriting x as the product of conversion, p, and initial concentration, [A]:

$$x = p \cdot [\mathrm{A}] \tag{47}$$

eq (45) simplifies to

$$\frac{K_a}{1 + K_a} ln\left(\frac{K_a}{K_a - p(1 + K_a)}\right) = k_1 t \tag{48}$$

or by rearranging:

$$p = \frac{K_a\left(1 - e^{\frac{-k_1 t(1+K_a)}{K_a}}\right)}{1 + K_a} \tag{49}$$

The experimental data that is the conversion, p, is fitted by eq (48) to yield the association constant, K_a, and the rate constant of the forward polymerization reaction, k_1. Figure 37 shows the corresponding nonlinear least square curve fit of the data by eq (48).

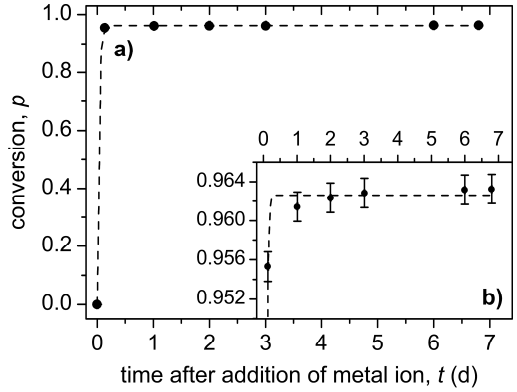

Figure 37. Plot of (a) conversion, p, vs. t according to a reversible first-order kinetic model with (b) being the inset, exemplary for the growth of Co-MEPE in acetic acid solution (75 vol %) at a temperature of 20 °C. The dashed line shows the nonlinear least square curve fitting of the data by eq (48) (χ^2_{red} = 4.4 × 10^{-7}, K_a and k_1 amount to (2.6 ± 0.02) × 10^1 and (3.9 ± 0.1) × 10^{-4} s^{-1}, respectively). Reprinted with permission from ref [188]. Copyright 2017 John Wiley and Sons.

The curve fitting of eq (48) to the data points in Figure 37 leads to χ^2_{red} = 4.4 × 10^{-7}, which is remarkably lower than χ^2 for the curve fitting of the irreversible first- and second-order kinetic models. K_a is calculated to (2.6 ± 0.02) × 10^1 and k_1 is calculated to (3.9 ± 0.1) × 10^{-4} s^{-1}. The rate constant for the reverse polymerization reaction, k_2, amounts to (1.5 ± 0.03) × 10^{-5} s^{-1}. Obviously, k_2 is smaller than k_1, in agreement with the binding of terpyridines and first row transition metal ions.

Finally, the analysis for the reversible second-order kinetic model is presented, where the metal ion, M^{2+} and **1** are regarded as bifunctional monomers (see Scheme 29a).

3.2.2.4 Reversible second-order kinetics

The reversible second-order kinetics of two species A and B, is described by

$$\mathrm{A} + \mathrm{B} \underset{k_2}{\overset{k_1}{\rightleftharpoons}} \mathrm{C} \tag{50}$$

with A and B representing the two polymerizable groups of the repeat unit and k_1 and k_2 being the rate constants for the forward and reverse polymerization reactions, respectively. Therefore, the rate of reaction, v, is defined as:[239, 272]

$$v = \frac{dx}{dt} = k_1([\mathrm{A}] - x)([\mathrm{B}] - x) - k_2([\mathrm{C}] + x) \tag{51}$$

If the initial concentrations [A] and [B] are equal, and the initial concentration of $[\mathrm{C}] = 0$, the rate expression is simplified according to

$$v = \frac{dx}{dt} = k_1([\mathrm{A}] - x)^2 - k_2 x \tag{52}$$

Integration using the above-mentioned limits:

$$\int_0^x \frac{1}{([\mathrm{A}] - x)^2 - \left(\frac{x}{K_a}\right)} dx = \int_0^t k_1 dt \tag{53}$$

where $K_a = k_1/k_2$ is the association constant of the polymerization reaction. Rewriting x as the product of conversion, p, and initial concentration, [A]:

$$x = p \cdot [\mathrm{A}] \tag{54}$$

eq (53) leads to

$$\frac{K_a}{\sqrt{4K_a[\mathrm{A}]+1}} \cdot \cdot ln\frac{\left(2K_a[\mathrm{A}]p-2K_a[\mathrm{A}]-\sqrt{4K_a[\mathrm{A}]+1}-1\right)\left(2K_a[\mathrm{A}]-\sqrt{4K_a[\mathrm{A}]+1}+1\right)}{\left(2K_a[\mathrm{A}]p-2K_a[\mathrm{A}]+\sqrt{4K_a[\mathrm{A}]+1}-1\right)\left(2K_a[\mathrm{A}]+\sqrt{4K_a[\mathrm{A}]+1}+1\right)} = k_1 t \tag{55}$$

or by rearranging

$$p = \frac{2K_a[\mathrm{A}]\left(e^{\frac{k_1 t\sqrt{4K_a[\mathrm{A}]+1}}{K_a}}-1\right)}{\left(2K_a[\mathrm{A}]+\sqrt{4K_a[\mathrm{A}]+1}+1\right)e^{\frac{k_1 t\sqrt{4K_a[\mathrm{A}]+1}}{K_a}}-2K_a[\mathrm{A}]+\sqrt{4K_a[\mathrm{A}]+1}-1} \tag{56}$$

Again, $[\mathrm{A}]$ is the initial concentration of either metal ion, M^{2+} or **1**. The experimental data that is the conversion, p, are fitted by eq (56) to yield the association constant, K_a, and the rate constant for the forward polymerization reaction, k_1. The resulting curve fit is shown in Figure 38 exemplary for Co-MEPE.

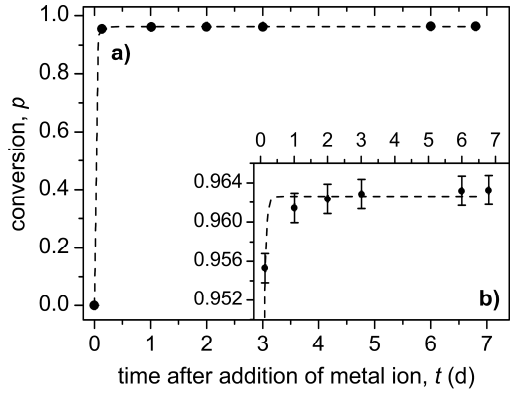

Figure 38. Plot of (a) conversion, p, vs. t according to a reversible second-order kinetic model with (b) being the inset, exemplary for the growth of Co-MEPE in acetic acid solution (75 vol %) at a temperature of 20 °C. The dashed line shows the nonlinear least square curve fitting of the data by eq (56) (χ^2_{red} = 4.4 × 10^{-7}, K_a and k_1 amount to (1.0 ± 0.02) × 10^5 M^{-1} and (3.9 ± 0.1) × 10^{-1} M^{-1} s^{-1}, respectively). Reprinted with permission from ref [188]. Copyright 2017 John Wiley and Sons.

This fit leads to χ^2_{red} = 4.4 × 10^{-7}, identical to the first-order reversible kinetics model. K_a amounts to (1.0 ± 0.02) × 10^5 M^{-1} and k_1 to (3.9 ± 0.1) × 10^{-1} M^{-1} s^{-1}, respectively. Therefore, the rate constant of the reverse polymerization reaction, k_2, results in a much smaller value of (3.9 ± 0.2) × 10^{-6} s^{-1}. Note that the rate constant of the forward polymerization reaction is a second-order rate constant in units of $M^{-1}s^{-1}$, whereas the reverse polymerization reaction rate constant is a first-order rate constant in units of s^{-1}.

Table 4 summarizes the curve fitting results of Co-MEPE growth according to irreversible and reversible first- and second-order kinetics models. In conclusion, the best fits, determined by χ^2_{red} of Co-MEPE growth are obtained by reversible first- and second-order rate laws. The models based on irreversible rate laws deviate from the experimentally determined conversion, providing strong evidence for the reversibility of the metal ion induced self-assembly of Co-MEPE. Also, the results present strong evidence for a step growth polymerization. The observed kinetics in a step growth polymerization should be the same independently whether the polymerization is described by the reaction of A-A and B-B monomers or by the self-reaction of an A-B monomer.[228]

Table 4. Curve fitting results χ^2_{red}, association constants, K_a, as well as the rate constants of the forward polymerization reaction, k_1, and the reverse polymerization reaction, k_2, respectively for the growth of Co-MEPE in acetic acid solution (75 vol %) at a temperature of 20 °C. Adapted with permission from ref [188]. Copyright 2017 John Wiley and Sons.

kinetic model	χ^2_{red}	association constant, K_a	forward polymerization rate constant, k_1	reverse polymerization rate constant, k_2
irreversible first-order	1.2×10^{-3}	-	$(2.6 \pm 0.6) \times 10^{-4}$ s^{-1}	-
irreversible second-order	9.8×10^{-4}	-	(0.2 ± 0.1) M^{-1} s^{-1}	-
reversible first-order	4.4×10^{-7}	$(2.6 \pm 0.02) \times 10^{1}$	$(3.9 \pm 0.1) \times 10^{-4}$ s^{-1}	$(1.5 \pm 0.03) \times 10^{-5}$ s^{-1}
reversible second-order	4.4×10^{-7}	$(1.0 \pm 0.02) \times 10^{5}$ M^{-1}	$(3.9 \pm 0.1) \times 10^{-1}$ M^{-1} s^{-1}	$(3.9 \pm 0.2) \times 10^{-6}$ s^{-1}

As predicted and summarized in Table 4, the forward polymerization rate constant, k_1, clearly exceeds the reverse rate constant, k_2, in a reversible first-order kinetic model. The quotient k_1/k_2 is the association constant, K_a, which reaches a value of $(2.6 \pm 0.02) \times 10^1$ in the case of the reversible first-order kinetic model and for the reversible second-order kinetic model, $K_a = (1.0 \pm 0.02) \times 10^5$ M^{-1}, respectively. The latter association constant can be compared to other well-known linear and columnar supramolecular polymers with a high degree of polymerization. The association constant, $K_a = (1.0 \pm 0.02) \times 10^5$ M^{-1} of Co-MEPEs is a "moderate" to "high" association constant if the classification of Meijer et al.[98] is used (see Chapter 1.3.2). As shown in Table 4, the forward polymerization rate constant, k_1, for the growth of Co-MEPEs is calculated to $(3.9 \pm 0.1) \times 10^{-1}$ M^{-1} s^{-1}, which is a high value, compared to other step polymerizations. Most step polymerizations proceed at slower rates at ordinary temperatures. High temperatures in the range of 150 - 200 °C and higher are frequently used to obtain reasonable polymerization rates. Typical rate constants of step polymerizations are in the order of 10^{-3} M^{-1} s^{-1}. There are a few exceptions of step

polymerizations with significantly larger rate constants, for example, the polymerization reaction between acid halides and alcohols (k_1 = 2.9 × 10^{-3} M^{-1} s^{-1} at a temperature of 58.8 °C).[228] However, compared to radical chain polymerizations, step growth of Co-MEPE proceeds at a remarkably lower rate constant. Normally, the rate constants for the propagation of radical chain polymerizations are in the range of k_1 = 10^2 - 10^4 M^{-1} s^{-1}.[228, 275]

3.2.2.5 Reversible second-order kinetics with [A] ≠ [B]

As discussed above, it is assumed that usage of a volume ratio of $V_{Co^{2+}}/V_{\mathbf{1}}$ = 0.913 leads to near-stoichiometric amounts of the reactants that is the metal ion to ligand ratio, y = 1. This assumption is verified by curve fitting of the conversion, p, according to a reversible second-order kinetic model, where the initial concentrations $[\mathrm{A}] \neq [\mathrm{B}]$. With $[\mathrm{A}] \neq [\mathrm{B}]$, eq (51) leads to

$$v = \frac{dx}{dt} = k_1([\mathrm{A}] - x)([\mathrm{B}] - x) - \frac{k_1}{K_a}x \tag{57}$$

where $K_a = k_1/k_2$ is the association constant of the polymerization reaction. This may be integrated after first multiplying with dt and then dividing by $([\mathrm{A}] - x)([\mathrm{B}] - x) - \frac{x}{K_a}$ to get the variables separated. The limits of integration are taken as $x = 0$ at $t = 0$ and $x = x$ at $t = t$, respectively:[239, 272]

$$\int_0^x \frac{1}{([\mathrm{B}]y - x)([\mathrm{B}] - x) - \left(\frac{x}{K_a}\right)} dx = \int_0^t k_1 dt \tag{58}$$

with $y = [\mathrm{A}]/[\mathrm{B}]$ as the metal ion to ligand ratio. Rewriting x as the product of conversion, p, and initial concentration, $[\mathrm{B}]$:

$$x = p \cdot [\mathrm{B}] \tag{59}$$

eq (58) leads to

$$\frac{1}{d} ln \frac{(K_a[\mathrm{B}](2p - y - 1) - K_a d - 1)(K_a d - K_a[\mathrm{B}](y + 1) + 1)}{(K_a[\mathrm{B}](2p - y - 1) + K_a d - 1)(K_a d + K_a[\mathrm{B}](y + 1) + 1)} = k_1 t \tag{60}$$

with

$$d = \sqrt{\frac{1}{{K_a}^2} + \frac{2[\mathrm{B}](y + 1)}{K_a} + [\mathrm{B}]^2(y - 1)^2} \tag{61}$$

Equations (60) and (61) can be rearranged:

$$p = \frac{2K_a[\mathrm{B}]y}{\left(\frac{2d}{e^{k_1 t d} - 1}\right) + k[\mathrm{B}](y + 1) + dK_a + 1} \tag{62}$$

In case of MEPE growth, [A] and [B] correspond to the initial concentrations of the metal ion, M^{2+}, and **1**. The experimental data that is the conversion, p, are fitted by eq (62) to yield the association constant, K_a, the rate constant for the forward polymerization reaction, k_1, and the metal ion to ligand ratio, y. Nonlinear least square curve fitting of the data from Figure 39 by eq (62) is performed applying the Levenberg-Marquardt algorithm.[273-274] The curve fitting is shown in Figure 39.

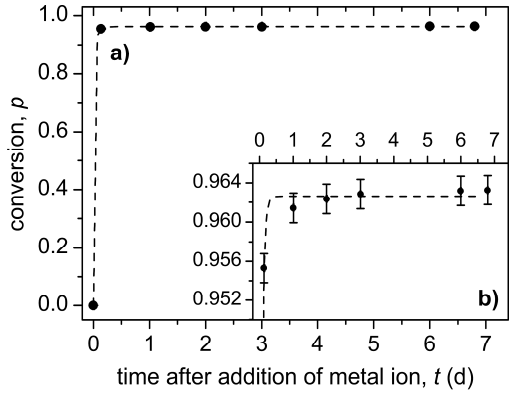

Figure 39. Plot of (a) conversion, p, vs. t according to a reversible second-order kinetic model ($[\mathrm{A}] \neq [\mathrm{B}]$) with (b) being the inset, exemplary for the growth of Co-MEPE in acetic acid solution (75 vol %) at a temperature of 20 °C. The dashed line shows the nonlinear least square curve fitting of the data by eq (62) (χ^2_{red} = 4.5 × 10^{-7}, K_a, k_1, k_2, and y are calculated to 1.1 × 10^5 M^{-1}, 0.39 M^{-1} s^{-1}, 3.5 × 10^{-6} s^{-1}, and 0.99938, respectively). Reprinted with permission from ref [188]. Copyright 2017 John Wiley and Sons.

K_a is calculated to 1.1 × 10^5 M^{-1} and k_1 is calculated to 0.39 M^{-1} s^{-1}. Therefore, the rate constant for the reverse polymerization reaction, k_2 results to 3.5 × 10^{-6} s^{-1} with χ^2_{red} leading to 4.5 × 10^{-7}. The curve fitting leads to a metal ion to ligand ratio y = 0.99938. All values are nearly the same as calculated for a reversible second-order kinetic model with $[\mathrm{A}] = [\mathrm{B}]$ (see Table 4). Thus, the synthesis protocol provides reproducible near-stoichiometric conditions for MEPE preparation.

3.2.2.6 Effect of salt addition on the growth of Co-MEPEs

In the following section, the effect of salt addition on the growth of MEPEs is examined. For this purpose, potassium acetate is added, which is expected to screen the electrostatic repulsion between neighboring charged metal complexes.[276] A solution of $Co(OAc)_2$ in acetic acid solution (75 vol %) is mixed with potassium acetate (0.1 M) and after that **1** is added to the mixture. Again, the growth of the resulting Co-MEPEs

is obtained by the time dependent weight average molar mass, $\bar{M}_w$. As discussed above the time dependent conversion, p, is calculated and the four different possible kinetic rate laws (reversible and irreversible first- and second-order kinetics) are tested on the data. The curve fitting results are shown in Figure 40 and Table 5.

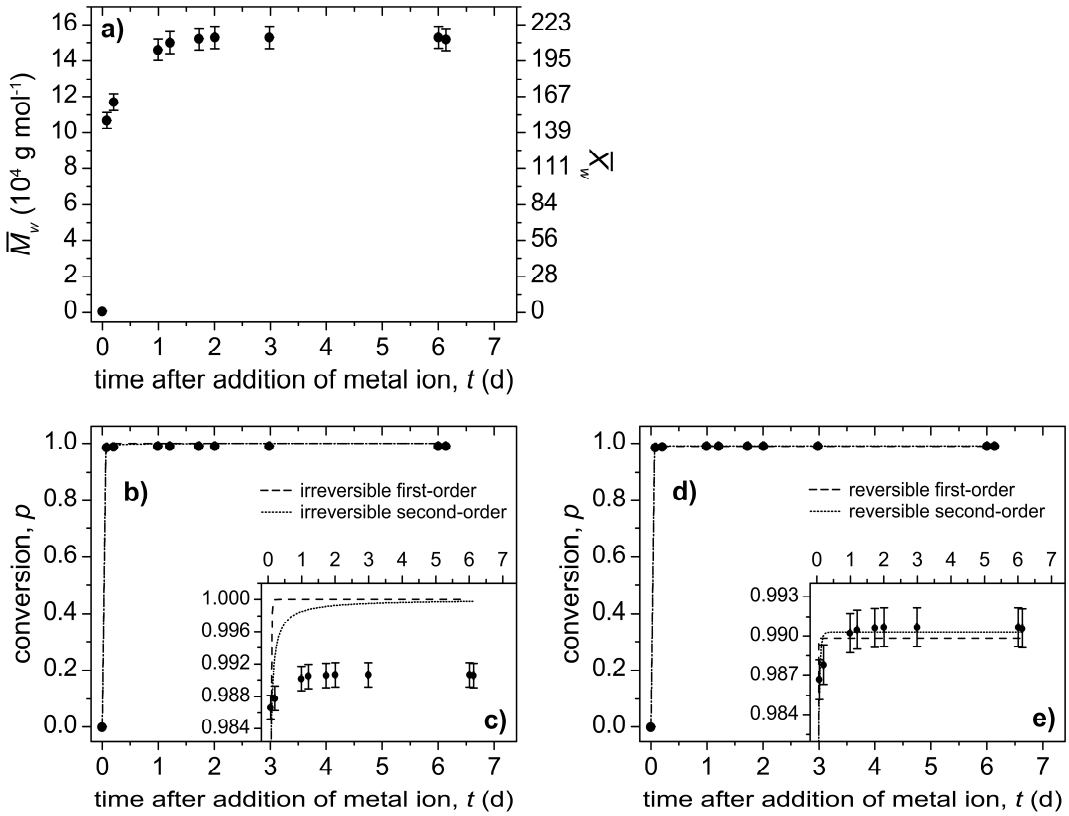

Figure 40. Time dependent growth of Co-MEPEs containing 0.1 M KOAc by monitoring (a) the weight average molar mass, $\bar{M}_w$, and plot of conversion, p, vs. t according to (b) irreversible kinetic models with (c) being the inset, and (d) reversible kinetic models with (e) being the inset in acetic acid solution (75 vol %) at a temperature of 20 °C. A volume ratio of $V_{Co^{2+}}/V_{\mathbf{1}}$ = 0.913 was used at Co-MEPE concentration of 4.8 g L^{-1}. The results of the nonlinear least square curve fitting of the data are summarized in Table 5. Reprinted with permission from ref [188]. Copyright 2017 John Wiley and Sons.

Table 5. Curve fitting results χ^2_{red}, association constants, K_a, as well as the rate constants for the forward polymerization reaction, k_1, and the reverse polymerization reaction, k_2, respectively for the growth of Co-MEPE containing 0.1 M KOAc in acetic acid solution (75 vol %) at a temperature of 20 °C. Adapted with permission from ref [188]. Copyright 2017 John Wiley and Sons.

kinetic model	χ^2_{red}	**association constant,** K_a	**forward polymerization rate constant,** k_1	**reverse polymerization rate constant,** k_2
irreversible first-order	8.6×10^{-5}	-	$(6.3 \pm 1.0) \times 10^{-4}$ s^{-1}	-
irreversible second-order	6.4×10^{-5}	-	(1.2 ± 0.5) M^{-1} s^{-1}	-
reversible first-order	2.2×10^{-6}	$(9.7 \pm 0.5) \times 10^{1}$	$(5.2 \pm 0.3) \times 10^{-3}$ s^{-1}	$(5.4 \pm 0.4) \times 10^{-5}$ s^{-1}
reversible second-order	7.3×10^{-7}	$(1.6 \pm 0.1) \times 10^{6}$ M^{-1}	(2.0 ± 0.2) M^{-1} s^{-1}	$(1.3 \pm 0.2) \times 10^{-6}$ s^{-1}

As already observed for Co-MEPE without salt addition, the growth can be described as first- or second-order reversible step growth polymerization. However, as shown in Table 5, χ^2_{red} reaches the lowest value, if a reversible second-order kinetics model is applied. The association constant, K_a, is calculated to $(1.6 \pm 0.1) \times 10^6$ M^{-1}, which is 16 times higher than K_a for Co-MEPE growth without addition of salt. The forward polymerization rate constant, k_1, is with (2.0 ± 0.2) M^{-1} s^{-1} about 5 times larger than the value obtained for the growth kinetics without salt addition.

However, the reverse rate constant, k_2, is with $(1.3 \pm 0.2) \times 10^{-6}$ s^{-1} lower (about a third) than the value obtained without salt addition. Thus, the addition of 0.1 M KOAc accelerates the growth of Co-MEPEs and causes a higher association constant presumably due to Debye screening between neighboring charged metal complexes as well as between charged MEPE chains.[276]

Likewise, the growth of Ni-, and Fe-MEPE with and without salt addition is examined. Again, the growth of the resulting Fe-, and Ni-MEPEs are obtained by the time dependent weight average molar mass, $\bar{M}_w$, which leads to the time dependent conversion, p, and the four different possible kinetic rate laws are tested on the data. The corresponding curve fitting graphics are shown in the following Chapters 3.2.2.7 to 3.2.2.10.

3.2.2.7 Growth of Fe-MEPE without salt addition

In order to describe the growth of Fe-MEPEs without salt addition, the applicability of different possible kinetic rate laws is tested on the data. The curve fitting procedure is analogous to the procedure, shown in Chapter 3.2 for the growth of Co-MEPEs without any salt addition. The curve fitting results are shown in Figure 41 and Table 6.

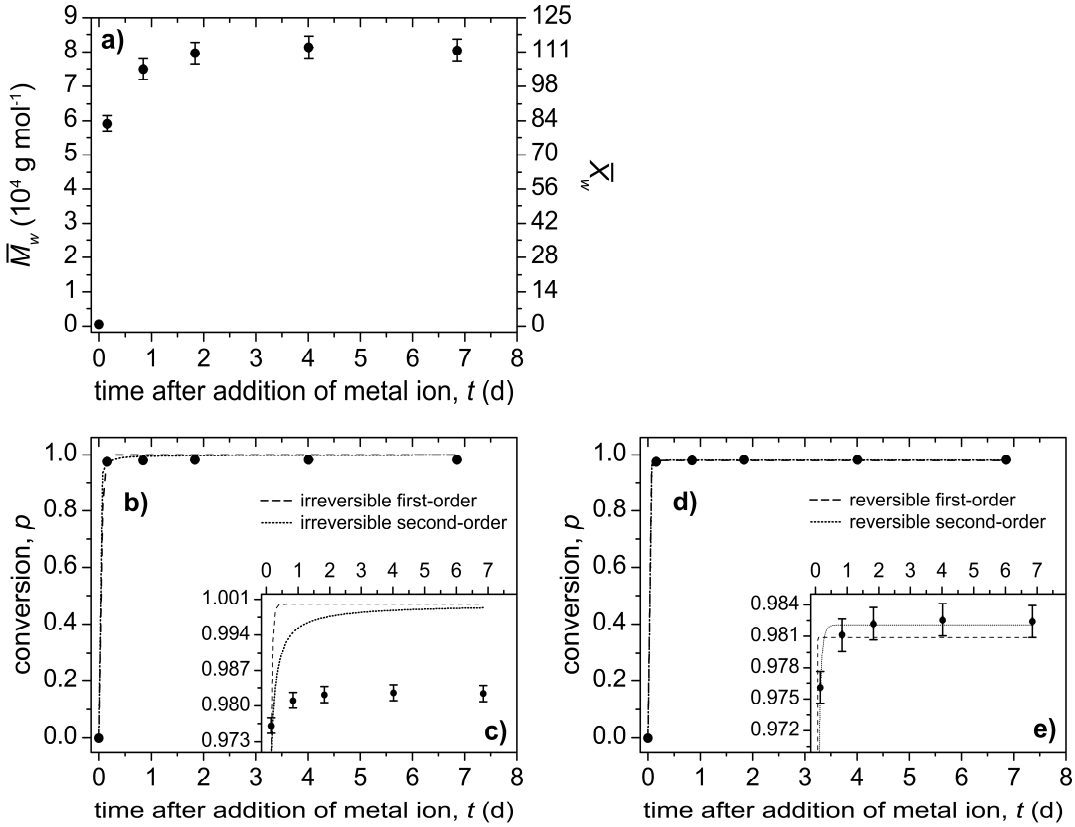

Figure 41. Time dependent growth of Fe-MEPEs without salt addition by monitoring (a) the weight average molar mass, $\bar{M}_w$, and plot of conversion, p, vs. t according to (b) irreversible kinetic models with (c) being the inset, and (d) reversible kinetic models with (e) being the inset in acetic acid solution (75 vol %) at a temperature of 20 °C. A volume ratio of $V_{Fe^{2+}}/V_1$ = 0.933 was used at Fe-MEPE concentration of 4.8 g L^{-1}. The results of the nonlinear least square curve fitting of the data are summarized in Table 6. Reprinted with permission from ref [188]. Copyright 2017 John Wiley and Sons.

Table 6. Curve fitting results χ^2_{red}, association constants, K_a, as well as the rate constants for the forward polymerization reaction, k_1, and the reverse polymerization reaction, k_2, respectively for the growth of Fe-MEPE without salt addition in acetic acid solution (75 vol %) at a temperature of 20 °C. The forward polymerization rate constants, k_1, obtained by using the irreversible kinetic models are shown in parentheses. Adapted with permission from ref [188]. Copyright 2017 John Wiley and Sons.

kinetic model	χ^2_{red}	**association constant,** K_a	**forward polymerization rate constant,** k_1	**reverse polymerization rate constant,** k_2
irreversible first-order	2.6×10^{-4}	-	$(2.7 \pm 0.5) \times 10^{-4}$ s^{-1}	-
irreversible second-order	2.0×10^{-4}	-	(0.4 ± 0.2) M^{-1} s^{-1}	-
reversible first-order	7.4×10^{-6}	$(5.1 \pm 0.3) \times 10^{1}$	$(2.9 \pm 0.2) \times 10^{-3}$ s^{-1}	$(5.7 \pm 0.5) \times 10^{-5}$ s^{-1}
reversible second-order	3.2×10^{-7}	$(4.5 \pm 0.1) \times 10^{5}$ M^{-1}	(0.6 ± 0.03) M^{-1} s^{-1}	$(1.3 \pm 0.1) \times 10^{-6}$ s^{-1}

3.2.2.8 Growth of Fe-MEPE containing 0.1 M KOAc

In order to describe the growth of Fe-MEPEs containing 0.1 M KOAc, the applicability of different possible kinetic rate laws is tested on the data. The curve fitting procedure is analogous to the procedure, shown in Chapter 3.2 for the growth of Co-MEPEs without any salt addition. The curve fitting results are shown in Figure 42 and Table 7.

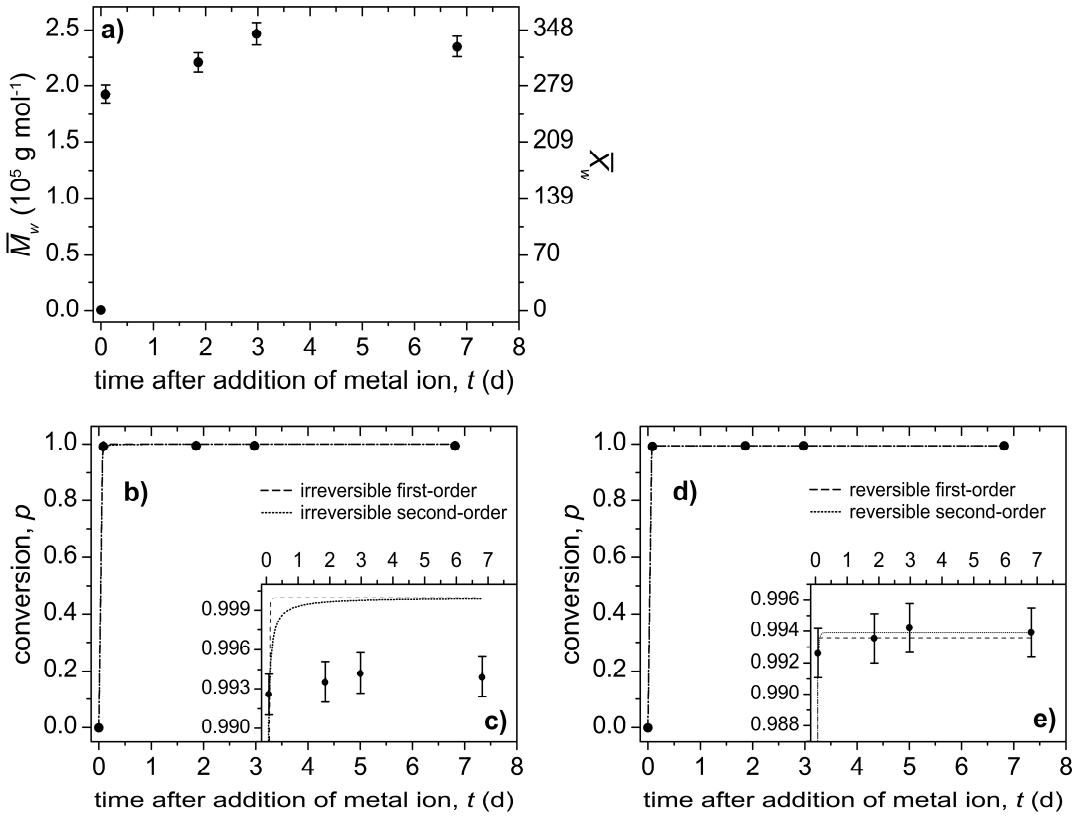

Figure 42. Time dependent growth of Fe-MEPEs containing 0.1 M KOAc by monitoring (a) the weight average molar mass, $\overline{M}_w$, and plot of conversion, p, vs. t according to (b) irreversible kinetic models with (c) being the inset, and (d) reversible kinetic models with (e) being the inset in acetic acid solution (75 vol %) at a temperature of 20 °C. A volume ratio of $V_{Fe^{2+}}/V_{\mathbf{1}}$ = 0.933 was used at Fe-MEPE concentration of 4.8 g L^{-1}. The results of the nonlinear least square curve fitting of the data are summarized in Table 7. Reprinted with permission from ref [188]. Copyright 2017 John Wiley and Sons.

Table 7. Curve fitting results χ^2_{red}, association constants, K_a, as well as the rate constants for the forward polymerization reaction, k_1, and the reverse polymerization reaction, k_2, respectively for the growth of Fe-MEPE containing 0.1 M KOAc in acetic acid solution (75 vol %) at a temperature of 20 °C. The forward polymerization rate constants, k_1, obtained by using the irreversible kinetic models are shown in parentheses. Adapted with permission from ref [188]. Copyright 2017 John Wiley and Sons.

kinetic model	χ^2_{red}	association constant, K_a	forward polymerization rate constant, k_1	reverse polymerization rate constant, k_2
irreversible first-order	2.8×10^{-5}	-	$(6.6 \pm 1.0) \times 10^{-4}$ s^{-1}	-
irreversible second-order	2.6×10^{-5}	-	(2.5 ± 1.6) M^{-1} s^{-1}	-
reversible first-order	4.9×10^{-7}	$(1.5 \pm 0.1) \times 10^{2}$	$(8.2 \pm 0.5) \times 10^{-3}$ s^{-1}	$(5.5 \pm 0.4) \times 10^{-5}$ s^{-1}
reversible second-order	7.5×10^{-8}	$(3.9 \pm 0.2) \times 10^{6}$ M^{-1}	(3.8 ± 0.3) M^{-1} s^{-1}	$(9.7 \pm 1.0) \times 10^{-7}$ s^{-1}

3.2.2.9 Growth of Ni-MEPE without salt addition

In order to describe the growth of Ni-MEPEs without salt addition, the applicability of different possible kinetic rate laws is tested on the data. The curve fitting procedure is analogous to the procedure, shown in Chapter 3.2 for the growth of Co-MEPEs without any salt addition. The curve fitting results are shown in Figure 43 and Table 8.

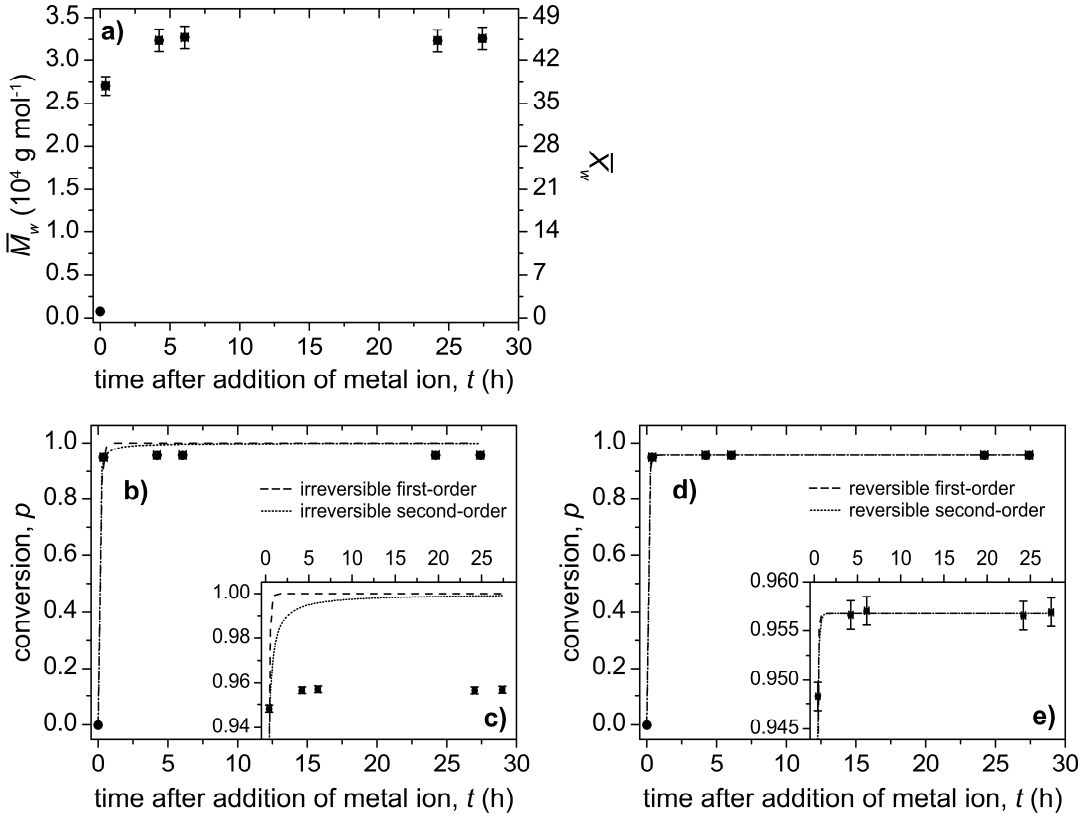

Figure 43. Time dependent growth of Ni-MEPEs without salt addition by monitoring (a) the weight average molar mass, $\bar{M}_w$, and plot of conversion, p, vs. t according to (b) irreversible kinetic models with (c) being the inset, and (d) reversible kinetic models with (e) being the inset in acetic acid solution (75 vol %) at a temperature of 20 °C. A volume ratio of $V_{Ni^{2+}}/V_{\mathbf{1}}$ = 0.977 was used at Ni-MEPE concentration of 4.8 g L^{-1}. The results of the nonlinear least square curve fitting of the data are summarized in Table 8. Reprinted with permission from ref [188]. Copyright 2017 John Wiley and Sons.

Table 8. Curve fitting results χ^2_{red}, association constants, K_a, as well as the rate constants for the forward polymerization reaction, k_1, and the reverse polymerization reaction, k_2, respectively for the growth of Ni-MEPE without salt addition in acetic acid solution (75 vol %) at a temperature of 20 °C. The forward polymerization rate constants, k_1, obtained by using the irreversible kinetic models are shown in parentheses. Adapted with permission from ref [188]. Copyright 2017 John Wiley and Sons.

kinetic model	χ^2_{red}	**association constant,** K_a	**forward polymerization rate constant,** k_1	**reverse polymerization rate constant,** k_2
irreversible first-order	1.5×10^{-3}	-	$(2.1 \pm 0.5) \times 10^{-3}$ s^{-1}	-
irreversible second-order	1.3×10^{-3}	-	(1.6 ± 1.0) M^{-1} s^{-1}	-
reversible first-order	4.0×10^{-8}	$(2.2 \pm 0.01) \times 10^{1}$	$(3.1 \pm 0.01) \times 10^{-3}$ s^{-1}	$(1.4 \pm 0.01) \times 10^{-4}$ s^{-1}
reversible second-order	4.0×10^{-8}	$(7.5 \pm 0.04) \times 10^{4}$ M^{-1}	(2.7 ± 0.03) M^{-1} s^{-1}	$(3.6 \pm 0.04) \times 10^{-5}$ s^{-1}

3.2.2.10 Growth of Ni-MEPE containing 0.1 M KOAc

In order to describe the growth of Ni-MEPEs containing 0.1 M KOAc, the applicability of different possible kinetic rate laws is tested on the data. The curve fitting procedure is analogous to the procedure, shown in Chapter 3.2 for the growth of Co-MEPEs without any salt addition. The curve fitting results are shown in Figure 44 and Table 9.

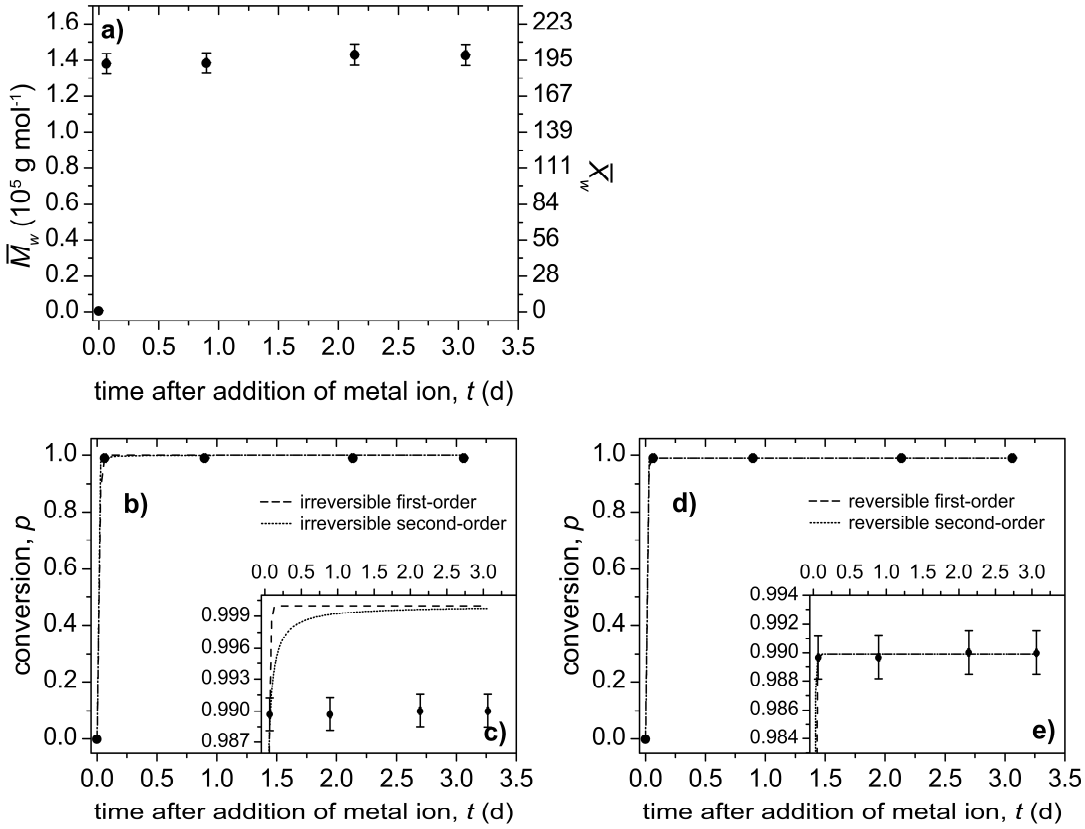

Figure 44. Time dependent growth of Ni-MEPEs containing 0.1 M KOAc by monitoring (a) the weight average molar mass, $\bar{M}_w$, and plot of conversion, p, vs. t according to (b) irreversible kinetic models with (c) being the inset, and (d) reversible kinetic models with (e) being the inset in acetic acid solution (75 vol %) at a temperature of 20 °C. A volume ratio of $V_{Ni^{2+}}/V_{\mathbf{1}}$ = 0.977 was used at Ni-MEPE concentration of 4.8 g L^{-1}. The results of the nonlinear least square curve fitting of the data are summarized in Table 9. Reprinted with permission from ref [188]. Copyright 2017 John Wiley and Sons.

Table 9. Curve fitting results χ^2_{red}, association constants, K_a, as well as the rate constants for the forward polymerization reaction, k_1, and the reverse polymerization reaction, k_2, respectively for the growth of Ni-MEPE containing 0.1 M KOAc in acetic acid solution (75 vol %) at a temperature of 20 °C. The forward polymerization rate constants, k_1, obtained by using the irreversible kinetic models are shown in parentheses. Adapted with permission from ref [188]. Copyright 2017 John Wiley and Sons.

kinetic model	χ^2_{red}	**association constant,** K_a	**forward polymerization rate constant,** k_1	**reverse polymerization rate constant,** k_2
irreversible first-order	7.6×10^{-5}	-	$(8.1 \pm 1.5) \times 10^{-4}$ s^{-1}	-
irreversible second-order	7.0×10^{-5}	-	(2.2 ± 1.6) M^{-1} s^{-1}	-
reversible first-order	2.3×10^{-8}	$(9.8 \pm 0.1) \times 10^{1}$	$(1.5 \pm 0.1) \times 10^{-3}$ s^{-1}	$(1.5 \pm 0.1) \times 10^{-5}$ s^{-1}
reversible second-order	2.3×10^{-8}	$(1.4 \pm 0.03) \times 10^{6}$ M^{-1}	(5.7 ± 0.9) M^{-1} s^{-1}	$(4.1 \pm 0.4) \times 10^{-6}$ s^{-1}

3.2.2.11 Overview of curve fitting results

All curve fitting results are summarized in Table 10 (reversible first-order kinetic model) and Table 11 (reversible second-order model).

Table 10. Curve fitting results χ^2_{red}, association constants, K_a, as well as the rate constants for the forward polymerization reaction, k_1, and the reverse polymerization reaction, k_2, respectively for the polymerization for a reversible first-order kinetic model of the different MEPEs in acetic acid solution (75 vol %) at a temperature of 20 °C. Adapted with permission from ref [188]. Copyright 2017 John Wiley and Sons.

reversible first-order kinetic model	χ^2_{red}	**association constant,** K_a	**forward polymerization rate constant,** k_1	**reverse polymerization rate constant,** k_2
Fe-MEPE without salt	7.4×10^{-6}	$(5.1 \pm 0.3) \times 10^{1}$	$(2.9 \pm 0.2) \times 10^{-3}$ s^{-1}	$(5.7 \pm 0.5) \times 10^{-5}$ s^{-1}
Fe-MEPE with 0.1 M KOAc	4.9×10^{-7}	$(1.5 \pm 0.1) \times 10^{2}$	$(8.2 \pm 0.5) \times 10^{-3}$ s^{-1}	$(5.5 \pm 0.4) \times 10^{-5}$ s^{-1}
Co-MEPE without salt	4.4×10^{-7}	$(2.6 \pm 0.02) \times 10^{1}$	$(3.9 \pm 0.1) \times 10^{-4}$ s^{-1}	$(1.5 \pm 0.03) \times 10^{-5}$ s^{-1}
Co-MEPE with 0.1 M KOAc	2.2×10^{-6}	$(9.7 \pm 0.5) \times 10^{1}$	$(5.2 \pm 0.3) \times 10^{-3}$ s^{-1}	$(5.4 \pm 0.4) \times 10^{-5}$ s^{-1}
Ni-MEPE without salt	4.0×10^{-8}	$(2.2 \pm 0.01) \times 10^{1}$	$(3.1 \pm 0.01) \times 10^{-3}$ s^{-1}	$(1.4 \pm 0.01) \times 10^{-4}$ s^{-1}
Ni-MEPE with 0.1 M KOAc	2.3×10^{-8}	$(9.8 \pm 0.1) \times 10^{1}$	$(1.5 \pm 0.1) \times 10^{-3}$ s^{-1}	$(1.5 \pm 0.1) \times 10^{-5}$ s^{-1}

Table 11. Curve fitting results χ^2_{red}, association constants, K_a, as well as the rate constants for the forward polymerization reaction, k_1, and the reverse polymerization reaction, k_2, respectively for the polymerization for a reversible second-order kinetic model of the different MEPEs in acetic acid solution (75 vol %) at a temperature of 20 °C. Adapted with permission from ref [188]. Copyright 2017 John Wiley and Sons.

reversible second-order kinetic model	χ^2_{red}	association constant, K_a	forward polymerization rate constant, k_1	reverse polymerization rate constant, k_2
Fe-MEPE without salt	3.2 × 10^{-7}	(4.5 ± 0.1) × 10^5 M^{-1}	(0.6 ± 0.03) M^{-1} s^{-1}	(1.3 ± 0.1) × 10^{-6} s^{-1}
Fe-MEPE with 0.1 M KOAc	7.5 × 10^{-8}	(3.9 ± 0.2) × 10^6 M^{-1}	(3.8 ± 0.3) M^{-1} s^{-1}	(9.7 ± 1.0) × 10^{-7} s^{-1}
Co-MEPE without salt	4.4 × 10^{-7}	(1.0 ± 0.02) × 10^5 M^{-1}	(3.9 ± 0.1) × 10^{-1} M^{-1} s^{-1}	(3.9 ± 0.2) × 10^{-6} s^{-1}
Co-MEPE with 0.1 M KOAc	7.3 × 10^{-7}	(1.6 ± 0.1) × 10^6 M^{-1}	(2.0 ± 0.2) M^{-1} s^{-1}	(1.3 ± 0.2) × 10^{-6} s^{-1}
Ni-MEPE without salt	4.0 × 10^{-8}	(7.5 ± 0.04) × 10^4 M^{-1}	(2.7 ± 0.03) M^{-1} s^{-1}	(3.6 ± 0.04) × 10^{-5} s^{-1}
Ni-MEPE with 0.1 M KOAc	2.3 × 10^{-8}	(1.4 ± 0.03) × 10^6 M^{-1}	(5.7 ± 0.9) M^{-1} s^{-1}	(4.1 ± 0.4) × 10^{-6} s^{-1}

The growth of MEPEs can be described as a first- or second-order reversible step growth polymerization process. However, χ^2_{red} reaches the lowest value, if a reversible second-order kinetic model is applied, as can be seen in Table 10 and Table 11. Thus, the focus is on the results of the reversible second-order kinetic model in the following. As can be seen in Table 11, all association constants, K_a, yield higher values (factor ~ 9, 16, and 19 for Fe-, Co-, and Ni-MEPE, respectively) in the presence of KOAc. Thus, increasing the ionic strength leads to higher molar masses for all MEPEs. Furthermore,

K_a follows the order Ni-MEPE < Co-MEPE < Fe-MEPE. Regarding the forward polymerization rate constants, k_1, also higher values by adding 0.1 M KOAc as a salt are obtained (factor ~ 6, 5, and 2 for Fe-, Co-, and Ni-MEPE, respectively).

Independent of salt addition, the forward polymerization rate constant, k_1, follows the order Co-MEPE < Fe-MEPE < Ni-MEPE. As shown in Table 1 in Chapter 1.2.2.2, $K_1 \cdot K_2$ follows the same order ($K_1 \cdot K_2$ = 2.0 × 10^{18}, 7.9 × 10^{20}, and 6.3 × 10^{21} for Co-, Fe-, and Ni-bisterpyridine complexes, respectively).[78] Thus, it is concluded that k_1 increases with an increasing total binding constant between metal ion and terpyridine receptor. On the other hand, the reverse polymerization rate constants, k_2, are smaller upon salt addition. They follow the order Fe-MEPE < Co-MEPE < Ni-MEPE, which is the opposite way regarding the order of K_a. Obviously, a lower association constant, K_a, correlates with an increased possibility of bond-breaking that is a higher reverse polymerization rate constant, k_2, and vice versa. This result supports the hypothesis that positively charged MEPE chains are stabilized in the presence of extra salt. Furthermore, the association constant, K_a, correlates well with the conversion, p, according to eq (63):[143, 195, 246, 261]

$$K_a \approx \frac{1}{4c(1-p)^2} \tag{63}$$

with c being the concentration. The results are shown in Table 12.

Table 12. Correlation of K_a with p according to eq (63). Adapted with permission from ref [188]. Copyright 2017 John Wiley and Sons.

reversible second-order kinetic model	p	**association constant, K_a, calculated according to eq (63)**
Fe-MEPE without salt	0.983	1.3×10^5 M^{-1}
Fe-MEPE with 0.1 M KOAc	0.994	1.0×10^6 M^{-1}
Co-MEPE without salt	0.963	2.7×10^4 M^{-1}
Co-MEPE with 0.1 M KOAc	0.990	3.7×10^5 M^{-1}
Ni-MEPE without salt	0.957	2.0×10^4 M^{-1}
Ni-MEPE with 0.1 M KOAc	0.990	3.7×10^5 M^{-1}

As can be seen in Table 12, the calculated association constants, K_a, are lower than the values found by application of the kinetic model (see Table 11), but are still in the same order of magnitude.

Regarding the weight average molar masses of the MEPEs, $\bar{M}_w$ is increasing up to 2.5×10^5 g mol^{-1} in Fe-MEPEs containing 0.1 M KOAc, which corresponds to a weight average degree of polymerization, $\bar{X}_w$ = 350 (see Figure 42). An overview of the achieved degrees of polymerization, $\bar{X}_w$, for the different MEPEs with and without salt addition is given in Figure 45.

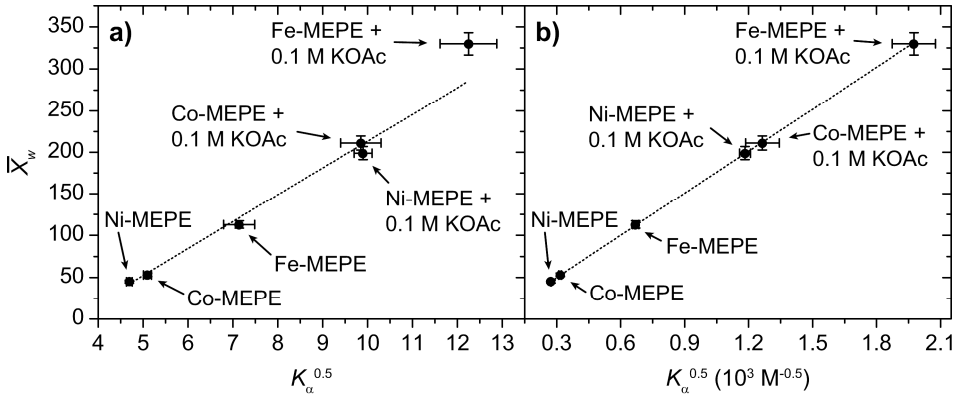

Figure 45. Plot of the weight average degree of polymerization, $\bar{X}_w$, vs. association constant, $K_a^{0.5}$, of the different MEPEs with and without salt addition according to the reversible (a) first- and (b) second-order kinetic model in acetic acid solution (75 vol %) at a temperature of 20 °C. The dotted lines show the linear curve fitting of the data by eq (64). Adapted with permission from ref [188]. Copyright 2017 John Wiley and Sons.

Without salt addition, $\bar{M}_w$ results to 8.1 × 10^4 g mol^{-1}, 3.8 × 10^4 g mol^{-1}, and 3.3 × 10^4 g mol^{-1} for Fe-, Co-, and Ni-MEPE, respectively. These values are in the same order of magnitude than the calculated values from Figure 18 in Chapter 1.2.3.2.4.2 (2.1 × 10^5 g mol^{-1}, 1.7 × 10^4 g mol^{-1}, and 7.7 × 10^4 g mol^{-1} for Fe-, Co-, and Ni-MEPE at pH = 1.8 and y = 1). As can be seen, both, $\bar{X}_w$, and association constant, K_a, increase in the order Ni-MEPE ~ Co-MEPE < Fe-MEPE. As known for isodesmic polymerizations,[107, 242] $\bar{X}_w$ is simply related to K_a by the approximate relationship:

$$\bar{X}_w \sim K_a^{0.5} \tag{64}$$

which is valid for K_a >> 1.[107, 242] As can be seen from Figure 45, the data calculated by the reversible second-order model (Figure 45b) are more suitable to eq (64) than the data calculated by the reversible first-order model (Figure 45a).

3.2.3 Microscopic Characterization

In order to investigate the structure and length of finally grown MEPEs, cryogenic Transmission Electron Microscopy (cryo-TEM) imaging is employed. After four-day aging, cryo-TEM images of a solution of finally grown and solid Fe-MEPE in water (10^{-4} M) revealed the formation of entangled bundles of molecular fibers which are (1.3 ± 0.2) nm in width and 100's nm to microns long (see Figure 46). To the best of knowledge, high-resolution cryo-TEM images of MEPEs are obtained for the first time. This data confirms the central hypothesis that metal ion induced self-assembly of ditopic ligands results in linear rigid-rod type macromolecules.

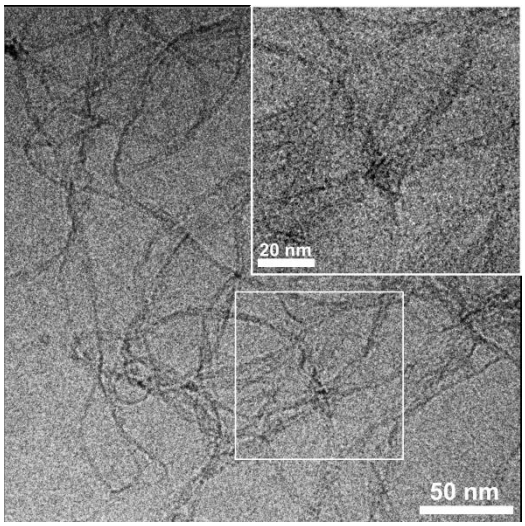

Figure 46. A representative cryo-TEM image of a solution of Fe-MEPE (10^{-4} M) in water after four days of aging, showing the formation of bundled molecular fibers (scale bar: 50 nm). The inset is the magnified image of the area inside the white frame. The fine structure of the bundles, which consists of molecular fibers, is illustrated (scale bar: 20 nm). Reprinted with permission from ref [188]. Copyright 2017 John Wiley and Sons.

3.3 Conclusions

In this Chapter concerning the metal ion induced self-assembly of metallo-supramolecular coordination polyelectrolytes (MEPEs), experiments are presented that elucidate the growth kinetics of Fe-, Co-, and Ni-MEPEs. The kinetics of polymerization can be best treated as a reversible first- and second-order step growth model. The irreversible models do not fit well. High molar masses are obtained and the association constants follow the order Ni-MEPE ~ Co-MEPE < Fe-MEPE, whereas the polymerization rate constants follow the order of Co-MEPE < Fe-MEPE < Ni-MEPE. Interestingly, the growth of MEPEs is accelerated by addition of potassium acetate. The extraordinary chain-length found in solution is confirmed by cryo-TEM data, revealing essentially plethora of filaments and bundles thereof.

4

Tailoring length and viscosity of dynamic metallo-supramolecular polymers in solution

This Chapter is based on: *"Tailoring length and viscosity of dynamic metallo-supramolecular polymers in solution",* S. M. Munzert, G. Schwarz, D. G. Kurth, *RSC Adv.* **2016**, 6, 15441-15450.

Abstract: Transition metal ions, like Fe^{2+}, Co^{2+} and Ni^{2+} coordinate to ditopic ligands such as 1,4-bis(2,2′:6′,2′′-terpyridin-4′-yl)benzene (**1**) forming sufficiently strong yet dynamic bonds in aqueous solutions, leading to extended, rigid-rod like metallo-supramolecular coordination polyelectrolytes (MEPEs). Here, a way is presented to adjust the average molar mass, chain-length and viscosity of MEPEs using the monotopic chain stopper 4′-(phenyl)-2,2′:6′,2′′-terpyridine (**2**). The systems are analyzed by light scattering and viscometry. The experiments indicate that chain-length and viscosity of the MEPEs are modifiable in predictable ways by adding the monotopic chain stopper, **2**. Light scattering is a suitable method for studying the molar mass and also the shape of the MEPEs.

4.1 Introduction

The ditopic ligand **1** and the chain stopping monotopic ligand **2** form rigid-rod like metallo-supramolecular coordination polyelectrolytes (MEPEs) in solution as shown in Scheme 30.

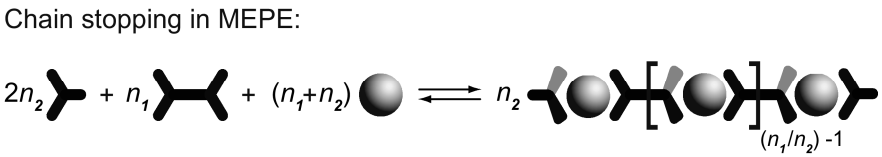

Scheme 30. Metal ion induced self-assembly of the metal ions Fe^{2+}, Co^{2+}, and Ni^{2+} with 1,4-bis(2,2′:6′,2′′-terpyridine-4′-yl)benzene (**1**) results in metallo-supramolecular coordination polyelectrolytes (MEPEs). 4′-(Phenyl)-2,2′:6′,2′′-terpyridine (**2**) acts as a stopping unit. n_1 is the number of monomers, $[M(\mathbf{1})]^{2+}$, and n_2 the number of the chain terminating complexes, $[M(\mathbf{2})_2]^{2+}$, in the solution. The acetate counterions are omitted for clarity. Adapted from ref [88] with permission from The Royal Society of Chemistry.

Due to the non-linear dependence of chain-length on the metal ion to ligand ratio, y, in particular in the vicinity of 1, small changes in y result in a varying chain-length and therefore in high viscosity changes of the final Fe-MEPE solutions (see Chapter 1.2.3.2.4.2). In order to control the length that is the viscosity of the solution, the molecular weight and therefore the length of the MEPE chains in solution based on Fe^{2+}, Co^{2+}, Ni^{2+}, and ligand **1**, the addition of the monotopic chain stopper 4′-(phenyl)-2,2′:6′,2′′-terpyridine (**2**) is employed (Scheme 30). Here, a comprehensive analysis of these chain stopper experiments is presented using light scattering and viscometry in solution.[88]

4.2 Results and discussion

Metal ion induced self-assembly of the ditopic ligand **1** and the monotopic ligand **2** is used in the following as model system to study the assembly of MEPEs. Under the assumption that the chain forming ligand **1** and the chain stopping ligand **2** show the same binding properties and that all species are involved in the chain formation, the number of repeat units in MEPEs and, therefore, the average molar mass of the polymer chains can be described as follows. The chain termination ratio, *z*, is defined as:

$$z = \frac{n_1}{n_1+2n_2}, \tag{65}$$

where n_1 is the number of monomers, $[M(\mathbf{1})]^{2+}$, and n_2 the number of the chain terminating complexes, $[M(\mathbf{2})_2]^{2+}$, in the solution. Chain termination occurs when the number of capping units exceeds the number of chains ends. According to the principle of "maximum site occupancy" the chain ends will then be terminated by monotopic ligand, **2** (see Scheme 30).[42] A stoichiometric ratio is chosen according to $n(M^{2+}) = (n_1 + n_2)$. If the number of complexes, n_2, is lower than (or equal to) the number of the monomers, n_1, that is $z \geq 1/3$, the number of MEPE chains in solution is equal to the number of chain terminating complexes $[M(\mathbf{2})_2]^{2+}$. If $z < 1/3$, the solution consists of $[(\mathbf{2})M(\mathbf{1})M(\mathbf{2})]^{2+}$-species and an excess of $[M(\mathbf{2})_2]^{2+}$. At $z = 1/3$ the chain stopping complex is absent. In this case, the length of the polymer chain depends on the concentration of monomers, $[M(\mathbf{1})]^{2+}$, and the metal ion to ligand ratio, *y*. Under the conditions that $1/3 < z < 1$, and that the concentration is low enough to enable the self-assembly of monomers with chain stopping complexes, the length of MEPE chains is independent of the binding constant and total concentration but is terminated solely by the number of complexes present in solution. Of course, the overall binding constant and the total concentration must exceed the threshold of self-assembly. Thus, the molar mass of a single MEPE chain is equal to the sum of the molar mass of

monomers, [M(**1**)]$^{2+}$, plus the molar mass of the chain terminating complex, [M(**2**)$_2$]$^{2+}$. Therefore, the number average molar mass, $\bar{M}_n$, equals to the sum of the molar mass of all monomers present in solution divided by n_2 and the molar mass of one [M(**2**)$_2$]$^{2+}$-complex that is M_c:

$$\bar{M}_n = \frac{n_1 M_m}{n_2} + M_c \tag{66}$$

for $1/3 \leq z < 1$ and with n_1 being the number of monomers, [M(**1**)]$^{2+}$, and M_m and M_c the molar masses of monomer, [M(**1**)]$^{2+}$, and chain terminating complex [M(**2**)$_2$]$^{2+}$, respectively. With eqs (65) and (66) the number average molar mass of the MEPE chains can be described as a function of z:

$$\bar{M}_n = \frac{2zM_m}{(1-z)} + M_c \tag{67}$$

for $1/3 \leq z < 1$.[88]

4.2.1 Weight average molar masses

With acetate as counter ion, the MEPEs are soluble in water, aqueous acetic acid and polar solvents like EtOH or MeOH. On the other hand, ligand **1** is soluble in aqueous acetic acid, but less soluble in polar solvents such as water, EtOH or MeOH. For this reason, preparation and analysis of the MEPEs are performed in acetic acid solution (75 vol %). For the MEPE synthesis the metal salt is added to a mixture of ligand **1** and **2** (see procedure I in Chapter 5.3) or the MEPEs are prepared by adding solid MEPE and solid complex, [M(**2**)$_2$]$^{2+}$ in pre-defined ratios, z, to acetic acid solution (75 vol %) (see procedure II in Chapter 5.3); also KOAc is added to the solution. In both procedures, the resulting MEPE solutions were allowed to equilibrate for at least 20 days. The

resulting weight average molar masses, $\overline{M}_w$, of the MEPEs are examined by static light scattering and the resulting viscosities by viscometry, respectively.

Light scattering is performed at a temperature of 23 °C and the data is evaluated according to the Guinier-Zimm plot:[72, 277]

$$ln\left(\frac{Kc}{R_\theta}\right) = ln\left(\frac{1}{\overline{M}_w\left(e^{-\frac{1}{3}r_g^2q^2}\right)} + 2A_2c\right) \quad (68)$$

with K being an optical constant, c the concentration of MEPEs in solution, R_θ the Rayleigh ratio, r_g, the radius of gyration, q the scattering vector, and A_2 the second virial coefficient (for details concerning the data analysis, see Chapter 5.4.3.1). As shown in Figure 47, the molar mass of the MEPEs is increasing with increasing chain termination ratio, *z*, that is with decreasing amount of chain terminating complex.

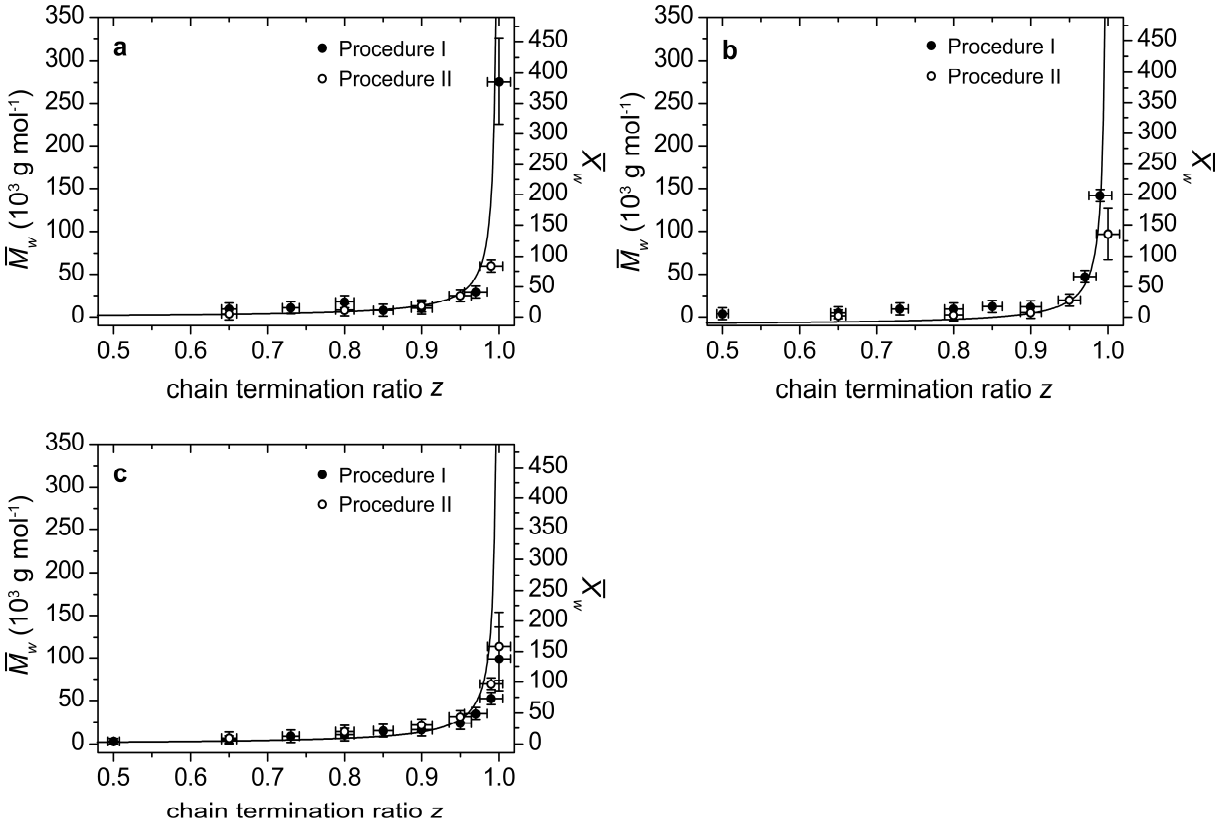

Figure 47. Weight average molar mass, $\bar{M}_w$, of (a) Fe-MEPE, (b) Co-MEPE, and (c) Ni-MEPE for different chain termination ratios, z, in 0.1 M KOAc acetic acid solution (75 vol %) at a temperature of 23 °C with a concentration of 4 g L^{-1}. The samples are prepared by procedure I and II, respectively (see Chapter 5.3). Each data point is obtained by using static light scattering leading to a Guinier-Zimm plot based on eq (68). The black solid lines show the corresponding number average molar masses, $\bar{M}_n$, calculated by eq (67). $\bar{X}_w$ is the corresponding weight average degree of polymerization, $\bar{X}_w = \bar{M}_w/M_m$. For details concerning the data analysis, see Chapter 5.4.3.1. Adapted from ref [88] with permission from The Royal Society of Chemistry.

The weight average molar masses, $\bar{M}_w$, measured by static light scattering are consistent with the number average molar masses, $\bar{M}_n$, calculated by eq (67) (black solid line in Figure 47) within an error of ± 7 × 10^3 g mol^{-1}, if $z < 1$. These results show that it is possible to adjust the chain-length of MEPEs by using a pre-defined amount of chain terminating complex.

Within the experimental error the average number of monomeric units per polymer chain is similar to the weight average degree of polymerization, $\bar{X}_w = \bar{M}_w/M_m$, ($z < 1$). As shown in Figure 47, $\bar{M}_w$ is determined up to 2.8 × 10^5 g mol^{-1}, which corresponds to a weight average degree of polymerization, $\bar{X}_w$ = 385.

In the following set of experiments solid MEPE and solid complex, $[M(\mathbf{2})_2]^{2+}$ are mixed in pre-defined ratios, z, in acetic acid solution (75 vol %) including 0.1 M KOAc (procedure II). The weight average molar masses, $\bar{M}_w$, obtained by this procedure are also included in Figure 47. The results are identical. This experiment proves the dynamic nature of the MEPE chains. The mixture of neat MEPE and chain stopper complex $[M(\mathbf{2})_2]^{2+}$ exchange and equilibrate resulting in chain-lengths determined by the ratio z independently of the preparation procedure. Also, these results confirm the hypothesis that the MEPE length depends only on the ratio of the components under these experimental conditions. The size of the MEPEs remains unchanged within the studied concentration range of 1 g L^{-1} to 4 g L^{-1} (see Chapter 5.4.3.2). However, as z approaches unity $\bar{M}_w$ exhibits larger error bars due to the strong depends of the chain-length on the metal ion to ligand ratio, y, and concentration, as described in the introduction.[72, 84, 88, 278]

4.2.2 Viscosities

In the following section, the viscosity data of the MEPE solutions is presented for $0.5 \leq z \leq 1$. The viscosity and SLS measurements are performed on the same samples. First, the specific viscosities, η_{sp}, are presented:

$$\eta_{sp} = \frac{\eta - \eta_0}{\eta_0} \tag{69}$$

with η being the measured dynamic viscosity of the solution, and η_0 the dynamic viscosity of the solvent that is the dynamic viscosity of acetic acid solution (75 vol %) mixed with 0.1 M KOAc. η_0 is determined to be 2.91 mPa s at a temperature of 23.0 °C. Figure 48 shows the specific viscosities, η_{sp}, of Fe-, Co-, and Ni-MEPE for different chain termination ratios, *z*, at a concentration of 3.0 g L^{-1}.

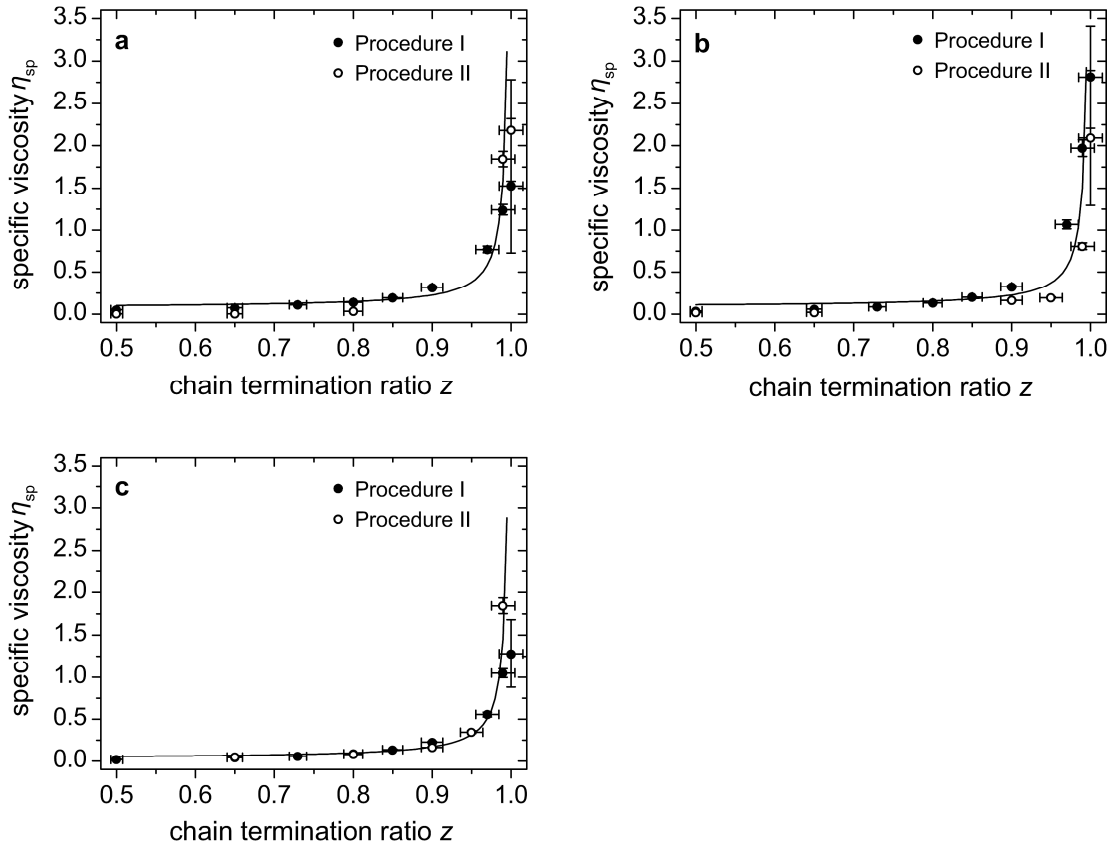

Figure 48. Specific viscosities of (a) Fe-MEPE, (b) Co-MEPE, and (c) Ni-MEPE for different chain termination ratios, *z*, at a temperature of 23.0 °C and a concentration of 3.0 g L^{-1} in 0.1 M KOAc acetic acid (75 vol %). The samples are prepared by procedures I and II, respectively (for details concerning the sample preparation see Chapter 5.3). The black solid lines show the corresponding curve fits according to eq (70), with $\eta_{sp,m}$ = (7.4 ± 0.3) × 10^{-3} and $\eta_{sp,c}$ = (9.1 ± 0.4) × 10^{-2}. Adapted from ref [88] with permission from The Royal Society of Chemistry.

The specific viscosities of MEPEs, η_{sp}, increase with increasing chain termination ratio, *z*, from 0.02 up to 2.81. Thus, the trend is the same as shown for the determined weight average molar masses, $\bar{M}_w$ (Figure 47), indicating that the chain-length increases with a decreasing amount of chain terminating complex, **2**. η_{sp} is growing analogous to eq (67) (see black solid lines in Figure 48):

$$\eta_{sp} = \frac{2z\eta_{sp,m}}{(1-z)} + \eta_{sp,c} \tag{70}$$

In comparison to eq (67), $\eta_{sp,m}$ corresponds to the specific viscosity of the monomers, $[M(\mathbf{1})]^{2+}$, and $\eta_{sp,c}$ corresponds to the specific viscosity of the $[M(\mathbf{2})_2]^{2+}$-complexes in the solution. If the corresponding solid compounds are dissolved in the solvent, the same specific viscosity data, η_{sp}, are obtained (Figure 48). By curve fitting according to eq (70), $\eta_{sp,m}$ results to (7.4 ± 0.3) × 10^{-3}, and $\eta_{sp,c}$ results to (9.1 ± 0.4) × 10^{-2}, for Fe-, Co-, and Ni-MEPE.

This corresponds to dynamic viscosities η_m = 2.93 mPa s and η_c = 3.17 ± 0.1 mPa s. As expected, these values are slightly higher than the dynamic viscosity of the solvent (2.91 mPa s) and are in good agreement with viscosity measurements of $[Fe(\mathbf{2})_2]^{2+}$, $[Co(\mathbf{2})_2]^{2+}$, and $[Ni(\mathbf{2})_2]^{2+}$ in 0.1 M KOAc acetic acid solution (75 vol %). The viscosity data are in full agreement with the light-scattering data supporting the hypothesis that MEPEs are dynamic structures and that chain terminating complexes can be used to tailor the chain-length and viscosity.

Figure 49 shows the specific viscosity, η_{sp}, of Fe-, Co-, and Ni-MEPE as a function of concentration (1.0 to 4.0 g L^{-1}) and chain termination ratios, *z*.

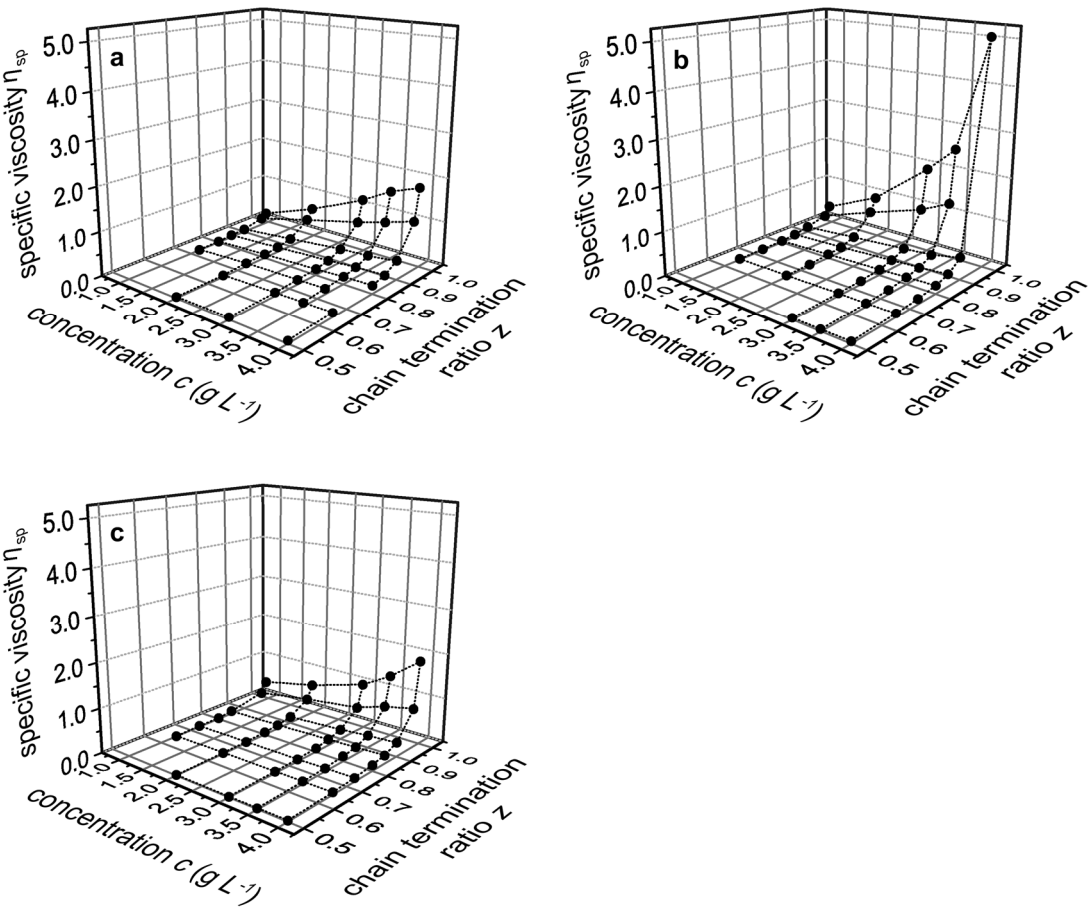

Figure 49. Specific viscosities, η_{sp}, of (a) Fe-MEPE, (b) Co-MEPE, and (c) Ni-MEPE as a function of the MEPE concentration, *c*, and at different chain termination ratios, *z*, measured at a temperature of 23 °C. Adapted from ref [88] with permission from The Royal Society of Chemistry.

The specific viscosity increases with an increasing concentration as well as an increasing chain termination ratio, *z*. As shown in Figure 49 and also previously shown in Figure 48, η_{sp} is increasing according to eq (70). In the present set of experiments the specific viscosity, η_{sp}, is changed from 0.01 to 5.06 simply by adjusting the concentration, *c*, and/or chain termination ratio, *z*. The dependence of the specific viscosity, η_{sp}, on the concentration, *c*, can be examined by Cate's model:[279]

$$\eta_{sp} \sim c^{\alpha} \tag{71}$$

with α being an exponent, relating η_{sp} to c. Regarding MEPEs, α is found to be 1.40 ± 0.04, 1.15 ± 0.05, and 1.04 ± 0.04, for Fe-, Co-, and Ni-MEPE, respectively. For noninteracting species of constant size Cate's model predicts a linear increase of η_{sp} with c, i.e. α = 1. The length of the MEPE chains should be independent on concentration in the presence of chain terminating complexes. Therefore, α is expected to be close to 1, which is indeed the case for Ni-MEPE; for Co- and Fe-MEPE α increases to 1.15 and 1.40, respectively. Values of α > 1 indicate that size increases with concentration as a result of a supramolecular polymerization or aggregation process.[279-281] The presence of chain terminating complex should prevent chain growth through metal ion coordination. The increase in α may, therefore, be associated with other yet unknown aggregation processes. The exponents, α, are in the same range, than reported by Rowan et al.[280] for metallo-supramolecular polymers, made from ditopic bis(benzimidazolyl)pyridine ligands and Fe^{2+} or Co^{2+}. Somewhat larger values are reported for DNA- and hydrogen-bonding based supramolecular solutions, where α = 1.3 - 1.8.[282-284] Finally, the examined concentration range is well below the overlap concentration, where Cate's model predicts a value of α = 3.5.[88, 279]

4.2.3 Kuhn-Mark-Houwink (KMH) constants

In the case of samples with the same polydispersity index, the dependence of viscosity on molar mass can be described by the Kuhn-Mark-Houwink (KMH) constants, relating the intrinsic viscosity, $[\eta]$, to the weight average molar mass, $\bar{M}_w$:[285-287]

$$[\eta] = K_\eta \bar{M}_w{}^{a_\eta} \tag{72}$$

with K_η and a_η being empirical constants, which are characteristic for a polymer-solvent system at a defined temperature. A KMH exponent of a_η = 0.5 is indicative of a coil,

dissolved in a theta solvent, and a_η = 0.8 is typical for coils in a good solvent. Larger exponents, a_η > 1, are frequently found for rigid macromolecules. For rigid-rod type polymers, such as tobacco mosaic virus, a_η is found to be 2.70 In order to calculate both KMH constants, the intrinsic viscosity, $[\eta]$, is determined. It is defined as:

$$[\eta] = \lim_{c \to 0} \left[\frac{\eta_{sp}}{c}\right] = \lim_{c \to 0} [\eta_{red}] \tag{73}$$

The intrinsic viscosity, $[\eta]$, is the contribution of a single particle to the solution's viscosity and is also known as Staudinger index.[285] The specific viscosity of MEPE solutions is measured as a function of concentration, the extrapolation to $c = 0$ gives the intrinsic viscosity, $[\eta]$. Thus, the intrinsic viscosity, $[\eta]$, is obtained from an extrapolation of the reduced viscosity, η_{red}, to $c = 0$, which is the so-called Huggins-plot,[288-289] as shown exemplary in Figure 50 for determination of $[\eta]$ by extrapolation of the reduced viscosities, η_{red}, of Fe-MEPE.

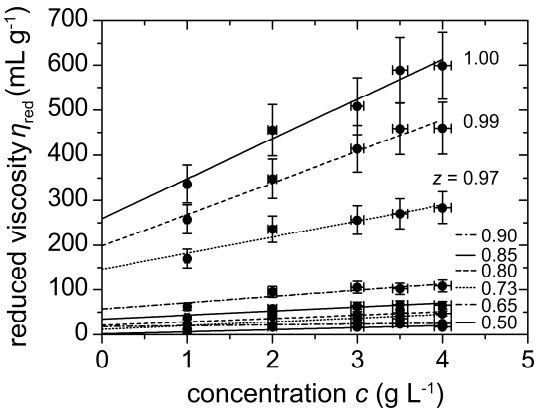

Figure 50. Huggins-plots of the reduced viscosity, η_{red}, of Fe-MEPE in acetic acid solution (75 vol %) with 0.1 M KOAc as a function of the MEPE concentration, *c*, and at different chain termination ratios, *z*, measured at a temperature of 23°C. Reprinted from ref [88] with permission from The Royal Society of Chemistry.

As can be seen in Figure 50, the reduced viscosity, η_{red}, increases linearly with concentration in 0.1 M KOAc acetic acid solution (75 vol %). Thus, the intrinsic viscosity, $[\eta]$, is reliably determined from the Huggins-plots.[290] As shown in Figure 51, the resulting values for $[\eta]$ are increasing up to 650 mL g^{-1} with increasing chain termination ratio, *z*.

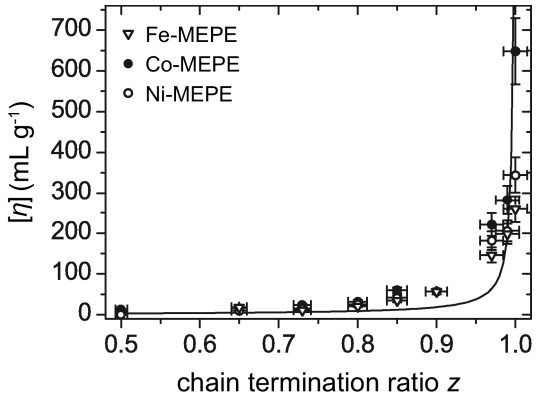

Figure 51. Intrinsic viscosities, $[\eta]$, of Fe-, Co-, and Ni-MEPE with different chain termination ratios, *z*, at a temperature of 23.0 °C. Each value is carried out by a linear plot of $\eta_{sp}c^{-1}$ to $c \rightarrow 0$ according to eq (73). The black solid line shows the corresponding curve fitting by eq (74) with $[\eta]_m$ = 1.0 mL g^{-1} and $[\eta]_c$ = 1.4 mL g^{-1}. Adapted from ref [88] with permission from The Royal Society of Chemistry.

Thus, the trend is the same as shown for the determined weight average molar masses, $\bar{M}_w$, indicating that the intrinsic viscosity grows with a decreasing amount of chain terminating complex. Analogous to eqs (67) and (70), the data follow

$$[\eta] = \frac{2z[\eta]_m}{(1-z)} + [\eta]_c \tag{74}$$

with $[\eta]_m$ = 1.0 mL g^{-1} and $[\eta]_c$ = 1.4 mL g^{-1}, which is relatively low, as expected. With the intrinsic viscosities, $[\eta]$, at hand, one can determine the values K_η and a_η of eq (72). A KMH plot is performed as shown in Figure 52 using the linearized eq (75):

$$\lg[\eta] = \lg\left[K_\eta\right] + a_\eta \lg[\bar{M}_w] \quad (75)$$

where $\lg[\eta]$ is obtained versus $\lg[\bar{M}_w]$, determined by static light scattering. $[\eta]$ is the intrinsic viscosity, $\bar{M}_w$ the weight average molar mass, and K_η and a_η are empirical constants, which are characteristic for a polymer-solvent system at a defined temperature.

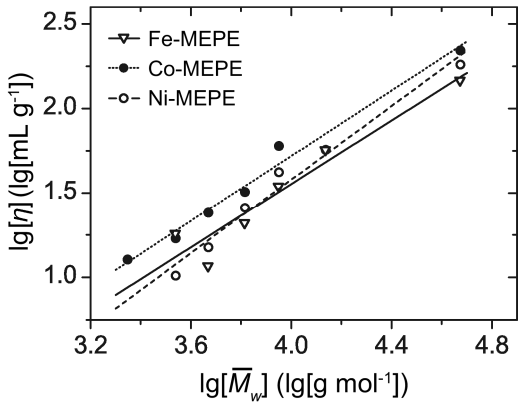

Figure 52. Kuhn-Mark-Houwink (KMH) fit of Fe-, Co-, and Ni-MEPE at a temperature of 23 °C according to eq (75). Adapted from ref [88] with permission from The Royal Society of Chemistry.

The KMH exponent, a_η, amounts to 0.94 ± 0.07, 0.97 ± 0.03 and 1.09 ± 0.04 and the constant, K_η, to (6.3 ± 0.5) × 10^{-3} mL g^{-1}, (7.2 ± 0.2) × 10^{-3} mL g^{-1}, and (1.7 ± 0.1) × 10^{-3} mL g^{-1} for Fe-, Co-, and Ni-MEPE, respectively, which is indicative of a semi-rigid (or stiff) polymer.[285] Again, there is an influence of the metal ion on the structures, as the stiffness increases in the order Fe-MEPE < Co-MEPE < Ni-MEPE.[88]

4.2.4 Second virial coefficients

The second virial coefficients, A_2, obtained from the light scattering data reveals information about the interactions of MEPEs in solution (for details concerning the theory of static light scattering, see Chapter 5.4.3.1). The second virial coefficients, A_2, are shown in Figure 53 for different chain termination ratios, *z*.

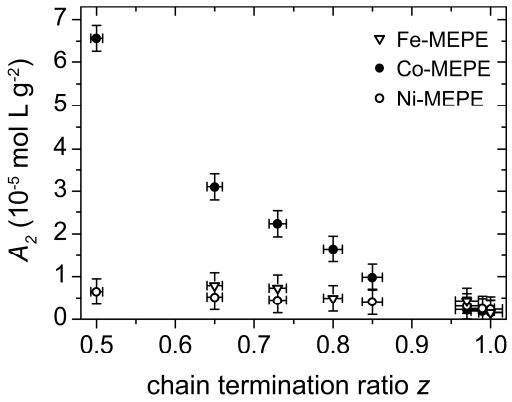

Figure 53. Second virial coefficients, A_2, of Fe-, Co-, and Ni-MEPE for different chain termination ratios, *z*, in 0.1 M KOAc in acetic acid solution (75 vol %) at a temperature of 23 °C. Each value is determined by an own Guinier-Zimm plot, resulting from static light scattering measurements by dilution of a stock solution (c = 4 g L^{-1}). Reprinted from ref [88] with permission from The Royal Society of Chemistry.

As shown in Figure 53, the second virial coefficients, A_2, are positive and decrease with increasing chain termination ratio, *z*. In general, if $A_2 = 0$, polymers act like ideal chains, assuming exactly their random walk coil dimensions. In this so-called "theta condition" the solvent neither expands nor contracts the macromolecule, which is said to be in its "unperturbed" state. A negative A_2 indicates the presence of an attractive interaction between the chains leading to macrophase separation ("salting-out effect"), whereas a positive A_2 value indicates repulsive forces between the polymers so that polymer-solvent interactions are favored over those between the polymers, and the solvent in

this case is referred to as a "good solvent" in a thermodynamic sense.[291-292] As can be seen in Figure 53, $A_2 > 0$, indicating that the interactions between the MEPEs and the solvent molecules are favored over those between the MEPEs and, therefore, acetic acid solution (75 vol %) can be referred as a "good solvent". Furthermore, an increasing $\bar{M}_w$ leads to a decreasing A_2 that is a decrease of repulsion forces between the MEPEs, which is a well-known phenomenon in polymer chemistry, due to the decrease of stiffness and increase of a worm-like structure of the polymers with increasing $\bar{M}_w$.[285] This tendency is more significant for Co-MEPE, than for Fe-, and Ni-MEPE.[88]

4.2.5 Shape and structure

Next, the focus is on the hydrodynamic radii, r_h, of Fe-, Co-, and Ni-MEPE which are shown in Figure 54 for different chain termination ratios, *z*. r_h is calculated by the Stokes-Einstein equation:[293]

$$r_h = \frac{k_B T}{6\pi\eta_0 D_0} \tag{76}$$

with k_B being the Boltzmann constant, T the temperature, η_0 the viscosity of the solvent, and D_0 the diffusion coefficient (for details concerning the application of a dynamic Zimm plot, see Chapter 5.4.3.3).

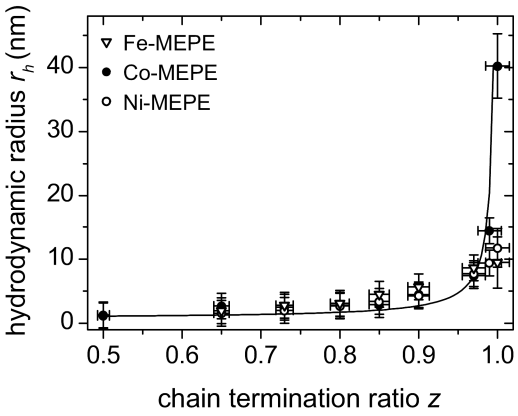

Figure 54. Hydrodynamic radii, r_h, of Fe-, Co-, and Ni-MEPE for different chain termination ratios, *z*, in 0.1 M KOAc in acetic acid solution (75 vol %) at a temperature of 23 °C. Each value is determined by an own dynamic Zimm plot, resulting from dynamic light scattering measurements by dilution of a stock solution (c = 4 g L^{-1}). Reprinted from ref [88] with permission from The Royal Society of Chemistry.

As expected and shown in Figure 54, the hydrodynamic radii, r_h, increase with increasing chain termination ratios, *z*, that is, with increasing weight average molar mass, $\bar{M}_w$. The trends are the same as shown for $\bar{M}_w$ in Figure 47.

With the hydrodynamic radii, r_h, at hand, the equation

$$r_h \sim \bar{M}_w{}^{\nu} \tag{77}$$

is used for determination of the dependence of radii to molar masses. A plot is performed as shown in Figure 55, using the linearized eq (78):

$$\lg[r_h] \sim \nu \cdot \lg[\bar{M}_w] \tag{78}$$

where $\lg[r_h]$ is plotted against $\lg[\bar{M}_w]$, determined by static light scattering.

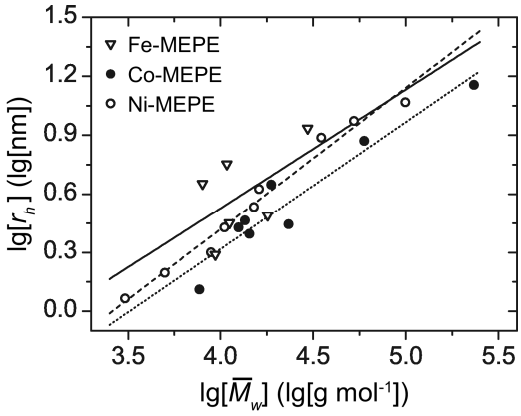

Figure 55. $\lg[r_h]$ versus $\lg[\overline{M}_w]$ of Fe-, Co-, and Ni-MEPE for different chain termination ratios, *z*, in 0.1 M KOAc acetic acid solution (75 vol %) at a temperature of 23 °C according to eq (78). Adapted from ref [88] with permission from The Royal Society of Chemistry.

The exponents, ν, result in 0.6 ± 0.2, 0.65 ± 0.04, and 0.72 ± 0.02 for Fe-, Co-, and Ni-MEPE, respectively, which is indicative of worm-like chains with an increased stiffness, comparable to covalent polymers.[294-295] The stiffness of the polymers increases in the order Fe-MEPE < Co-MEPE < Ni-MEPE, as already noticed above.

Further information about the shape and structure of the MEPEs is possible by a comparison of r_h with the radius of gyration, r_g, which can be achieved by the Guinier-Zimm plot, described above, according to eq (68) and as described in Chapter 5.4.3.1 Calculation of the radius of gyration is possible, if $r_g > \lambda_0/20$, with λ_0 being the wavelength of the incident laser light in vacuum. In this case, interference of the scattered light emitted from an individual particle leads to a nonisotropic angular dependence of the scattered light intensity. If $r_g < \lambda_0/20$, only a negligible phase difference exists between light emitted from the various scattering centers within the given particle. In this case, the detected scattered intensity is independent of the scattering angle and only depends on the molar mass of the particle, which is proportional to the total number of scattering centers one particle contains.[293] That means that for light scattering on Co-, and Ni- MEPE, r_g has to be > 32 nm, since the

wavelength of the incident laser, λ_0 = 632.8 nm. Light scattering on Fe-MEPE, requires a laser wavelength of λ_0 = 784.0, due to absorption effects. Therefore r_g of Fe-MEPE has to be > 40 nm. Thus, determination of weight average molar mass, $\overline{M}_w$, second virial coefficient, A_2, and hydrodynamic radius, r_h, is possible by light scattering measurements, but r_g of Co-, and Ni-MEPE can only be regarded as a trend (see Table 13). The determination of r_g of Fe-MEPE is not possible.[293]

Table 13. Radius of gyration, r_g, of Co-, and Ni-MEPE for different chain termination ratios, *z*, mixed with 0.1 M KOAc in acetic acid solution (75 vol %) at a temperature of 23 °C. Each value is determined by an own Guinier-Zimm plot, resulting from static light scattering measurements by dilution of a stock solution (c = 4 g L^{-1}). Adapted from ref [88] with permission from The Royal Society of Chemistry.

chain termination ratio, *z*	**r_g of Co-MEPE (nm)**	**r_g of Ni-MEPE (nm)**
0.50	7.8 ± 0.6	7.5 ± 0.6
0.65	-	(1.1 ± 0.1) × 10^1
0.73	8.6 ± 0.7	(1.0 ± 0.1) × 10^1
0.80	(1.3 ± 0.1) × 10^1	-
0.85	-	(1.1 ± 0.1) × 10^1
0.90	-	(1.1 ± 0.1) × 10^1
0.97	-	(2.0 ± 0.2) × 10^1
0.99	(2.5 ± 0.2) × 10^1	(2.4 ± 0.2) × 10^1
1.00	(3.2 ± 0.4) × 10^1	(2.7 ± 0.4) × 10^1

Nevertheless, a comparison of r_g to r_h is done, since the ratio, ρ, of radii of gyration and hydrodynamic radii

$$\rho = \frac{r_g}{r_h} \tag{79}$$

is a characteristic parameter of the particle architecture.[296] It has to be mentioned that the results for ρ can only be regarded as a trend. As shown in Table 14, ρ is decreasing with increasing chain termination ratio, *z*, which is indicative of a decreasing rigid-rod

like structure and an increasing worm-like structure, due to increasing weight average molar masses, $\bar{M}_w$.[296]

Table 14. Ratio, ρ, of radii of gyration, r_g, and hydrodynamic radii, r_h, of Co-, and Ni-MEPE for different chain termination ratios, *z*, mixed with 0.1 M KOAc in acetic acid solution (75 vol %) at a temperature of 23.0 °C. Each value of r_g is determined by an own Guinier-Zimm plot, resulting from static light scattering measurements, and each value of r_h is determined by an own dynamic Zimm plot by dilution of a stock solution (c = 4 g L^{-1}). Adapted from ref [88] with permission from The Royal Society of Chemistry.

chain termination ratio, *z*	ρ of Co-MEPE	ρ of Ni-MEPE
0.50	6.0 ± 0.4	6.5 ± 0.4
0.65	-	7.2 ± 0.5
0.73	3.5 ± 0.2	5.1 ± 0.3
0.80	4.5 ± 0.3	-
0.85	-	3.2 ± 0.2
0.90	-	2.5 ± 0.2
0.97	-	2.6 ± 0.2
0.99	1.7 ± 0.1	2.5 ± 0.2
1.00	0.8 ± 0.1	2.3 ± 0.1

The trend of the ratios, ρ, regarding the architecture of the MEPEs is in agreement with the trend, shown in Figure 53, where the second virial coefficient, A_2, is examined and indicates that the stiffness of the MEPEs is decreasing with increasing $\bar{M}_w$.[88]

4.3 Conclusion

In this Chapter on metal ion induced self-assembly of metallo-supramolecular coordination polyelectrolytes (MEPEs) chain stopping experiments are carried out in order to adjust the chain-length of Co-, Ni-, and Fe-MEPEs. A theoretical model is established, which can easily be used to receive a polymer of desired average molecular weight and thus, the viscosity, which is an important parameter in technological applications of MEPEs. This model should be applicable to (linear) supramolecular polymerization that form through reversible interactions of ditopic species in solution under equilibrium conditions. The validity of the theoretical model is confirmed by static light scattering and viscometry and it is shown that tailoring of the chain-length is reproducible, due to the dynamic nature of the MEPEs. The Kuhn-Mark-Houwink constants, a_η, are determined to 0.94 ± 0.07, 0.97 ± 0.03 and 1.09 ± 0.04 and the constants, K_η, to (6.3 ± 0.5) × 10^{-3} mL g^{-1}, (7.2 ± 0.2) × 10^{-3} mL g^{-1}, and (1.7 ± 0.1) × 10^{-3} mL g^{-1} for Fe-, Co-, and Ni-MEPE, respectively, by which it is possible to convert average molar masses to viscosities of the polyelectrolytes. The polymers exhibit a rigid-rod like structure in solution and the stiffness of the polymers seems to increase in the order Fe-MEPE < Co-MEPE < Ni-MEPE.[88]

5

Experimental Section

Parts of this Chapter are based on the publications listed on page VIII.

5.1 Synthesis

The ligands 1,4-bis(2,2′:6′,2′′-terpyridine-4′-yl)benzene (**1**)[297] and 4′-phenyl-2,2′:6′,2′′-terpyridine (**2**)[298] were synthesized and characterized according to literature procedures. 2,2′:6′,2′′-Terpyridine (**3**) and all other chemicals were purchased from Aldrich and used without further purification. All used metal acetates were synthesized from the corresponding neat metals under reflux in acetic acid according to literature procedures.[299]

5.2 Conductometric titrations

The MEPEs investigated were prepared by metal ion induced self-assembly of the ditopic ligand 1,4-bis(2,2′:6′,2′′-terpyridine-4′-yl)benzene (**1**) in acetic acid solution (75 vol %) with Fe^{2+}, Co^{2+}, or Ni^{2+}, respectively. The synthesis of MEPE was done under conductometric control because the chain-length of MEPE depends critically on the stoichiometry, $\delta = [M^{2+}]/[L]$ that is the ratio of the concentrations of metal ion, $[M^{2+}]$, and ligand, [L].[227] The ligands 4′-phenyl-2,2′:6′,2′′-terpyridine (**2**) and 2,2′:6′,2′′-terpyridine (**3**) form mononuclear complexes, which are used for control experiments. Conductometric titrations were performed with a Metrohm 905 Titrando instrument. The titroprocessor was controlled by Tiamo 2.2.

26.1 mg (468 µmol) iron powder was dispersed in 26 mL of degassed acetic acid solution (75 vol %). The dispersion was heated under reflux and under argon until the iron powder had completely disappeared and reacted to 81.4 mg (468 µmol) $Fe(OAc)_2$, which took ~2 h. In a separate 100 mL two-necked flask equipped with a conductivity sensor, ligand **1** (243 mg, 450 µmol) was dissolved in 50 mL of acetic acid solution (75 vol %). The solution containing the freshly synthesized $Fe(OAc)_2$ was cooled to room

temperature and titrated under argon to the ligand solution while the conductivity was metered. Each addition is accompanied by a corresponding decrease in the conductivity. Because of the small amount that was added (100 µL), the end point or 1:1 stoichiometry was recognized by the observation that the conductivity did not change for two consecutive additions. Whenever solid MEPE was needed, the solvent was removed under reduced pressure, and the MEPE was isolated as solid powder.

A typical titration procedure for $[Fe(\mathbf{2})_2]^{2+}$ and $[Fe(\mathbf{3})_2]^{2+}$, respectively, is as follows: 58.8 mg (338 µmol) $Fe(OAc)_2$ was prepared as described above. In a separate 100 mL two-necked flask equipped with a conductivity sensor, ligand **2** (201 mg, 650 µmol) and ligand **3** (282 mg, 650 µmol), respectively, was dissolved in 50 mL of acetic acid solution (75 vol %). The solution containing the synthesized $Fe(OAc)_2$ was titrated to the ligand solution while the conductivity was metered as described above.

5.3 Sample preparation

5.3.1 Sample preparation for light scattering and viscometry

For measuring light scattering and viscometry, the MEPE samples were prepared according to two procedures. In procedure I, the ligands **1**, **2**, and the respective metal ion (Fe^{2+}, Co^{2+}, or Ni^{2+}) were solved in acetic acid solution (75 vol %) including 0.1 M KOAc and the ligand solution was mixed with the solution of the respective metal ion in predefined ratios, z. In procedure II, the MEPEs were prepared by adding solid MEPE and solid complexes, $[M(\mathbf{2})_2]^{2+}$ in predefined ratios, z, to acetic acid solution (75 vol %) including 0.1 M KOAc.

5.3.2 Sample preparation for cryo-TEM imaging

The samples for cryo-TEM imaging were prepared according to ref [255].

5.4 Methods

5.4.1 UV/Vis and fluorescence spectroscopy

Absorbance spectra were recorded on a JASCO V-650 spectrophotometer, emission spectra were measured on a JASCO FP-8300 spectrofluorometer. The spectra were recorded at 20 °C with solutions of the different MEPEs and monotopic complexes all containing a constant ligand concentration of 10^{-3} M in UV/Vis measurements and 10^{-5} M in fluorescence spectroscopy measurements.

5.4.2 Stopped-flow

The stopped-flow measurements were performed using the fluorescent substances (**1**, **2**, and **3**) at different concentrations between 10^{-5} and 10^{-4} M ultrasonicated in EtOH for at least 30 min. The measurements were carried out in EtOH instead of acetic acid solution (75 vol %) to avoid possible corrosion to the stopped-flow apparatus. To make sure that the ligands **1**, **2**, and **3** are dissolved in EtOH, emission spectra were monitored and the intensity of the Rayleigh scattering band was checked. A low intensity of the band indicated that the ligands were dissolved and that there were no scattering aggregates present in solution. These dissolved substances were reacted with different concentrations in the range of 5×10^{-5} to 10^{-3} M of the respective quenching substances $Fe(OAc)_2 \cdot 4H_2O$, $Co(OAc)_2 \cdot 4H_2O$, and $Ni(OAc)_2 \cdot 4H_2O$ in EtOH. The coordination kinetics of MEPE and metal complexes were monitored by fluorescence detection using a BioLogic SFM-300 stopped-flow module attached to a JASCO J-815

spectropolarimeter with an addition photomultiplier tube for fluorescence detection. For the concentration range between 10^{-5} and 10^{-4} M a calibration curve was recorded that relates ligand concentration of **1**, **2**, and **3** to the emission signal, which follows a linear relationship. The slope of the calibration curves correlates the emission signal to the concentration of the ligand. Ligand **1** was excited at λ_e = 292 nm, ligand **2** at λ_e = 289 nm and ligand **3** at λ_e = 281 nm. Emission intensity between 387 and 447 nm was detected using a cutoff filter supplied by Bio-Logic. The dead time of these experiments was 3.8 ms. Every stopped-flow mixing experiment was performed with 151 µL of ligand, dissolved in EtOH and 151 µL of metal acetate, dissolved in EtOH, each with a flow rate of 4.00 mL s^{-1}. The temperature was set to 20 °C with a FL 300 Julabo temperature controller. Fluorescence-time traces were monitored using Biokine32 (BioLogic). The concentration of ligand is related to the emission intensity via a calibration curve. In the concentration range of 10^{-5} to 10^{-4} M a linear relationship between concentration of ligand and emission signal is observed. Every concentration/time plot was fitted to the following equation:

$$w(t) = \alpha t + \beta + \gamma e^{(-\kappa t)} \tag{80}$$

Slope α and offset β correspond to the baseline, which is subtracted after fitting. Amplitude γ and exponent κ are parameters of the exponential term of the graph. After subtracting the baseline, the rate v of every single exponential curve $w(t) = \gamma e^{(-\kappa t)}$ at the commencement of the reaction, was determined by calculating the slope of the exponential curve, and thus the first derivation at $t = 0$:

$$w'(0) = -\kappa\gamma \tag{81}$$

$$v = |-\kappa\gamma| \tag{82}$$

The stopped-flow experiments were repeated with different initial concentrations of **1**, **2**, and **3**, during coordination to Fe^{2+}, Co^{2+}, and Ni^{2+} leading to 45 curves in total, similar to the curves, shown in Figure 27a.

Likewise, the experiments were repeated by using a constant initial concentration of the metal ions Fe^{2+}, Co^{2+}, and Ni^{2+} and varied initial concentrations of ligands **1**, **2**, and **3**, to determine the reaction order in ligands **1**, **2**, and **3**, leading to additional 45 decreasing exponential curves.

5.4.3 Static and Dynamic Light Scattering (SLS/DLS)

Dynamic and static light scattering measurements were performed with an ALV CGS-3 Multi Detection Goniometry System (ALV, Langen, Germany), equipped with a He-Ne laser (22 mW at λ = 632.8 nm) for investigation of Co-, and Ni-MEPEs, and an infrared laser (70 mW at λ = 784 nm) for investigation of Fe-MEPE, and 8 fiber optical detection units including 8 simultaneously working APD avalanche diodes. The measurements were conducted at scattering angles from 20° to 140° in steps of 8°. The samples were thermostated in a cell with temperature stability of ± 0.1 °C. All solutions were filtered separately before measuring light scattering using 0.2 µm syringe filters in order to remove dust particles. The specific refractive index increment (dn/dc) of every polymer sample was measured at 20.0 °C using a differential refractive index detector BI-DNDC WGE DR Bures from Wyatt Technologies. For details concerning the theory of dynamic and static light scattering, see the following Chapter.

5.4.3.1 Theory and data analysis

In static light scattering experiments, macromolecules in solution are irradiated by laser light of wavelength, λ_0, which scatters in all directions (Rayleigh scattering). The intensity of the scattered laser light depends on the scattering angle, θ, if scattered by macromolecules larger in size than $\lambda_0/20$. The Rayleigh ratio, R_θ, is determined in the following way. The scattered intensity of three different liquids is recorded that is the toluene, $I_{standard}$, the solvent $I_{solvent}$, and the solution of MEPE, I_{MEPE}. If the scattered intensities are measured using the same experimental setup, R_θ can be calculated as

$$R_\theta = \frac{I_{MEPE} - I_{solvent}}{I_{standard}} R_{standard} \cdot \left(\frac{n_{solvent}}{n_{standard}}\right)^2 \quad (83)$$

with $R_{standard}$ as the Rayleigh ratio of the standard that is toluene and the refractive indices of solvent, $n_{solvent}$, and standard, $n_{standard}$.[285, 293, 300] $R_{standard}$ is known as 1.4×10^{-3} m^{-1} at an irradiation wavelength of λ_0 = 632.8 nm and as 5.8×10^{-4} m^{-1} at an irradiation wavelength of λ_0 = 784.0 nm. Both values refer to a sample temperature of 20 °C.[301-302] The scattering vector, q, is given by:[285, 293]

$$q = \frac{4\pi n_{solvent}}{\lambda_0} \cdot sin\left(\frac{\theta}{2}\right) \quad (84)$$

with $n_{solvent}$ being the refractive index of the solvent at 20 °C and θ the scattering angle. The optical constant, K, is calculated as

$$K = \frac{4\pi^2 n_{solvent}^2}{N_A \lambda_0^4} \cdot \left(\frac{dn_s}{dc}\right)^2 \quad (85)$$

with N_A being the Avogadro number, c the concentration of MEPEs in solution, and $\frac{dn_s}{dc}$ the refractive index increment of the solution, which is defined as

$$\left(\frac{dn_s}{dc}\right) = \frac{n_s - n_{solvent}}{c} \tag{86}$$

where n_s is the refractive index of the solute. The refractive index increment, $\frac{dn_s}{dc}$, depends on the difference in polarizability of solute and solvent.[285, 293]

In order to calculate the weight average molar mass, $\bar{M}_w$, and the radius of gyration, r_g, of the MEPEs, a solution is prepared and diluted. The intensity of the scattered light depends on variation of the concentration, c, and the scattering angle, θ, which results in different Rayleigh ratios, R_θ. The obtained Rayleigh ratios, R_θ can be plotted via a Zimm plot,[285, 293, 303] which is based on the formula

$$\frac{Kc}{R_\theta} = \frac{1}{\bar{M}_w\left(1 - \frac{1}{3}r_g^2 q^2\right)} + 2A_2 c \tag{87}$$

where A_2 is the second virial coefficient. The evaluation of static light scattering measurements requires two extrapolations: On the one hand, the KcR_θ^{-1} values are extrapolated to an interference-free condition that is $\theta \to 0$, which leads to an extrapolation of the scattering vector, $q^2 \to 0$, on the other hand the values are extrapolated to an interaction-free condition that is $c \to 0$. For this purpose, a Zimm plot is carried out, considering Guinier's method.[296, 304] Guinier and Fournet[304-305] showed that the scattering vector can be approximated over a wide range of q^2 by:

$$1 - \frac{1}{3}r_g^2 q^2 = e^{-\frac{1}{3}r_g^2 q^2} \tag{88}$$

With the approximation at hand, Wesslau[277, 304] proposed the Guinier–Zimm plot

$$ln\left(\frac{Kc}{R_\theta}\right) = ln\left(\frac{1}{\bar{M}_w\left(e^{-\frac{1}{3}r_g^2 q^2}\right)} + 2A_2 c\right) \tag{89}$$

where $\ln\left(KcR_\theta^{-1}\right)$ is plotted against $(q^2 + bc)$, as shown exemplary in Figure 56 for the static light scattering measurement of a Ni-MEPE solution at time, t = 21.5 d after adding Ni^{2+} to ligand **1**. b is an arbitrary constant, a scaling factor which is freely selectable.

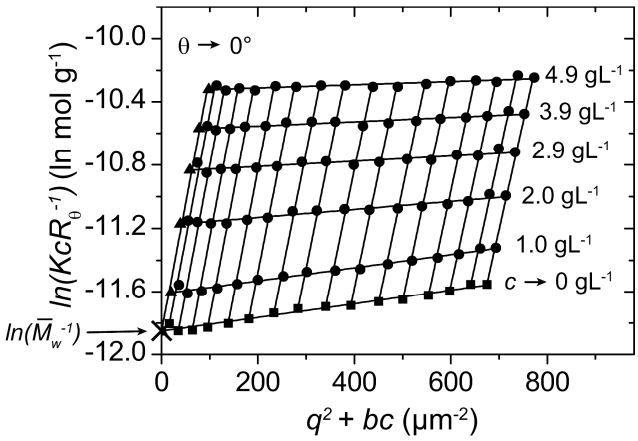

Figure 56. Guinier-Zimm plot of Ni-MEPE at time, t = 21.5 d after adding Ni^{2+} to ligand **1** in 0.1 M KOAc acetic acid solution (75 vol %) at a temperature of 20 °C. The Rayleigh ratio, R_θ, is measured for five different concentrations, ranging from 1 g L^{-1} to 4.9 g L^{-1} and from 16 different angle positions of the detectors, ranging from 20° to 140°. The scaling factor b of the Zimm plot is set to 20 L g^{-1} μm^{-2}. The $\ln\left(KcR_\theta^{-1}\right)$ values are extrapolated to $\theta \to 0$ that is $q^2 \to 0$, (triangles) and to $c \to 0$ (rectangles). Adapted with permission from [89]. Copyright 2016 American Chemical Society.

From the intercept of the extrapolation curve, $q^2 \to 0$, the weight average molar mass, $\bar{M}_w$, can be estimated as follows (see also Figure 56):

$$\lim_{\substack{q^2 \to 0 \\ c \to 0}} \left(ln\left(\frac{Kc}{R_\theta}\right)\right) = ln\left(\frac{1}{\bar{M}_w}\right) \tag{90}$$

The radius of gyration, r_g, or more exactly, the z-average of the squared radius of gyration, $\langle r_g^2 \rangle_z$, is defined as the average of the squared distance between a point of a polymer and the center of mass, r_i:

$$\langle r_g^2 \rangle_z = \frac{1}{N} \sum_{i=1}^{N} |r_i|^2 \tag{91}$$

Also r_g can be obtained from the slope of the extrapolation curve of $\ln\left(KcR_\theta^{-1}\right)$ to $c \to 0$:

$$\frac{d\left(\lim_{c\to 0}\left(ln\left(\frac{Kc}{R_\theta}\right)\right)\right)}{d(q^2)} = \frac{r_g^2}{3} \tag{92}$$

From the slope of the extrapolation curve, $q^2 \to 0$, the second virial coefficient, A_2, respectively, can be estimated:[285, 293, 304]

$$\frac{d\left(\lim_{q^2\to 0}\left(\frac{Kc}{R_\theta}\right)\right)}{dc} \cdot b = 2A_2 \tag{93}$$

The applicability of static light scattering measurements on noncovalent polymers is discussed in the next Chapter.

5.4.3.2 Size of polymers during static light scattering measurements

To apply the method of Guinier and Zimm[277, 304] it is generally required that the size of particles remains unchanged within the studied concentration range.[293, 306] MEPEs are consisting of reversible noncovalent bonds and the polymer length may vary while preparing different concentrations for static light scattering measurements. For this reason, the dependence of size on concentration is examined and compared to a well-known covalent polymer system, i.e. polystyrene, where polymer length is known to be independent on concentration. The experimental dependence of $\bar{\Gamma}$ on the square of the scattering vector, q^2, at different concentrations, c, is shown in Figure 57 for Ni-MEPE and polystyrene.

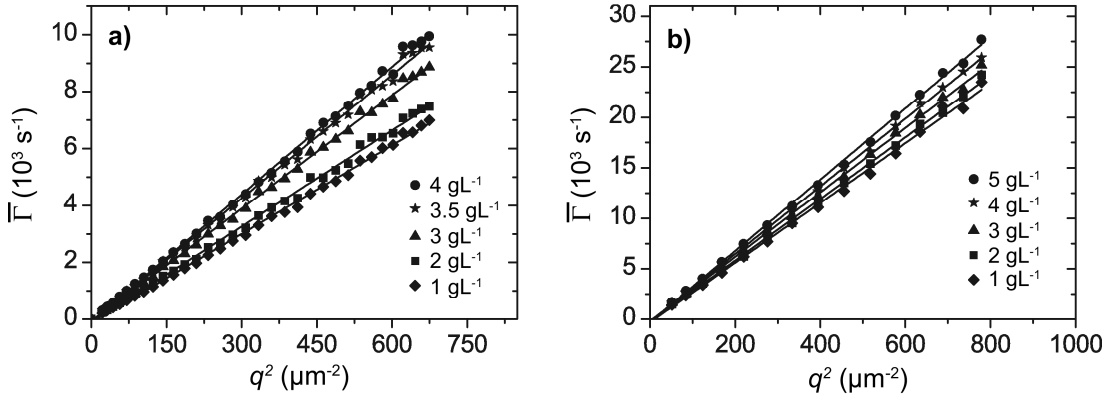

Figure 57. Experimental dependence of $\overline{\Gamma}$ on q^2 of (a) Ni- MEPE at t = 21.5 d after adding Ni^{2+} to ligand **1** in 0.1 M KOAc acetic acid solution (75 vol %), and (b) polystyrene at different concentrations. Adapted with permission from [89]. Copyright 2016 American Chemical Society.

As can be seen in Figure 57, the linear dependence of $\overline{\Gamma}$ on q^2,

$$\overline{\Gamma} = Dq^2 \tag{94}$$

is well approximated by the straight lines passing through the coordinate origin. Diffusion coefficients, D, of the MEPEs calculated from the slopes is independent on solution concentration within an error of ± 7.8 % within the studied concentration range of 1 gL^{-1} to 4 gL^{-1}. Thus, static light scattering is a suitable method for studying the molar mass and also the shape of MEPEs.

5.4.3.3 Dynamic light scattering (DLS)

A dynamic Zimm plot is generated by measuring the diffusion coefficients, D, and extrapolating the data in the same way as the KcR_θ^{-1} values, shown in the Guinier-Zimm plot described above (Figure 56), to an interference-free condition that is $\theta \rightarrow 0$,

which leads to an extrapolation of the scattering vector, $q^2 \rightarrow 0$, and to an interaction-free condition that is $c \rightarrow 0$. The extrapolation leads to the diffusion coefficient, D_0. With D_0 at hand, the hydrodynamic radius, r_h, is calculated.[293]

5.4.4 Viscosity

Viscosity measurements were conducted using a capillary viscometer (Lovis 2000M, Anton-Paar, Ostfildern, Germany) under precise temperature control (± 0.01 °C) based on the rolling ball viscosity method employing a steel ball moving in a glass capillary. The density of the solutions analyte was determined with a density sensor (DMA 4100M, Anton-Paar, Ostfildern, Germany) to obtain both, dynamic and kinematic viscosity.

5.4.5 Cryogenic transmission electron microscopy (cryo-TEM) imaging

Cryo-TEM imaging was performed according to ref [255].

5.4.6 Nonlinear curve fitting according the Levenberg-Marquardt algorithm

Nonlinear fitting is performed using Origin (OriginLab, Northampton, MA) applying the Levenberg-Marquardt algorithm. Application of the algorithm leads to a minimization of the squares of the deviations, χ^2, between the fitted curve and the experimental data and gives the corresponding value for the polymerization rate constant, k. That means that k is refined iteratively, until χ^2 is reduced to χ^2_{red} and changes no more. χ^2_{red} is calculated by the sum of the squares of the deviations between the theoretical curve and the experimental data points according to

$$\chi^2_{red} = \sum_{i=1}^{n} \left(p_{fit} - p_{exp}\right)^2 \quad (95)$$

with n being the number of data points, p_{fit} being the theoretical conversion at a time, t, and p_{exp} being the experimental value at the same time, t. The lower χ^2_{red}, the better the curve fits to the experimental data.

5.5 Notes on data analysis and experimental uncertainty

Data of fluorescence intensities, rates, monomer conversions, dynamic, specific, reduced and intrinsic viscosities, weight average molar masses, weight average degrees of polymerization, second virial coefficients, hydrodynamic radii and association constants are given as mean ± SD (n = 3) in the corresponding figures. Impurities, weighing and dilution uncertainties of stoichiometries, concentrations, volume ratios and chain termination ratios are given with absolute error bars in the corresponding figures.

6

Summary

Parts of this Chapter are based on the publications listed on page VIII.

In this work the overall rates of the coordination reaction of terpyridine ligands and Fe^{2+}, Co^{2+}, and Ni^{2+} are presented by usage of fluorescence quenching experiments. The rates are such that the reactions can be followed by stopped-flow measurements. The coordination reactions occur within a few seconds and the overall order of the coordination reactions of **1** and M^{2+} is second order. In EtOH the reaction rates decrease in the order Fe^{2+} > Co^{2+} > Ni^{2+}, due to the electron configuration and the ionic radii with k = (3.9 ± 0.8) × 10^5 M^{-1} s^{-1}, (1.8 ± 0.1) × 10^5 M^{-1} s^{-1}, and (8.0 ± 0.4) × 10^3 M^{-1} s^{-1}, respectively. On the other side, the monotopic ligands **2** or **3** show similar reaction rates. However, coordination reactions of the ditopic ligand **1** proceed approximately twice as fast than the monotopic ligands.

Furthermore, experiments are presented that elucidate the growth kinetics of Fe-, Co-, and Ni-MEPEs. The polymer growth occurs within days and can be best treated as a reversible first- and second-order step growth model. The irreversible kinetic models do not fit well for the polymerization of the MEPEs. High weight average molar masses are obtained. In acetic acid solution (75 vol %), $\bar{M}_w$ follows the order Fe-MEPE > Co-MEPE ~ Ni-MEPE with 8.1 × 10^4 g mol^{-1}, 3.8 × 10^4 g mol^{-1}, and 3.3 × 10^4 g mol^{-1} for Fe-, Co-, and Ni-MEPE, respectively. By usage of acetic acid solution (75 vol %) containing 0.1 M KOAc, $\bar{M}_w$ increases to 2.5 × 10^5 g mol^{-1}, 1.5 × 10^5 g mol^{-1}, and 1.4 × 10^5 g mol^{-1} for Fe-, Co-, and Ni-MEPE, respectively. These values are in the same order of magnitude than calculated at pH = 1.8. The chain-length determined by light scattering in solution is confirmed by cryo-TEM data, revealing essentially plethora of filaments and bundles thereof. Appropriately, the association constants follow the same order with K_a = (4.5 ± 0.1) × 10^5 M^{-1}, (1.0 ± 0.02) × 10^5 M^{-1}, and (7.5 ± 0.04) × 10^4 M^{-1} for Fe-, Co-, and Ni-MEPE, respectively, in acetic acid solution (75 vol %) and (3.9 ± 0.2) × 10^6 M^{-1}, (1.6 ± 0.1) × 10^6 M^{-1}, and (1.4 ± 0.03) × 10^6 M^{-1} for Fe-, Co-, and Ni-MEPE, respectively, in acetic acid solution (75 vol %) containing 0.1 M KOAc. The

forward polymerization rate constants follow the order of Co-MEPE < Fe-MEPE < Ni-MEPE with k = (3.9 ± 0.1) × 10^{-1} M^{-1} s^{-1}, (0.6 ± 0.03) M^{-1} s^{-1}, and (2.7 ± 0.03) M^{-1} s^{-1} for Co-, Fe-, and Ni-MEPE, respectively, in acetic acid solution (75 vol %) and (2.0 ± 0.2) M^{-1} s^{-1}, (3.8 ± 0.3) M^{-1} s^{-1}, and (5.7 ± 0.9) M^{-1} s^{-1} for Co-, Fe-, and Ni-MEPE, respectively, in acetic acid solution (75 vol %) containing 0.1 M KOAc. Thus, the growth of MEPEs is accelerated by presence of potassium acetate as electrolyte.

Furthermore, chain stopping experiments are carried out in order to adjust the chain-length of Co-, Ni-, and Fe-MEPEs. A theoretical model is established, which can be used to receive a polymer of desired average molecular weight and thus, the viscosity. This model should be applicable to (linear) supramolecular polymers that form through reversible interactions of ditopic species in solution under equilibrium conditions. The validity of the theoretical model is confirmed by static light scattering and viscometry and it is shown that tailoring of the chain-length is reproducible, due to the dynamic nature of the MEPEs. In acetic acid solution (75 vol %) the Kuhn-Mark-Houwink constants, a_η, are determined to 0.94 ± 0.07, 0.97 ± 0.03 and 1.09 ± 0.04 and the constants, K_η, to (6.3 ± 0.5) × 10^{-3} mL g^{-1}, (7.2 ± 0.2) × 10^{-3} mL g^{-1}, and (1.7 ± 0.1) × 10^{-3} mL g^{-1} for Fe-, Co-, and Ni-MEPE, respectively, by which it is possible to convert average molar masses to viscosities of the polyelectrolytes. The polymers exhibit a rigid-rod like structure in solution and the stiffness of the polymers increases in the order Fe-MEPE < Co-MEPE < Ni-MEPE.

7

Zusammenfassung

In dieser Arbeit wird die Kinetik der Koordinationsreaktion von Terpyridin-Liganden mit Fe^{2+}, Co^{2+} und Ni^{2+} mit Hilfe der Fluorenzlöschung untersucht. Die Geschwindigkeitskonstanten können mittels Stopped-flow-Messungen bestimmt werden. Die Koordinationsreaktion zwischen dem Liganden **1** und M^{2+} findet innerhalb weniger Sekunden statt und verläuft nach einer Reaktionskinetik zweiter Ordnung. Aufgrund der unterschiedlichen Elektronenkonfigurationen und Ionenradien der Metallionen, nehmen die entsprechenden Geschwindigkeitskonstanten in der Reihe Fe^{2+} > Co^{2+} > Ni^{2+} ab und betragen k = (3.9 ± 0.8) × 10^5 M^{-1} s^{-1}, (1.8 ± 0.1) × 10^5 M^{-1} s^{-1} und (8.0 ± 0.4) × 10^3 M^{-1} s^{-1} für Fe^{2+}, Co^{2+} bzw. Ni^{2+} in Ethanol.

Zudem wird in dieser Arbeit die Wachstumskinetik der Fe-, Co- und Ni-MEPE beschrieben. Das Polymerwachstum findet innerhalb von Tagen statt und kann am besten anhand einer reversiblen Stufenwachstumspolymerisation erster oder zweiter Ordnung beschrieben werden. Die irreversiblen kinetischen Modelle eignen sich hingegen nicht für die Beschreibung der Polymerisation der MEPE. Die MEPE weisen hohe gewichtsmittlere molare Massen auf. In 75% HOAc nehmen sie in der Reihe Fe-MEPE > Co-MEPE ~ Ni-MEPE ab und betragen $\bar{M}_w$ = 8.1 × 10^4 g mol^{-1}, 3.8 × 10^4 g mol^{-1} und 3.3 × 10^4 g mol^{-1} für Fe-, Co- bzw. Ni-MEPE. Bei Vorlage von 0.1 M KOAc in 75% HOAc steigt $\bar{M}_w$ auf 2.5 × 10^5 g mol^{-1}, 1.5 × 10^5 g mol^{-1} und 1.4 × 10^5 g mol^{-1} bei Fe-, Co- bzw. Ni-MEPE. Die Werte liegen in der gleichen Größenordnung wie für pH = 1.8 theoretisch berechnet. Die mittels Lichtstreuung in Lösung bestimmten Kettenlängen können durch cryo-TEM-Messungen bestätigt werden. Die Gleichgewichtskonstanten des Polymerwachstums betragen in 75% HOAc K_a = (4.5 ± 0.1) × 10^5 M^{-1}, (1.0 ± 0.02) × 10^5 M^{-1} und (7.5 ± 0.04) × 10^4 M^{-1} für Fe-, Co- bzw. Ni-MEPE und bei Vorlage von 0.1 M KOAc in 75% HOAc K_a = (3.9 ± 0.2) × 10^6 M^{-1}, (1.6 ± 0.1) × 10^6 M^{-1} und (1.4 ± 0.03) × 10^6 M^{-1} für Fe-, Co- bzw. Ni-MEPE. Die Geschwindigkeitskonstanten der Hinreaktion nehmen in der Reihe Co-MEPE < Fe-MEPE < Ni-MEPE zu und betragen in

75% HOAc k = (3.9 ± 0.1) × 10^{-1} M^{-1} s^{-1}, (0.6 ± 0.03) M^{-1} s^{-1} und (2.7 ± 0.03) M^{-1} s^{-1} für Co-, Fe- bzw. Ni-MEPE und bei Vorlage von 0.1 M KOAc in 75% HOAc (2.0 ± 0.2) M^{-1} s^{-1}, (3.8 ± 0.3) M^{-1} s^{-1} und (5.7 ± 0.9) M^{-1} s^{-1} für Co-, Fe- bzw. Ni-MEPE. Das Wachstum der MEPE kann somit durch die Anwesenheit des Elektrolyten Kaliumacetat beschleunigt werden.

In dieser Arbeit wird außerdem eine Methode beschrieben, um die Kettenlänge der MEPE mit Hilfe von Kettenstoppern einzustellen. Hierfür wird zunächst ein theoretisches Modell beschrieben, mit dessen Hilfe ein Polymer mit gewünschter mittlerer Molmasse und Viskosität erhalten werden kann. Dieses Modell sollte auf andere (lineare) supramolekulare Polymerisationen anwendbar sein, sofern sich die Polymere reversibel aus ditopen Spezies in Lösung oder unter Gleichgewichtsbedingungen bilden. Die Gültigkeit dieses theoretischen Modells wird durch statische Lichtstreuung und Viskositätsmessungen bestätigt. Aufgrund der Dynamik der MEPE ist das Einstellen der Kettenlängen reproduzierbar. Die Kuhn-Mark-Houwink-Konstanten a_η sind bestimmt worden und betragen in 75% HOAc 0.94 ± 0.07, 0.97 ± 0.03 und 1.09 ± 0.04 für Fe-, Co- bzw. Ni-MEPE. Die Konstanten K_η betragen (6.3 ± 0.5) × 10^{-3} mL g^{-1}, (7.2 ± 0.2) × 10^{-3} mL g^{-1} und (1.7 ± 0.1) × 10^{-3} mL g^{-1} für Fe-, Co-, bzw. Ni-MEPE. Mit diesen Konstanten ist es nun möglich, die mittlere molare Masse der Polyelektrolyte in deren Viskosität umzurechnen. Die Polymere weisen eine stäbchenartige Form auf, deren Steifheit in der Reihe Fe-MEPE < Co-MEPE < Ni-MEPE zunimmt.

8

References

[1] M. W. Hosseini, *Acc. Chem. Res.* **2005**, *38*, 313-323.
[2] L. Brammer, *Chem. Soc. Rev.* **2004**, *33*, 476-489.
[3] O. Delgado-Friedrichs, M. D. Foster, M. O'Keeffe, D. M. Proserpio, M. M. Treacy, O. M. Yaghi, *J. Solid State Chem.* **2005**, *178*, 2533-2554.
[4] O. M. Yaghi, M. O'keeffe, N. W. Ockwig, H. K. Chae, M. Eddaoudi, J. Kim, *Nature* **2003**, *423*, 705-714.
[5] M. Eddaoudi, D. B. Moler, H. Li, B. Chen, T. M. Reineke, M. O'keeffe, O. M. Yaghi, *Acc. Chem. Res.* **2001**, *34*, 319-330.
[6] D. G. Kurth, M. Higuchi, *Soft Matter* **2006**, *2*, 915-927.
[7] S. Leininger, B. Olenyuk, P. J. Stang, *Chem. Rev.* **2000**, *100*, 853-908.
[8] M. Fujita, M. Aoyagi, K. Ogura, *Inorg. Chim. Acta* **1996**, *246*, 53-57.
[9] P. J. Stang, K. Chen, A. M. Arif, *J. Am. Chem. Soc.* **1995**, *117*, 8793-8797.
[10] A.-K. Duhme, S. C. Davies, D. L. Hughes, *Inorg. Chem.* **1998**, *37*, 5380-5382.
[11] B. Hasenknopf, J.-M. Lehn, G. Baum, D. Fenske, *Proc. Natl. Acad. Sci. USA* **1996**, *93*, 1397-1400.
[12] C. Piguet, G. Bernardinelli, G. Hopfgartner, *Chem. Rev.* **1997**, *97*, 2005-2062.
[13] D. L. Caulder, K. N. Raymond, *Angew. Chem., Int. Ed. Engl.* **1997**, *36*, 1440-1442.
[14] B. Hasenknopf, J. M. Lehn, B. O. Kneisel, G. Baum, D. Fenske, *Angew. Chem., Int. Ed. Engl.* **1996**, *35*, 1838-1840.
[15] O. Mamula, A. von Zelewsky, G. Bernardinelli, *Angew. Chem., Int. Ed.* **1998**, *37*, 289-293.
[16] J. Libman, Y. Tor, A. Shanzer, *J. Am. Chem. Soc.* **1987**, *109*, 5880-5881.
[17] M. Albrecht, *Synlett* **1996**, *6*, 565-567.
[18] C. R. Woods, M. Benaglia, J. S. Siegel, F. Cozzi, *Angew. Chem., Int. Ed. Engl.* **1996**, *35*, 1830-1833.
[19] D. A. McMorran, P. J. Steel, *Angew. Chem., Int. Ed.* **1998**, *37*, 3295-3297.
[20] J. R. Hall, S. J. Loeb, G. K. Shimizu, G. Yap, *Angew. Chem., Int. Ed.* **1998**, *37*, 121-123.
[21] M. Fujita, O. Sasaki, T. Mitsuhashi, T. Fujita, J. Yazaki, K. Yamaguchi, K. Ogura, *Chem. Commun.* **1996**, *13*, 1535-1536.
[22] R. D. Schnebeck, L. Randaccio, E. Zangrando, B. Lippert, *Angew. Chem., Int. Ed.* **1998**, *37*, 119-121.
[23] S. W. Lai, M. C. W. Chan, S. M. Peng, C. M. Che, *Angew. Chem., Int. Ed.* **1999**, *38*, 669-671.
[24] F. A. Cotton, L. M. Daniels, C. Lin, C. A. Murillo, *J. Am. Chem. Soc.* **1999**, *121*, 4538-4539.
[25] S. Mann, G. Huttner, L. Zsolnai, K. Heinze, *Angew. Chem., Int. Ed. Engl.* **1996**, *35*, 2808-2809.
[26] T. Habicher, J. F. Nierengarten, V. Gramlich, F. Diederich, *Angew. Chem., Int. Ed.* **1998**, *37*, 1916-1919.
[27] A. Varvoglis, *Tetrahedron* **1997**, *53*, 1179-1255.
[28] P. J. Stang, V. V. Zhdankin, *Chem. Rev.* **1996**, *96*, 1123-1178.
[29] P. J. Stang, B. Olenyuk, K. Chen, *Synthesis* **1995**, *8*, 937-938.
[30] P. J. Stang, K. Chen, *J. Am. Chem. Soc.* **1995**, *117*, 1667-1668.
[31] B. Olenyuk, J. A. Whiteford, P. J. Stang, *J. Am. Chem. Soc.* **1996**, *118*, 8221-8230.
[32] D. L. Caulder, K. N. Raymond, *J. Chem. Soc., Dalton Trans.* **1999**, *8*, 1185-1200.
[33] D. L. Caulder, K. N. Raymond, *Acc. Chem. Res.* **1999**, *32*, 975-982.
[34] P. Jones, K. Byrom, J. Jeffery, J. McCleverty, M. Ward, *Chem. Commun.* **1997**, 1361-1362.
[35] B. Dietrich, J. Lehn, J. Sauvage, *Tetrahedron Lett.* **1969**, *10*, 2885-2888.
[36] M. Fujita, S. Nagao, K. Ogura, *J. Am. Chem. Soc.* **1995**, *117*, 1649-1650.
[37] P. Jacopozzi, E. Dalcanale, *Angew. Chem., Int. Ed. Engl.* **1997**, *36*, 613-615.
[38] P. N. Baxter, J. M. Lehn, G. Baum, D. Fenske, *Chem. Eur. J.* **1999**, *5*, 102-112.

[39] P. N. Baxter, J. M. Lehn, B. O. Kneisel, G. Baum, D. Fenske, *Chem. Eur. J.* **1999**, *5*, 113-120.
[40] L. Zhao, Z. Xu, L. K. Thompson, S. L. Heath, D. O. Miller, M. Ohba, *Angew. Chem., Int. Ed.* **2000**, *39*, 3114-3117.
[41] L. K. Thompson, L. Zhao, Z. Xu, D. O. Miller, W. M. Reiff, *Inorg. Chem.* **2003**, *42*, 128-139.
[42] M. Ruben, J. Rojo, F. J. Romero-Salguero, L. H. Uppadine, J.-M. Lehn, *Angew. Chem., Int. Ed.* **2004**, *43*, 3644-3662.
[43] J. Rojo, F. J. Romero-Salguero, J. M. Lehn, G. Baum, D. Fenske, *Eur. J. Inorg. Chem.* **1999**, *9*, 1421-1428.
[44] V. Patroniak, P. N. Baxter, J. M. Lehn, M. Kubicki, M. Nissinen, K. Rissanen, *Eur. J. Inorg. Chem.* **2003**, *22*, 4001-4009.
[45] M. Barboiu, G. Vaughan, R. Graff, J.-M. Lehn, *J. Am. Chem. Soc.* **2003**, *125*, 10257-10265.
[46] E. Breuning, G. S. Hanan, F. J. Romero-Salguero, A. M. Garcia, P. N. Baxter, J. M. Lehn, E. Wegelius, K. Rissanen, H. Nierengarten, A. van Dorsselaer, *Chem. Eur. J.* **2002**, *8*, 3458-3466.
[47] M. Grätzel, *J. Photoch. Photobio. C* **2003**, *4*, 145-153.
[48] U. Beckmann, S. Brooker, *Coord. Chem. Rev.* **2003**, *245*, 17-29.
[49] J. England, C. C. Scarborough, T. Weyhermüller, S. Sproules, K. Wieghardt, *Eur. J. Inorg. Chem.* **2012**, *29*, 4605-4621.
[50] F. Han, M. Higuchi, D. G. Kurth, *Adv. Mater.* **2007**, *19*, 3928-3931.
[51] F. S. Han, M. Higuchi, D. G. Kurth, *J. Am. Chem. Soc.* **2008**, *130*, 2073-2081.
[52] M. Schott, M. Beck, F. Winkler, H. Lorrmann, D. G. Kurth, *J. Chem. Educ.* **2014**, *92*, 364-367.
[53] M. Schott, W. Szczerba, D. G. Kurth, *Langmuir* **2014**, *30*, 10721-10727.
[54] D. Evans, L. Truesdale, G. Carroll, *J. Chem. Soc., Chem. Commun.* **1973**, 55-56.
[55] M. Fujita, Y. J. Kwon, S. Washizu, K. Ogura, *J. Am. Chem. Soc.* **1994**, *116*, 1151-1152.
[56] M. Hayashi, Y. Miyamoto, T. Inoue, N. Oguni, *J. Chem. Soc., Chem. Commun.* **1991**, 1752-1753.
[57] B. Hoskins, R. Robson, *J. Am. Chem. Soc.* **1990**, *112*, 1546-1554.
[58] J. Lee, O. K. Farha, J. Roberts, K. A. Scheidt, S. T. Nguyen, J. T. Hupp, *Chem. Soc. Rev.* **2009**, *38*, 1450-1459.
[59] H. Minamikawa, S. Hayakawa, T. Yamada, N. Iwasawa, K. Narasaka, *Bull. Chem. Soc. Jpn.* **1988**, *61*, 4379-4383.
[60] A. Mori, H. Ohno, H. Nitta, K. Tanaka, S. Inoue, *Synlett* **1991**, 563-564.
[61] H. K. Chae, D. Y. Siberio-Pérez, J. Kim, Y. Go, M. Eddaoudi, A. J. Matzger, M. O'keeffe, O. M. Yaghi, *Nature* **2004**, *427*, 523-527.
[62] M. Eddaoudi, J. Kim, N. Rosi, D. Vodak, J. Wachter, M. O'keeffe, O. M. Yaghi, *Science* **2002**, *295*, 469-472.
[63] F. Gándara, H. Furukawa, S. Lee, O. M. Yaghi, *J. Am. Chem. Soc.* **2014**, *136*, 5271-5274.
[64] H. Li, M. Eddaoudi, M. O'Keeffe, O. M. Yaghi, *Nature* **1999**, *402*, 276-279.
[65] N. L. Rosi, J. Eckert, M. Eddaoudi, D. T. Vodak, J. Kim, M. O'keeffe, O. M. Yaghi, *Science* **2003**, *300*, 1127-1129.
[66] J. B. Beck, S. J. Rowan, *J. Am. Chem. Soc.* **2003**, *125*, 13922-13923.
[67] M. B. Duriska, S. M. Neville, J. Lu, S. S. Iremonger, J. F. Boas, C. J. Kepert, S. R. Batten, *Angew. Chem., Int. Ed.* **2009**, *48*, 8919-8922.
[68] M. B. Duriska, S. M. Neville, B. Moubaraki, J. D. Cashion, G. J. Halder, K. W. Chapman, C. Balde, J.-F. Létard, K. S. Murray, C. J. Kepert, S. R. Batten, *Angew. Chem., Int. Ed.* **2009**, *48*, 2549.
[69] J. M. Lehn, *Polym. Int.* **2002**, *51*, 825-839.
[70] T. Vermonden, J. van der Gucht, P. de Waard, A. T. Marcelis, N. A. Besseling, E. J. Sudhölter, G. J. Fleer, M. A. Cohen Stuart, *Macromolecules* **2003**, *36*, 7035-7044.

[71] M. Burnworth, L. Tang, J. R. Kumpfer, A. J. Duncan, F. L. Beyer, G. L. Fiore, S. J. Rowan, C. Weder, *Nature* **2011**, *472*, 334-337.
[72] C.-C. Chen, E. E. Dormidontova, *Polym. Prepr.* **2004**, *45*, 391-392.
[73] E. C. Constable, A. Thompson, *J. Chem. Soc., Dalton Trans.* **1992**, *24*, 3467-3475.
[74] P. Cordier, F. Tournilhac, C. Soulié-Ziakovic, L. Leibler, *Nature* **2008**, *451*, 977-980.
[75] R. Dobrawa, M. Lysetska, P. Ballester, M. Grüne, F. Würthner, *Macromolecules* **2005**, *38*, 1315-1325.
[76] V. A. Friese, D. G. Kurth, *Coord. Chem. Rev.* **2008**, *252*, 199-211.
[77] S. Graber, K. Doyle, M. Neuburger, C. E. Housecroft, E. C. Constable, R. D. Costa, E. Ortí, D. Repetto, H. J. Bolink, *J. Am. Chem. Soc.* **2008**, *130*, 14944-14945.
[78] R. Holyer, C. Hubbard, S. Kettle, R. Wilkins, *Inorg. Chem.* **1966**, *5*, 622-625.
[79] U. Kolb, K. Büscher, C. A. Helm, A. Lindner, A. F. Thünemann, M. Menzel, M. Higuchi, D. G. Kurth, *Proc. Natl. Acad. Sci. USA* **2006**, *103*, 10202.
[80] G. Moad, E. Rizzardo, S. H. Thang, *Aust. J. Chem.* **2005**, *58*, 379-410.
[81] G. U. Priimov, P. Moore, L. Helm, A. E. Merbach, *BioInorg. React. Mech.* **2001**, *3*, 1-24.
[82] M. Schütte, D. G. Kurth, M. Linford, H. Cölfen, H. Möhwald, *Angew. Chem., Int. Ed.* **1998**, *37*, 2891.
[83] G. Schwarz, I. Haßlauer, D. G. Kurth, *Adv Colloid Interface Sci* **2014**, *207*, 107-120.
[84] G. Schwarz, T. Sievers, Y. Bodenthin, I. Hasslauer, T. Geue, J. Koetz, D. G. Kurth, *J. Mater. Chem.* **2010**, *20*, 4142-4148.
[85] J. I. Bullock, P. W. G. Simpson, *J. Chem. Soc., Faraday Trans. I* **1981**, *77*, 1991-1997.
[86] K.-Y. Kim, G. H. Nancollas, *J. Phys. Chem.* **1977**, *81*, 948-952.
[87] K. Nakamoto, *J. Phys. Chem.* **1960**, *64*, 1420-1425.
[88] S. M. Munzert, G. Schwarz, D. G. Kurth, *RSC Adv.* **2016**, *6*, 15441-15450.
[89] S. M. Munzert, G. Schwarz, D. G. Kurth, *Inorg. Chem.* **2016**, *55*, 2565-2573.
[90] D. G. Kurth, A. Meister, A. F. Thünemann, G. Förster, *Langmuir* **2003**, *19*, 4055-4057.
[91] D. Akcakayiran, D. Mauder, C. Hess, T. K. Sievers, D. Kurth, I. Shenderovich, H.-H. Limbach, G. Findenegg, *J. Phys. Chem. B* **2008**, *112*, 14637-14647.
[92] G. Schwarz, Y. Bodenthin, Z. Tomkowicz, W. Haase, T. Geue, J. Kohlbrecher, U. Pietsch, D. G. Kurth, *J. Am. Chem. Soc.* **2011**, *133*, 547-558.
[93] V. Berl, M. Schmutz, M. J. Krische, R. G. Khoury, J.-M. Lehn, *Chem.-Eur.J.* **2002**, *8*, 1227-1244.
[94] M.-J. Brienne, J. Gabard, J.-M. Lehn, I. Stibor, *J. Chem. Soc. Chem. Commun.* **1989**, *24*, 1868-1870.
[95] S. P. Dudek, M. Pouderoijen, R. Abbel, A. P. Schenning, E. Meijer, *J. Am. Chem. Soc.* **2005**, *127*, 11763-11768.
[96] B. J. Folmer, R. Sijbesma, R. Versteegen, J. Van der Rijt, E. Meijer, *Adv. Mater.* **2000**, *12*, 874-878.
[97] B. J. B. Folmer, E. Cavini, R. P. Sijbesma, E. W. Meijer, *Chem. Commun.* **1998**, *17*, 1847-1848.
[98] J. K. Hirschberg, A. Ramzi, R. P. Sijbesma, E. Meijer, *Macromolecules* **2003**, *36*, 1429-1432.
[99] M. Kotera, J.-M. Lehn, J.-P. Vigneron, *Tetrahedron* **1995**, *51*, 1953-1972.
[100] R. P. Sijbesma, F. H. Beijer, L. Brunsveld, B. J. Folmer, J. K. Hirschberg, R. F. Lange, J. K. Lowe, E. Meijer, *Science* **1997**, *278*, 1601-1604.
[101] S. Bode, L. Zedler, F. H. Schacher, B. Dietzek, M. Schmitt, J. Popp, M. D. Hager, U. S. Schubert, *Adv. Mater.* **2013**, *25*, 1634-1638.
[102] T. Jungst, W. Smolan, K. Schacht, T. Scheibel, J. r. Groll, *Chem. Rev.* **2016**, *116*, 1496-1539.
[103] D. G. Kurth, *Ann. N.Y. Acad. Sci.* **2002**, *960*, 29-38.

[104] J.-M. Lehn, *Supramolecular chemistry, Vol. 1*, VCH Weinheim, **1995**.
[105] J. M. Lehn, *Angew. Chem., Int. Ed.* **1990**, *29*, 1304-1319.
[106] X. Lu, X. Li, Y. Cao, A. Schultz, J. L. Wang, C. N. Moorefield, C. Wesdemiotis, S. Z. Cheng, G. R. Newkome, *Angew. Chem., Int. Ed.* **2013**, *52*, 7728-7731.
[107] U. Michelsen, C. A. Hunter, *Angew. Chem., Int. Ed.* **2000**, *39*, 764-767.
[108] D. Philp, J. F. Stoddart, *Angew. Chem. Int. Ed.* **1996**, *35*, 1154-1196.
[109] U. S. Schubert, A. Winter, G. R. Newkome, *Terpyridine-based materials: for catalytic, optoelectronic and life science applications*, John Wiley & Sons, **2012**.
[110] J. Wang, A. de Keizer, R. Fokkink, Y. Yan, M. A. Cohen Stuart, J. van der Gucht, *J. Phys. Chem. B* **2010**, *114*, 8313-8319.
[111] A. Winter, C. Friebe, M. Chiper, U. S. Schubert, M. Presselt, B. Dietzek, M. Schmitt, J. Popp, *ChemPhysChem* **2009**, *10*, 787-798.
[112] L. Yang, X. Tan, Z. Wang, X. Zhang, *Chem. Rev.* **2015**, 7196-7239.
[113] M. A. Aboudzadeh, M. E. Muñoz, A. Santamaría, R. Marcilla, D. Mecerreyes, *Macromol. Rapid Commun.* **2012**, *33*, 314-318.
[114] A. Harada, M. Okada, *Polym. J.* **1999**, *31*, 1095-1098.
[115] A. Harada, S. Suzuki, M. Okada, M. Kamachi, *Macromolecules* **1996**, *29*, 5611-5614.
[116] A. Harada, Y. Takashima, H. Yamaguchi, *Chem. Soc. Rev.* **2009**, *38*, 875-882.
[117] T. Kakuta, Y. Takashima, M. Nakahata, M. Otsubo, H. Yamaguchi, A. Harada, *Adv. Mater.* **2013**, *25*, 2849-2853.
[118] M. Miyauchi, T. Hoshino, H. Yamaguchi, S. Kamitori, A. Harada, *J. Am. Chem. Soc.* **2005**, *127*, 2034-2035.
[119] S. S. Babu, V. K. Praveen, A. Ajayaghosh, *Chem. Rev.* **2014**, *114*, 1973-2129.
[120] E. H. Beckers, S. C. Meskers, A. P. Schenning, Z. Chen, F. Würthner, R. A. Janssen, *J. Phys. Chem. A* **2004**, *108*, 6933-6937.
[121] F. C. De Schryver, T. Vosch, M. Cotlet, M. Van der Auweraer, K. Müllen, J. Hofkens, *Acc. Chem. Res.* **2005**, *38*, 514-522.
[122] C. D. Dimitrakopoulos, P. R. Malenfant, *Adv. Mater.* **2002**, *14*, 99.
[123] S. Ghosh, X. Q. Li, V. Stepanenko, F. Wuerthner, *Chem. Eur. J.* **2008**, *14*, 11343-11357.
[124] F. Graser, E. Hädicke, *Liebigs Ann. Chem.* **1984**, *3*, 483-494.
[125] J. Hak Oh, S. Liu, Z. Bao, R. Schmidt, F. Würthner, *Appl. Phys. Lett.* **2007**, *91*, 212107.
[126] B. A. Jones, M. J. Ahrens, M. H. Yoon, A. Facchetti, T. J. Marks, M. R. Wasielewski, *Angew. Chem.* **2004**, *116*, 6523-6526.
[127] T. E. Kaiser, H. Wang, V. Stepanenko, F. Würthner, *Angew. Chem. Int. Ed.* **2007**, *46*, 5541-5544.
[128] C. Karapire, C. Zafer, S. İçli, *Synth. Met.* **2004**, *145*, 51-60.
[129] A. Kraft, A. C. Grimsdale, A. B. Holmes, *Angew. Chem. Int. Ed.* **1998**, *37*, 402-428.
[130] H. Langhals, J. Karolin, L. B.-Å. Johansson, *J. Chem. Soc. Faraday Trans.* **1998**, *94*, 2919-2922.
[131] P. R. Malenfant, C. D. Dimitrakopoulos, J. D. Gelorme, L. L. Kosbar, T. O. Graham, A. Curioni, W. Andreoni, *Appl. Phys. Lett.* **2002**, *80*, 2517-2519.
[132] J. Mizuguchi, *J. Appl. Phys.* **1998**, *84*, 4479-4486.
[133] M. O'Neil, M. Niemczyk, W. Svec, D. Gosztola, G. Gaines, M. Wasielewski, *Science* **1992**, *257*, 63-65.
[134] A. Prodi, C. Chiorboli, F. Scandola, E. Iengo, E. Alessio, R. Dobrawa, F. Würthner, *J. Am. Chem. Soc.* **2005**, *127*, 1454-1462.
[135] M. S. Rodríguez-Morgade, T. Torres, C. Atienza-Castellanos, D. M. Guldi, *J. Am. Chem. Soc.* **2006**, *128*, 15145-15154.

[136] A. Sautter, B. K. Kaletas, D. G. Schmid, R. Dobrawa, M. Zimine, G. Jung, I. H. van Stokkum, L. De Cola, R. M. Williams, F. Würthner, *J. Am. Chem. Soc.* **2005**, *127*, 6719-6729.
[137] R. Schmidt, M. M. Ling, J. H. Oh, M. Winkler, M. Könemann, Z. Bao, F. Würthner, *Adv. Mater.* **2007**, *19*, 3692-3695.
[138] L. Schmidt-Mende, A. Fechtenkötter, K. Müllen, E. Moons, R. H. Friend, J. MacKenzie, *Science* **2001**, *293*, 1119-1122.
[139] C. W. Struijk, A. B. Sieval, J. E. Dakhorst, M. van Dijk, P. Kimkes, R. B. Koehorst, H. Donker, T. J. Schaafsma, S. J. Picken, A. M. van de Craats, *J. Am. Chem. Soc.* **2000**, *122*, 11057-11066.
[140] C. W. Tang, *Appl. Phys. Lett.* **1986**, *48*, 183-185.
[141] F. Würthner, R. Schmidt, *ChemPhysChem* **2006**, *7*, 793-797.
[142] S. Yagai, T. Seki, T. Karatsu, A. Kitamura, F. Würthner, *Angew. Chem. Int. Ed.* **2008**, *47*, 3367-3371.
[143] T. F. De Greef, M. M. Smulders, M. Wolffs, A. P. Schenning, R. P. Sijbesma, E. Meijer, *Chem. Rev.* **2009**, *109*, 5687-5754.
[144] E. Krieg, M. M. Bastings, P. Besenius, B. Rybtchinski, *Chem. Rev.* **2016**, *116*, 2414-2477.
[145] C. Kulkarni, S. Balasubramanian, S. J. George, *ChemPhysChem* **2013**, *14*, 661-673.
[146] M. R. Molla, S. Ghosh, *Phys. Chem. Chem. Phys.* **2014**, *16*, 26672-26683.
[147] C. Rest, R. Kandanelli, G. Fernández, *Chem. Soc. Rev.* **2015**, *44*, 2543-2572.
[148] S. Yagai, *Bull. Chem. Soc. Jpn.* **2015**, *88*, 28-58.
[149] J. M. Fréchet, *Proc. Nat. Acad. Sci.* **2002**, *99*, 4782-4787.
[150] O. Sato, *Accounts Chem. Res.* **2003**, *36*, 692-700.
[151] Y. Bodenthin, U. Pietsch, J. Grenzer, T. Geue, H. Möhwald, D. Kurth, *J. Phys. Chem. B* **2005**, *109*, 12795-12799.
[152] M. Alvaro, C. Aprile, B. Ferrer, F. Sastre, H. García, *Dalton Trans.* **2009**, *36*, 7437-7444.
[153] P. Calero, M. Hecht, R. Martínez-Máñez, F. Sancenón, J. Soto, J. L. Vivancos, K. Rurack, *Chem. Commun.* **2011**, *47*, 10599-10601.
[154] S. Cousinié, L. Mauline, M. Gressier, S. R. Kandibanda, L. Datas, C. Reber, M.-J. Menu, *New J. Chem.* **2012**, *36*, 1355-1367.
[155] M. Guerrero, N. J. Costa, L. L. Vono, L. M. Rossi, E. V. Gusevskaya, K. Philippot, *J. Mater. Chem. A* **2013**, *1*, 1441-1449.
[156] D. Hobara, S. Kondo, M. S. Choi, Y. Ishioka, S. Hirata, M. Murata, K. Azuma, J. Kasahara, *Phys. Status Solidi A* **2007**, *204*, 1706-1711.
[157] E. Jin Cho, S. Jung, K. Lee, H. Joo Lee, K. Chun Nam, H.-J. Bae, *Chem. Commun.* **2010**, *46*, 6557-6559.
[158] G. Li, E. M. Sproviero, W. R. McNamara, R. C. Snoeberger III, R. H. Crabtree, G. W. Brudvig, V. S. Batista, *J. Phys. Chem. B* **2010**, *114*, 14214-14222.
[159] M. Montalti, L. Prodi, N. Zaccheroni, M. Beltrame, T. Morotti, S. Quici, *New J. Chem.* **2007**, *31*, 102-108.
[160] U. S. Schubert, A. Alexeev, P. R. Andres, *Macromol. Mater. Eng.* **2003**, *288*, 852-860.
[161] P. H. Seeberger, S. J. Danishefsky, *Acc. Chem. Res.* **1998**, *31*, 685-695.
[162] R. Shenhar, E. Jeoung, S. Srivastava, T. B. Norsten, V. M. Rotello, *Adv. Mater.* **2005**, *17*, 2206-2210.
[163] L. A. Thompson, J. A. Ellman, *Chem. Rev.* **1996**, *96*, 555-600.
[164] D. S. Thorpe, S. Walle, *Biochem. Biophys. Res. Commun.* **2000**, *269*, 591-595.
[165] A. Winter, M. D. Hager, G. R. Newkome, U. S. Schubert, *Advanced Materials* **2011**, *23*, 5728-5748.

[166] B. L. Feringa, *Molecular switches, Vol. 42*, Wiley Online Library, **2001**.
[167] P. Gütlich, Y. Garcia, T. Woike, *Coord. Chem. Rev.* **2001**, *219*, 839-879.
[168] G. Schwarz, S. Maisch, S. Ullrich, J. Wagenhöfer, D. G. Kurth, *Appl. Mater. Interfaces* **2013**, *5*, 4031-4034.
[169] S. R. Batten, N. R. Champness, X.-M. Chen, J. Garcia-Martinez, S. Kitagawa, L. Öhrström, M. O'Keeffe, M. Paik Suh, J. Reedijk, *Pure Appl. Chem.* **2013**, *85*, 1715-1724.
[170] T. R. Cook, Y.-R. Zheng, P. J. Stang, *Chem. Rev.* **2013**, *113*, 734-777.
[171] H. Buser, D. Schwarzenbach, W. Petter, A. Ludi, *Inorg. Chem.* **1977**, *16*, 2704-2710.
[172] S. Roche, C. Haslam, S. L. Heath, J. A. Thomas, *Chem. Commun.* **1998**, *16*, 1681-1682.
[173] M. Eigen, R. G. Wilkins, *Adv. Chem. Ser.* **1965**, *49*, 55.
[174] H. Bennetto, E. Caldin, *J. Chem. Soc. A* **1971**, 2191-2198.
[175] R. G. Pearson, P. Ellgen, *Inorg. Chem.* **1967**, *6*, 1379-1385.
[176] D. T. Richens, *Chem. Rev.* **2005**, *105*, 1961-2002.
[177] H. Ma, C. Wan, A. H. Zewail, *Proc. Natl. Acad. Sci. USA* **2008**, *105*, 12754-12757.
[178] T. Swaddle, *Comment. Inorg. Chem.* **1991**, *12*, 237-258.
[179] R. G. Wilkins, *Kinetics and Mechanism of Reactions of Transition Metal Complexes, 2nd Thoroughly Revised Edition*, VCH, **1991**.
[180] I. M. Henderson, R. C. Hayward, *J. Mater. Chem.* **2012**, *22*, 21366-21369.
[181] J. Burgess, C. D. Hubbard, *Adv. Inorg. Chem.* **2003**, *54*, 71-155.
[182] Y. Ducommun, K. E. Newman, A. E. Merbach, *Inorg. Chem.* **1980**, *19*, 3696-3703.
[183] D. Benton, P. Moore, *J. Chem. Soc., Dalton Trans.* **1973**, 399-404.
[184] R. Mohr, R. Van Eldik, *Inorg. Chem.* **1985**, *24*, 3396-3399.
[185] R. Holyer, C. Hubbard, S. Kettle, R. Wilkins, *Inorg. Chem.* **1965**, *4*, 929-935.
[186] D. W. Margerum, *ACS Symp. Ser.* **1982**, *198*, 3-38.
[187] C. Goze, G. Ulrich, L. Charbonnière, M. Cesario, T. Prangé, R. Ziessel, *Chem. Eur. J.* **2003**, *9*, 3748-3755.
[188] S. M. Munzert, G. Schwarz, D. G. Kurth, *Chem. Eur. J.* **2017**, doi: 10.1002/chem.201701417.
[189] E. C. Constable, G. Baum, E. Bill, R. Dyson, R. van Eldik, D. Fenske, S. Kaderli, D. Morris, A. Neubrand, M. Neuburger, *Chem. Eur. J.* **1999**, *5*, 498-508.
[190] R. Tsuchida, *B. Chem. Soc. Jpn.* **1938**, *13*, 388-400.
[191] A. N. Carolan, A. E. Mroz, M. El Ojaimi, D. G. VanDerveer, R. P. Thummel, R. D. Hancock, *Inorg. Chem.* **2012**, *51*, 3007-3015.
[192] W. Knoben, N. Besseling, L. Bouteiller, M. A. C. Stuart, *Phys. Chem. Chem. Phys.* **2005**, *7*, 2390-2398.
[193] W. Knoben, N. Besseling, M. A. C. Stuart, *Phys. Rev. Lett.* **2006**, *97*, 068301.
[194] W. Knoben, N. Besseling, M. A. C. Stuart, *J. Chem. Phys.* **2007**, *126*, 024907.
[195] W. Knoben, N. A. Besseling, M. A. Cohen Stuart, *Macromolecules* **2006**, *39*, 2643-2653.
[196] F. Lortie, S. Boileau, L. Bouteiller, C. Chassenieux, F. Lauprêtre, *Macromolecules* **2005**, *38*, 5283-5287.
[197] S. Yagai, T. Iwashima, T. Karatsu, A. Kitamura, *Chem. Commun.* **2004**, 1114-1115.
[198] P. A. Korevaar, S. J. George, A. J. Markvoort, M. M. Smulders, P. A. Hilbers, A. P. Schenning, T. F. De Greef, E. Meijer, *Nature* **2012**, *481*, 492-496.
[199] A. Winter, U. S. Schubert, *Chem. Soc. Rev.* **2016**, *45*, 5311-5357.
[200] A. Wild, A. Winter, F. Schlütter, U. S. Schubert, *Chem. Soc. Rev.* **2011**, *40*, 1459-1511.
[201] A. S. Abd-El-Aziz, P. O. Shipman, B. N. Boden, W. S. McNeil, *Progr. Polym. Sci.* **2010**, *35*, 714-836.

[202] C.-C. You, F. Würthner, *Org. Lett.* **2004**, *6*, 2401-2404.
[203] A. J. Boydston, J. D. Rice, M. D. Sanderson, O. L. Dykhno, C. W. Bielawski, *Organometallics* **2006**, *25*, 6087-6098.
[204] E. Peris, R. H. Crabtree, *Coord. Chem. Rev.* **2004**, *248*, 2239-2246.
[205] A. J. Boydston, K. A. Williams, C. W. Bielawski, *J. Am. Chem. Soc.* **2005**, *127*, 12496-12497.
[206] A. J. Boydston, D. M. Khramov, C. W. Bielawski, *Tetrahedron Lett.* **2006**, *47*, 5123-5125.
[207] D. M. Khramov, A. J. Boydston, C. W. Bielawski, *Angew. Chem., Int. Ed.* **2006**, *45*, 6186-6189.
[208] C.-S. Wu, Y.-T. Lee, Y. Chen, *Polymer Chemistry* **2012**, *3*, 2776-2784.
[209] T. Kuhlmann, S. Roth, J. Rozière, W. Siebert, *Angew. Chem., Int. Ed. Engl.* **1986**, *25*, 105-107.
[210] W. Siebert, *Pure Appl. Chem.* **1988**, *60*, 1345-1348.
[211] T. Kuhlmann, S. Roth, J. Roziere, W. Siebert, U. Zenneck, *Synth. Met.* **1987**, *19*, 757-762.
[212] W. Siebert, *Angew. Chem., Int. Ed. Engl.* **1985**, *24*, 943-958.
[213] W. Siebert, *Russ. Chem. Rev.* **1991**, *60*, 784-791.
[214] M. Rosenblum, H. M. Nugent, K.-S. Jang, M. Labes, W. Cahalane, P. Klemarczyk, W. M. Reiff, *Macromolecules* **1995**, *28*, 6330-6342.
[215] R. Arnold, S. A. Matchett, M. Rosenblum, *Organometallics* **1988**, *7*, 2261-2266.
[216] B. M. Foxman, D. A. Gronbeck, M. Rosenblum, *J. Organomet. Chem.* **1991**, *413*, 287-294.
[217] B. M. Foxman, M. Rosenblum, V. Sokolov, N. Khrushchova, *Organometallics* **1993**, *12*, 4805-4809.
[218] H. M. Nugent, M. Rosenblum, P. Klemarczyk, *J. Am. Chem. Soc.* **1993**, *115*, 3848-3849.
[219] B. Bush, J. Lagowski, *Organometallics* **1988**, *7*, 1945-1948.
[220] T. Hirao, M. Kurashina, K. Aramaki, H. Nishihara, *J. Chem. Soc., Dalton Trans.* **1996**, *14*, 2929-2933.
[221] H. Jacobson, W. H. Stockmayer, *J. Chem. Phys.* **1950**, *18*, 1600-1606.
[222] R. Dobrawa, F. Würthner, *J. Polym. Sci., Part A: Polym. Chem.* **2005**, *43*, 4981-4995.
[223] Q. Cheng, V. Pavlinek, Y. He, A. Lengalova, C. Li, P. Saha, *Colloids Surf., A* **2008**, *318*, 169-174.
[224] M. S. Cho, H. J. Choi, W.-S. Ahn, *Langmuir* **2004**, *20*, 202-207.
[225] F. F. Fang, H. J. Choi, W.-S. Ahn, *Microporous Mesoporous Mater.* **2010**, *130*, 338-343.
[226] Y. D. Liu, F. F. Fang, H. J. Choi, Y. Seo, *Colloids Surf., A* **2011**, *381*, 17-22.
[227] G. Schwarz, Y. Bodenthin, T. Geue, J. Koetz, D. G. Kurth, *Macromolecules* **2010**, *43*, 494-500.
[228] G. Odian, *Principles of polymerization, Vol. 4*, Wiley-Interscience New York, **2004**.
[229] A. E. Martell, R. M. Smith, R. J. Motokaitis, *NIST Standard Reference Database 46, Critically selected stability constants of metal complexes* **2004**, *Version 8.0*.
[230] P. Payamyar, B. T. King, H. C. Öttinger, A. D. Schlüter, *Chem. Commun.* **2016**, *52*, 18-34.
[231] R. J. Young, P. A. Lovell, *Introduction to polymers*, CRC press, **2011**.
[232] M. Chanda, S. K. Roy, *Plastics technology handbook, Vol. 72*, CRC press, **2006**.
[233] M. Szwarc, M. Levy, R. Milkovich, *J. Am. Chem. Soc.* **1956**, *78*, 2656-2657.
[234] M. Szwarc, *Nature* **1956**, *178*, 1168-1169.
[235] R. J. Palmer, in *Encyclopedia of Polymer Science and Technology*, John Wiley & Sons, Inc., **2002**.
[236] V. Serini, in *Ullmann's Encyclopedia of Industrial Chemistry*, Wiley-VCH Verlag GmbH & Co. KGaA, **2000**.
[237] W. Carothers, *J. Am. Chem. Soc.* **1929**, *51*, 2548-2559.
[238] E. Delebecq, J.-P. Pascault, B. Boutevin, F. o. Ganachaud, *Chem. Rev.* **2013**, *113*, 80-118.
[239] D. Zhao, J. S. Moore, *Org. Biomol. Chem.* **2003**, *1*, 3471-3491.
[240] W. H. Carothers, *T. Faraday. Soc.* **1936**, *32*, 39-49.
[241] A. Ciferri, *Macromol. Rapid Commun.* **2002**, *23*, 511-529.

[242] A. Ciferri, *Supramolecular Polymers*, CRC press, **2005**.
[243] T. F. De Greef, E. Meijer, *Nature* **2008**, *453*, 171-173.
[244] J. F. Douglas, J. Dudowicz, K. F. Freed, *J. Chem. Phys.* **2008**, *128*, 224901.
[245] J. Dudowicz, K. F. Freed, J. F. Douglas, *J. Chem. Phys.* **2003**, *119*, 12645-12666.
[246] R. B. Martin, *Chem. Rev.* **1996**, *96*, 3043.
[247] P. R. Andres, U. S. Schubert, *Synthesis* **2004**, *8*, 1229-1238.
[248] P. R. Andres, U. S. Schubert, *Macromol. Rapid Commun.* **2004**, *25*, 1371-1375.
[249] M. A. Meier, D. Wouters, C. Ott, P. Guillet, C.-A. Fustin, J.-F. Gohy, U. S. Schubert, *Macromolecules* **2006**, *39*, 1569-1576.
[250] T. J. Cho, C. N. Moorefield, S. H. Hwang, P. Wang, L. A. Godínez, E. Bustos, G. R. Newkome, *Eur. J. Org. Chem.* **2006**, *18*, 4193-4200.
[251] E. C. Constable, B. Hermann, C. E. Housecroft, M. Neuburger, S. Schaffner, L. J. Scherer, *New J. Chem.* **2005**, *29*, 1475-1481.
[252] E. C. Constable, C. E. Housecroft, M. Neuburger, S. Schaffner, E. J. Shardlow, *Dalton Trans.* **2005**, 234-235.
[253] S. Ogi, K. Sugiyasu, S. Manna, S. Samitsu, M. Takeuchi, *Nat. Chem.* **2014**, *6*, 188-195.
[254] P. J. Stals, P. A. Korevaar, M. A. Gillissen, T. F. de Greef, C. F. Fitié, R. P. Sijbesma, A. R. Palmans, E. Meijer, *Angew. Chem. Int. Ed.* **2012**, *124*, 11459-11463.
[255] Y. Tidhar, H. Weissman, D. Tworowski, B. Rybtchinski, *Chem.-Eur.J.* **2014**, *20*, 10332-10342.
[256] J. Baram, H. Weissman, B. Rybtchinski, *J. Phys. Chem. B* **2014**, *118*, 12068-12073.
[257] E. Krieg, H. Weissman, E. Shimoni, A. Bar On, B. Rybtchinski, *J. Am. Chem. Soc.* **2014**, *136*, 9443-9452.
[258] D. Zhao, J. S. Moore, *J. Am. Chem. Soc.* **2003**, *125*, 16294-16299.
[259] D. Zhao, K. Yue, *Macromolecules* **2008**, *41*, 4029-4036.
[260] T. D. Clark, J. M. Buriak, K. Kobayashi, M. P. Isler, D. E. McRee, M. R. Ghadiri, *J. Am. Chem. Soc.* **1998**, *120*, 8949-8962.
[261] L. Brunsveld, B. Folmer, E. Meijer, R. Sijbesma, *Chem. Rev.* **2001**, *101*, 4071-4098.
[262] S. Lahiri, J. L. Thompson, J. S. Moore, *J. Am. Chem. Soc.* **2000**, *122*, 11315-11319.
[263] H. Zeng, X. Yang, A. L. Brown, S. Martinovic, R. D. Smith, B. Gong, *Chem. Commun.* **2003**, *13*, 1556-1557.
[264] X. J. Zhao, R. X. He, M. Li, N. W. Zhao, Y. F. Li, C. Z. Huang, *RSC Adv.* **2013**, *3*, 111-116.
[265] Y. Bodenthin, G. Schwarz, Z. Tomkowicz, T. Geue, W. Haase, U. Pietsch, D. G. Kurth, *J. Am. Chem. Soc.* **2009**, *131*, 2934-2941.
[266] J. Lakowicz, *Principles of fluorescence spectroscopy*, Springer Verlag, **2006**.
[267] B. Bodenant, F. Fages, M.-H. Delville, *J. Am. Chem. Soc.* **1998**, *120*, 7511-7519.
[268] L. Fabbrizzi, M. Licchelli, P. Pallavicini, A. Perotti, A. Taglietti, D. Sacchi, *Chem. Eur. J.* **1996**, *2*, 75-82.
[269] J. A. Kemlo, T. M. Shepherd, *Chem. Phys. Lett.* **1977**, *47*, 158-162.
[270] A. W. Varnes, R. B. Dodson, E. Wehry, *J. Am. Chem. Soc.* **1972**, *94*, 946-950.
[271] L. Helm, G. M. Nicolle, R. E. Merbach, *Adv. Inorg. Chem.* **2005**, *57*, 327-379.
[272] J. W. Moore, R. G. Pearson, *Kinetics and mechanism*, John Wiley & Sons, **1961**.
[273] K. Levenberg, *Q. Appl. Math.* **1944**, *2*, 164-168.
[274] D. W. Marquardt, *J. Soc. Ind. Appl. Math.* **1963**, *11*, 431-441.
[275] F. S. Dainton, W. D. Sisley, *Trans. Faraday Soc.* **1963**, *59*, 1369-1376.
[276] J.-F. Gohy, B. G. Lohmeijer, S. K. Varshney, U. S. Schubert, *Macromolecules* **2002**, *35*, 7427-7435.

[277] V. H. Wesslau, *Makromol. Chem.* **1963**, *69*, 213-219.
[278] S. Schmatloch, A. M. van den Berg, A. S. Alexeev, H. Hofmeier, U. S. Schubert, *Macromolecules* **2003**, *36*, 9943-9949.
[279] A. Tessa ten Cate, R. P. Sijbesma, *Macromol. Rapid Commun.* **2002**, *23*, 1094-1112.
[280] J. B. Beck, J. M. Ineman, S. J. Rowan, *Macromolecules* **2005**, *38*, 5060-5068.
[281] M. Cates, *Macromolecules* **1987**, *20*, 2289-2296.
[282] B. Lahn, M. Rehahn, *e-Polymers* **2002**, *2*, 1-33.
[283] T. Shikata, D. Ogata, K. Hanabusa, *J. Phys. Chem. B* **2004**, *108*, 508-514.
[284] J. Xu, E. A. Fogleman, S. L. Craig, *Macromolecules* **2004**, *37*, 1863-1870.
[285] K.-F. Arndt, G. Müller, *Polymercharakterisierung*, Hanser, **1996**.
[286] M. H. Ottøy, K. M. Vårum, B. E. Christensen, M. W. Anthonsen, O. Smidsrød, *Carbohydr. Polym.* **1996**, *31*, 253-261.
[287] C. Tanford, *Physical chemistry of macromolecules*, Wiley, New York, **1961**.
[288] A.-A. A. Abdel-Azim, A. M. Atta, M. S. Farahat, W. Y. Boutros, *Polymer* **1998**, *39*, 6827-6833.
[289] M. L. Huggins, *J. Am. Chem. Soc.* **1942**, *64*, 2716-2718.
[290] P. Suresha, M. V. Badiger, B. A. Wolf, *RSC Advances* **2015**, *5*, 27674-27681.
[291] A. George, W. W. Wilson, *Acta. Crystallogr. D* **1994**, *50*, 361-365.
[292] T. Radeva, *Physical Chemistry of Polyelectrolytes*, Marcel Dekker: New York, **2001**.
[293] W. Schärtl, *Light Scattering from Polymer Solutions and Nanoparticle Dispersions*, Springer, **2007**.
[294] L. Fetters, N. Hadjichristidis, J. Lindner, J. Mays, *J. Phys. Chem. Ref. Data* **1994**, *23*, 619-640.
[295] H. Lee, R. M. Venable, A. D. MacKerell, R. W. Pastor, *Biophys. J.* **2008**, *95*, 1590-1599.
[296] W. Burchard, *Adv. Polym. Sci.* **1983**, *48*, 1.
[297] A. Winter, A. M. J. v. d. Berg, R. Hoogenboom, G. Kickelbick, U. S. Schubert, *Synthesis* **2006**, *17*, 2873-2878.
[298] J. Wang, G. Hanan, *Synlett* **2005**, *8*, 1251-1254.
[299] H. D. Hardt, W. Möller, *Z. Anorg. Allg. Chem.* **1961**, *313*, 57-69.
[300] J. Hermans, S. Levinson, *J. Opt. Soc. Am.* **1951**, *41*, 460-464.
[301] W. Kaye, J. McDaniel, *Appl. Opt.* **1974**, *13*, 1934-1937.
[302] H. Wu, *Chem. Phys.* **2010**, *367*, 44-47.
[303] B. H. Zimm, *J. Chem. Phys.* **1948**, *16*, 1099-1116.
[304] T. Röder, B. Morgenstern, *Polymer* **1999**, *40*, 4143-4147.
[305] A. Guinier, G. Fournet, *Small angle scattering of X-rays*, J. Wiley & Sons, New York, **1955**.
[306] I. Topchieva, I. Panova, B. Kurganov, V. Spiridonov, E. Matukhina, S. Filippov, A. Lezov, *Colloid Journal* **2008**, *70*, 356-365.

DOCUMENTATION OF AUTHORSHIP

This section contains a list of the individual contribution for each author to the publications reprinted in this thesis.

A S. M. Munzert, G. Schwarz, D. G. Kurth, *"Kinetic Studies of the Coordination of Mono- and Ditopic Ligands with First Row Transition Metal Ions", Inorg. Chem.* **2016**, 55, 2565-2573.

Author	**1**	**2**	**3**	**-**	**-**	**-**
Synthesis and sample preparation	x					
Absorption and fluorescence spectroscopy	x					
Stopped-Flow measurements	x					
Static light scattering (SLS)	x					
Study design / concept development	x		x			
Data analysis and interpretation	x	x	x			
Manuscript planning	x		x			
Manuscript writing	x					
Correction of manuscript		x	x			
Supervision of S. M. Munzert		x	x			

B S. M. Munzert, S. P. Stier, G. Schwarz, H. Weissman, B. Rybtchinski, D. G. Kurth, *"The kinetics of growth of metallo-supramolecular polyelectrolytes in solution", Chem. Eur. J.* **2017**, doi: 10.1002/chem.201701417.

Author	**1**	**2**	**3**	**4**	**5**	**6**
Synthesis and sample preparation	x					
Conductometric titrations	x					
Static light scattering (SLS)	x					
Viscosity measurements	x					
Modeling the chain-length of MEPEs		x				
Cryo-TEM imaging				x	x	
Study design / concept development	x					x
Data analysis and interpretation	x	x	x	x	x	x
Manuscript planning	x					x
Manuscript writing	x					
Correction of manuscript			x			x
Supervision of S. M. Munzert			x			x

C S. M. Munzert G. Schwarz, D. G. Kurth, *"Tailoring length and viscosity of dynamic metallo-supramolecular polymers in solution", RSC Advances* **2016**, 6, 15441-15450.

Author	**1**	**2**	**3**	**-**	**-**	**-**
Synthesis and sample preparation	x					
Viscosity measurements	x					
Static light scattering (SLS)	x					
Dynamic light scattering (DLS)	x					
Study design / concept development	x		x			
Data analysis and interpretation	x	x	x			
Manuscript planning	x		x			
Manuscript writing	x					
Correction of manuscript		x	x			
Supervision of S. M. Munzert		x	x			

Erklärung zu den Eigenanteilen des Doktoranden sowie der Koautoren an Publikationen und Zweitpublikationsrechten bei einer kumulativen Dissertation

Für alle in dieser kumulativen Dissertation verwendeten Manuskripte liegen die notwendigen Genehmigungen der Verlage ("reprint permission") für die Zweitpublikation vor. Dieser Umstand wird durch die genaue Angabe der Literaturstelle der Erstpublikation auf der ersten Seite des betreffenden Kapitels deutlich gemacht. Die Mitautoren der in dieser kumulativen Dissertation verwendeten Manuskripte sind sowohl über die Nutzung als auch über die oben angegebenen Eigenanteile informiert und stimmen dem zu. Die Beiträge der Mitautoren an den Publikationen sind in den vorausgehenden Tabellen aufgeführt.

Würzburg, den

Stefanie Martina Munzert

Erklärung

Hiermit erkläre ich an Eides statt, dass ich die Dissertation mit dem Titel „Coordination of dynamic metallo-supramolecular polymers (MEPEs)“ selbständig angefertigt und keine anderen als die von mir angegebenen Quellen und Hilfsmittel benutzt habe.

Ich erkläre außerdem, dass diese Dissertation weder in gleicher noch in anderer Form bereits in einem anderen Prüfungsverfahren vorgelegen hat.

Ich habe außer den mit dem Zulassungsgesuch urkundlich vorgelegten Graden keine weiteren akademischen Grade erworben oder zu erwerben versucht.

Würzburg, den

Stefanie Martina Munzert